

Light-induced charge-transfer dynamics in Ruthenium-polypyridine complexes

DISSERTATION

zur Erlangung des akademischen Grades
doctor rerum naturalium (Dr. rer. nat.)



seit 1558

vorgelegt dem Rat der Chemisch-Geowissenschaftlichen Fakultät
der Friedrich-Schiller-Universität Jena

von Diplomchemiker Christian Kuhnt
geboren am 12.05.1983

Gutachter:

1. Prof. Dr. Jürgen Popp

2. Prof. Dr. Benjamin Dietzek

Datum der Verteidigung: 08.05.2013

Contents

List of Figures	iv
List of Abbreviations	v
List of Substances	vii
1. Introduction	1
2. Rudppz - a model system	7
2.1. Ground-state properties	9
2.2. Excited-state properties	11
2.2.1. Controlling the luminescence by regioselective substitution	11
2.2.2. Adjustment of an excited-state equilibrium by regioselective substitution	13
3. Modification of the Bridging Ligand	17
3.1. Bromination of the tpphz bridging ligand	19
3.1.1. Bromine-induced stabilization of the ³ MLCT	19
3.1.2. Substitution- and solvent-effects on the charge-transfer path	21
3.2. Introduction of tpac as bridging ligand	24
3.2.1. General spectroscopic characteristics of the Rutpac-complexes	25
3.2.2. Characterization of interactions between the solvent and the photocatalyst	26
4. Homodinuclear Rutpphz complexes	30
4.1. General spectroscopic characteristics of the homodinuclear complexes	31
4.2. Interaction of the photocentres after excitation	32
5. Conclusion	37
6. Zusammenfassung	40
Literaturverzeichnis	43

Contents

A. Publikationen	54
[CK1] Investigation of substitution effects on novel Ru–dppz complexes by Raman spectroscopy in combination with DFT methods	54
[CK2] Substitution-controlled ultrafast excited-state processes in Ru-dppz-derivatives	66
[CK3] Tuning of Photocatalytic Hydrogen Production and Photoinduced Intramolecular Electron Transfer Rates by Regioselective Bridging Ligand Substitution	79
[CK4] Synthesis and photophysics of a novel photocatalyst for hydrogen production based on a tetrapyridoacridine bridging ligand	89
[CK5] Excited-state annihilation in a homodinuclear ruthenium complex	99
[CK6] The impact of bromine substitution on the photophysical properties of a homodinuclear Ru–tpphz–Ru complex	102
B. Autorenschaft der Publikationen	109
C. Liste der im Rahmen der Arbeit erzielten Veröffentlichungen	115
D. Danksagung	117
E. Lebenslauf	119
F. Selbständigkeitserklärung	120

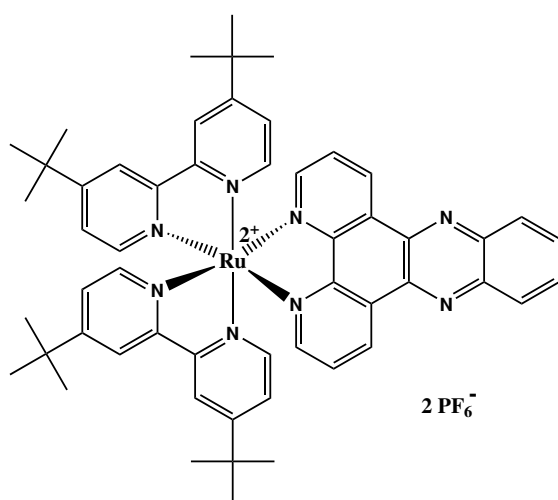
List of Figures

1.1. The three components of RuPd1	4
2.1. Localization of excited states in Rudppz	8
2.2. Absorption and emission spectra of Rudppz1 , Rudppz4 and Rudppz5 .	12
2.3. Transient absorption spectra and transient kinetics of Rudppz1 , Rudppz4 and Rudppz5	14
2.4. Schematic energy diagram for Rudppz1 , Rudppz4 and Rudppz5	15
3.1. Schematic illustration of the catalytic functionality of RuPd1	18
3.2. Catalytical data of RuPd1 , RuPd2 and RuPd3	19
3.3. UV/vis absorption and emission spectra of RuPd2	20
3.4. Transient absorption data of RuPd2	22
3.5. UV/vis absorption and emission spectra of Rutpac and RuPd3	25
3.6. Transient absorption spectra of Rutpac and RuPd3	27
3.7. Transient kinetics of Rutpac and RuPd3	28
4.1. Absorption and emission spectra of RuRu1 and RuRu2	31
4.2. Transient absorption spectra of RuRu1 and RuRu2	33
4.3. Transient absorption kinetics of RuRu1 and RuRu2	34
4.4. Schematic energy diagram of the excited states of RuRu1 and RuRu2 . .	35

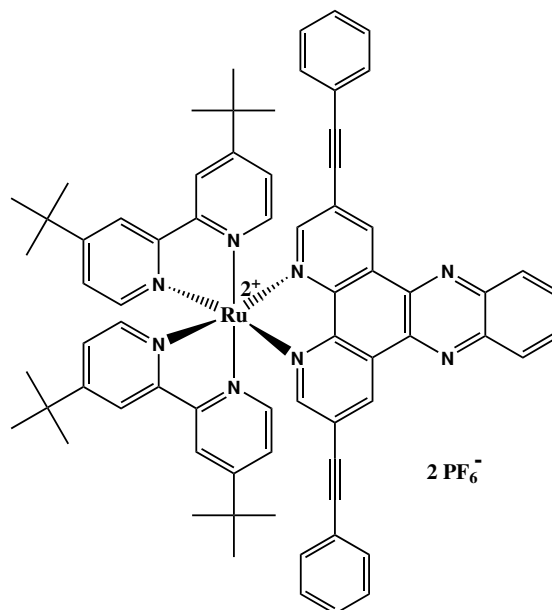
List of Abbreviations

bpy	2,2'-bipyridine
TEA	triethylamine
UV/vis	ultra-violet/visible
MLCT	metal-to-ligand charge-transfer
ISC	inter-system crossing
Φ	emission quantum yield
tbbpy	4,4'-di-tert-butyl-2,2'-bipyridine
tpphz	tetrapyrido[3,2- <i>a</i> :2',3' <i>c</i> :3'',2'',- <i>h</i> :2''',3'''- <i>j</i>]phenazine
dppz	dipyrido[3,2- <i>a</i> :2',3,3'- <i>c</i>]phenazine
phen	phenanthroline (part of dppz or tpphz)
phz	phenazine (part of tpphz)
tpac	tetrapyrido[3,2- <i>a</i> :2',3'- <i>c</i> :3'',2''- <i>h</i> :2''',3'''- <i>j</i>]acridine
DFT	density functional theory
phac	phenylacetylene
ACN	acetonitrile
RR	Resonance Raman
τ	time constant of a light-induced process
cm^{-1}	wavenumber, 1 cm^{-1} correlates with 0.000124 eV
GSB	ground-state bleach
TON	turn-over number
DCM	dichloromethane
LMCT	ligand-to-metal charge-transfer
ESA	excited-state absorption
ILCT	inter-ligand charge-transfer
DAS	decay-associated spectra
ϵ	dielectric coefficient
phenan	1,10-phenanthroline

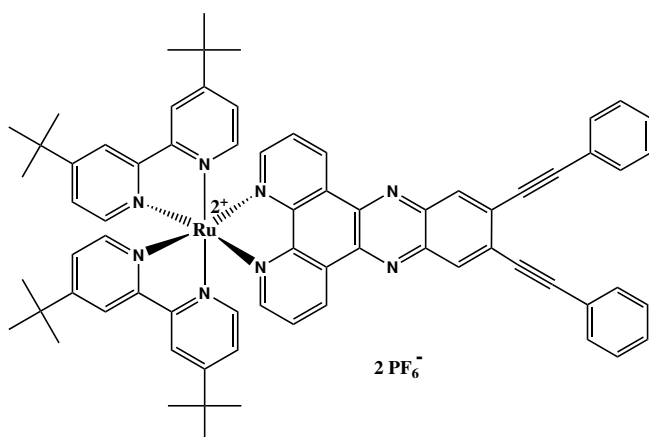
List of Substances



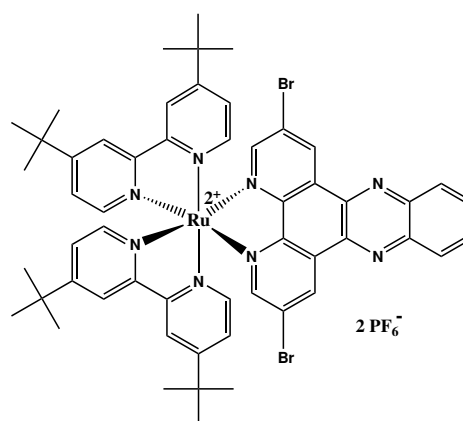
Rudppz1



Rudppz2

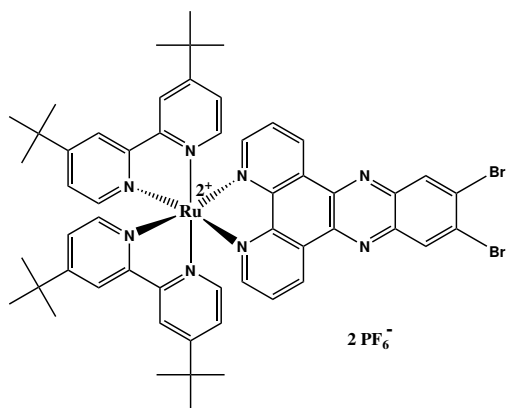


Rudppz3

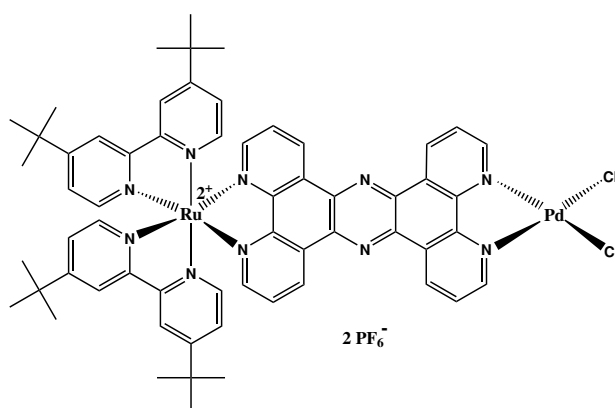


Rudppz4

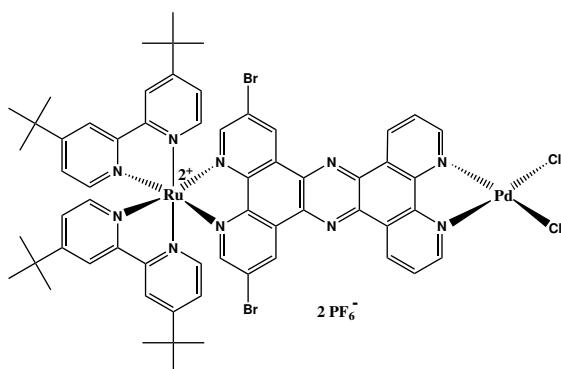
List of Substances



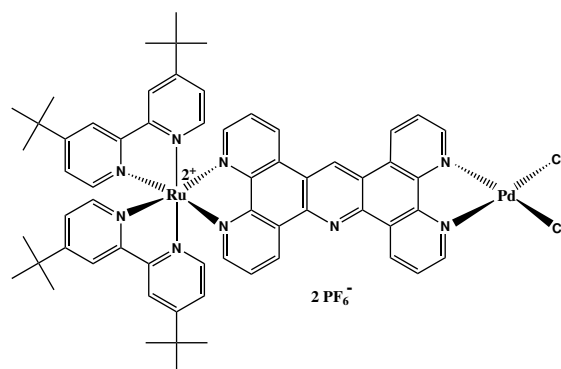
Rudppz5



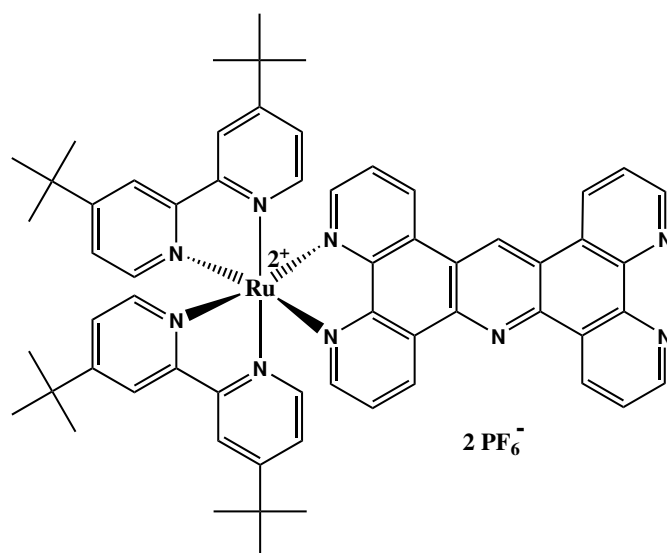
RuPd1



RuPd2

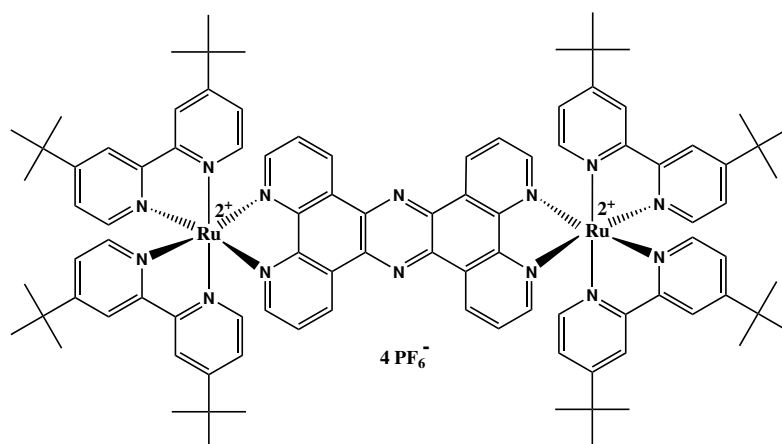


RuPd3

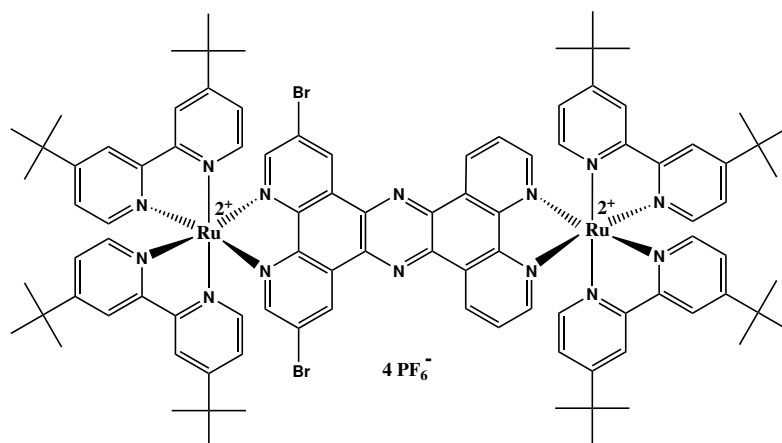


Rutpac

List of Substances



RuRu1



RuRu2

1. Introduction

Facing the world-wide growing demand for energy will be one of the major challenges of the 21st century. The production of energy nowadays is mainly based on fossil fuels such as coal, oil or gas. Their consumption will confront mankind with two enormous problems: 1) The production of a vast amount of greenhouse gases that contributes to global warming and a change of the existing world climate with uncertain consequences for the planet.[1] 2) These fossil resources will be depleted in a foreseeable time-period which requires the search for alternatives. Ideally such alternative energy sources should have no impact on the world climate or - at least - less impact than fossil fuels.[2, 3]

The most promising alternatives to fossil energy carriers nowadays are photovoltaics and the use of wind-power. But both methods show a major drawback as it is quite difficult and expensive to store the collected energy in order to bridge longer periods of sky cover or calm. Hence, the demand of different alternative ways for energy production and storage is still unmet. One promising opportunity is the direct conversion of solar energy into chemical energy for instance by the production of molecular hydrogen. Given its high energy density and the fact, that its combustion only produces water and no greenhouse gases, molecular hydrogen is a promising candidate as energy carrier of the future. However, molecular hydrogen is not available from natural sources on earth and needs to be produced from hydrogen containing substances like water or hydrocarbons. Current industrial methods for hydrogen production on a large scale, like the steam reforming process or the water gas reaction, are very inefficient. Consequently they are energy-consuming and thus contribute directly to the consumption of fossil energy sources.[4]

One promising possibility for future hydrogen production is the utilization of the biggest available energy source on earth - the sun: A photoactive cell capable of producing elemental hydrogen by photocatalytic water splitting would be the ideal sustainable energy source. In fact, the process of photocatalytic water splitting is one of the most fundamental chemical reactions in nature, as it is a crucial step in natural photosynthesis, solar energy is converted into chemical energy, performed by every green plant on the planet.[5, 6]

Up to now, several approaches aiming at artificial photosynthesis have been developed.

1. Introduction

Since the 1970's photocatalytic water-splitting is subject of research.[7, 8, 9, 10] The most basic approach in this field utilizes electrical current of a conventional solar cell to split water electrochemically.[11] Furthermore, several metal oxide semiconductor systems based on nanoparticles and thin films were developed.[12] Unfortunately semiconductor systems have a small efficiency as they only use a fraction of the solar spectrum. Thus, efforts have been made to extend the absorption of metal oxide photocatalysts.[13] The attempts to develop a visible-light responsive photocatalyst for the water splitting reaction resulted in a three component concept, combining a photosensitizer, an intermolecular electron relay and a hydrogen evolving catalyst. In the late 1970's such systems were reported independently by Lehn [8] and Grätzel [9]. The hydrogen evolving system reported by Grätzel contained the transition metal dye $[Ru(bpy)_3]^{2+}$ (bpy = 2,2'-bipyridine), as photosensitizer, a methylviologen as electron relay and Adam's catalyst, an aqueous solution of PtO_2 , which is supposed to form colloidal Pt in the course of reaction, which then serves as the hydrogen evolving catalyst. Lehn reported a system, where $[Rh(bpy)_3]^{2+}$ acts as the electron relay. However, these photocatalytic systems deal with only one part of the water splitting reaction, i.e. the reduction of protons. Consequently a sacrificial electron donor like triethylamine (TEA) has to be added, in order to regenerate the catalyst. Aside from the systems mentioned before, e.g. several Iridium- [14, 15] or Cobalt(II)-tetraphenylporphyrin complexes [16, 17] have been reported as photosensitizers.

The concept of a three-component system was also realized in homogeneous catalysis, which has the major advantage that the charge-transfer can be controlled by specific structural modification of the homogeneous catalyst. Therefore a light-harvesting unit, capable of absorbing visible light, is utilized to initiate a charge transfer. This light-harvesting centre is covalently connected to a catalytic unit based on a metal-complex, which has the ability to reduce protons to molecular hydrogen. Following the design strategy of connecting the light-harvesting with the catalytic-active centre to form a homogeneous catalyst, several groups developed supramolecular devices, employing a Ruthenium metal-centre as light-harvesting unit. Those were connected to Rh[18], Pt[19], Co[20] or Pd[21, 22] as catalytically active species. One other significant advantage of homogeneous supramolecular photocatalysts as compared to heterogeneous systems is the possibility to observe the light-induced charge-transfer processes directly by spectroscopic methods like UV/vis-absorption and -emission or ultrafast transient absorption spectroscopy. Based on the insights obtained on actual hydrogen producing systems it is possible to introduce model systems focussing on the investigation of individual charge-transfer steps. The optimiza-

1. Introduction

tion of single charge-transfer steps can be a key for the improvement of such catalytic systems. This is due to the fact that in the case of competing photochemical processes the fastest process determines the further fate of the photoexcited species.[5, 23] Thus, the desired photocatalytic charge-transfer steps ideally run on a timescale that is at least one order of magnitude faster than competing pathways. Hence, it is necessary to obtain detailed knowledge about all participating relaxation channels after photoexcitation in order to be able to improve photocatalytic systems.

For the realization of complex homogeneous catalysts the molecular bridge connecting both metal-centres plays a pivotal role. This unit has the important task to transport the light-activated charge to the catalytic centre, serve as an electron reservoir and mediate the interaction between the photocentre and the catalytic unit. To fulfill these manifold requirements polypyridines have proven to be suitable.[18, 19, 20, 21] The reason therefor is found in the versatile and well investigated photophysical properties of the well known Ru-polypyridine complexes.[24, 25] These species show, independent on their environment, a metal-to-ligand charge-transfer (MLCT) in the visible range between 400 and 500 nm.[26, 27] The photophysical processes initiated by this MLCT-absorption are described exemplarily for the complex $[Ru(bpy)_3]^{2+}$ as this is one of the best examined and described representatives of Ru-polypyridine complexes. Immediately after photoexcitation a charge-transfer state delocalized over all bpy-ligands is formed [28, 29, 30] which undergoes an inter-system-crossing (ISC) and localizes onto one of the bpy-ligands within several hundred femtoseconds, resulting in a long-living $^3\text{MLCT}$ -state.[26, 31, 32] The subsequent cooling process is completed within the first couple of picoseconds, depending on the solvent environment.[33] The depopulation of the $^3\text{MLCT}$ -state occurs roughly within one microsecond by radiationless and radiative (quantum yield $\Phi = 0.28$ in H_2O [34]) decay.[27] Due to these characteristic photophysical properties Ru-polypyridines found manifold applications as optical sensors for DNA-sampling and cell imaging [35, 36, 37, 38] or as dyes for dye-sensitized solar cells.[39, 40]

For the work at hand the polypyridine ligand tetrapyrido[3,2-*a*: 2',3'*c*: 3'',2'',-*h*: 2''',3'''-*j*]phenazine (tpphz) was employed to form the hydrogen evolving photocatalyst $[(tbbpy)_2Ru(tpphz)PdCl_2](PF_6)_2$, (**RuPd1**, tbbpy = 4,4'-di-tert-butyl-2,2'-bipyridine, Figure 1.1).[22] This heterodinuclear complex is able to reduce protons, provided by TEA or water, to form molecular hydrogen within a light-driven photocatalytic reaction.[22, 41] Hereby, visible light with a wavelength between 400 and 500 nm initiates a MLCT transition and a subsequent cascade of electron transfer-steps to finally transport the charge to the Pd-metal-centre.[42] After repetition of this charge-transfer two electrons can be

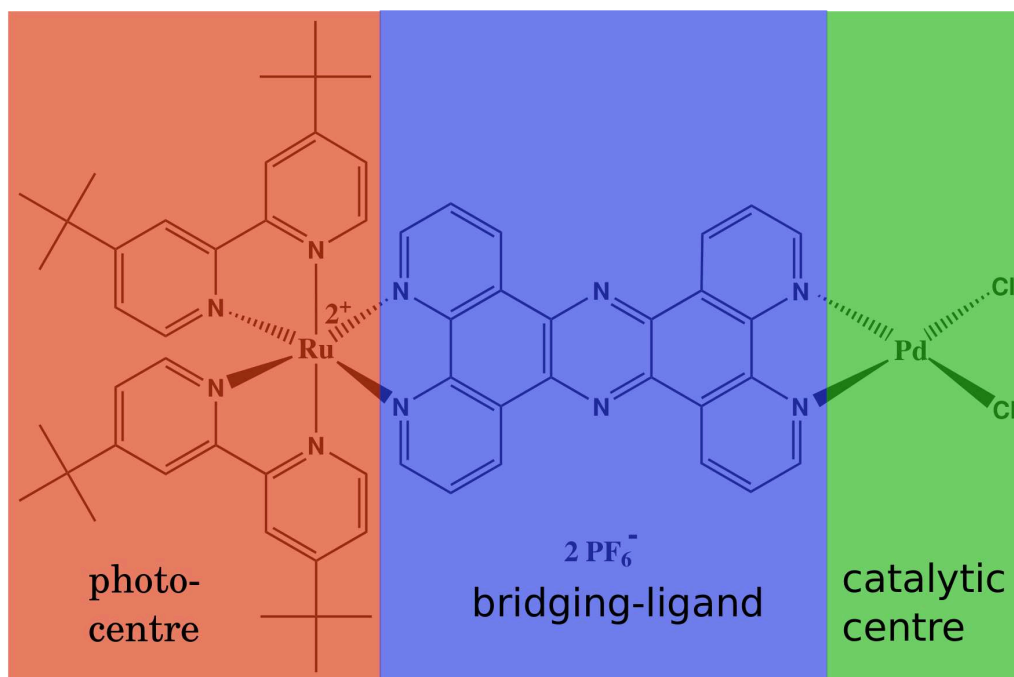


Figure 1.1.: The three components of photocatalyst **RuPd1** are highlighted: By excitation of the photocentre charge is transferred via the bridging-ligand to the catalytic centre.

transferred to two incoming protons to form molecular hydrogen. To close the catalytic cycle the oxidized Ru-centre is finally re-reduced by TEA, or another sacrificial electron-donor, which is added to the reaction mixture. The efficiency of this catalytic reaction depends on several parameters, e.g. the duration and wavelength of the irradiation, the solvent and the concentration of water and TEA.[22, 41] Within this set of parameters, the role of the bridging-ligand tpphz is versatile, thus its optimization with the help of chemical variation offers great potential towards the improvement of the entire catalytic system. Accordingly, the purpose of this work is to investigate the impact of substitutions on the properties of the molecular bridge tpphz and on the initial charge-transfer cascade after light-exposure.

In the beginning of the investigations the model system $[(tbbpy)_2Rudppz]^{2+}$ (**Rudppz1**, dppz = dipyrido[3,2-*a*:2',3,3'-*c*]phenazine) is introduced which is structurally related to **RuPd1**. In general Rudppz complexes constitute a class of very interesting Ru-polypyridine species as their photophysical properties are very sensitive to environmental parameters such as solvent or the temperature.[43, 36, 44, 45]. In the first part of this thesis investigations are presented, which are concerned with regiospecific substitutions on **Rudppz1**. The underlying approach bases on the solvent dependent luminescence of Rudppz1 complexes: While in polar solvents no emission can be detected, bright lumi-

1. Introduction

nescence is found in unpolar solvents. This so-called light-switch effect can be exploited for DNA-detection [35, 36, 46] and is explained by the interplay of two excited triplet states, which are both associated with the dppz scaffold. However, while the luminescent state resides on the phenanthroline-moiety (phen), the dark state is located on the phenazine-part (phz).[47, 43, 48] In order to figure out how the equilibrium between the two states can be affected and controlled by intramolecular parameters, the role of electron withdrawing bromine substituents placed either on the phen- or on the phz-part of dppz is investigated.

Building on the results on the photophysical impact of bromination of **Rudppz1**, the second part of this thesis is concerned with the impact of bromine substituents on the photophysical properties of the catalytic active system **RuPd1**. The effect of bromination is discussed in relation to the differences of the catalytic performances in the absence/presence of the bromine substituents. Beside the bromination a second modification of **RuPd1** is introduced: In $[(tbbpy)_2RutpacPdCl_2](PF_6)_2$ (**RuPd3**, tpac = tetrapyrido[3,2-*a*:2',3'-*c*:3'',2''-*h*:2''',3'''-*j*]acridine) the central phenazine ring of the tpacz ligand is replaced by a acridine ring. All three catalytic active complexes show dependencies in their catalytic activities to the water content.[CK3,CK4] Thus the role of water on the light-induced charge-transfer reactions of these complexes are discussed.

Finally, another aspect closely related to the design of supramolecular systems for artificial photosynthesis is investigated. To improve the ability of light-harvesting in photocatalytic systems they may be equipped with more than one light-harvesting unit per catalytic center.[18, 49, 50] But beside a higher efficiency in providing the catalytically active centre with electrons, interactions between the multiple photocentres need to be taken into account. In order to reproduce such interactions the photophysical behaviour of the model-complex $[(tbbpy)_2RutpaczRu(tbbpy)_2](PF_6)_4$ (**RuRu1**) was analyzed. Hereby, the dependence of the photoinduced dynamics on the intensity of the excitation light was evaluated to investigate whether the two photocentres of the model compound interact when both are excited at the same time. Furthermore, the effect of bromine substituents on this system is described as well.

Alltogether, the aim of this work is to show in which way photophysical properties of a new homogeneous photocatalytic Ru-complex can be influenced by chemical variations. For this purpose a complete photophysical characterization of the derivatives of the photocatalyst is necessary. Therefore, at first these variations were examined for model-complexes by the means of Raman-spectroscopy with the help of quantum chemical calculations, by UV/vis-absorption and emission spectroscopy and by ultrafast transient-

1. Introduction

absorption spectroscopy. With the help of these results light is shed on the photophysical behaviour of the varied catalytic systems under consideration of the impact of the solvent on the photoinduced charge-transfer. In a last step the interaction of two connected light-harvesting unit, especially in dependence on the intensity of the excitation light, is studied.

2. Rudppz - a model system

Parts of this chapter are published in:

[CK1] C. Kuhnt, S. Tschierlei, M. Karnahl, S. Rau, B. Dietzek, M. Schmitt., J. Popp; INVESTIGATION OF SUBSTITUTION EFFECTS ON NOVEL RU-DPPZ COMPLEXES BY RAMAN SPECTROSCOPY IN COMBINATION WITH DFT METHODS, *J. Raman Spectrosc.*, **2010**, *41*, 922-932

[CK2] C. Kuhnt, M. Karnahl, S. Tschierlei, K. Griebenow, M. Schmitt, B. Schäfer, S. Krieck, H. Görls, S. Rau, B. Dietzek, J. Popp, SUBSTITUTION-CONTROLLED ULTRAFAST EXCITED-STATE PROCESSES IN RU-DPPZ-DERIVATIVES, *Phys. Chem. Chem. Phys.*, **2010**, *12*, 1357-1368

Complexes of dipyridophenazin with Ruthenium as a central atom were developed in the late eighties of the last century.[46] These complexes were found to be chemically stable and redox-active[51, 31, 24], thus they are potentially useful as model systems for artificial photosynthesis [52], dye-sensitized solar cells [39, 53] or light driven catalysis.[54] Because of the sensitivity of their photophysics towards environmental properties they can be used as analytical tools to detect e.g. metal-ions[55, 56, 57], oxygen[58] or biological macromolecules like DNA[59, 46, 35, 60, 47, 43]. One major photophysical feature of Ru-dppz complexes is the so called 'light-switch effect': Dissolved in water Rudppz complexes do not show emission, which changes after the addition of DNA to the solution. Beside the ability of Rudppz complexes to intercalate into the DNA double-strand this effect roots in the interaction of two excited states within the dppz framework. Both states are localized on the dppz ligand, the non-luminescent on the phz-sphere ($^3\text{MLCT-phz}$) and the luminescent on the phen-sphere ($^3\text{MLCT-phen}$, see Fig. 2.1). These two states are populated subsequently to photoexcitation of the MLCT of Rudppz with visible light between 400 and 500 nm. Afterwards the fraction of population of each state and hence, the intensity of the emission, depends on the environment of the complex: In unpolar solvents high emission is observed due to predominant population of the phen-centred state. In polar solvents no emission is found because the phz-centred state is mostly populated. This behaviour can be explained by the different dipole moments of the excited states. While the phen-centred state is in the vicinity of the Ru-centre its dipole moment is smaller than that of the phz-centred state. Therefore, in the polar solvent water the phz-

2. Rudppz - a model system

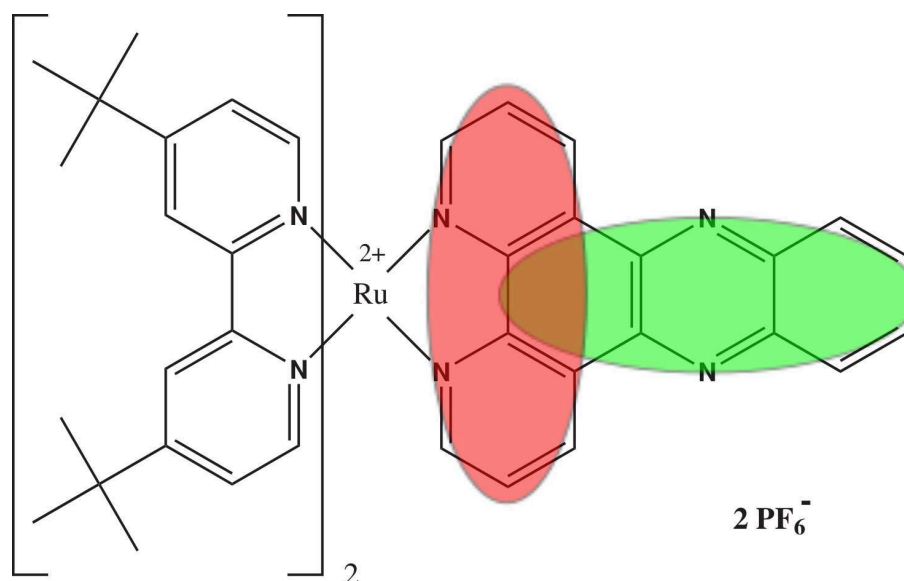


Figure 2.1.: **Rudppz1** and the schematic localization of the luminescent (red) and non-luminescent (green) excited state.

centred state is populated and no emission can be observed. In the case of water a second effect must be considered: As water is protic hydrogen-bonds between the protons and the phz-nitrogen atoms are built which additionally lowers the energy of the phz-located excited state.[61] After addition of DNA Rudppz intercalates into the major grooves of the double-strands, which inhibits the interaction of water molecules with the complexes thus enables emission.[47, 43, 44, 48]

The nature of these ambivalent photophysical behaviour of Rudppz complexes was topic of several studies, which focussed on the equilibrium between both states. It was found that also temperature and viscosity of the solvent are suitable to influence the equilibrium between the phen- and phz-located states.[43, 44, 45, 62, 61, 63, 64, 65, 66, 67] As such a well investigated species these Rudppz-complexes present valuable model compounds for the more complex system **RuPd1**. With their help it was possible to investigate the impact of substitution on a smaller molecular fragment. In particular, the impact of substituents at the phen- and phz-parts of the dppz ligand was examined to gain better understanding of the interplay and dependency between both moieties. The effect of such substitutions on the properties of the ground and the excited state are investigated within this chapter.

The method of choice for the investigation of the ground state was Raman spectroscopy in combination with density-functional theory (DFT) calculations. Raman spectroscopy is a powerful tool to collect structural and electronical information on molecular systems.[68] However, the interpretation of Raman spectra is often very challenging or even impossible as experimentally observed Raman bands can hardly be assigned to specific and localized

2. Rudppz - a model system

molecular vibrations. Thus, for a reliable band assignment a comparison with computationally calculated spectra is essential.[69, 70]

Especially DFT methods have developed into a powerful tool: They are computationally much less demanding compared to conventional quantum chemical methods and take into account the effect of electron correlation.[71] In combination with vibrational spectroscopic methods the major advantage of these calculations is the output of normal coordinates of each molecular vibration. Thus, it is possible to obtain explicit information about molecular properties and accordingly about the way such properties may be influenced by changing intramolecular parameters, e.g., substituents.

For the observation of excited state properties of **Rudppz1** and its derivatives **Rudppz4** and **Rudppz5** steady-state absorption and emission spectroscopy in combination with ultrafast transient absorption spectroscopy were employed. Both steady-state techniques yield insight into the effect of the substitution on the excited states that are responsible for the luminescence behavior of Rudppz complexes. With the help of transient absorption spectroscopy it is possible to follow the electron dynamics after excitation of the MLCT of these complexes.

2.1. Ground-state properties

Detailed knowledge about the ground-state properties of a substance is necessary to perform a proper investigation of its excited state. Thus, at first substitution effects on the ground-state properties of different Rudppz-complexes are discussed. For this purpose bromine and phenylacetylene (phac) groups were attached to the dppz framework with special attention to effects on the two moieties of dppz. The investigations focus on two aspects: The structural variations induced by the substituents and the resultant vibrational differences. For the first aspect solely the results of quantum chemical calculation are interpreted and for the latter one the calculations were analyzed in combination with the Raman spectra. Thus it was possible to take normal coordinates into account. The objects of the investigations were the complexes **Rudppz1 - Rudppz3** and **Rudppz5**, hence two different substitution patterns could be compared at two different positions on the dppz framework.

Comparing bond lengths and angles the impact on the structure of the dppz ligand by both substituents, bromine and phenylacetylene, are minor and only relevant for bonds in the direct vicinity of the substitutions. For **Rudppz5** no significant effect on the dppz framework could be found. Only the bonds in direct vicinity of the bromine substituents

2. Rudppz - a model system

are influenced. In contrast, the phac groups disturb the dppz's planarity and its symmetry due to sterical interactions. The reason for this is found in the spacial vicinity of both alpha-H atoms of the phac groups to the according H atoms of dppz. This vicinity leads to repulsion and a torsion of the phac's phenyl rings with respect to the dppz plane. By this the dppz π -system is disturbed slightly leading to a loss of planarity and consequently to a loss of the symmetry.

Further insight in the effects of structural modifications on the ground-state properties of dppz is obtained by Raman spectroscopy data in combination with the DFT calculations. The focus of these investigations lies on the structural subunits of dppz, namely the phenazine- and the phenanthroline-part. Observing the normal coordinates of each molecular vibration some specific vibrations were found suitable to show the effects of substitution on this subunits. In this context three different types of vibrations are highlighted: Those that are either located solely on the phen-(i) or the phz-moiety(ii) and, in contrast to that, those that are delocalized over the complete dppz framework (iii). In the following the effect of the substituents on such characteristic vibrations is detailed.

(i) Vibrations where only atoms of the phen-moiety are involved are solely influenced by structural variations at the phen-part of the ligand. This behaviour shows that influences of the phz-moiety do not have an effect on the phen-part. This concept does not work in the opposite direction: (ii) Vibration modes including only the phz-moiety shift in their energy also when substituents are introduced in the phen-moiety. This means that such vibrations, e.g. the ring-breathing mode of the central pyrazine ring, undergo a wavenumber shift when comparing **Rudppz1** with **Rudppz2** or **Rudppz5**. This shows, that a coupling between the two moieties is existent in the electronic ground state. That behaviour is furthermore observable by the presence of modes that are delocalized over the entire dppz structure (iii). Such vibrations are also influenced by each of the investigated substitutions.

In summary the examination of **Rudppz1** and its derivatives in the electronic ground-state yielded that the division of dppz in two separate spheres is existent. This is shown by molecular vibrations that are located only on one sphere, which are influenced only by regiospecific substitutions. But a total decoupling of both parts in the electronic ground state cannot be confirmed as also vibrations are found which are delocalized over the entire molecular framework of dppz and which are shifted by substitutions on either of the subunits.

2.2. Excited-state properties

Studies on the properties of the excited states aiming at a better understanding of the photoinitiated electron-migration in Rudppz complexes were performed with **Rudppz1**, **Rudppz4** and **Rudppz5** with acetonitrile (ACN) as solvent. Bromine was chosen as substituent because it is known to affect the photophysics of related complexes.[72, 73] Furthermore it can be excluded that observed photophysical effects stem from steric interactions as bromine is very small compared to other possible substituents, e.g. methyl-, tert-butyl- or phenyl-groups. The substitution pattern of **Rudppz5** with bromine in the 11,12 position is already known from the literature from a different context[74]. The presented investigation is the first detailed comparative study on the influence of substitution on both moieties of dppz.

2.2.1. Controlling the luminescence by regioselective substitution

UV/vis absorption spectroscopy The influence of the bromine substituents is already observable within the steady-state absorption and emission spectra (Figure 2.2). Above 330 nm the absorption spectra are dominated by two distinct electronic transitions. The first shortwave-absorption band (in the range between 350 and 400 nm) is attributed to a $\pi - \pi^*$ transition located on the dppz ligand. The second one (above 400 nm) is assigned to a MLCT transition and lies in the visible part of the spectrum. In comparison to **Rudppz1** the $\pi - \pi^*$ transition of **Rudppz5** is shifted to lower energies. In contrast, for **Rudppz4** this absorption band is unchanged while here the MLCT is modified: a splitting of this band can be observed yielding one transition roughly at 430 nm and a pronounced long-wave shoulder at 490 nm. The origin of this double-peaked MLCT band is revealed with the help of Resonance Raman (RR) spectroscopy. This spectroscopical technique is able to highlight the Franck-Condon active vibrational modes, i.e. modes coupled to the electronic transitions.[75] The RR spectra of **Rudppz1** after excitation of the MLCT with several excitation wavelengths show enhanced Raman bands which can be assigned to vibrations of the tbbpy and the dppz ligands. For **Rudppz4** a different situation is found. Here the RR spectra upon short-wavelength excitation at 458 nm also show bands that can be assigned to both the tbbpy and dppz ligands. But long-wave excitation results in dominant contributions from the dibromo-dppz ligand. This explains the presence of the double peaked MLCT bands for **Rudppz4** and it is concluded that bromination in the 2,7 position of dppz lowers the energy of the according Ru \rightarrow dppz MLCT transition, while leaving the Ru \rightarrow tbbpy MLCT transition unaffected. In contrast for **Rudppz5**

2. Rudppz - a model system

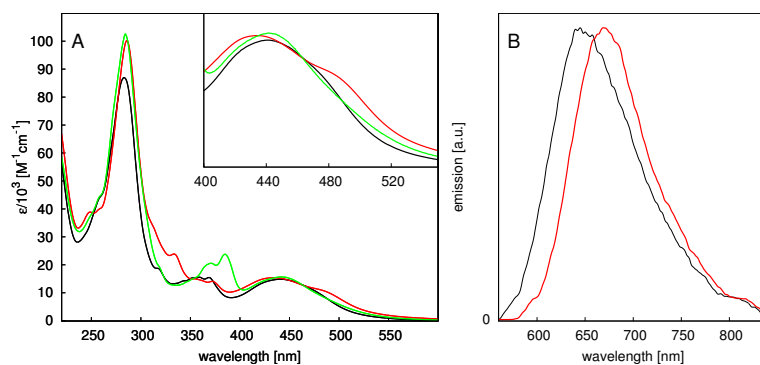


Figure 2.2.: A: Absorption (A) spectra of **Rudppz1** (black), **Rudppz4** (red) and **Rudppz5** (green) dissolved in ACN. The shape of the MLCT absorption is highlighted in the inset. B: Emission spectra of **Rudppz1** (black) and **Rudppz4** (red) normalized to the maximum of the emission. **Rudppz5** does not show detectable emission.

such changes of the character of the MLCT cannot be observed, which was also shown in an earlier study.[74] As a result the bromine substituents at the phz-moiety have no influence on the structural subunits which participate in the MLCT transition. Furthermore, it could be confirmed, that the bromine substituents lower the energies of the excited states localized in their vicinity.

Emission spectroscopy The emission characteristics also show a substituent depending behaviour. The emission maximum, the luminescence quantum yields and lifetimes (τ), differ notably between the three different Rudppz complexes. The quantum yield increases by a factor of two for **Rudppz4** (2×10^{-2}) compared to **Rudppz1** (1×10^{-2}). For **Rudppz5** the contrary effect can be observed i.e., the quantum yield decreases drastically and no emission could be detected. Comparing the emission spectra of **Rudppz1** and **Rudppz4** a redshift of the emission maxima of 640 cm^{-1} from 650 to 670 nm is found. Thus, the bromination in 2,7-position of the dppz energetically stabilizes the bright (i.e., the luminescent) state. This also becomes obvious in the temperature dependent behavior of the emission lifetime. For **Rudppz1** it is known from the literature that the emission lifetime differs (in a range between 200 to 1300 ns) with the temperature (in a range between 150 and 350 K) because of the equilibrium between the bright and the dark state.[45] Contrarily this is not the case for **Rudppz4** where the emission lifetime is almost constant around 190 ns over a broad temperature range between 225 to 305 K. This means that for this compound the charge-transfer to the dark phz-centered state can be excluded, as well as the deactivation *via* Ru-centered excited states, which is well known for Ru-polypyridine complexes.[62, 61, 76] Otherwise **Rudppz5** is non-luminescent, i.e.

2. Rudppz - a model system

the excited state of this complex is deactivated *via* the non-luminescent state that is located on the phz-unit.

The results from steady-state absorption and emission spectroscopy clearly show the separation of the phen- and the phz-centered excited state, which was already discussed in the context of electrochemistry experiments.[47] Already the considerations on the absorption spectra suggest that bromination in the 2,7-positions of dppz selectively influence the electronic structure of the phen-moiety. Meanwhile the modification of the phz-part (**Rudppz5**) leaves the electronic structure of the phen unaffected while the dppz $\pi \rightarrow \pi^*$ transition, which dominantly concerns π -electrons from the phz-moiety, is influenced selectively. The assumption of phen-phz-separation is supported by taking the substitution dependent luminescence into account. In Rudppz complexes luminescence originates from the phen-centered state, while population of a phz-centered state leads to quenching of the luminescence.[43, 45, 77] In this context the increased emission quantum yield of **Rudppz4** compared to **Rudppz1** is remarkable as well as the fact that no emission can be detected for **Rudppz5**. Thus, the luminescence properties of Rudppz-complexes can be controlled by intramolecular alterations and not only by environmental modifications, as it was known before.[35, 43]

2.2.2. Adjustment of an excited-state equilibrium by regioselective substitution

The studies of the influence of substitution on the excited state properties of **Rudppz1** are completed by investigations of the photoinduced excited-state dynamics with the help of ultrafast transient absorption spectroscopy. The charge-transfer dynamics were initialized by photoexcitation of the MLCT transition with pump pulses at 510 nm. The subsequent processes were tracked with a supercontinuum that served as probe-pulse. With the experimental setup that was employed, it was possible to record the photoinduced charge-transfer processes within a temporal window from 0.5 to 1800 ps.

The transient absorption spectra (see Figure 2.3A) of all three compounds are comparable. After photoabsorption the rise of a positive differential absorption band is detected, while in the spectral region that was probed, i.e. 520 to 685 nm, no ground-state bleach (GSB) or stimulated emission bands are observable. The shape of the differential absorption spectra is in general comparable to spectra that were recorded for related complexes.[78, 42] All three complexes show relatively structureless excited-state absorption in between 520 and 680 nm with a maximum between 580 and 590 nm. For proper data analysis the differential absorption signal as a function of delay time between

2. Rudppz - a model system

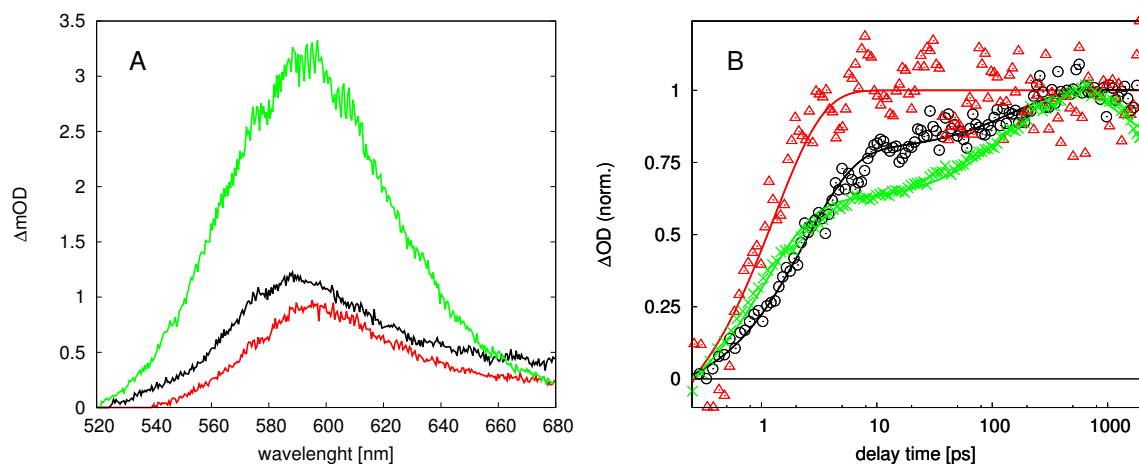


Figure 2.3.: A: Representative transient absorption spectra for **Rudppz1** (black), **Rudppz4** (red) and **Rudppz5** (green) 10 ps after excitation of the MLCT. B: Transient kinetic signals for **Rudppz1** (black), **Rudppz4** (red) and **Rudppz5** (green), which were integrated over the whole recorded spectral region and afterwards normalized to the maximum of the differential absorption for comparability. The dots are used for the measured data while the results of the fit are shown as solid lines.

	Rudppz1	Rudppz4	Rudppz5
τ_1 /ps	2.4	1.3	1.0
τ_2 /ps	150	–	200
τ_3 /ns	–	–	10

Table 2.1.: Summary of the characteristic decay times τ_i obtained from the global fit of the differential absorption data. While τ_1 and τ_2 refer to a build-up of the signal, τ_3 is assigned to a decay. The latter one also represents only an estimate due to the limited delay time accessible with the experimental setup.

the pump- and the probe-pulse was subjected to a global fit routine as, e.g., described in [79, 80]. The result from the data analysis which is depicted in Figure 2.3B yields specific kinetic components for each observed complex, which are characteristic for the individual charge-transfer processes.

The prominent substitution-induced effects on the excited state dynamics is revealed in the analysis of the relaxation kinetics for each complex, which is summarized in Figure 2.4. For all three compounds a fast ps-component (τ_1) is found that is manifested by a rise of the differential absorption signal. For **Rudppz1** and **Rudppz5** this is followed by a second rise-component (τ_2) in the range of 150 to 200 ps. Only for **Rudppz5** a slow component (τ_3), larger than 1 ns, is found, which appears as a decay of the signal. The characteristic time-constants are summarized in Table 2.1.

2. Rudppz - a model system

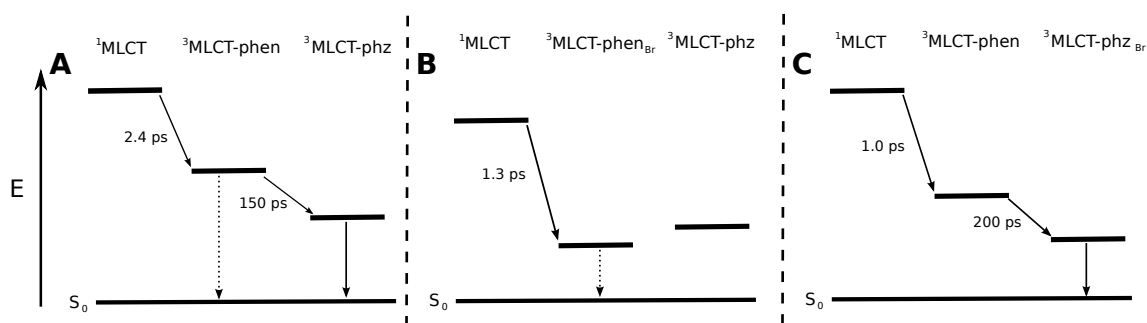


Figure 2.4.: Energy diagram of the excited states involved in the charge-transfer processes of the observed Rudppz-complexes in dependence to the substitution pattern. Solid arrows represent non-emissive while dashed lines represent emissive transition. In comparison to **Rudppz1** (panel A) the $^3\text{MLCT-phen}$ state in **Rudppz4** (panel B) is energetically stabilized, hence emission is enhanced for this complex. In **Rudppz5** (panel C) the non-emissive $^3\text{MLCT-phz}$ state is stabilised and hence, emission cannot be observed.

To assign excited-state relaxation processes to each of the kinetic components that were found in the differential absorption data the general photophysical processes in Rudppz complexes are reconsidered. After excitation within the MLCT transition an ultrafast ISC occurs from the initial $^1\text{MLCT}$ to the $^3\text{MLCT}$.^[28] This ISC proceeds within the first 200 fs and thus escapes detection within the experimental setup used.^[32] The fastest process detected in our setup, which occurs on a ps time-scale, is assigned to the thermal equilibration of the rapidly formed $^3\text{MLCT}$ state as previously also observed for related complexes.^[75, 30, 33, 32] Subsequently the system relaxes to the phz-centered excited state on a 100 ps timescale, which is in agreement with reports on related complexes in ACN.^[78] Interestingly this charge-transfer step is absent in the case of **Rudppz4** and only found for **Rudppz1** and **Rudppz5**. The third kinetic component is only found for **Rudppz5**. Due to the experimental limitation of the delay time to 1.8 ns the value for this decay component τ_3 can only be approximated to roughly 10 ns. But nonetheless, the exact value of τ_3 is of only minor importance for the following argumentation. This kinetic component is characterized by a decay of the entire differential absorption band and thus assigned to an overall non-radiative decay of excited-state population back to the ground state.

The different relaxation behaviors of the three complexes show the influence of the bromine substitution on the excited states of Rudppz. The RR data and experiments on related complexes^[44, 81] suggests that the process that is characterized by τ_1 leads to population of the phen-centered MLCT on the dppz-ligand. This state is energetically lowered compared to the tbbpy-centered MLCT-states. After that the excited state dy-

2. Rudppz - a model system

namics of **Rudppz4** stop. To rationalise this result the changes on the luminescence properties, that are induced by bromination in the 2,7-position, must be considered. The bromine substituents on the phz-moiety increase the emission quantum yield and induce a red-shift of the wavelength of the emission, which means, the emissive bright MLCT state, located on the phen, is stabilized with respect to the phz-centered state. The result of the transient absorption experiments show, that this stabilization inhibits the relaxation from the phen-centered to the phz-centered state, as only the first rise component is found for **Rudppz4**. For **Rudppz1** and **Rudppz5** this electron transfer channel is still open as revealed by the presence of τ_2 . Following the argumentation for **Rudppz4** the bromine substituents stabilize the phz-centered excited state in **Rudppz5** and hence the emission quantum yield is decreased. Furthermore, the non-radiative decay rate of this phz-centered state is increased to an extent, that this process becomes visible within the experimental accessible range of delay times.

The experimental data presented in this chapter clearly show a structure-dynamic relation. Ground-state properties, luminescence behavior and ultrafast excited-state dynamics are controlled by local substitution and not by environmental parameters as it was known from previous, conventional light-switch experiments. In **Rudppz4** bromine is introduced to the dppz's phen-moiety and the correspondent excited state is stabilized, leading to a red-shifted and more intense emission and quenching the charge-transfer to the phz-located excited state. In contrast the phz-located excited state can be also stabilized by bromination. Thus, **Rudppz5** is found non-emissive and the transient-absorption experiments show an accelerated ground-state recovery for this complex. Altogether, the ultrafast experiments show that it is possible to modify photoinitiated charge-transfers not only by blocking relaxation channels but also by increasing the gradient for an electron transfer. This shows the potential that is given by combination of intramolecular effects to control the charge-transfer dynamics in Ru-polypyridine complexes. Especially for the further development of supramolecular photocatalysts like **RuPd1** this is an interesting route to follow.

3. Photophysical effects of modified bridging ligands in supramolecular photocatalysts

Parts of this chapter are published in:

[CK3] M. Karnahl, C. Kuhnt, F. Ma, A. Yartsev, M. Schmitt, B. Dietzek, S. Rau, J. Popp, TUNING OF PHOTOCATALYTIC HYDROGEN PRODUCTION AND PHOTOINDUCED INTRAMOLECULAR ELECTRON TRANSFER RATES BY REGIOSELECTIVE BRIDGING LIGAND SUBSTITUTION, *Chem. Phys. Chem.*, **2011**, *12*, 2101-2109

[CK4] M. Karnahl, C. Kuhnt, F. W. Heinemann, M. Schmitt, S. Rau, J. Popp, B. Dietzek, SYNTHESIS AND PHOTOPHYSICS OF A NOVEL PHOTOCATALYST FOR HYDROGEN PRODUCTION BASED ON A TETRAPYRIDOACRIDINE BRIDGING LIGAND, *Chem. Phys.*, **2012**, *393*, 65-73

Supramolecular catalysts that are capable of reducing protons to molecular hydrogen upon absorption of visible light are typically composed of at least three essential molecular building blocks: the photoactive center is connected to the catalytic active center by a molecular bridge [54, 22, 52, 82, 19, 83] (for a schematic illustration see Figure 3.1). But the prominent role of the molecular bridge is not only to connect the two metals. It serves as an electron reservoir, should allow direct electron transfer and tune the interaction between both metal centers. Furthermore it should ensure vectorial electron transfer, i.e. already the initially photoexcited state should be located on the bridging ligand itself in order to assure that the charge-transfer leads to the right direction within the molecular frame.[41] Thus, the potential for improvement of supramolecular photocatalysts by variation of the bridging ligand is immense.

A detailed understanding of the underlying photophysical processes, which are induced by the modifications of the catalytic system should play a key role in order to achieve a directed evolutionary development of such systems. With this in mind, the impact of structural modifications on the excited-state properties and the photoinduced electron relaxation of the hydrogen evolving catalyst **RuPd1** is investigated. One modification that is taken into account within this work is bromination of the tp-phz bridging ligand at the 3,16

3. Modification of the Bridging Ligand

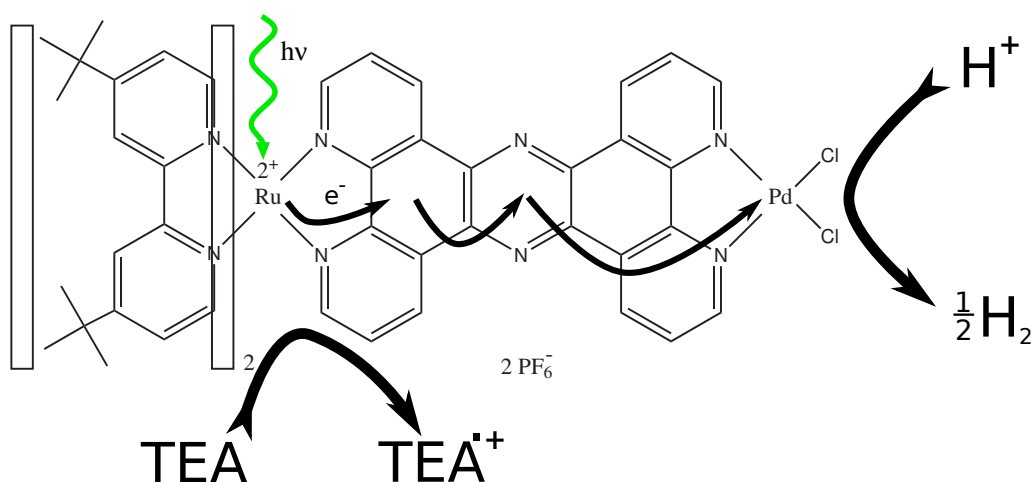


Figure 3.1.: Schematic illustration of the functionality of the photocatalyst **RuPd1**. Initial absorption of the photoactive Ru-centre is followed by a charge-transfer cascade which leads to reduction of the Pd-centre. The charge-transfer must be repeated to reduce the Pd-centre a second time. Then, by electron-transfer to incoming protons molecular hydrogen is formed. The electron-donor TEA is responsible for re-reduction of the oxidized Ru-centre.

position, e.g., the phen-moiety (**RuPd2**), in analogy to the Rudppz model complexes previously investigated (see Chapter 2). The second alteration concerns the tpphz's central pyrazine ring, which is exchanged with acridine to build the complex **RuPd3**.

The reason for the investigation of the second modification is the dependency of the photocatalytic proton-reduction on the water-content in the reaction mixture, which is shown in Figure 3.2. The effectivity of each catalyst is expressed with the help of the turn-over number (TON) which shows that only **RuPd1** is catalytically active without water. For **RuPd2** the maximum catalytic activity is obtained at a water content of 8 vol% in ACN while, in contrast, the TON of **RuPd3** is rising with the water content (see also [CK3] and [CK4]). This different behaviour might be rationalised by the fact that the central acridine ring in the tpac bridging-ligand possesses only one N-atom and thus it is expected to be less influenced by water.

For both of the modified supramolecular photocatalysts the photophysical properties are investigated with respect to changes of the solvent composition: The influence of the modification of the bridging ligand tpphz and the environment are investigated by means of UV/vis absorption, steady-state emission and ultrafast transient absorption spectroscopy.

3. Modification of the Bridging Ligand

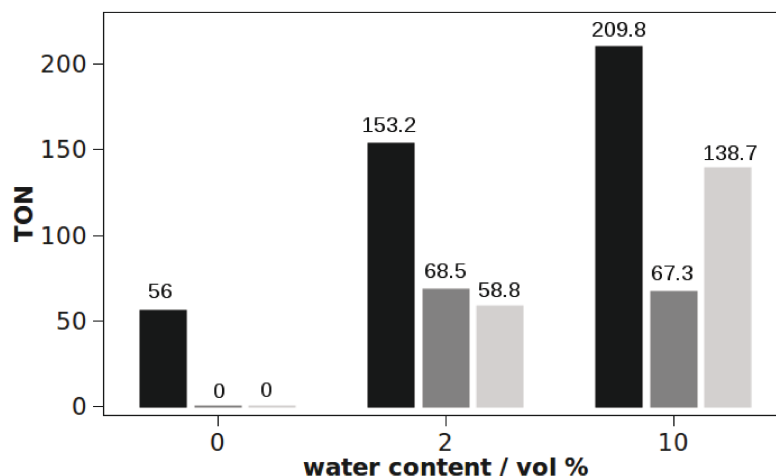


Figure 3.2.: The turn-over number (TON) of the three complexes **RuPd1** (black), **RuPd2** (dark gray) and **RuPd3** (light gray) in dependency on the water content in the reaction mixture while all other parameters (wavelength, intensity and time of irradiation, solvent, molarity of catalyst and TEA) were held constant. The evaluation of this data was carried out by Michael Karnahl.

3.1. Bromation of the tpphz bridging ligand

The investigations of the solvent dependent photophysics of **RuPd2** are considered in comparison to the unsubstituted **RuPd1**.^[42] By this comparison conclusions about the resulting structure-dynamic relationship can be deduced. For the solvent-dependent experiments ACN, dichloromethane (DCM) and a mixture of ACN with 10vol% H₂O were used. While for the experiments with UV/vis absorption and steady-state emission spectroscopy only ACN and DCM were used to detail effects of solvent polarity. As the catalytic activity of **RuPd1** and **RuPd2** is strongly dependent on the water concentration (Figure 3.2) the question to be addressed is whether water shows an effect on the charge-transfer properties on these complexes. Therefore, the transient absorption experiments, which are capable of following charge-transfer processes were also carried out with the ACN/H₂O mixture.

3.1.1. Bromine-induced stabilization of the ³MLCT

UV/vis absorption spectroscopy The absorption spectra show the features that were described before for Rudppz complexes (see Figure 3.3A): In the UV region a $\pi - \pi^*$ transition of the tbbpy ligands at 286 nm and two $\pi - \pi^*$ -transitions of the tpphz ligand at 361 and 381 nm are observed. These absorption features are rather unaffected by the

3. Modification of the Bridging Ligand

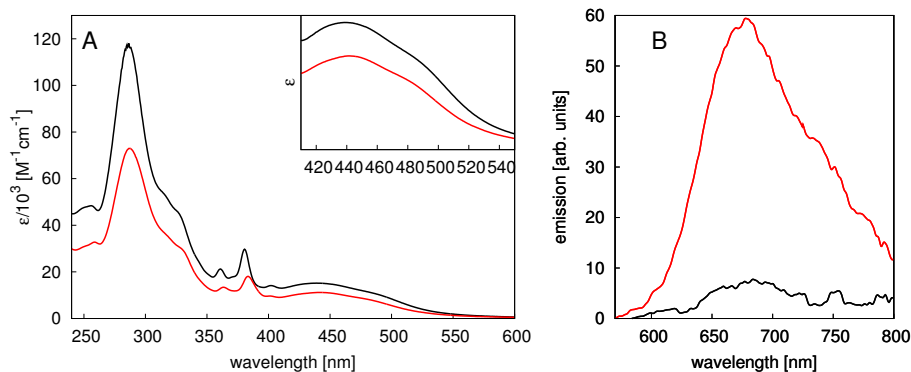


Figure 3.3.: A: UV/vis absorption of **RuPd2** in ACN (black) and DCM (red). The inset highlights the spectral shape of the MLCT band. B: Emission spectra of **RuPd2** in ACN (black) and DCM (red) after excitation of the MLCT

bromine substitution. The MLCT absorption band in the visible part of the spectrum in contrast is significantly affected by the introduction of bromine at the tpphz's phen-moiety. Compared to **RuPd1** the absorption maximum of the MLCT is shifted to lower wavelength for **RuPd2** and a shoulder appears at 484 nm. As in the case of the bromine-substituted **Rudppz4** the appearance of this shoulder reveals the presence of two distinct MLCT states. These two states, which are associated with either the tbbpy or the tpphz ligand are approximately degenerated in **RuPd1**. The introduction of the bromine substituents energetically lowers the tpphz-associated MLCT and hence the aforementioned shoulder appears in the spectrum.

Emission spectroscopy In contrast to **RuPd1**, which appears non-emissive, **RuPd2** shows solvent-dependent luminescence. An increase of the solvent-polarity leads to a decrease of the emission quantum yield. While in DCM $\Phi = 2.4 \times 10^{-2}$, this value reduces to 0.3×10^{-2} when ACN is used as solvent. A similar effect is obtained for the emission lifetime which shortens from 198 ns in DCM to 84 ns in ACN.

The reason of this luminescence behavior is found in the nature of the excited states that are involved in the photoinduced charge-transfer pathway. As described for Rudppz complexes, the relaxation process starts with an ultrafast ISC from the initially excited $^1\text{MLCT}$ to the $^3\text{MLCT}$, which is promoted by the presence of the heavy Ru atom. [26, 31, 28, 84] The lowest lying $^3\text{MLCT}$ in **RuPd1** and **RuPd2** is located on the tpphz's phen-moiety from where the relaxation can proceed in two possible ways: One possibility is intraligand charge-transfer to the short-living excited state located on the phz-moiety which is followed by further ligand-to-metal charge-transfer (LMCT) to the Pd metal ion. A competing process is the radiative decay of the phen-centered MLCT.[85, 45, 61, 61] Compar-

3. Modification of the Bridging Ligand

ison between the phen- and the phz-centered charge-transfer states shows that the molecular dipole moment of the latter one is larger. Thus the phz-centered state is stabilized in more polar solvents and consequently the excited-state equilibrium is shifted towards this state in polar solvents and Φ and τ are decreased. The luminescence characteristics of **RuPd1** compared to **RuPd2** shows that the bromine-substitution at the phen-moiety stabilizes the phen-centered MLCT and consequently **RuPd2** appears luminescent.

3.1.2. Substitution- and solvent-effects on the charge-transfer path

The excited-state relaxation of **RuPd2** is observed with the help of ultrafast transient absorption spectroscopy. As already described for the Rudppz complexes the MLCT was excited by a pump pulse at 510 nm and the subsequent processes were recorded with a supercontinuum white-light probe. At first the transient absorption recorded with ACN as solvent is discussed. Afterwards this data is compared to the situation with different solvent environments.

The transient absorption data in ACN, including transient absorption spectra, transient kinetics and the according decay-associated spectra (DAS), which depict the spectroscopic signature of the individual kinetic processes, are summarized in Figure 3.4. The broad structureless differential absorption band, with the maximum at 590 nm, is a signal built-up within the first tens of picoseconds, which is followed by a decrease of the signal at longer delay times towards the longest experimentally available delay time, i.e., 1.8 ns. Within this time window only slight spectral shifts of the transient absorption bands can be observed. A quantitative data analysis by global fitting reveals that three kinetic components τ_i , whose spectral signatures are depicted in the DAS (Figure 3.4 C) are necessary to fit a kinetic model to the data. The fastest of these processes ($\tau_1 = 1.1$ ps) describes the build-up of the excited-state absorption (ESA) which is followed by a second rise step ($\tau_2 = 8.2$ ps) which slightly increases the blue part of the differential absorption spectrum. The third process ($\tau_3 = 460$ ps) is accompanied with a signal decay over the entire spectral range.

The discussion of the molecular nature of these findings **RuPd2** is done in comparison to **RuPd1** as the photophysics of this compound has been published earlier.[42] Thus, the initial process (τ_1) is assigned to equilibration of the $^3\text{MLCT}$ on the tpzhz ligand, which most likely contains contributions from interligand hopping processes, vibrational cooling and intramolecular vibrational energy redistribution.[33, 50, 86, 30] For both **RuPd2** and **RuPd1** the duration of this process is found to be 1.1 ps. The DAS of the second, i.e., 8.2 ps component in **RuPd2** resembles the spectral features of a 5-ps component that was

3. Modification of the Bridging Ligand

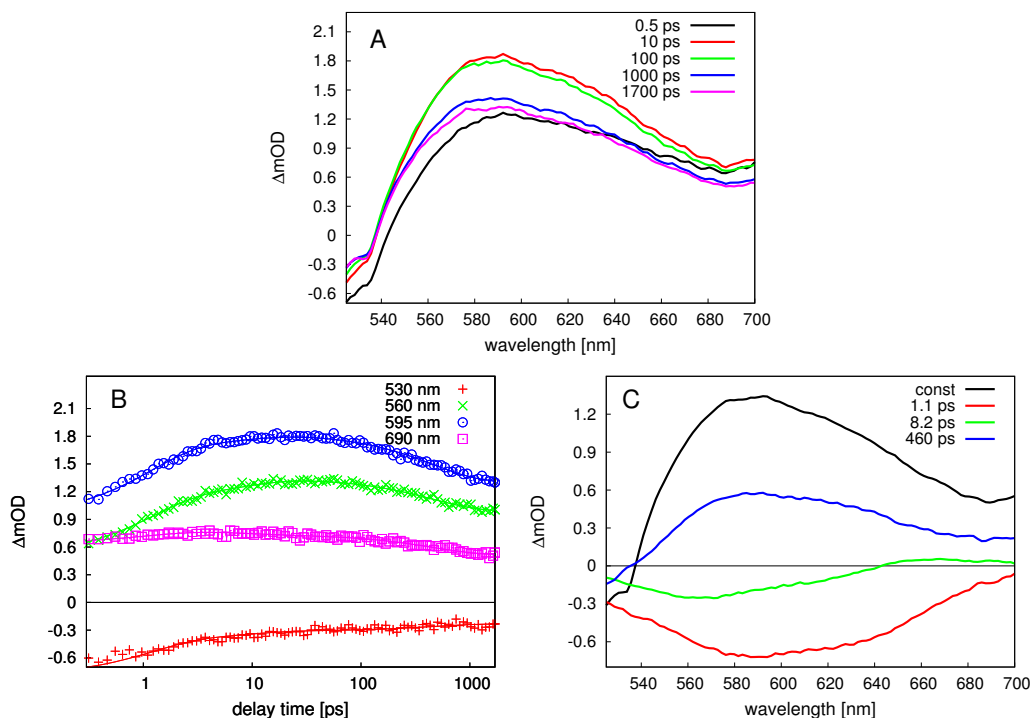


Figure 3.4.: Transient absorption data of **RuPd2** in ACN after excitation of the MLCT at 510 nm. A: Differential absorption spectra at given delay times after excitation. B: Kinetic development of the transient absorption at chosen wavelength. C: DAS which depict the spectral signatures of the kinetic components τ_i (which are denoted in the upper right corner).

found for **RuPd1** and is therefore assigned to an inter-ligand charge-transfer (ILCT) yielding a phz-centered excited state. Compared to the Rudppz-complexes, where this ILCT was also found, the population of the phz-centered state is accelerated as a consequence of the presence of the catalytically active Pd-centre. The spectral characteristics of the third process (τ_3) lead to the assignment of this component to a LMCT from the tpphz bridge to the Pd metal centre. This assignment stems from the kinetic and spectral analogies between **RuPd1** and **RuPd2** and $[(bpy)_2Ru^{II}tpphzOs^{III}(bpy)_2]^{4+}$ complexes.[85, 87].

The most notable difference in the charge-transfer dynamics of **RuPd1** and **RuPd2** is that the second and third kinetic components appear decelerated upon the introduction of bromine to the tpphz's phen-moiety. This finding can be rationalized by the characteristic spectral shape of the DAS of the second component τ_2 which is 30 nm red-shifted for **RuPd2** as compared to **RuPd1**. The underlying process is assigned to an ILCT from the phen- to the phz-centered state on dppz. As the spectral information of the DAS involves relative energy differences between the two excited states, this red-shift shows the stabilization of the phen-centered state with respect to the phz-centered state. Consequently the electron transfer between both states becomes less favored and appears decelerated. As

3. Modification of the Bridging Ligand

the same effect is also observed for the LMCT, it is indicated that the introduction of the bromine flattens the charge-transfer gradient across the entire bridging ligand leading to a deceleration of all photoinduced charge-transfer steps. This finding constitutes the first example for this class of Ru complexes, for which the chemical variation of one part of the molecular framework influences the entire charge-transfer across the supramolecular framework.

Additionally to the described data the development of the GSB in the spectral region below 520 nm is recorded with a second experimental setup that enables a time-window up to 15 ns. For both complexes, **RuPd1** and **RuPd2** a decay of the GSB signal on a ns-timescale is observed. The according ns-component (τ_4) indicates ground-state recovery, i.e., the decay of the charge-transfer state. Remarkably this deactivation process is quite faster for **RuPd2** ($\tau_4 = 7.2$ ns) than for **RuPd1** ($\tau_4 \geq 30$ ns). As for the catalysis the charge residing on the Pd-centre is crucial, such ground-state-recovery is directly a competing process. Hence, faster recovery of the ground state might be one of the reasons why **RuPd2** is less catalytic active than **RuPd1**

Solvent effects: Polarity When DCM is used as solvent instead of ACN it is expected that the stabilization of the charge-transfer state is reduced because of the reduced solvent polarity. ($\epsilon_{ACN} = 37.5$, $\epsilon_{DCM} = 8.9$ [88]) Hence, the driving force for intramolecular electron transfer is decreased. Accordingly in DCM the same processes that were observed in ACN could be found, but all of them appear decelerated. The charge-separation, interligand-hopping and vibrational cooling takes place within 2.8 ps (τ_1) followed by the ILCT to the phz-sphere within 52 ps (τ_2). The process assigned to LMCT (τ_3) has a time constant of 1000 ps. The DAS of the latter two processes reveal a red-shift as it was found for τ_2 for **RuPd2** compared to **RuPd1**. Thus, a solvent-induced decrease of the energy gap between the phen- and phz-located excited states can be observed, too. As a result the driving force for the charge-transfer processes is reduced resulting in decelerated excited-state relaxation in the less polar solvent.

Solvent effects: Addition of Water With the addition of water to neat ACN the catalytic activity of **RuPd1** rises significantly (Figure 3.2 and [41], TON rises from 56 without H₂O to 210 with 10vol% H₂O) while **RuPd2** is only photocatalytically active in a mixture of these both solvents. Such behaviour shows that water plays some role in the catalytic cycle but the mechanism of this interference is still unclear. In order to shed light on the molecular origin of this behavior, the transient absorption experiments were performed in a mixture of ACN and 10vol% H₂O. The results for both photocatalysts show

3. Modification of the Bridging Ligand

only minor qualitative differences in the charge-transfer behaviour after the light-induced MLCT for the mixture compared to neat ACN: The shape of the transient absorption spectra and the DAS remained unaltered. Hence, the photophysics of **RuPd1** and **RuPd2** in the solvent mixture is the same as it was detailed above for neat ACN. However, the rates of the individual charge-transfer steps were affected. Upon addition of water the rate of the fastest process, i.e., charge-separation, interligand hopping and vibrational cooling, is nearly retained for **RuPd1** ($\tau_1 = 1.2$ ps) and **RuPd2** ($\tau_1 = 1$ ps), which also applies for the ILCT from the phen- to the phz-centered state on the tpphz bridging ligand ($\tau_2 = 6.1$ ps for **RuPd1** and $\tau_2 = 10.5$ ps for **RuPd2**). The biggest effect of water addition is found for the rate of the third step, i.e., the LMCT from tpphz to the Pd-metal centre. The according kinetic component τ_3 rises significantly for both complexes from 310 to 850 ps for **RuPd1** and from 460 to 800 ps for **RuPd2**, respectively.

It is shown that the addition of water affects the photoinduced charge-transfer processes within the first nanosecond after photoexcitation of both complexes in the same way. Remarkably for the solvent mixture is that the rates for the LMCT are nearly equal for **RuPd1** and **RuPd2**. This points to the fact that the substitution induced alterations of the electron transfer gradient are compensated by the intermolecular effect of water. But contrary to the behavior in DCM the reason here cannot be the polarity. ($\epsilon_{H_2O} = 80.4$ [88]) While in DCM the whole charge-transfer dynamic is decelerated compared to neat ACN the addition of water has only a minor effect on the two initial processes of charge separation. Thus, other effects like specific molecular interaction between water and the complexes must be taken in account.

3.2. Introduction of tpac as bridging ligand

The catalytic activity of **RuPd1** and **RuPd2** was found to be strongly dependent on the water content in the reaction mixture. (see Figure 3.1) Already minor amounts of water significantly increase the catalytic hydrogen production and the optimum concentration of water lies between 10 and 15 vol% in ACN. The reason for the existence of such a turn-over point has to lie in an ambivalent role of water: On the one hand it serves as a substrate for the hydrogen production. On the other hand direct intermolecular interaction between water molecules and the complexes reduce the overall charge-transfer gradient after the initial photoexcitation which is limiting the catalytic turnover. Hence the introduction of bridging ligands with a decreased water sensitivity is an interesting route to follow. Accordingly the complex **RuPd3** is introduced with tpac as molecular bridge.

3. Modification of the Bridging Ligand

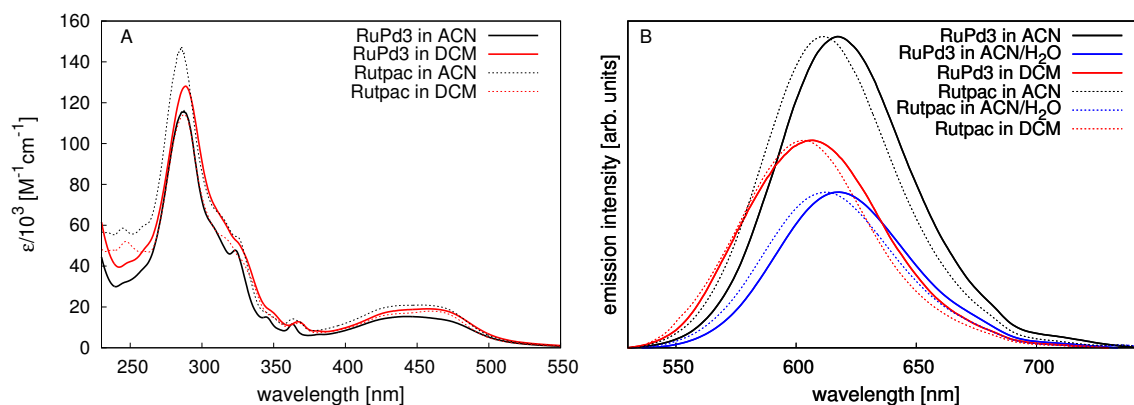


Figure 3.5.: A: UV/vis absorption of **Rutpac** and **RuPd3** in different solvents. B: Emission spectra of **Rutpac** and **RuPd3**. The emission maxima are normalized in pairs to provide better comparability.

This ligand has similar coordination spheres, compared to *tpphz*, and a central acridine moiety. Previous investigation on the photophysical properties of $[(phenan)_2Ru(tpac)]^{2+}$ and $[(phenan)_2Ru(tpac)Ru(phenan)_2]^{4+}$ (phenan = 1,10-phenanthroline) showed that for these complexes the excited states which are located on the *tpac* ligand are less sensitive towards water.[89, 90, 91] In order to achieve better insight into the photophysics of **RuPd3** the study performed in the context of this work includes the monomolecular precursor complex **Rutpac**, which lacks the catalytic active unit.

3.2.1. General spectroscopic characteristics of the Rutpac-complexes

UV/vis absorption spectroscopy The UV/Vis absorption spectra of **Rutpac** and **RuPd3** show three absorption maxima in the spectral region above 300 nm (see Figure 3.5). At 350 and 370 nm the $\pi - \pi^*$ -transition of the *tpac* ligands can be seen. The broad band between 400 and 500 nm is assigned to the MLCT from the central Ru-ion to the terminal *tbbpy*- and to the *tpac*-ligand. The transitions to both ligands are distinguished by two apparent, solvent-independent shoulders: The shoulder at approximately 430 nm belongs mainly to the MLCT from Ru to the *tbbpy*-ligands and the shoulder at 475 nm is assigned mainly to the MLCT from Ru to the *tpac*-ligand. In general the absorption spectra are quite similar to those of **RuPd1** and **RuPd2** with slightly shifted MLCT maxima.[42]

Emission spectroscopy Both complexes **Rutpac** and **RuPd3** show solvent-dependent emission after excitation of the MLCT (see Figure 3.5 and Table 3.1). In analogy to the *Rudppz* and the *Rutpphz* complexes the emission properties of the *Rutpac* complexes

3. Modification of the Bridging Ligand

Complex	λ_{em} [nm]			$\Phi \times 10^{-2}$			τ_{em} [ns]		
	ACN	DCM	ACN/H ₂ O	ACN	DCM	ACN/H ₂ O	ACN	DCM	ACN/H ₂ O
Rutpac	612	603	612	1.6	4.6	1.8	153	900	162
RuPd3	617	607	617	0.8	0.8	0.6	180	170	90

Table 3.1.: Emission data (i.e. emission maxima λ_{em} , quantum yield Φ and lifetime τ_{em}) of **Rutpac** and **RuPd3** in dependence to the solvent environment.

are determined by the equilibrium between two states. The first and emissive ³MLCT is located on the phen-part of the tpac-ligand (³MLCT-phen). The second, non-emissive excited state is assumed to reside on the acridine moiety (³MLCT-ac). [90, 87, 92, 45] The emission of **Rutpac** in ACN has a maximum at 612 nm and a quantum yield of 1.6×10^{-2} with a life-time of of 153 ns. Addition of 10vol% water to ACN induces rather small changes: Without a shift of the emission wavelength the quantum yield rises to 1.8×10^{-2} and the life-time to 162 ns. When **Rutpac** is solved in DCM the emission quantum yield rises to 4.6×10^{-2} accompanied with an increased emission lifetime of 900 ns. As observed for Rudppz- and Rutpphz-complexes this effect stems from the decreased solvent-polarity by which the population of the luminescent and long-living ³MLCT-phen state is favoured.

The introduction of the *PdCl₂*-unit leads to a small redshift of the emission by 5 nm (130 cm^{-1}) and a decreased luminescence quantum yield independent to the solvent. Especially the drop of the quantum yield shows the presence of an additional non-radiative deactivation channel in **RuPd3**. In analogy to **RuPd1** and **RuPd2** this deactivation path is attributed to the electron transfer to the Pd-metal centre. The effect of the solvent polarity as observed for **Rutpac** is nearly negligible for **RuPd3**. When the complex is solved in DCM the same quantum yield as in ACN is measured and the emission lifetime undergoes a minor decrease to 170 ns. In contrast the addition of water has a more significant effect: The luminescence quantum yield drops to 0.6×10^{-2} and the lifetime decreases to 90 ns. That solvent-dependent luminescence behavior of **RuPd3** cannot be reasoned with the polarity. Further, these finding indicate direct interaction between water molecules and the *PdCl₂*-unit, e.g., by exchange of a *Cl⁻* ion as also discussed for **RuPd1**. [42]

3.2.2. Characterization of interactions between the solvent and the photocatalyst

The wavelength- and time-dependent transient absorption data for **Rutpac** and **RuPd3** are recorded in neat ACN, ACN/H₂O and DCM. For excitation light at 480 nm was used and

3. Modification of the Bridging Ligand

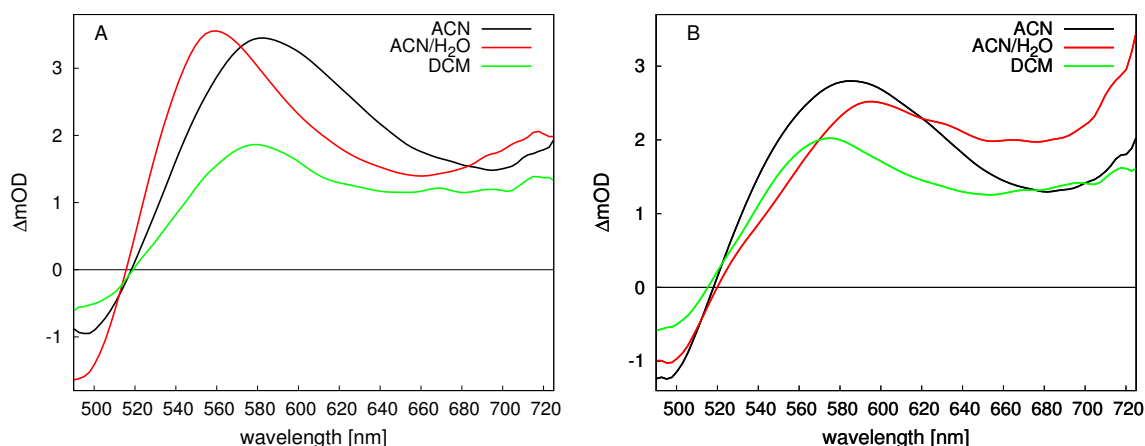


Figure 3.6.: A: Representative transient absorption spectra of **Rutpac** in different solvent environments ten ps after excitation of the MLCT with 480 nm. B: Representative transient absorption spectra of **RuPd3** ten ps after excitation in three different solvent environments after excitation of the MLCT with 480 nm.

the subsequent charge-transfer processes were recorded in a spectral window between 490 and 720 nm within a time-range from 0.5 to 1600 ps. The transient spectra of both species (see Figure 3.6) show similar features in all three solvents: GSB is observed below 520 nm and ESA bands are recorded with solvent-specific maxima for longer probe wavelength.

The solvent dependency of the transient absorption behavior of **Rutpac** can be seen merely in the maxima of the ESA. While this appears at 585 nm in ACN it is blue-shifted to 580 nm in DCM and to 560 nm upon addition of H₂O to ACN. The transient absorption spectra show nearly no dependence to the delay-time between pump- and probe-pulse, irrespective of the solvent. This is also reflected in the transient kinetics (Figure 3.7 A) where temporal evolution is nearly insignificant. Such kinetic behavior might arise from several origin: (1) The excited-state dynamics might be faster than the available temporal resolution, i.e. proceeding within the first 500 fs. (2) The charge-transfer processes might be too slow and cause significant changes of the differential absorption only after 1.6 ns. (3) The spectral changes induced by the photoinduced processes might be too small and thus be invisible within the experimentally accessible signal-to-noise ratio.

The transient absorption spectra of **RuPd3** in neat ACN and DCM are nearly similar to those of **Rutpac** and only small spectral shifts can be found (see Figure 3.6). When the ACN/H₂O mixture is used as solvent a different situation is found. Here the introduction of the Pd-centre causes a red-shift of the ESA maximum from 550 to 590 nm. The temporal evolution of the ESA signals differs significantly between **Rutpac** and **RuPd3** (see Figure 3.7). The transient kinetics of the latter system reveal two features irrespective of the solvent: On a short time-scale a hypsochromic shift of the ESA-band can be observed

3. Modification of the Bridging Ligand

and on a long time-scale the signal globally decays. In ACN the according time constants are fitted to $\tau_1 = 4.4$ and $\tau_2 = 580$ ps. The assignment of these kinetic components to the underlying charge-transfer processes is done in comparison to **RuPd1** and **RuPd2**. [42] This shows that the slow process belongs to the LMCT from the tpac-ligand to the Pd-centre. This LMCT originates from the $^3\text{MLCT-ac}$ state and thus it is expected that the previous steps, i.e., ISC and ILCT (from $^3\text{MLCT-phen}$ to $^3\text{MLCT-ac}$), occur on a time-scale faster than 4.4 ps. This finding sheds some light on the previous discussion about the uniform transient kinetics of **Rutpac**. It can be argued that also in the mononuclear complex the initial charge-transfer steps take place rather rapidly associated with only small spectral changes. Thus, the possibility (2), i.e., that a slow charge-transfer dynamics is present, appears unlikely.

If DCM and the ACN/H₂O mixture is used as solvent, kinetics found for **RuPd3** do not differ qualitatively but quantitatively. As it was already observed for **RuPd1** and **RuPd2** in DCM the kinetics are decelerated to $\tau_1 = 42$ ps and $\tau_2 = 1200$ ps, which is explained by the fact that the excited states, due to their higher dipole moment, are destabilized in unpolar solvents, like DCM. When H₂O is added to ACN the impact on the two time-constants differ: The first process, reflecting the charge-localization on the tpac-ligand is slightly decelerated to $\tau_1 = 5.5$ ps and in contrast the LMCT appears faster. Thus, the addition of water has a minor effect on the charge-transfer reactions related with the tpac bridging-ligand and a significant impact on the charge-transfer to the catalytic Pd-metal centre. This result is in good agreement with the finding of the steady-state emission spectroscopy that water interacts directly with the Pd-centre and not with the tpac bridging ligand.

The described steady-state and ultrafast charge-transfer behaviour shows that the ex-

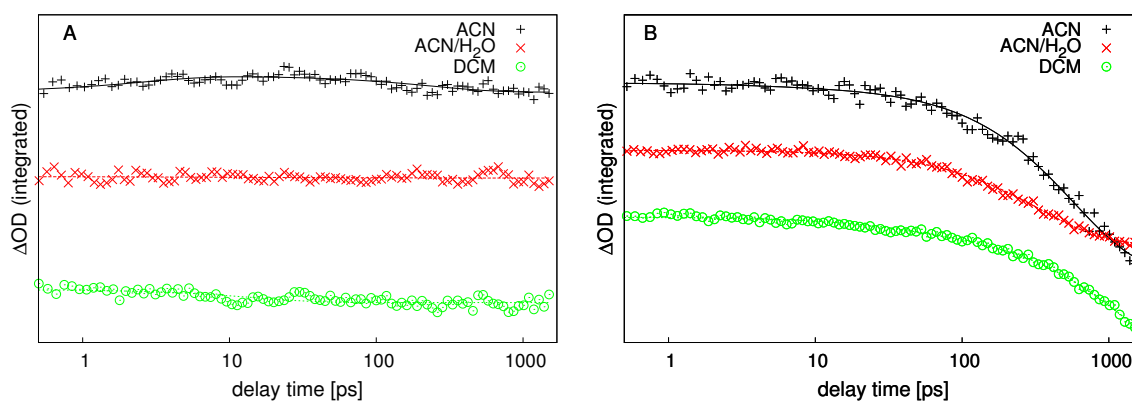


Figure 3.7.: A: Integrated transient kinetics of **RuPd3** in three different solvents. B: Integrated transient kinetics of **RuPd3** in three different solvents.

3. Modification of the Bridging Ligand

change of the central phenazine-ring by a acridine-ring changes the location of interaction between water and the catalytic system: It does no longer take place between the bridging ligand and water molecules, instead this interaction is observed between water and the catalytic Pd-centre.

4. Excited state interaction in homodinuclear RuTPPhz model complexes

Parts of this chapter are published in:

[CK5] C. Kuhnt, M. Karnahl, M. Schmitt, S. Rau, B. Dietzek, J. Popp, EXCITED-STATE ANNIHILATION IN A HOMODINUCLEAR RUTHENIUM COMPLEX, *Chem. Comm.*, **2011**, 47, 3820-3821

[CK6] C. Kuhnt, M. Karnahl, S. Rau, M. Schmitt, B. Dietzek, J. Popp, THE IMPACT OF BROMINE SUBSTITUTION ON THE PHOTOPHYSICAL PROPERTIES OF A HOMODINUCLEAR RU-TPPHZ-RU COMPLEX, *Chem. Phys. Lett.* **2011**, 516, 45-50

Beside the attempts to tune individual structural motifs of supramolecular photocatalysts to increase the catalytic efficiency other strategies can be followed to reach that goal. One possibility is to mimic the design strategies of natural photosynthetic systems and to increase the number of light-harvesting units per catalytic centre. [50, 18, 49] As the absorption cross-section of Ru-polypyridine complexes scales almost linearly with the number of Ru-units, increasing the numbers of photoactive Ru-centres increases the number of harvested photons. [93, 94, 95] Recently it was proven that tpphz as bridging ligand is well suited for this task as it is able to form dendrimeric structures to connect several Ru-units. [93, 96] Another advantage of this strategy is the possibility to introduce multiple structural distinct chromophoric units in order to tune the absorption spectrum of the catalytic complex. This can be realized by the introduction of substituents to the chromophoric units, which shift the energetic positions of the MLCT states involved in the visible light absorption. Hence, the absorption spectrum of the catalyst can be broadened to cover a larger part of the solar spectrum.

A major drawback of multiple chromophoric units that are directly connected to each other is the possibility of direct unwanted interactions between individually photoexcited chromophores. Such interactions, which might lead to annihilation of excited states are well known for systems with high number of light-harvesting units like conjugated poly-

4. Homodinuclear Rutpphz complexes

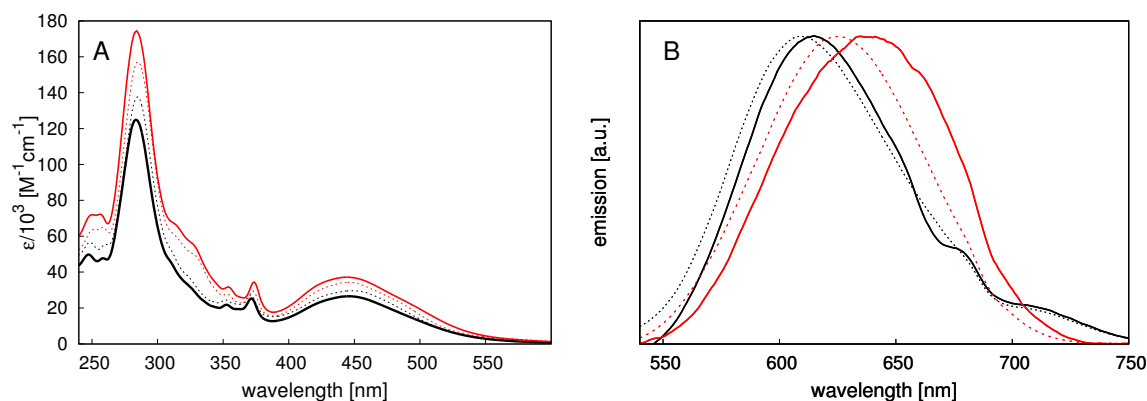


Figure 4.1.: A: Absorption spectra of **RuRu1** (black) and **RuRu2** (red) in ACN (full line) and DCM (dashed line). B: Emission spectra of **RuRu1** and **RuRu2** after excitation of the MLCT.

mers or dendrimers.[97, 98, 99] In order to examine such processes in Ru-polypyridine complexes the homodinuclear model complexes **RuRu1** and **RuRu2** are investigated with respect to their pump-intensity dependent photophysics. With the help of this examination interactions between the two photocentres can be detected as they should only appear if the pump-power is high enough to excite both Ru-centres. By comparing this dependency of both complexes the interaction of non-degenerated excited-states is taken into account, which can be found in **RuRu2**.

4.1. General spectroscopic characteristics of the homodinuclear complexes

UV/vis absorption spectroscopy The absorption spectra of **RuRu1** and **RuRu2** show the well known features that were observed for the other Ru-polypyridine complexes (see Figure 4.1). For **RuRu1** (**RuRu2**) the $\pi - \pi^*$ -transitions of the tpphz ligands are found at 351 nm (354 nm) and 371 nm (374 nm). Compared to the Rudppz- and mononuclear Rutpphz-complexes the red-shift induced by the bromine substituents is rather small. [73] The broad and unshaped MLCT-band with a maximum at 445 nm, irrespective of solvent or substitution, does not show the shoulder that was typical for **Rudppz4** or **RuPd2**.

Emission spectroscopy After excitation of the MLCT **RuRu1** and **RuRu2** show weak emission in ACN (see Figure 4.1 and Table 4.1). As it was observed for related mononuclear species the bromine substitution stabilizes the emissive ³MLCT-phen state and hence the emission is bathochromatically shifted from 616 nm (**RuRu1**) to 637 nm (**RuRu2**).

4. Homodinuclear Rutpphz complexes

Complex	λ_{em} [nm]		$\Phi \times 10^{-3}$	
	ACN	DCM	ACN	DCM
RuRu1	616	605	1.6	8.1
RuRu2	637	626	0.8	7.3

Table 4.1.: Maximum of the emission (λ_{em}) and emission quantum yield (Φ) of the homodinuclear complexes in dependence on the solvent.

Against expectations this stabilization does not increase the emission quantum yield, actually the opposite is found: $\Phi = 1.6 \times 10^{-3}$ for **RuRu1** and $\Phi = 0.8 \times 10^{-3}$ for **RuRu2**. This finding is attributed to the asymmetric substitution pattern in **RuRu2**, which causes the presence of two distinct $^3\text{MLCT-phen}$ states on the tpphz-ligand. These two states shall be denoted $^3\text{MLCT-phen}_{Br}$ for the substituted part and $^3\text{MLCT-phen}_H$ for the unsubstituted part. In **RuRu1** two degenerated emissive $^3\text{MLCT-phen}_H$ states exist from which emission originate. In **RuRu2** both states, the $^3\text{MLCT-phen}_{Br}$ and the $^3\text{MLCT-phen}_H$ state might be emissive. But the red-shift of the emission and the absence of a secondary emission shoulder in the luminescence spectra of **RuRu2** shows that only $^3\text{MLCT-phen}_{Br}$ is responsible for the emission. Furthermore, as it was shown for **RuPd2** the bromine substitution stabilizes not only the $^3\text{MLCT-phen}$ state but also the $^3\text{MLCT-phz}$ state in the direct vicinity. In **RuRu2** this increases the energy-gap between the $^3\text{MLCT-phz}$ and the $^3\text{MLCT-phen}_H$, which is schematically depicted in Figure 4.4. Hence, in **RuRu2** emission of the $^3\text{MLCT-phen}_H$ state is effectively quenched.

When DCM is used as solvent the emission of both complexes is blue-shifted and an increased quantum yield is observed. The higher quantum yield in the unpolar solvent is explained because of the larger dipole-moment of the non-emissive $^3\text{MLCT-phz}$ state compared to the emissive $^3\text{MLCT-phen}$ state.

4.2. Interaction of the photocentres after excitation

The experiments on the transient absorption spectroscopy were performed in dependence on the excitation-light intensity. Following the experimental design the discussion in this chapter is splitted into two parts: low-intensity excitation (pump-intensity of $9.3 \times 10^{15} \text{ photons cm}^{-2}$) and a high-intensity excitation (pump-intensity of $4.6 \times 10^{16} \text{ photons cm}^{-2}$) are discussed separately. In both cases the excitation wavelength was 505 nm which lies in the red flank of the MLCT absorption band and the probe-window lies between 525 and 750 nm.

4. Homodinuclear Rutpphz complexes

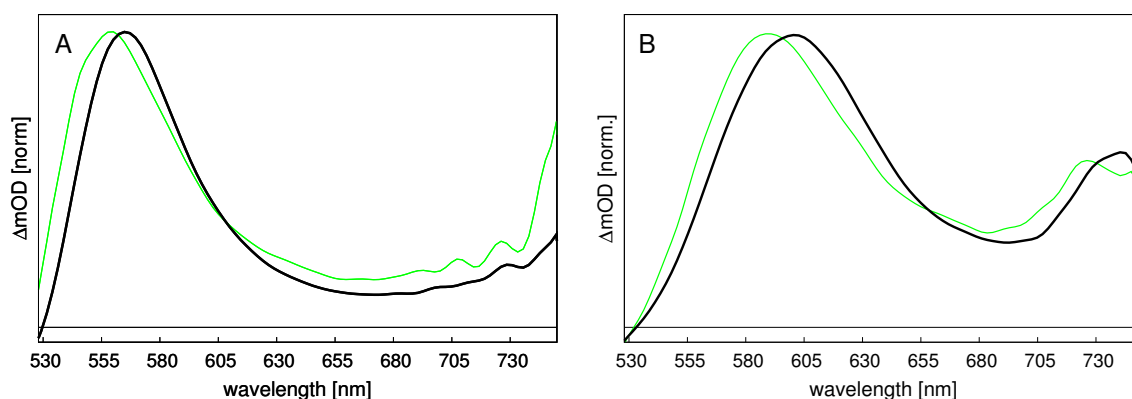


Figure 4.2.: A: Typical transient absorption spectra ten picoseconds after excitation of **RuRu1** for low-intensity (green) and high-intensity (black) excitation. For reasons of comparability the spectra are normalized to the maximum of the ESA band. B: Typical transient absorption spectra ten picoseconds after excitation of **RuRu2**

Low-intensity excitation In the low-intensity regime a GSB below 530 nm for **RuRu1** (below 540 nm for **RuRu2**) and an ESA band with a maximum at 560 nm (590 nm) can be observed within the complete experimentally accessible time-window between 0.5 to 1800 ns (see Figure 4.2). For **RuRu2** a second ESA band appears at 730 nm, which is absent for **RuRu1**. This band most likely indicates the presence of discrete triplett-states that are energetically higher than the $^3\text{MLCT-ph}_{\text{en}}$ and $^3\text{MLCT-ph}_{\text{z}}$ states. Apparentely the bromine substitution either introduces novel states or shifts the energy of this states to increase the ESA gap compared to **RuRu1**

The stabilization of the $^3\text{MLCT-ph}_{\text{en}}$ state by introduction of bromine substituents, can be observed by comparison of the transient absorption spectra of both complexes (Figure 4.2): The ESA band of **RuRu2** is red-shifted compared to **RuRu1** by 25 nm. This substitution induced red-shift shows that the energy of the $^3\text{MLCT-ph}_{\text{en}_{\text{Br}}}$ state is reduced compared to the $^3\text{MLCT-ph}_{\text{en}_{\text{H}}}$ state. Furthermore, the ESA band of **RuRu2** is broadened compared to **RuRu1**, which points to the mixed excitation of both states. The transient absorption data shows only negligible spectral shifts within the experimental accessible time-window between 0.5 and 1700 ps. Thus, the temporal evolution of the ESA signal-intensity is used to interpret the data (normalized transient kinetics are depicted in Figure 4.3). For both complexes a bimodal rise of the ESA over the entire delay-time can be observed. Accordingly, data treatment by the global fitting routine yields two kinetic components. The assignment of these kinetic components to charge-transfer processes is done in comparison to related Ru-polypyridine complexes. Thus, for **RuRu1**, the first component with a characteristic time constant of $\tau_1 = 1.5$ ps is assigned to charge-localization

4. Homodinuclear Rutpphz complexes

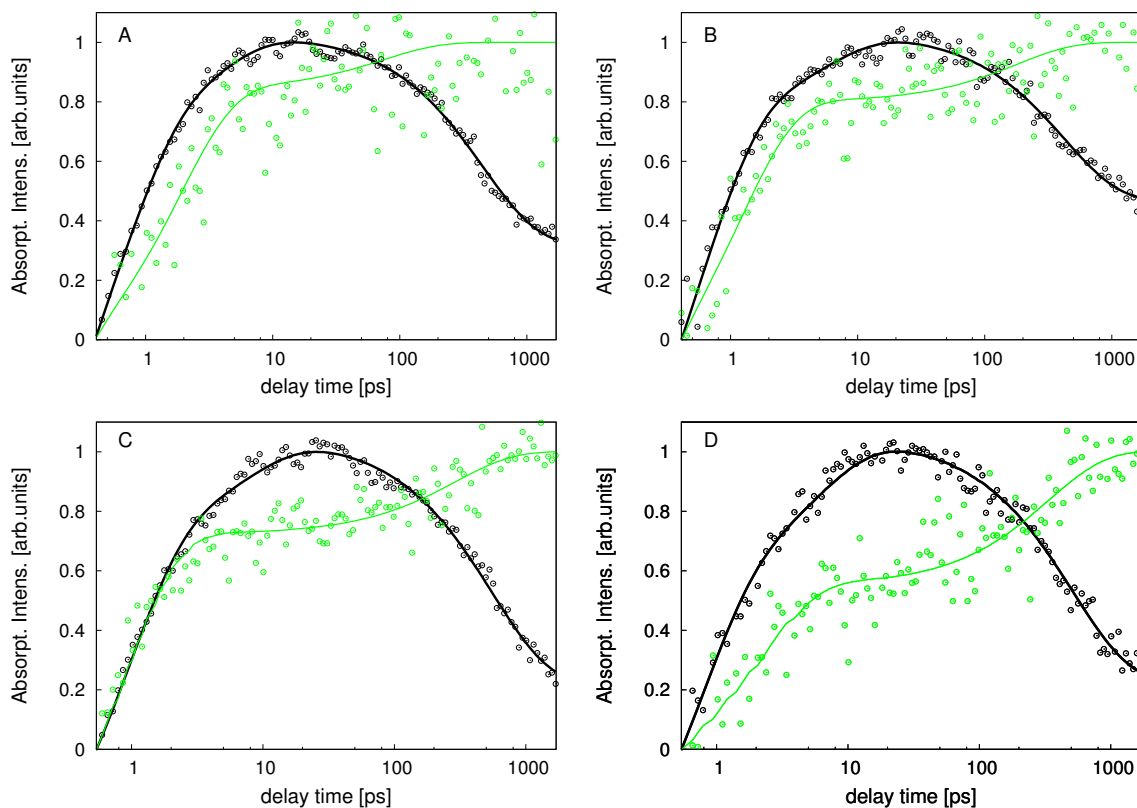


Figure 4.3.: Transient absorption kinetics of both homodinuclear complexes for low (green) and high (black) pump-intensity. A: Kinetics of **RuRu1** at high concentration of the complex. B Kinetics of **RuRu1** at low concentration. C: Kinetics of **RuRu2** at high concentration. D: Kinetics of **RuRu2** at low concentration.

on the tpphz-ligand and vibrational cooling within the $^3\text{MLCT-phn}$ state.[33, 30, 86] The subsequent process, revealing a time constant of $\tau_2 = 58$ ps, is assigned to ILCT from the $^3\text{MLCT-phn}$ to the $^3\text{MLCT-phz}$ state.[42] The stabilization of the $^3\text{MLCT-phn}$ state by the introduction of bromine is reflected in the time-constants yielded for **RuRu2**: The first process is accelerated to 0.8 ps, which - for **RuRu2** - represents a mixture of the localization process on either of the two non-degenerated $^3\text{MLCT}$ -states. The second process, the ILCT from the tpphz's phen- to the phz-moiety, is decelerated to 290 ps. Especially the slower ILCT shows that the energy-gap between the $^3\text{MLCT-phn}_{Br}$ and the $^3\text{MLCT-phz}$ states is reduced and hence the driving force of the corresponding transition is decreased. The charge-transfer-paths of both complexes are schematically shown in Figure 4.4. The impact of the bromine substituents on the homodinuclear complex **RuRu1** can be compared to the results found for heterodinuclear complexes **RuPd1** and **RuPd2**: In both cases the general charge-transfer gradients after MLCT is reduced resulting in a substitution-induced deceleration of the electron migration.

4. Homodinuclear Rutpphz complexes

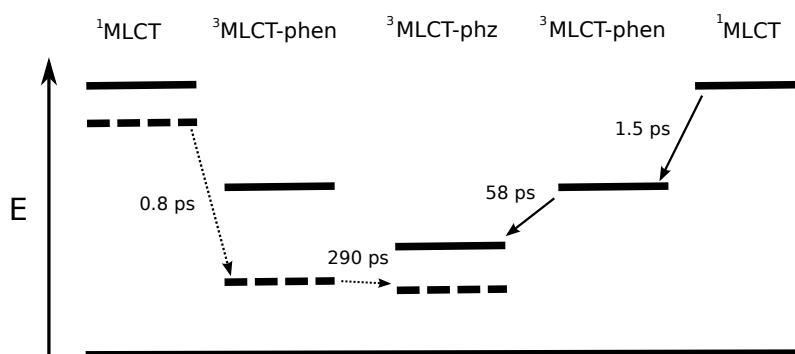


Figure 4.4.: Energy diagram of the excited states involved in the charge-transfer processes of **RuRu1** and **RuRu2**. Horizontal bars represent the excited states while the influence of the bromine-substitution is illustrated by the dashed bars. Notably in **RuRu2** only one Ru-polypyridine center is affected by the bromine-substitution (here shown in the left part of the diagram). The characteristic time-constants describe intramolecular charge-transfer processes at low pump-intensities.

High-intensity excitation Increasing the pump-intensity for MLCT excitation leads to only minor spectral changes. The ESA of both complexes are slightly red-shifted (see Figure 4.2). However, a significant impact of the pump-intensity is observed in the transient kinetics. The bimodal rise of the signal, that is found to be explicitly accelerated upon increased pump intensity ($\tau_1 = 0.6$ ps and $\tau_2 = 5.5$ ps for **RuRu1**) is now followed by an overall ESA decay. The underlying molecular mechanism of the strong acceleration of the first two charge-transfer processes, which is also observed for **RuRu2** ($\tau_1 = 0.9$ ps and $\tau_2 = 7$ ps), is not yet understood. However, the reduced driving force for the ILCT upon bromine substitution is again apparent as the characteristic time-constants for **RuRu2** are longer than for **RuRu1**.

The time-constant for the third, the decay-process, which is introduced by increasing the pump intensity is 420 ps for **RuRu1** and 560 ps for **RuRu2**. The overall decay of the ESA associated with this process indicates a deactivation mechanism induced by interaction of individual photoexcited states. The nature of such interaction can be either inter- or intramolecular. As several related Ru-polypyridine complexes are known to form π -stacking dimers at high concentrations (in the range of 10^{-3} mol/l) [73, 100, 101] the dependence of the decay on the intensity of the excitation-light was studied also for high concentrations (Figure 4.3 A and C). Rising the concentration up to one order of magnitude shows that the decay behavior is independent on the concentration. Thus, the deactivation mechanism is supposed to be intramolecular. This means that the increased pump-intensity can lead to excitation of both photoactive centres in the homodinuclear

4. Homodinuclear *Rutpphz* complexes

complexes. After the ILCT occurred the $^3\text{MLCT-phz}$ states interacts with one of the $^3\text{MLCT-phen}$ states resulting in deactivation of one excited state and finally the $^3\text{MLCT-phz}$ state is formed. As bromine substitution generally slows down excited state transfer-rates in Ru-polypyridines the deceleration of the annihilation process of **RuRu2** compared to **RuRu1** fits quite well.

This is the first time that an exciton-exciton annihilation is found in a homodinuclear complex, where two photoactive metal centres are connected by an electron relaying ligand. Such phenomena has been observed beforehand for e.g. conducting polymers or dendrimeric complexes. [102, 98] In dendrimers of chromophoric units and in polymers, connecting assemblies of chromophores, such processes are known as triplet-triplet or singlet-singlet annihilation.[97, 103] The discovery of that annihilation process in **RuRu1** and **RuRu2** must be taken into account for the future development of photocatalysts with multiple chromophoric units. This means that for such devices mechanisms must be implemented that avoid direct interaction of the single light-absorbing units. Furthermore it was shown that pump-intensity transient absorption spectroscopy is suitable to obtain annihilation processes even in relatively small molecules with a small amount of chromophores.

5. Conclusion

This thesis constitutes a comprehensive overview of the photophysical properties of several new Ru-polypyridine complexes. The goal of the investigations was to characterize the impact of substitutions on the light-induced charge-transfer of a photocatalytic active species. Therefore a variety of spectroscopic methods, i.e. UV/vis-absorption and emission spectroscopy, measurements of emission quantum yields, time-correlated single-photon counting and ultrafast transient absorption spectroscopy, were applied. The repertoire was complemented by quantum chemical calculations. This ensemble of techniques enabled a detailed insight into the possibilities of tuning the photophysical properties of supramolecular photocatalysts, which are based on Ru-polypyridines as photoactive units and are able to reduce protons to molecular hydrogen. To achieve such tunability, simple variations like substitutions at the bridging ligand, which connects the photoactive unit with the catalytic unit, or by alteration of the solvent environment are shown to be sufficient.

In a first examination on regiospecificly substituted Rudppz complexes (dppz = dipyrrodo[3,2-*a*:2',3,3'-*c*]phenazine), which are well suited model complexes for the supramolecular species such as [(*tbbpy*)₂Ru(*tpphz*)PdCl₂](PF₆)₂ (*tbbpy* = 4,4'-di-*tert*-butyl-2,2'-bipyridine, *tpphz* = tetrapyrrodo[3,2-*a*:2',3'*c*:3'',2'',-*h*:2''',3'''-*j*]phenazine, **RuPd1**), a combination of Raman spectroscopy with DFT calculation was applied. It could be shown that, after the introduction of several substituents, in the electronic ground-state a strict separation of the phenanthroline- (phen) and the phenazine-moieties (phz), which are located on the dppz ligand, does not exist.

Substitutions on both, the phen- and phz-, spheres with bromine do also have an impact on the excited-state properties of Rudppz. With the help of the relatively simple bromine substituents the photoinduced charge-transfer behavior can be controlled: By substitution on the emissive phen-moiety the luminescence is significantly enhanced and otherwise, when the phz-part is substituted, reduced. With the help of transient absorption spectroscopy the underlying mechanism leading to this luminescence behavior could be elucidated. It is found that the electron-withdrawing bromine-substituents energetically

5. Conclusion

stabilize the excited state located on the substituted part of dppz, leading to a substitution-controlled equilibrium. Hence, relaxation pathways are quenched or accelerated, depending on the position of the bromine, and accordingly the weak luminescence of the unsubstituted complex is significantly enhanced or - alternatively - switched off completely. This shows the drastic influence of even minimal alterations on the photophysics of Ru-polypyridines.

After the discovery of the strong effect of bromination on the model compound the next step was to monitor the impact of a similar substitution pattern on **RuPd1**. Bromination of the photocatalytic active complex in proximity to the photoactive metal-ion decreases the overall charge-transfer gradient across the entire bridging ligand. This result shows that the strict separation of the properties of the phen- and the phz-centered located state in tpphz (and most likely in other polypyridines) is invalid. Furthermore, the impact of water-addition to the solvent was examined, because the addition of water increases the catalytic activity of the photocatalysts. It could be shown by investigations on the ground-state-recovery that direct interactions between water molecules and the catalysts take place. These interactions accelerate recovery of the ground-state and thus open or at least favor a reaction channel which directly competes with the charge-transfer that leads to reduction of the catalytic Pd-centre. By this result the ambivalent role of water within the catalytic reaction of both complexes is shown: On the one hand, small amounts of water increase the efficiency of both catalysts but on the other hand it influences the charge-transfer reactions in a negative way. This could be one reason that the catalytic efficiency decreases at a higher water content.

A second alteration of the bridging ligand, namely introduction of a central acridine- instead of a phenazine-ring in the tpphz-scaffold, forming another photocatalytic active complex $[(tbbpy)_2Ru^{II}tpacPdCl_2](PF_6)_2$ (tpac = tetrapyrido[3,2-*a*:2',3'-*c*:3'',2''-*h*:2''',3'''-*j*]acridine, **RuPd3**) is presented. This variation especially aims at the interaction between the catalyst and water molecules, which should be decreased as the acridine-ring has fewer N-atoms available compared to the phenazine-ring. It could be shown that tpac is less prone to interact with water than tpphz and that the changes of the photodynamics are minor. But instead, the impact of water on **RuPd3** is attributed to direct interactions between the catalytic Pd-centre and water molecules.

In the last chapter the effect of connection of two photoactive Ru-polypyridine units was examined. The experiments show a pump-intensity depending charge-transfer behavior: When the intensity of the photoexcitation is low and only one of the photocentres is excited, the typical excited-state dynamics is observed as e.g. for Rudppz. Upon increasing

5. Conclusion

the pump-intensity both light-harvesting units are excited and the deactivation mechanism switches to an annihilation process by intramolecular interaction between the two excited states. Such a process is observed for the first time in a homodinuclear metal-complex and was only known for polymers or dendrimers with a high amount of chromophores.

Altogether the results show the great opportunities of supramolecular photocatalysts. As one of their major advantages the photophysical properties of such systems can be observed directly. Thereby with the help of several spectroscopic techniques the great impact of regiospecific variations like bromination is presented. As these, rather small, modifications lead to explicit alteration in the photophysical behaviour, the possibilities for the introduction of larger organic substituents to control the charge-transfer properties by extension of the molecular framework should be enormous.

6. Zusammenfassung

Diese Arbeit liefert einen zusammenfassenden Überblick der photophysikalischen Eigenschaften verschiedener Rutheniumpolypyridinkomplexe. Das übergeordnete Ziel bestand darin, den Einfluss von Substitutionen auf den lichtinduzierten Ladungstransfer der Photokatalysatoren zu charakterisieren. Dabei fanden eine Vielzahl spektroskopischer Methoden Anwendung: Die UV/vis-Absorptions- und Emissionsspektroskopie, die Messung von Emissionsquantenausbeuten, das *time-correlated single-photon counting* sowie die femtosekundenzeitaufgelöste transiente Absorptionsspektroskopie. Dieses Methodenrepertoire wurde durch die Verwendung quantenchemischer Rechnungen vervollständigt. Der Einsatz dieser spektroskopischen Techniken ermöglichte einen Einblick in die Möglichkeiten welche sich bieten um die rutheniumpolypyridin-basierten photokatalytischen Systeme zu verbessern. Es konnte hierbei gezeigt werden, dass schon einfachste Veränderungen am Brückenliganden, welcher das photoaktive mit dem katalytisch aktiven Zentrum des Photokatalysators verbindet, oder der Lösungsumgebung ausreichen um gravierende Veränderungen am photophysikalischen Verhalten dieser komplexen Systeme zu erhalten.

Die Grundlage für diese Studie bilden die Untersuchungen an regioselektiv substituierten Rudppz (dppz = dipyrido[3, 2' - a : 2', 3, 3' - c]phenazin) Komplexen, welche sich als geeignete Modelle für das supramolekulare System $[(tbbpy)_2RutpphzPdCl_2](PF_6)_2$ (tbbpy = 4,4'-di-tert-butyl-2,2'-bipyridin, tpphz = tetrapyrido[3, 2 - a : 2', 3'c : 3'', 2'' - h : 2''', 3''' - j]phenazin, **RuPd1**), erwiesen haben. An diesen verschiedenen substituierten Modellkomplexen konnte mit einer Kombination aus Raman-Spektroskopie und quantenchemischen Rechnungen gezeigt werden, dass im elektronischen Grundzustand die strikte Trennung des dppz-Liganden in Phenanthrolin (phen) und Phenazin-Sphäre (phz) nicht möglich ist.

Auch die elektronisch angeregten Zustände der Rudppz-komplexe werden durch die Substitutionen an der phen- und phz-Sphäre beeinflusst. So lässt sich mit Hilfe von einfacher Bromierung der lichtinduzierte Ladungstransfer innerhalb des Komplexes steuern: Erfolgt die Bromierung am phen, so wird die Lumineszenz signifikant verstärkt, während

6. Zusammenfassung

der gegenteilige Effekt durch Bromierung des phz erreicht wird. Der zugrundeliegende Mechanismus konnte mit Hilfe der transienten Absorptionsspektroskopie aufgeklärt werden: Durch die elektronenziehenden, induktiven Eigenschaften der Bromsubstituenten wird der am substituierten Molekülteil lokalisierte angeregte Zustand energetisch stabilisiert. Folglich wird nach der elektronischen Anregung für die Rückkehr in den Grundzustand der Relaxationsweg bevorzugt, welcher über den bromsubstituierten Teil des dppz läuft. Da nur der auf dem phen lokalisierte Zustand lumineszent ist, ist es möglich, die schwache Emission des Ru-dppz-Komplexes mit der phen-zentrierten Bromierung drastisch zu erhöhen, beziehungsweise mit der phz-zentrierten Bromierung vollständig zu unterdrücken. Somit konnte in diesem Fall ein substitutionskontrolliertes Gleichgewicht der angeregten Zustände beobachtet werden.

Nachdem anhand des Modellkomplexes deutlich wurde, dass die Bromierung einen sehr großen Einfluss auf dessen Photophysik ausübt, bestand der nächste Schritt darin, aufzuzeigen, wie diese sich auf den Photokatalysator **RuPd1** auswirkt. Hierbei wurde beobachtet, dass die Bromierung an der dem Photozentrum benachbarten phen-Sphäre des tp-phz-Brückenliganden den Ladungstransfergradienten im gesamten Molekül senkt. Dies bedeutet, dass, wie im Modellkomplex, die einzelnen phen- und phz-zentrierten angeregten Zustände der beiden Photokatalysatoren nicht unabhängig voneinander betrachtet werden dürfen. Außerdem wurde anhand der Zugabe von Wasser zu reinem Acetonitril als Lösungsmittel eine direkte Wechselwirkung zwischen den Wassermolekülen und den Komplexen deutlich, welche sich in einer schnelleren Rückkehr zum Grundzustand manifestiert. Durch diese Wechselwirkung wird, neben dem Ladungstransfer zum katalytisch wirkenden Pd-Zentrum, ein weiterer photoinduzierter Reaktionsweg ermöglicht oder zumindest bevorzugt, welcher in direkter Konkurrenz zum gewünschten Ladungstransfer steht. Anhand dieses Ergebnisses wird die ambivalente Rolle des Wassers bei der katalytischen Reaktion beider Komplexe deutlich: Zum einen wird die katalytische Aktivität durch Zugabe kleiner Mengen Wasser erhöht, zum anderen behindert die Wechselwirkung von Wasser den gewünschten Ladungstransfer zum katalytisch aktiven Pd-Zentrum. Dies könnte einen der Gründe darstellen, weswegen die katalytische Aktivität beider Komplexe bei zu hoher Wasserkonzentration sinkt.

Entsprechend dieser ungewünschten Wechselwirkung zwischen Wasser und den betrachteten Photokatalysatoren folgte die photophysikalische Charakterisierung des katalytisch aktiven Komplexes $[(tbbpy)_2RutpacPdCl_2](PF_6)_2$ (tpac = tetrapyrido [3,2-a:2',3'-c:3'',2''-h:2''',3'''-j]acridin, **RuPd3**). Diese Variation zielt darauf ab, dass der Brückenligand tpac aufgrund der kleineren Anzahl der Stickstoffatome im Vergleich

6. Zusammenfassung

zum tp_{phz} eine verminderte Wechselwirkung mit Wasser zeigen sollte. Der Einfluss des neuen Brückenliganden auf die Photodynamik des Komplexes ist gering und es konnte gezeigt werden, dass die Interaktion zwischen tp_{ac} und Wasser kleiner ist. Allerdings wurde auch beobachtet, dass diese Wechselwirkung bei **RuPd3** nun stärker am katalytisch aktiven Pd-zentrum stattfindet.

Der letzte Abschnitt dieser Arbeit behandelt den Effekt den zwei direkt benachbarte Lichtsammelinheiten aufeinander ausüben. Dafür wurden die Experimente der transienten Absorption in Abhängigkeit zur Intensität des eingestrahltten Lichtes durchgeführt. Ist diese Intensität gering, wird nur eines der beiden Photozentren angeregt und eine für Ru-polypyridinkomplexe normale Photodynamik beobachtet. Durch Erhöhung der Lichtintensität wird die Anregung beider Lichtsammelzentren erreicht. Dadurch ändert sich der Deaktivierungsmechanismus in einen Annihilationsprozess, der durch eine direkte Wechselwirkung zwischen beiden angeregten Zuständen zustande kommt; ein Effekt wie er bisher zum ersten mal an homodinuklearen Metallkomplexen beobachtet werden konnte und bisher nur für Polymere und Dendrimere mit einer hohen Anzahl an Chromophoren bekannt war.

Die Zusammenfassung dieser Ergebnisse zeigt die vorhandenen Möglichkeiten supra-molekularer homogener Photokatalysatoren auf. Einer der größten Vorteile ist, dass die photophysikalischen Eigenschaften derartiger Systeme direkt beobachtet werden können. Dementsprechend trägt die vorliegende Arbeit dazu bei, mit Hilfe verschiedener spektroskopischer Techniken den Einfluss chemischer Variationen auf die Photokatalysatoren zu ergründen. Der enorme Einfluss auf die Photodynamiken, der anhand der sehr moderaten Variationen schon erreicht werden kann, zeigt dabei auf, dass die Einführung komplexerer organischer Substituenten in das molekulare Grundgerüst eine enorme Vielfalt an Möglichkeiten bieten wird um die photophysikalischen Eigenschaften dieser katalytisch aktiven Systeme in die gewünschte Richtung zu verändern.

Bibliography

- [1] METZ, B.; DAVIDSON, O. R.; BOSCH, P. R.; DAVE, R.; MEYER, L. A. (: In: *IPCC Fourth Assessment Report: Climate Change 2007* (2007).
- [2] LEWIS, N.S.; NOCERA, D.G.: Powering the planet: Chemical challenges in solar energy utilization. In: *PNAS* 103 (2006), S. 15729–15735.
- [3] NOCERA, D.: Living healthy on a dying planet. In: *Chem. Soc. Rev.* 38 (2009), S. 13–15.
- [4] LUBITZ, W.; TUMAS, W.: Hydrogen: An Overview. In: *Chem. Rev.* 107 (2007), S. 3900–3903.
- [5] SUNDSTRÖM, V.: Light in elementary biological reactions. In: *Prog. Quant. Elec.* 24 (2000), S. 187–238.
- [6] BARBER, J.; ANDERSSON, B.: Revealing the blueprint of photosynthesis. In: *Nature* 370 (1994), S. 31–35.
- [7] FUJISHIMA, A.; HONDA, K.: Electrochemical Photolysis of Water at a Semiconductor Electrode. In: *Nature* 238 (1972), S. 37–38.
- [8] LEHN, J.-M.; SAUVAGE, J.-P.: Chemical storage of light energy Catalytic generation of hydrogen by visible light or sunlight. Irradiation of neutral aqueous solutions. In: *Nouv. J. Chim.* 1 (1977), S. 449–451.
- [9] KALYANASUNDARAM, K.; KIWI, J.; GRÄTZEL, M.: Hydrogen Evolution from Water by Visible Light, a Homogeneous three Component Test System for Redox Catalysis. In: *Helv. Chim. Acta* 61 (1978), S. 2720–2730.
- [10] BALZANI, V.; MOGGI, L.; MANFRIN, M. F.; BOLLETTA, F.; GLERIA, M.: Solar Energy Conversion by Water Photodissociation. In: *Science* 189 (1978), S. 852–856.

Bibliography

- [11] KHASELEV, O.; TURNER, J. A.: A Monolithic Photovoltaic-Photoelectrochemical Device for Hydrogen Production via Water Splitting. In: *Science* 280 (1998), S. 425–427.
- [12] KUDO, A.; MISEKI, Y.: Heterogeneous photocatalyst materials for water splitting. In: *Chem. Soc. Rev.* 38 (2009), S. 253–278.
- [13] GRÄTZEL, M.; MOSER, M. E.: *Electron Transfer in Chemistry*. Bd. Vol. 5. Wiley-VCH: Weinheim, Germany, 2001, S. 589–644.
- [14] TINKER, L. L.; MCDANIEL, N. D.; CURTIN, P. N.; SMITH, C. K.; IRELAND, M. J.; BERNHARD, S.: Visible Light Induced Catalytic Water Reduction without an Electron Relay. In: *Chem. Eur. J.* 13 (2007), S. 8726 – 8732.
- [15] MOURTZIS, N.; CONTRERAS CARBALLADA, P.; FELICE, M.; NOLTE, R. J. M.; WILLIAMS, R. M.; DE COLA, L.; FEITERS, M. C.: Cyclodextrin-based systems for photoinduced hydrogen evolution. In: *Phys. Chem. Chem. Phys.* 13 (2011), S. 7903–7909.
- [16] HAGIWARA, H.; ONO, N.; INOUE, T.; MATSUMOTO, H.; ISHIHARA, T.: Dye-Sensitizer Effects on a Pt/KTa(Zr)O₃ Catalyst for the Photocatalytic Splitting of Water. In: *Angew. Chem. Int. Ed.* 45 (2006), S. 1420 –1422.
- [17] NGWENIFORM, P.; KUSUMOTO, Y.; IKEDA, M.; SOMEKAWA, S.; AHMAD, B.: Conformation-dependent photoinduced hydrogen evolution with Co(II)tetraphenylporphyrin–poly(l-glutamate) complex. In: *J. Photochem. Photobiol. A* 189 (2007), S. 198–204.
- [18] ELVINGTON, M.; BROWN, J.; ARACHCHIGE, S.M.; BREWER, K.J.: Photocatalytic Hydrogen Production from Water Employing A Ru, Rh, Ru Molecular Device for Photoinitiated Electron Collection. In: *J. Am. Chem. Soc.* 129 (2007), S. 10644–10645.
- [19] OZAWA, H.; HAGA, M.; SAKAI, K.: A Photo-Hydrogen-Evolving Molecular Device Driving Visible-Light-Induced EDTA-Reduction of Water into Molecular Hydrogen. In: *J. Am. Chem. Soc.* 128 (2006), S. 4926–2927.
- [20] FIIHRI, A.; ARTERO, V.; PEREIRA, A.; FONTECAVE, M.: Efficient H₂-producing photocatalytic systems based on cyclometalated iridium- and tricarbonylrhenium-diimine photosensitizers and cobaloxime catalysts. In: *Dalton Trans.* (2008), S. 5567–5569.

Bibliography

- [21] LEI, P.; HEDLUND, M.; LOMOTH, R.; RENSMO, H.; JOHANSSON, O.; HAMMARSTRÖM, L.: The Role of Colloid Formation in the Photoinduced H₂ Production with a Ru^{II}-Pd^{II} Supramolecular Complex: A Study by GC, XPS, and TEM. In: *J. Am. Chem. Soc.* 130 (2008), S. 26–27.
- [22] RAU, S.; SCHÄFER, B.; GLEICH, D.; ANDERS, E.; RUDOLPH, M.; FRIEDRICH, M.; GÖRLS, H.; HENRY, W.; VOS, J.G.: Ein supramolekularer Photokatalysator zur Erzeugung von Wasserstoff und zur selektiven Hydrierung von Tolan. In: *Angew. Chem.* 118 (2006), S. 6361–6364.
- [23] SCHOENLEIN, R. W.; PETEANU, L. A.; MATHIES, R. M.; SHANK, C. V.: The first step in vision: femtosecond isomerization of rhodopsin. In: *Science* 254 (1991), S. 412–415.
- [24] CAMPAGNA, S.; PUNTORIERO, F.; NASTASI, F.; BERGAMINI, G.; BALZANI, V.: Photochemistry and Photophysics of Coordination Compounds II. In: *Top. Curr. Chem.* 280 (2007), S. 117–214.
- [25] HAMMARSTRÖM, L.; JOHANSSON, O.: Expanded bite angles in tridentate ligands. Improving the photophysical properties in bistridentate Ru^{II} polypyridine complexes. In: *Coord. Chem. Rev.* 254 (2010), S. 2546–2559.
- [26] JURIS, A.; BALZANI, V.; BARIGELLETTI, F.; CAMPAGNA, S.; BELSER, P.; VON ZELEWSKI, A.: Ru(II) Polypyridine Complexes: Photophysics, Photochemistry, Electrochemistry and Chemiluminescence. In: *Coord. Chem. Rev.* 84 (1988), S. 85–277.
- [27] DURHAM, B.; CASPAR, J. V.; NAGLE, J. K.; MEYER, T. J.: Photochemistry of Ru(bpy)₃²⁺. In: *J. Am. Chem. Soc.* 104 (1982), S. 4803–4810.
- [28] DAMRAUER, N.; CERULLO, G.; YEH, A.; BOUSSIE, T.R.; SHANK, C.V.; MCCUSKER, J.K.: Femtosecond Dynamics of Excited-State Evolution in [Ru(bpy)₃]²⁺. In: *Science* 275 (1997), S. 54–58.
- [29] YEH, A.T.; SHANK, C.V.; MCCUSKER, J.K.: Ultrafast Electron Localization Dynamics Following Photo-Induced Charge Transfer. In: *Science* 289 (2000), S. 935–938.
- [30] WALLIN, S.; DAVIDSSON, J.; MODIN, J.; HAMMARSTRÖM, L.: Femtosecond Transient Absorption Anisotropy Study on [Ru(bpy)₃]²⁺ and [Ru(bpy)(py)₄]²⁺.

Bibliography

- Ultrafast Interligand Randomization of the MLCT State. In: *J. Phys. Chem. A* 109 (2005), S. 4697–4704.
- [31] BALZANI, V.; VENTURI, M.; CAMAGNA, S.; SERRONI, S.: Luminescent and Redox-Active Polynuclear Transition Metal Complexes. In: *Chem. Rev.* 96 (1996), S. 759–833.
- [32] DIETZEK, B.; AKIMOV, D.; KIEFER, W.; RAU, S.; POPP, J.; SCHMITT, M.: Excited-state dynamics of $\text{Ru}(\text{tbbpy})_3^{2+}$ investigated by femtosecond time-resolved four-wave mixing. In: *Laser Phys. Lett.* 4 (2007), S. 121–125.
- [33] BHASIKUTTAN, A.C.; SUZUKI, M.; NAKASHIMA, S.; OKADA, T.: Ultrafast Fluorescence Detection in Tris(2,2'-bipyridine)ruthenium(II) Complex in Solution: Relaxation Dynamics Involving Higher Excited States. In: *J. Am. Chem. Soc.* 124 (2002), S. 8398–8405.
- [34] NAKAMURA, K.: Synthesis, Luminescence Quantum Yields, and Lifetimes of Trischelated Ruthenium(II) Mixed-ligand Complexes Including 3,3'-Dimethyl-2,2'-bipyridyl. In: *Bull. Chem. Soc. Jap.* 55 (1982), S. 2697–1705.
- [35] JENKINS, Y.; FRIEDMAN, A.E.; TURRO, N.J.; BARTON, J.K.: Characterization of dipyridophenazine complexes of ruthenium(II): The light switch effect as a function of nucleic acid sequence and conformation. In: *Biochemistry* 31 (1992), S. 10809–10816.
- [36] TURRO, C.; BOSSMANN, S.H.; JENKINS, Y.; BARTON, J.K.; TURRO, N.J.: Proton Transfer Quenching of the MLCT Excited State of $\text{Ru}(\text{phen})_2\text{dppz}^{2+}$ in Homogeneous Solution and Bound to DNA. In: *J. Am. Chem. Soc.* 117 (1995), S. 9026–9032.
- [37] NEUGEBAUER, U.; PELLEGRIN, Y.; DEVOCELLE, M.; FORSTER, R. J.; SIGNAC, W.; MORAN, N.; KEYES, T. E.: Ruthenium polypyridyl peptide conjugates: membrane permeable probes for cellular imaging. In: *Chem. Comm.* (2008), S. 5307–5309.
- [38] FERNANDEZ-MOREIRA, V.; THORP-GREENWOOD, F. L.; COOGAN, M. P.: Application of d^6 transition metal complexes in fluorescence cell imaging. In: *Chem. Comm.* 46 (2010), S. 186–202.
- [39] GRÄTZEL, M.: Photoelectrochemical cells. In: *Nature* 414 (2001), S. 338–344.

Bibliography

- [40] GRAY, H. B.; WINKLER, J. R.: Long-Range Electron Transfer Special Feature: Long-range electron transfer. In: *Proc. Nat. Acad. Science* 102 (2005), S. 3534–3539.
- [41] TSCHIERLEI, S.; KARNAHL, M.; PRESSELT, M.; DIETZEK, B.; GUTHMULLER, J.; GONZALES, L.; SCHMITT, M.; RAU, S.; POPP, J.: Photochemisches Schicksal: Der erste Schritt bestimmt die Effizienz der H₂-Bildung mit einem supramolekularen Photokatalysator. In: *Ang. Chemie* 122 (2010), S. 4073–4076.
- [42] TSCHIERLEI, S.; PRESSELT, M.; KUHN, C.; YARTSEV, A.; PASCHER, T.; SUNDSTRÖM, V.; KARNAHL, M.; SCHWALBE, M.; SCHÄFER, M.; RAU, S.; SCHMITT, M.; DIETZEK, B.; POPP, J.: Photophysics of an Intramolecular Hydrogen-Evolving Ru–Pd Photocatalyst. In: *Chem. Eur. J.* 15 (2009), S. 7678–7688.
- [43] OLSON, E.J.C.; HU, D.; HÖRMANN, A.; JONKMANN, A.M.; ARKIN, M.R.; STEMP, E.D.A.; BARTON, J.K.; BARBARA, P.F.: First Observation of the Key Intermediate in the “Light-Switch” Mechanism of [Ru(phen)₂dppz]²⁺. In: *J. Am. Chem. Soc.* 119 (1997), S. 11458–11467.
- [44] SCHOONOVER, J.R.; BATES, W.D.; MEYER, T. J.: Application of Resonance Raman Spectroscopy to Electronic Structure in Metal Complex Excited States. Excited-State Ordering and Electron Delocalization in Dipyrido[3,2-*a*:2',3'-*c*]phenazine (dppz): Complexes of Re(I) and Ru(II). In: *Inorg. Chem.* 34 (1995), S. 6421–6422.
- [45] BRENNAMAN, M.K.; ALSTRUM-ACEVEDO, J.H.; FLEMING, C.N.; JANG, P.; MEYER, T.J.; PAPANIKOLAS, J.M.: Turning the [Ru(bpy)₂dppz]²⁺ Light-Switch On and Off with Temperature. In: *J. Am. Chem. Soc.* 124 (2002), S. 15094–15098.
- [46] FRIEDMAN, A.E.; CHAMBRON, J.C.; SAUVAGE, J.P.; TURRO, N.J.; BARTON, J.K.: Molecular “Light Switch” for DNA *Ru(bpy)₂(dppz)²⁺*. In: *J. Am. Chem. Soc.* 112 (1990), S. 4960–4962.
- [47] FEES, J.; KAIM, W.; MOSCHEROSCH, M.; MATHEIS, W.; KLIMA, J.; KREJCIK, M.; ZALIS, S.: Electronic structure of the “molecular light switch” bis(bipyridine)dipyrido[3,2-*a*:2',3'-*c*]phenazineruthenium(2+). Cyclic voltammetric, UV/visible and EPR/ENDOR study of multiply reduced complexes and ligands. In: *Inorg. Chem.* 32 (1993), S. 166–174.

Bibliography

- [48] SUN, Y.; LUTTERMAN, D.A.; TORRO, C.: Role of Electronic Structure on DNA Light-Switch Behavior of Ru(II) Intercalators. In: *Inorg. Chem.* 47 (2008), S. 6427–6434.
- [49] PILZ, T. D.; ROCKSTROH, N.; RAU, S.: Synthesis and characterisation of heterooligonuclear ruthenium complexes with tri(phenanthroline)hexaazatriphenylene ligands. In: *J. Coord. Chem.* 63 (2010), S. 2727.
- [50] DIETZEK, B.; KIEFER, W.; BLUMHOFF, J.; BÖTTCHER, L.; RAU, S.; WALTHER, D.; UHLEMAN, U.; SCHMITT, M.; POPP, J.: Ultrafast Excited-State Excitation Dynamics in a Quasi-Two-Dimensional Light-Harvesting Antenna Based on Ruthenium(II) and Palladium(II) Chromophores. In: *Chem. Eur. J.* 12 (2006), S. 5105–5115.
- [51] LEHN, J.; SANDERS, J.K. (Hrsg.): *Supramolecular Chemistry: Concept and Perspectives*. VCH Verlagsgesellschaft, Weinheim, 1995.
- [52] ESSWEIN, A. J.; NOCERA, D. C.: Hydrogen Production by Molecular Photocatalysis. In: *Chem. Rev.* 107 (2007), S. 4022–4047.
- [53] GRÄTZEL, M.: Solar Energy Conversion by Dye-Sensitized Photovoltaic Cells. In: *Inorg. Chem.* 44 (2005), S. 6841–6851.
- [54] RAU, S.; WALTHER, D.; VOS, J. G.: Inspired by nature: light driven organometallic catalysis by heterooligonuclear Ru(II) complexes. In: *Dalton Trans.* (2007), S. 915–919.
- [55] COOPER, J. B.; DREW, M. G. B.; BEER, P. D.: In: *J. Chem. Soc., Dalton Trans.* (2001), S. 392–401.
- [56] BEER, P. D.; HAYES, E. J.: In: *Coord. Chem. Rev.* 240 (2003), S. 167–189.
- [57] RAU, S.; BÜTTNER, T.; TEMME, C.; RUBEN, M.; GÖRLS, H.; WALTHER, D.; DUATI, M.; FANNI, S.; VOS, J. G.: In: *Inorg. Chem.* 39 (2003), S. 1621–1624.
- [58] MACGRAITH, B. D.; MCDONAGH, C. M.; O'KEEFE, G.; KEYES, E. T.; VOS, J. G.; O'KELLY, B.; MCGILP, J. F.: In: *Analyst* 118 (1993), S. 385–388.
- [59] CHAMBRON, J.-C.; SAUVAGE, J.-P.; AMOUYAL, E.; KOFFI, P.: In: *New. J. Chem.* 9 (1985), S. 527–529.

Bibliography

- [60] HARTSHORN, R.M.; BARTON, J.K.: Novel dipyrrophenazine complexes of ruthenium(II): exploring luminescent reporters of DNA. In: *J. Am. Chem. Soc.* 114 (1992), S. 5919–5925.
- [61] OLOFSSON, J.; ÖNFELT, B.; LINCOLN, P.: Three-State Light Switch of $[Ru(phen)_2dppz]^{2+}$: Distinct Excited-State Species with Two, One, or No Hydrogen Bonds from Solvent. In: *J. Phys. Chem. A* 108 (2004), S. 4391–4398.
- [62] BRENNAMAN, M.K.; MEYER, T.J.; PAPANIKOLAS, J.M.: $[Ru(bpy)_2dppz]^{2+}$ Light-Switch Mechanism in Protic Solvents as Studied through Temperature-Dependent Lifetime Measurements. In: *J. Phys. Chem. A* 108 (2004), S. 9938–9944.
- [63] FANTACCI, S.; DE ANGELIS, F.; SGAMELLOTTI, A.; RE, N.: A TDDFT study of the ruthenium(II) polyazaaromatic complex $[Ru(dppz)(phen)_2]^{2+}$ in solution. In: *Chem. Phys. Lett.* 396 (2004), S. 43–48.
- [64] BATISTA, E. R.; MARTIN, R. L.: In: *J. Phys. Chem. A* 109 (2005), S. 3128–3133.
- [65] ATSUMI, M.; GONZALES, L.; CHANTAL, D.: Spectroscopy of Ru(II) polypyridyl complexes used as intercalators in DNA: Towards a theoretical study of the light switch effect. In: *J. Photochem. Photobiol., A: Chemistry* 190 (2007), S. 310–320.
- [66] CHEN, W.; TURRO, C.; FRIEDMANN, L.A.; BARTON, J.K.; TURRO, N.J.: Resonance Raman Investigation of $Ru(phen)_2(dppz)^{2+}$ and Related Complexes in Water and in the Presence of DNA. In: *J. Phys. Chem. B* 101 (1997), S. 6995–7000.
- [67] COATES, C.G.; OLOFSSON, J.; COLETTI, M.; MCGARVEY, J.J.; ÖNFELT, B.; LINCOLN, P.; NORDEN, B.; TUIE, E.; MATOUSEK, P.; PARKER, A.W.: Picosecond Time-Resolved Resonance Raman Probing of the Light-Switch States of $[Ru(Phen)_2dppz]^{2+}$. In: *J. Phys. Chem. B* 105 (2001), S. 12654–12664.
- [68] SCHMITT, M.; POPP, J.: Raman spectroscopy at the beginning of the twenty-first century. In: *J. Raman Spectrosc.* 37 (2006), S. 20–28.
- [69] JALKANEN, K. J.; WÜRTZ JÜRGENSEN, V.; CLAUSSEN, A.; RAHIM, A.; JENSEN, G. M.; WADE, R. C.; NARDI, F.; JUNG, C.; DEGTYARENKO, I. M.; NIEMINEN, R. M.; HERRMANN, F.; KNAPP-MOHAMMADY, M.; NIEHAUS, T. A.; FRIMAND, K.; SUHAI, S.: Use of vibrational spectroscopy to study protein and DNA structure, hydration, and binding of biomolecules: A combined theoretical and experimental

Bibliography

- approach. In: *International Journal of Quantum Chemistry* 106 (2006), S. 1160–1198.
- [70] HERRMANN, C.; REIHER, M.: First-Principles Approach to Vibrational Spectroscopy of Biomolecules. In: *Top Curr. Chem.* 268 (2006), S. 85–132.
- [71] KOCH, W.; HOLTHAUSEN, M. C.: *A Chemist's Guide to Density Functional Theory*. Wiley-VCH, 2000.
- [72] KARNAHL, M.; KRIECK, S.; GÖRLS, H.; TSCHIERLEI, S.; SCHMITT, M.; POPP, J.; CHARTRAND, D.; HANAN, G.S.; GROARKE, R.; VOS, J. G.; RAU, S.: Synthesis and Photophysical Properties of 3,8-Disubstituted 1,10-Phenanthrolines and Their Ruthenium(II) Complexes. In: *Eur. J. Inorg. Chem.* 33 (2009), S. 4962–4971.
- [73] KARNAHL, M.; TSCHIERLEI, S.; KUHN, C.; DIETZEK, B.; SCHMITT, B.; POPP, J.; SCHWALBE, M.; KRIECK, S.; GÖRLS, H.; HEINEMANN, F. W.; RAU, S.: Synthesis and characterization of regioselective substituted tetrapyrrophenazine ligands and their Ru(II) complexes. In: *Dalton Trans.* 39 (2010), S. 2359–2370.
- [74] SCHÄFER, B.; GÖRLS, H.; PRESSELT, M.; SCHMITT, M.; POPP, J.; HENRY, W.; VOS, J.G.; RAU, S.: Derivatives of dipyrido[3,2-*a*:2',3'-*c*]phenazine and its ruthenium complexes, influence of aryl substitution on photophysical properties. In: *Dalton Trans.* 18 (2006), S. 2225–2231.
- [75] MYERS, A. B.: Resonance Raman Intensities and Charge-Transfer Reorganization Energies. In: *Chem. Rev.* 96 (1996), S. 911–926.
- [76] BARIGELLETTI, F.; DE COLA, L.; BALZANI, V.; BELSER, P.; VON ZELEWSKI, A.; VÖGTLE, F.; EBMAYER, F.; GRAMMENDI, S.: Caged and Uncaged Ruthenium(II)-Polypyridine Complexes. Comparative Study of the Photochemical, Photophysical, and Electrochemical Properties. In: *J. Am. Chem. Soc.* 111 (1989), S. 4662–4668.
- [77] OLOFSSON, J.; WILHELMSSON, L.M.; LINCOLN, P.: Effects of Methyl Substitution on Radiative and Solvent Quenching Rate Constants of $[Ru(phen)_2dppz]^{2+}$ in Polyol Solvents and Bound to DNA. In: *J. Am. Chem. Soc.* 126 (2004), S. 15458–15465.
- [78] COATES, C. G.; CALLAGHAN, P.; MCGARVEY, J. J.; KELLY, J. M.; JAQUET, L.; KIRSCH-DE MESMAECKER, A.: Spectroscopic studies of structurally similar

Bibliography

- DNA-binding Ruthenium (II) complexes containing the dipyrrophenazine ligand. In: *J. Mol. Struct.* 598 (2001), S. 15–25.
- [79] HOLZWARTH, A. R.: In: *Adv. Photosynth.* 3 (1996), S. 75–92.
- [80] DIETZEK, B.; TSCHIERLEI, S.; HERMANN, G.; YARTSEV, A.; PASCHER, T.; SUNDSTRÖM, V.; SCHMITT, M.; POPP, J.: Protochlorophyllide a: A Comprehensive Photophysical Picture. In: *ChemPhysChem* 10 (2009), S. 144–150.
- [81] BROWNE, W.R.; MCGARVEY, J.J.: Raman scattering and photophysics in spin-state-labile d6 metal complexes. In: *Coord. Chem. Rev.* 250 (2006), S. 1697–1706.
- [82] RANGAN, K.; ARACHCHIGE, S. M.; BROWN, J. R.; BREWER, K. J.: Solar energy conversion using photochemical molecular devices: photocatalytic hydrogen production from water using mixed-metal supramolecular complexes. In: *Energy Environ. Sci.* 2 (2009), S. 410–419.
- [83] INAGAKI, A.; AKITA, M.: Visible-light promoted bimetallic catalysis. In: *Coordination Chemistry Reviews* 254 (2010), S. 1220 – 1239.
- [84] CANNIZZO, A.; VAN MOURIK, F.; GAWELDA, W.; ZGRABLIC, G.; BRESSLER, C.; CHERGUI, M.: Broadband Femtosecond Fluorescence Spectroscopy of $[Ru(bpy)_3]^{2+}$. In: *Angew. Chem. Int. Ed.* 45 (2006), S. 3174–3176.
- [85] CHIORBOLI, C.; BIGNOZZI, C.A.; SCANDOLA, F.; ISHOW, E.; GORDON, A.; LAUNAY, J.-P.: Photophysics of Dinuclear Ru(II) and Os(II) Complexes Based on the Tetrapyrrodo[3,2-a:2',3'-c:3'',2''-h:2'''-3'''-j]phenazine (tpphz) Bridging Ligand. In: *Inorg. Chem.* 38 (1999), S. 2402–2410.
- [86] BENKÖ, Gábor; KALLIOINEN, Jani; KORPPI-TOMMOLA, Jouko E. I.; YARTSEV, Arkady P.; SUNDSTRÖM, Villy: Photoinduced Ultrafast Dye-to-Semiconductor Electron Injection from Nonthermalized and Thermalized Donor States. In: *Journal of the American Chemical Society* 124 (2002), S. 489–493.
- [87] CHIORBOLI, C.; ROGER, M.A.J.; SCANDOLA, F.: Ultrafast Processes in Bimetallic Dyads with Extended Aromatic Bridges. Energy and Electron Transfer Pathways in Tetrapyrrophenazine-Bridged Complexes. In: *J. Am. Chem. Soc.* 125 (2003), S. 483–491.
- [88] REICHARDT, C.: Empirische Parameter der Lösungsmittelpolarität. In: *Angew. Chem.* 77 (1965), S. 30–40.

Bibliography

- [89] DEMEUNYNCK, M.; MOUCHERON, C.; KIRSCH-DE MESMAEKER, A.: Tetrapyrido[3,2-*a*:2',3'-*c*:3'',2''-*h*:2''',3'''-*j*]acridine (tpac): a new extended polycyclic bis-phenanthroline ligand. In: *Tetrahedron Lett.* 43 (2002), S. 261–264.
- [90] ELIAS, B.; HERMAN, L.; MOUCHERON, C.; KIRSCH-DE MESMAEKER, A.: Dinuclear Ru^{II}PHEHAT and -TPAC Complexes: Effects of the Second Ru^{II} Center on Their Spectroelectrochemical Properties. In: *Inorg. Chem.* 46 (2007), S. 4979–4988.
- [91] HERMAN, A.; ELIAS, B.; PIERARD, C.; KIRSCH-DE MESMAEKER, A.: Effects of Protonation on the Spectroscopic Properties of Tetrapyridoacridine (TPAC) Mono- and Dinuclear Ru(II) Complexes in Their Ground and ³MLCT Excited States. In: *J. Phys. Chem. A* 111 (2007), S. 9756–9763.
- [92] KOMATSUZAKI, N.; KATOH, R.; HIMEDA, Y.; SUGIHARA, H.; H., Arakawa; KASUGA, K.: Structure and photochemical properties of ruthenium complexes having dimethyl-substituted DPPZ or TPPHZ as a ligand. In: *J. Chem. Soc., Dalton Trans.* (2000), S. 3053–3054.
- [93] CAMPAGNA, S.; SERRONI, S.; BODIGE, S.; MACDONNELL, F. M.: Absorption Spectra, Photophysical Properties, and Redox Behavior of Stereochemically Pure Dendritic Ruthenium(II) Tetramers and Related Dinuclear and Mononuclear Complexes. In: *Inorg. Chem.* 38 (1999), S. 692–701.
- [94] BODIGE, S.; TORRES, A. S.; MALONEY, D. J.; TATE, D.; KINSEL, G. R.; WALKER, A. K.; MACDONNELL, F. M.: First-Generation Chiral Metallodendrimers: Stereoselective Synthesis of Rigid D₃-Symmetric Tetranuclear Ruthenium Complexes. In: *J. Am. Chem. Soc.* 119 (1997), S. 10364–10369.
- [95] FLEMING, C. N.; MAXWELL, K. A.; DESIMONE, J. M.; MEYER, T.J.; PAPANIKOLAS, J. M.: Ultrafast Excited-State Energy Migration Dynamics in an Efficient Light-Harvesting Antenna Polymer Based on Ru(II) and Os(II) Polypyridyl Complexes. In: *J. Am. Chem. Soc.* 123 (2001), S. 10336–10347.
- [96] ISHOW, E.; GOURDON, A.; LAUNAY, J.-P.; LECANTE, P.; VERELST, M.; CHIORBOLI, C.; SCANDOLA, F.; BIGNOZZI, C.-A.: Tetranuclear Tetrapyrido[3,2-*a*:2',3'-*c*:3'',2''-*h*:2''',3'''-*j*]phenazineruthenium Com-

Bibliography

- plex: Synthesis, Wide-Angle X-ray Scattering, and Photophysical Studies. In: *Inorg. Chem.* 37 (1998), S. 3603–3609.
- [97] LARSEN, J.; BRÜGGEMANN, B.; POLIVKA, T.; SUNDSTRÖM, V.; AKESSON, E.; SLY, J.; CROSSLEY, M. J.: Energy Transfer within Zn-Porphyrin Dendrimers: Study of the Singlet-Singlet Annihilation Kinetics. In: *J. Phys. Chem. A* 109 (2005), S. 10654–10662.
- [98] SCHEBLYKIN, I. G.; YARTSEV, A.; PULLERITS, T.; GULBINAS, V.; SUNDSTRÖM, V.: Excited State and Charge Photogeneration Dynamics in Conjugated Polymers. In: *J. Phys. Chem. B* 111 (2007), S. 6303–6321.
- [99] LAQUAI, F.; PARK, Y.-S.; KIM, J.-J.; BASCHE, T.: Excitation Energy Transfer in Organic Materials: From Fundamentals to Optoelectronic Devices. In: *Macromolecular Rapid Communications* 30 (2009), Nr. 14, S. 1203–1231.
- [100] GUT, D.; GOLDBERG, I.; KOL, M.: Eilatin as a Bridging Ligand in Ruthenium(II) Complexes: Synthesis, Crystal Structures, Absorption Spectra and Electrochemical Properties. In: *Inorganic Chemistry* 42 (2003), S. 3483–3491.
- [101] FUJITA, M.; ISHIDA, A.; MAJIMA, T.; TAKAMUKU, S.: Lifetimes of Radical Anions of Dicyanoanthracene, Phenazine, and Anthraquinone in the Excited State from the Selective Electron-Transfer Quenching. In: *J. Phys. Chem.* 100 (1996), S. 5382–5387.
- [102] HODGKISS, J. M.; CAMPBELL, A. R.; MARSH, R. A.; RAO, A.; ALBERTSEIFRIED, S.; FRIEND, R. H.: Subnanosecond Geminate Charge Recombination in Polymer-Polymer Photovoltaic Devices. In: *Phys. Rev. Lett.* 104 (2010), S. 177701.
- [103] SHAW, G. B.; PAPANIKOLAS, J. M.: Triplet-Triplet Annihilation of Excited States of Polypyridyl Ru(II) Complexes Bound to Polystyrene. In: *J. Phys. Chem. B* 106 (2002), S. 6156–6162.

A. Publikationen

[CK1] Investigation of substitution effects on novel Ru–dppz complexes by Raman spectroscopy in combination with DFT methods

Der Nachdruck der folgenden Publikation erfolgt mit freundlicher Genehmigung von John Wiley & Sons Ltd..

Reproduced with permission from:

C. Kuhnt, S. Tschierlei, M. Karnahl, S. Rau, B. Dietzek, M. Schmitt., J. Popp; INVESTIGATION OF SUBSTITUTION EFFECTS ON NOVEL RU–DPPZ COMPLEXES BY RAMAN SPECTROSCOPY IN COMBINATION WITH DFT METHODS, *J. Raman Spectrosc.*, **2010**, *41*, 922-932.

Copyright 2009 John Wiley & Sons, Ltd.

Investigation of substitution effects on novel Ru–dppz complexes by Raman spectroscopy in combination with DFT methods

Christian Kuhnt,^{a†} Stefanie Tschierlei,^{a†} Michael Karnahl,^b Sven Rau,^c Benjamin Dietzek,^{a,d} Michael Schmitt^a and Jürgen Popp^{a,d*}

We present a combined Raman–density functional theory (DFT) study of novel dipyrldophenazine (dppz) derivatives and their Ru–bipyridine complexes. Our results show that the molecular architecture of dppz and its Ru complexes can be considered to consist of two independent moieties, the structural ground state properties of which can be tuned independently by means of side-specific substitution. These results are expected to be of importance for the design of highly specific dppz-based DNA sensors. Methodologically, the results presented in this paper highlight the power of a combined Raman–DFT approach to unravel the details of the structural properties of complex molecules. Copyright © 2009 John Wiley & Sons, Ltd.

Keywords: Raman spectroscopy; ruthenium complexes; DFT calculations; dipyrldophenazine

Introduction

Raman spectroscopy has matured into a powerful tool in a variety of branches of science ranging from solid-state physics through planetary research to medical diagnostics.^[1] However, the interpretation of Raman spectra solely based on experimental data is very often challenging if not impossible since a clear assignment of the measured Raman bands to specific vibrations is partly unclear and often ambiguous. The only way to realize a reliable assignment of the experimentally observed Raman bands and hence to obtain a detailed understanding of the geometric and electronic structure of the analyte is by a thorough comparison with theoretically calculated spectra. Over the last two decades, quantum chemical calculations have emerged, which turned out to be highly successful in coping with this task.^[2]

Particularly, density functional theory (DFT) methods have developed into a powerful computational tool.^[3] Compared to conventional quantum chemical approaches, they are computationally much less demanding and take into account the effects of electron correlation. Hence, quantum chemical calculations, and in particular DFT, are nowadays an almost indispensable complement to experimental Raman studies. One of the most useful aspects of these calculations is the output of normal coordinates of each vibration. These normal coordinates provide explicit information about the properties of molecules and hence a deeper knowledge about the way these may be influenced or directed by changing intramolecular parameters, e.g. with substitutions, or intermolecular parameters, e.g. by changing the solvent.

In the present study, novel derivatives of dipyrldo[3,2-a:2',3'-c]phenazine (dppz) and [Ru(tbbpy)₂dppz]²⁺ (tbbpy = 4,4'-di-*tert*-butyl-2,2'-bipyridine) are introduced and investigated by a combination of Raman spectroscopy and DFT calculations. Ruthenium polypyridine complexes show in general high potential as model systems for investigation of photochemical processes as well as light-driven catalysis, and as building blocks for supramolecular arrays or multielectron storage systems.^[4–12] Especially, the

ruthenium dppz complexes are important photosensitizers^[13–17] and show the so-called light-switch effect that makes them suitable sensor molecules for DNA.^[18–22] Generally, the complex and rich photophysics of dppz and its complexes depend on a wide range of environmental parameters.^[23–28] Hence, photophysical processes occurring in such complexes have been the subject of extensive basic research.^[29–32]

To construct a basis for the investigation of the photophysics and photochemistry of these new Ru–dppz complexes, a detailed knowledge about the ground state properties of such compounds is essential. Thus, the investigations presented here aim at the examination of substitution effects on the ground state properties of novel dppz derivatives and their ruthenium complexes. To do so, bromine (Br) and phenylacetylene (phac) groups were attached to the dppz backbone (Fig. 1), for which the existence of two independent moieties, i.e. a phenanthroline and a phenazine sphere, is discussed in the literature in the context of the excited state properties of Ru–dppz complexes.^[16,24,33] To further investigate this conceptual model, we investigate the effect of side-specific substitution, i.e. substitution on either moiety, on the ground state structural properties of the molecule (Fig. 1). As the

* Correspondence to: Jürgen Popp, Institute for Physical Chemistry, Friedrich-Schiller-University Jena, Helmholtzweg 4, 07743 Jena, Germany.
E-mail: juergen.popp@uni-jena.de

† These authors have contributed equally to the presented work.

a Institute for Physical Chemistry, Friedrich-Schiller University Jena, 07743 Jena, Germany

b Institute for Anorganic and Analytical Chemistry, Friedrich-Schiller-University Jena, 07743 Jena, Germany

c Department for Chemistry and Pharmacy, Friedrich-Alexander-University Erlangen Nürnberg, 91058 Erlangen, Germany

d Institute of Photonic Technology Jena e.V., 07745 Jena, Germany

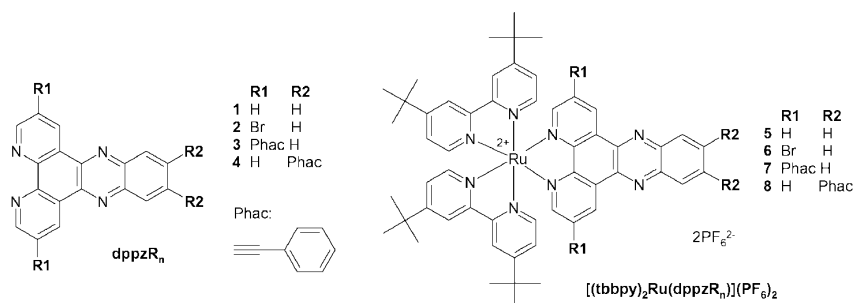


Figure 1. Chemical structures of the dppz-based ligands investigated in this study (1–4) and the corresponding ruthenium polypyridine complexes (5–8).

method of choice, Raman spectroscopy is chosen as it constitutes a structure-sensitive tool for the investigation of molecular properties. The Raman spectroscopic results are combined with results from DFT calculations to obtain optimized structures of the systems under investigation and to obtain detailed insight into the behavior of dppz.

This paper is organized as follows: A summary of the central experimental details is followed by a short discussion about the structure of the dppz derivatives, as obtained from DFT calculations, and their ruthenium complexes. Subsequently, a discussion of the experimental Raman spectra is presented. Finally, we discuss the additional insight into the structural properties as reflected by vibrational spectra obtained from the computational results. Here, a detailed analysis of both the experimental and calculated Raman spectra is presented, and some characteristic normal modes are chosen to highlight the influence of side-specific substitutions on the dppz backbone.

Experimental

Materials

The synthesis of the dppzR_n ligands and the corresponding ruthenium complexes will be published in due course elsewhere.

NIR micro-Raman spectroscopy

Non-resonant Raman spectra of the solids excited at 830 nm were recorded with a micro-Raman setup (LabRam invers, Jobin–Yvon–Horiba). This setup is equipped with an Olympus IX70 microscope and a video camera. The scattered light was detected by an air-cooled CCD camera operating at 298 K. An Olympus LMPlanSI 50× 0.5 BD objective focused the laser light on the solid samples. The grating of the spectrometer had 300 lines/mm and the validation of the wavenumber axis was done by using the Raman signals of TiO₂ (anatase). For excitation, an external cavity semiconductor laser (TEC100 Raman, Sacher Lasertechnik) with a wavelength of 830 nm was used.

Computational details

For calculations, the program package TURBOMOLE 5.71 suite^[34] was used. Structure optimizations as well as calculations of Raman wavenumbers and Raman intensities were performed with the BP86 functional by Becke^[35] and Perdew^[36] in combination with the RI-density approximation.^[37] A triple-zeta basis set named TZVPP that uses Schäfer *et al.*'s^[38] TZV-core and additional

polarization functions taken from the cc-pVTZ basis by Dunning^[39] and Woon and Dunning^[40,41] was used as implemented in TURBOMOLE. To account for the mass effect of the second-row metal ruthenium, the effective core potential mwb28 of the Stuttgart group^[42] was used as implemented in TURBOMOLE in our calculations.

For calculations of Raman wavenumbers, the program package SNF^[43] was employed. Hence, wavenumbers and Raman intensities were calculated numerically. No scaling factors for readjusting the calculated wavenumbers were applied.

Results and Discussion

Calculated molecular structures

As a starting point for our discussion of the substitution-dependent ground state properties of dipyrindophenazine derivatives and their respective Ru complexes, we will present first the structural results of the quantum chemical calculations. For cross-validation of this data, we exemplarily compare the calculated structure of **5** to the structural data of the related complex [Ru(tbbpy)₂(dppz-11,12-Br₂)](PF₆)₂ as obtained from X-ray diffraction analysis.^[22] For this complex, Ru–N bond lengths of 206.3 pm to the dppz donor nitrogens and of 205.3 pm to the tbbpy were found. Our calculations are in very good agreement with these experimental values: the calculated Ru–N(dppz) bond lengths of the complex [Ru(tbbpy)₂dppzR₅]²⁺ are 207.4 pm and 206.7 pm for the Ru–N(tbbpy) bonds. The angle N4–Ru–N5 was found to be 79.2° in both our calculations and the X-ray structure of [Ru(tbbpy)₂(dppz-11,12-Br₂)](PF₆)₂. Hence, we conclude that our approach of discussing the calculated molecular structures is valid and yields results with reasonable accuracy.

Structure of the ligands

Before considering the geometrical structure of the Ru complexes in detail, the influence of the substitutions on the structure of the unbound ligands is investigated first. For the ligands **1–3** (Fig. 1), where the phenanthroline sphere is varied by the substituents, planar structures with C_{2v} symmetry are found. The bond lengths obtained from the calculations are depicted in Table 1. The influences of the introduced substituents on the dppz core structure result in general in alterations of bond lengths of less than 1 pm, which are exclusively observed in the direct vicinity of the substituents. A more pronounced effect is observed only in the case of phac groups at the R1 position. Here, the bonds directly

Table 1. Summary of the chosen bond length in picometers. Numbering of atoms is according to Fig. 2

	Unbound ligands				Complexes			
	1	2	3	4	5	6	7	8
C ₁ –C ₂	138.4	138.2	139.9	138.4	138.9	139	140.9	138.7
C ₂ –C ₃	140.5	140.8	142.5	140.5	139.9	140.3	141.9	140
C ₃ –N ₄	133	132.7	132.2	133.1	134.8	134.6	134	134.7
N ₄ –C ₁₆	135	135	135.4	135	137.2	137.2	137.3	137.2
C ₁₆ –C ₁₇	147.5	147	146.4	147.4	143.9	143.5	143	143.6
C ₁₇ –N ₅	135	135	135.4	135	137.2	137.2	137.4	137.1
N ₅ –C ₆	133	132.7	132.2	133	134.8	134.6	134	134.7
C ₆ –C ₇	140.5	140.8	142.5	140.6	139.9	140.3	141.9	140
C ₇ –C ₈	138.4	138.2	139.9	138.3	138.8	139	140.9	138.7
C ₈ –C ₁₈	140.7	140.7	140	140.8	140.6	140.4	139.6	140.8
C ₁ –C ₁₅	140.7	140.7	140	140.7	140.6	140.4	139.6	140.8
C ₁₅ –C ₂₂	146.1	146.2	146.4	146	146.2	146.3	146.6	145.8
C ₁₈ –C ₁₉	146.1	146.2	146.4	146	146.2	146.3	146.6	145.8
C ₁₉ –C ₂₂	144.1	143.9	144	144.2	143.7	143.7	143.8	143.5
C ₂₀ –C ₂₁	144	144.3	144.4	144	145	145.1	144.8	145.4
C ₁₁ –C ₁₂	142.1	142.1	141.5	145.7	142.4	142.4	142.3	146.6
C ₂₀ –N ₉	133.2	133.1	133.1	133.3	133.1	133.1	133.1	133.6
C ₂₂ –N ₁₄	133.2	133.1	133.1	133.4	133.1	133.1	133.1	133.6
C ₁₀ –C ₁₁	137.8	137.7	137.8	139.1	137.7	137.7	137.7	139.3
C ₁₂ –C ₁₃	137.8	137.7	137.8	139.1	137.7	137.7	137.7	139.3

linked to the substitution, i.e. the bonds C₁–C₂ and C₂–C₃ (C₆–C₇, C₇–C₈) (Fig. 2), are elongated by 1.5 and 2.0 pm, respectively. In contrast to the fairly pronounced impact of phac, the influence of Br on the molecular structure is minor – resulting only in bond length changes of less than 0.5 pm.

The substitution on the phenazine moiety of dppz (R2) with phac groups perturbs the symmetry of the dppz core, which originates from significant steric interactions. The spatial proximity of the two alpha-H atoms of the phac phenyl rings leads to a repulsion and thus to a torsion of these rings with respect to the dppz plane (Fig. 3). Hence, the rings are twisted oppositely around the C–C triple-bond axis with an angle of approximately 15°. The dppz π -system might be slightly disturbed by the participation of the

twisted phac groups. Due to this, the C_{2v} symmetry of the noncoordinated ligand is broken and dihedral angles of at most 0.5° are found in the dppz backbone. Other effects on the dppz backbone were not found except a bond elongation in the direct neighbourhood to the substitution (C₁₀–C₁₁, C₁₁–C₁₂, C₁₂–C₁₃, Table 1). This finding is in agreement to the results obtained for **2** and **3**.

Altogether, the dppz structure is only marginally affected by the substituents on the phenanthroline sphere. Only bonds in direct vicinity of the substituents are affected by the substitution. In contrast, the steric repulsion of the phac groups on the phenazine sphere perturbs the planarity of dppz. Consequently, the symmetry of the ligand and the π -system is disturbed.

Structure of the complexes

On the basis of the calculated geometry data, the influence of complexation with the [Ru(tbbpy)₂]²⁺ moiety on bond lengths and angles of the ligand is explored. In order to reduce computational costs, the *tert*-butyl groups on the tbbpy ligands were replaced by methyl groups (Fig. 3) in the calculations. Generally, the introduction of the Ru moiety results in larger changes of the dppz core as compared to the influence of the different substitutions. This is in agreement with the results obtained for Ru–terpyridine complexes.^[44] In all cases, the planarity and hence the symmetry of dppz are lost. The covalent bonds between Ru and the pyridine donor atoms of the dppzR_n ligands, which are built up by the nitrogen lone pairs, lead to a small sp³ contribution to the nitrogen hybridization and to the dihedral angles up to 1° in the pyridine rings. Consequently, the related C–N bonds are extended by 1.4%. Due to the altered hybridization, the repulsion of the nitrogen lone pairs is reduced. This results in a contraction of the pyridine–pyridine distance along the C₁₆–C₁₇ bond, which shows a dominant single bond character in the unbound ligand **1**. The length of this bond is shortened from 147.5 pm (unbound ligand) to 143.9 pm (complex).

Regardless of the specific substitution, the coordination has only an effect on the phenanthroline moiety of the dppz ligand. The geometrical changes in the phenazine part are, if at all present, negligible (see also Ref. 23). In contrast to these purely geometrical considerations, this strict separation of phenanthroline and phenazine sphere will break down when considering the vibrational normal modes discussed below. There, we will argue

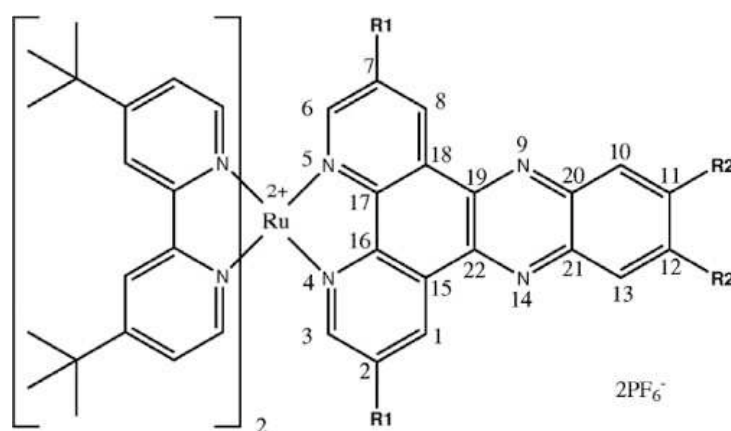


Figure 2. Scheme to assign the atomic numbering that is used to label individual atoms of the dppz ligands (1–4) and the respective ruthenium complexes (5–8).

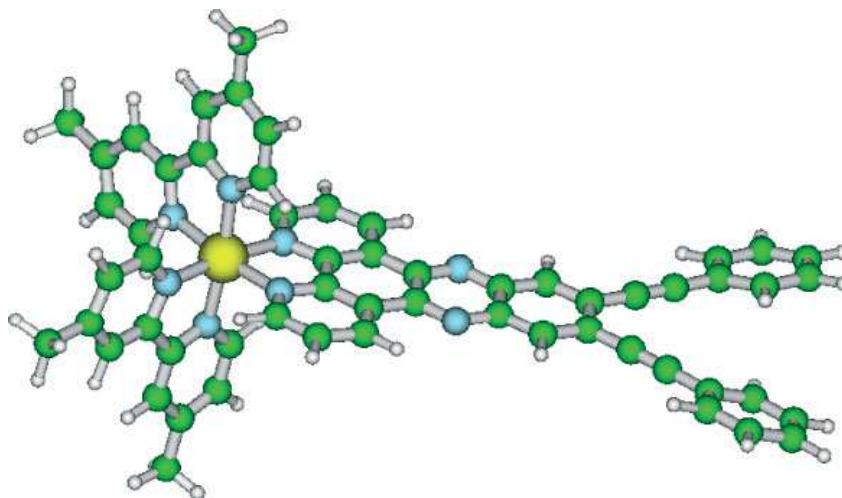


Figure 3. Calculated structure of **8**. The phac groups are twisted by steric stress resulting in a nonplanar geometry of the substituted dppz ligand.

that complexation induces vibrational coupling between normal modes centered on either moiety of the dppz ligand.

Experimental Raman spectra

Solid-state Raman spectra could be recorded for the compounds **1–3** and **5–7** (Fig. 1) with an excitation wavelength of 830 nm (Fig. 4). A comprehensive Raman band assignment can be found in Table 2. For the unbound ligands, the spectra are normalized to band 22 (nomenclature refers to Table 2). The Raman spectra of the complexes are normalized to band 46. A fluorescence background makes the ligand **4** and the complex **8** inaccessible for recording Raman spectra (this fluorescence originates from highly fluorescent salts that were needed for synthesis and could not be removed completely by any purification processes).^[1] In order to interpret the influence of the introduction of substituents or complexation on a molecular level, the experimental Raman spectra are analyzed by comparing them to the DFT calculated spectra.

Raman spectra of noncoordinated ligands

To be able to differentiate between effects due to substitution and due to complexation with the ruthenium metal center, the Raman spectra of the noncoordinated ligands are discussed separately from those of the complexes. First, the substitution effects on the unbound dppz ligands are described. The Raman spectra of **1** and **2** (Fig. 4) are dominated by the peaks at 1405 and 1412 cm^{-1} , respectively, and show in general quite similar bands and intensity patterns. All Raman bands of **1** are also found in the Raman spectrum of **2**, except the band at 1433 cm^{-1} which is observed exclusively in **1** (Fig. 4). However, the Raman spectrum of **2** shows four additional bands at 737, 1280, 1305 and 1340 cm^{-1} , which are absent in the spectrum of **1**. Taking only the experimental data into account, it is unclear whether these bands are absent in the Raman spectra of **1** or whether they are supercomposed with other bands. This will be discussed later in the section where we discuss the calculated spectra.

A significant wavenumber shift induced by the Br substitution can be found for the pyridine ring-breathing mode (band 16) which shifts from 1032 cm^{-1} in (**1**) to 1087 cm^{-1} in (**2**) (Fig. 4).

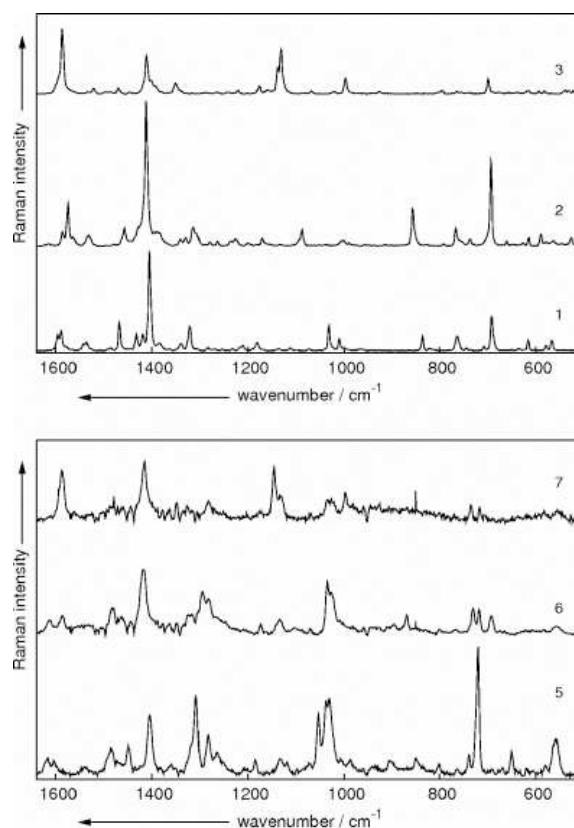


Figure 4. Experimental Raman Spectra of the compounds **1–3** and **5–7**. The Raman spectra were recorded as solids with an excitation wavelength of 830 nm.

Additionally, band 51 is shifted from 1543 (**1**) to 1565 cm^{-1} (**2**). These modes can be assigned to pyridine ring-deformation modes, and the substitution-induced wavenumber shift indicates that the mode might be directly influenced by Br.

Table 2. Wavenumber positions (in cm^{-1}) of the experimental and calculated Raman bands of all investigated molecules 1–8

No.	Experimental						Sym	Calculated										
	1	2	3	5	6	7		1	2	3	4	5	6	7	8			
1		527	522															
2	566	563	583	557	556	555						558	557	558	558			δ_{sym} -ring, tbbpy
3	579	590	588	580	580	583	a_1	571	573	578	548	573	581	580	544			δ_{sym} -ring, dppz
4	616	615	617	650			a_1	609	610	612	611							δ_{sym} -ring, dppz
5	693	694	700	721	719	718	a_1	680	683	687	686	712	721	726	713			δ_{asym} -ring, dppz
6	708			739	731	735						734	735	734	734			δ_{asym} -ring, tbbpy
7		737				693								682		644		δ_{asym} -ring, phenan
8	765	767	765	801	800		a_1	758	760	757	766	752	758	754	758			δ_{sym} -ring, phenan
9	836	857	796	850	869		a_1	829	847	793	815	840	864		820			δ_{sym} -ring, phenan + δ_{sym} -ring, phenaz
10			997			998	a_1			990	990			990	990			Ring-breath, phac
11	1010	1001		1007		1025	a_1	1005		1014		1003	1005	1005	1003			Ring-breath, phenaz
12												1004	1007	1003	1004			Ring-breath $_{\text{asym}}$, tbbpy
13												1007	1009	1006	1006			Ring-breath $_{\text{asym}}$, tbbpy
14				1030	1027	1032						1008	1010	1008	1008			Ring-breath $_{\text{asym}}$, tbbpy
15				1038	1035							1018	1020	1020	1019			Ring-breath $_{\text{sym}}$, tbbpy
16	1032	1087	927	1052	1069	925	a_1	1025	1073	924	1026	1046	1083	922	1046			Ring-breath $_{\text{sym}}$, phenan
17			1068			1069	a_1			1051	1063				1059	1071		Ring-breath $_{\text{asym}}$, phenan + ring breath $_{\text{asym}}$, phac
18				1118										1113		1109		δ -CH, phenan + δ -CH, tbbpy
19				1133	1133									1116	1118	1115		δ -CH, phenan + δ -CH, tbbpy
20			1131			1131	a_1			1123	1121				1130	1123		Ring-breath $_{\text{sym}}$ + δ -CH, phac + phenan
21			1138			1146	a_1		1136	1139		1151	1146	1144				δ -CH, phenaz
22	1181	1171	1156	1184	1173	1177	a_1	1172	1160	1164	1171	1175	1164	1164	1173			δ -CH, phenan
23							a_1			1170	1168			1173	1169			δ -CH, phac
24											1222				1214			δ -CH, phac
25	1211	1226	1176				b_1	1206	1192	1192	1198							δ -CH, phenaz
26				1264	1268							1253	1253	1253	1252			δ -CH, tbbpy
27												1256	1258	1258	1256			
28	1219	1236																
29		1280		1282	1283		a_1	1262	1263			1275						δ -CH, phenan
30	1284	1262	1262	1308	1296	1283	a_1	1272	1249	1246	1265	1289	1265	1262	1323			δ -CH, dppz
31		1305					a_1	1306	1298	1285	1312	1306	1306	1298	1305			ν_{asym} -ring, phenan
32		1340	1350	1318	1319		a_1	1332	1338	1380	1332	1303	1305	1355	1303			ν_{sym} , C–N phenan, + ν_{asym} , phenaz
33												1307	1307	1304	1306			
34	1321	1329	1340				a_1	1329	1327	1357	1303							ν_{asym} , C–N phenan, + ν_{sym} , phenaz
35	1339	1314					a_1	1337	1308	1335	1338	1336	1320	1324	1340			ν_{asym} -ring, phenan + δ -CH, phenan
36											1359				1366			ν_{sym} -ring, phenaz + ν_{sym} -ring, phac
37				1358	1362	1363						1368	1368	1369	1369			δ -CH, Methyl
38					1348													
39	1384	1384	1402															
40	1405	1412	1411	1404	1419	1416	a_1	1381	1382	1383	1371	1390	1396	1394	1382			ν_{sym} -ring, phenaz
41												1443			1440			ν_{sym} -ring, phenaz + ν_{sym} -ring, phac
42												1463			1454			ν_{sym} -ring, dppz + ν_{sym} -ring, phac
43	1419	1428			1444	1444	b_1	1403	1395	1431	1395		1404		1391			ν_{sym} -ring, phenaz
44	1433	1390		1449			a_1	1406	1374		1409	1422		1375	1421			ν_{sym} -ring, phenan
45	1468	1458	1470				a_1	1450	1441	1455	1453	1458	1457	1463	1463			ν_{sym} -ring, dppz
46				1486	1480	1480						1470	1469	1470	1470			ν -CC, tbbpy
47			1522				a_1		1468	1502	1499	1479	1470	1513	1499			ν_{sym} -ring, dppz
48	1537	1533					b_1	1516	1513	1517	1506	1506	1502	1509	1480			ν_{asym} -ring, pyrazin
49												1523	1526	1522	1523			ν_{sym} -ring, tbbpy
50	1543						a_1	1527	1511	1546	1485			1531	1538	1482		ν_{sym} -ring, phenaz + ν_{sym} -ring, phenan
51	1589	1575					a_1	1574	1550	1483	1575	1552	1519	1481	1550			ν_{sym} -ring, phenan
52	1577	1565					a_1	1550	1544	1562	1543	1569	1557	1555	1563			ν_{asym} -ring, phenan
53							b_1	1551	1534	1526	1550	1571	1554	1539	1561			ν_{asym} -ring, phenan

Table 2. (Continued)

No.	Experimental						Sym	Calculated								
	1	2	3	5	6	7		1	2	3	4	5	6	7	8	
54							a ₁			1560				1557	1556	$\nu_{\text{asym}}\text{-ring, phac}$
55						1562				1580					1580	$\nu_{\text{asym}}\text{-ring, phac}$
56	1596	1586		1604	1586		a ₁	1586	1568	1580	1589	1563	1547	1568	1559	$\nu_{\text{asym}}\text{-ring, phenan}$
57			1587				a ₁			1594	1592			1592	1590	$\nu_{\text{sym}}\text{-ring, phac}$
58			1600									1600	1601	1601	1601	$\nu_{\text{asym}}\text{-ring, tbbpy}$
59				1616	1612							1605	1607	1606	1605	$\nu_{\text{sym}}\text{-ring, tbbpy}$

The nominated symmetry (Sym) is referred to the highly symmetric ligands 1–3.

Upon phac substitution on the phenanthroline moiety (**3**), the overall number of atoms is increased compared to **1** and **2** while the molecular symmetry remains unchanged according to the calculated geometries (Table 1). This leads to a higher number of normal modes and should accordingly lead to a more complex Raman spectrum. However, against this expectation the number of observed Raman bands is decreased as can be seen in Fig. 4. This finding might be explained by the increased polarizability of (**3**) as compared to (**1**) and (**2**) induced by the larger π -system of (**3**). This larger π -system leads to a strongly increased Raman intensity of bands, which can be assigned to vibrations of the phac-substituted phenanthroline part. Additionally, bands that are assigned to vibrations coupled to the phac groups might experience an increase in Raman intensity, too. Due to the normalization of all spectra to band 22, which is assigned to a CH deformation on the phenanthroline sphere and thus experiences an increased Raman cross-section upon phac substitution, there may be some bands that cannot be found in the Raman spectrum of **3** because of their relatively low intensity as compared to band 22. Consequently, the Raman bands that are not observed in the Raman spectrum of **3** can be assigned to vibrations of the phenazine part. On the other hand, bands with relative high intensity can be assigned to the vibrations of the phac group themselves. Alternatively, these intense bands might be also assigned to vibrations coupled to phac. An example for an isolated vibration of the phac group is the band at 1130 cm^{-1} , which is present only in the Raman spectrum of **3** and corresponds to a ring deformation mode of the phenyl ring within phac (Fig. 4). Two additional modes dominate the Raman spectrum of **3**, namely the bands at 1411 and 1587 cm^{-1} , which arise from ring deformations of the dppz phenazine sphere. This assignment is based on the fact that these modes are also present in the Raman spectra of **1** and **2**. The enhancement of the Raman cross-sections of the latter two modes upon introduction of the phac at the R1 position indicates that this mode is an example for modes directly coupled to the phac unit.

The Raman spectra of the ligands **1–3** (Fig. 4) show a strong influence of the substituents on the overall intensity pattern. These changes in intensity together with the wavenumber shifts allow a distinction to be made between Raman bands belonging to vibrations on the phenanthroline sphere, where the substituents are introduced, and vibrations centered on the phenazine sphere.

Raman spectra of Ru–dppz_n complexes

Based on the results obtained from the Raman analysis of the noncoordinated ligands, the changes in the Raman spectra due

to complexation are expected to occur predominantly for bands that emerge from vibrations of the phenanthroline sphere, where the Ru metal is bound. The first thing to mention is a fluorescent background of the spectra of the Ru complexes **5–7** (Fig. 4), which is caused by irremovable fluorescent residues from synthesis. This background was subtracted by baseline correction with a fifth order polynomial exponential fit. Due to this, the spectra show a reduced signal-to-noise ratio compared to the spectra of the unbound ligand (Fig. 4). As expected, the Raman spectrum of **5** contains several new bands as compared to the Raman spectrum of the unbound dppz ligand **1** (bands at 1038 , 1118 , 1133 , 1264 , 1282 , 1358 and 1486 cm^{-1}). These bands are assigned to vibrations of the tbbpy ligands. The spectra are normalized to band 46 at 1486 cm^{-1} of the tbbpy bands to ensure insensitivity of the normalized standard to dppz substitution. Nevertheless, a comparison of relative intensities clearly indicates a different intensity pattern in the Raman spectra of **5** and **6** as compared to **1** and **2** (Fig. 4). This is in agreement with the new electronic situation in the phenanthroline moiety caused by complexation. Therefore, bands assigned to vibrations of the phenanthroline sphere will change in relative intensity. This can be predominantly seen for the bands 5, 16, 32 and 40 (Fig. 4 in comparison with Table 2). Following this argument, the large wavenumber shifts indicate that the corresponding vibrations belong to a vibration of the phenanthroline moiety, which is the case for the bands 8, 9, 30, 32 and 43 (Table 2). On the other hand, Raman bands whose positions are insensitive to complexation and which show a lower relative intensity, may tentatively be assigned to vibrations of dppz phenazine moiety. Details of this argument will be discussed later within the context of the DFT-calculated Raman spectra.

Complexation with the $[\text{Ru}(\text{tbbpy})_2]^{2+}$ moiety leads to the same changes in the Raman spectrum of **6** as for **5**, compared to the unbound ligand Raman spectra (Fig. 4). Otherwise, the changes in the Raman spectra of the noncoordinated ligands induced by the presence of Br are also found for the Raman spectra of the corresponding Ru complexes, e.g. the band 7, which is present only in the spectra of both ligand **2** and its complex **6**, or the shift of the band 16. Surprisingly, the most intense band in the Raman spectrum of **5** exhibits low intensity in the spectrum of **6**, even compared to the spectrum of the unbound ligand **2**. This fact will be rationalized later during the discussion of the calculated Raman spectra.

Due to the significant fluorescence background,^[1] the signal-to-noise ratio of the Raman spectrum of **7** is worse than those of **5** and **6**, while its general pattern is very similar to that of the corresponding ligand **3** (Fig. 4). Because of the poor signal-to-noise ratio of the Raman spectrum of **7**, several bands are absent

as compared to the spectrum of the noncoordinated ligand **3**. In the spectrum of **7**, the Raman bands 5, 16, 22, 30 and 40 (referring to Table 2) are assigned to bands that were also observed in the Raman spectra of **5** and **6**. For these bands, complexation induces identical Raman shifts irrespective of substitution, which additionally does not alter the relative intensities of these bands as compared to the unbound ligands. In analogy to the behavior of the ligand, phac substitution at the position R1 in the complex yields increased Raman intensities for the bands 40 and 57. Finally, there are modes due to the vibrational pattern of the phac substituent. These bands appear in the Raman spectra of **3** and **7** at the same wavenumber positions and are seemingly independent of the rest of the molecule (Fig. 4). The band at 1587 cm^{-1} exhibits the same wavenumber position in the Raman spectra of **3** and its Ru complex **7**, and even the Raman intensities of both bands are comparable (Fig. 4). Consequently, this band at 1587 cm^{-1} is assigned to a vibration of the phac groups of the unbound ligand **3**. With a reversed argument, the band 40 can be assigned to a dppz vibration on the phenazine moiety coupled to the phac groups.

By analyzing the Raman spectra of the complexes and comparing them to the spectra of the unbound dppz ligands, it was possible to pick out the bands of the tbbpy groups. The remaining bands of dppz could be assigned to vibrations of either its phenanthroline or phenazine part, which indicates the possibility of treating these spheres separately. Unfortunately, further assignment of Raman bands is not possible based on experimental data only. Therefore, in the remainder of the paper we will turn to the discussion of the calculated Raman spectra to obtain detailed insight into the structural properties of the dppz derivatives and their respective Ru–bipyridine complexes.

Calculated Raman spectra

The theoretically derived Raman spectra shown in Fig. 5 are obtained by convoluting the quantum chemically calculated line spectra with Gaussian functions (15 cm^{-1} width). The resultant spectra are corrected for the ω^4 dependency on the excitation wavelength. Normalization of the spectra ensures comparability to the experimental spectra and was performed with respect to band 22 for the unbound ligands and band 46 for the complexes.

Discussion of ligand spectra

In general, it can be seen that the calculated spectra resemble the experimental ones fairly well (Figs 4 and 5). The influence of the substitution discussed above can also be found in the calculated spectra. However, the calculation allows us to interpret these influences on a molecular level by considering the displacement vectors of the normal modes which are affected by substitution or complexation.

It was found that, generally, the calculated wavenumber values are smaller than the experimental values (Table 2). One exception is band 34, for which the calculation yields a higher wavenumber for **1** and **3**.

Wavenumber shifts due to Br substitution manifest themselves in the calculated spectra in the same way as in the experimental ones. An analysis of the associated normal modes of vibrations with a large shift reveals that displacements of atoms of the phenanthroline moiety contributes most to these vibrations. With one exception (mode 25 (Table 2)), the Br-induced wavenumber shifts are predicted quite well in the calculations.

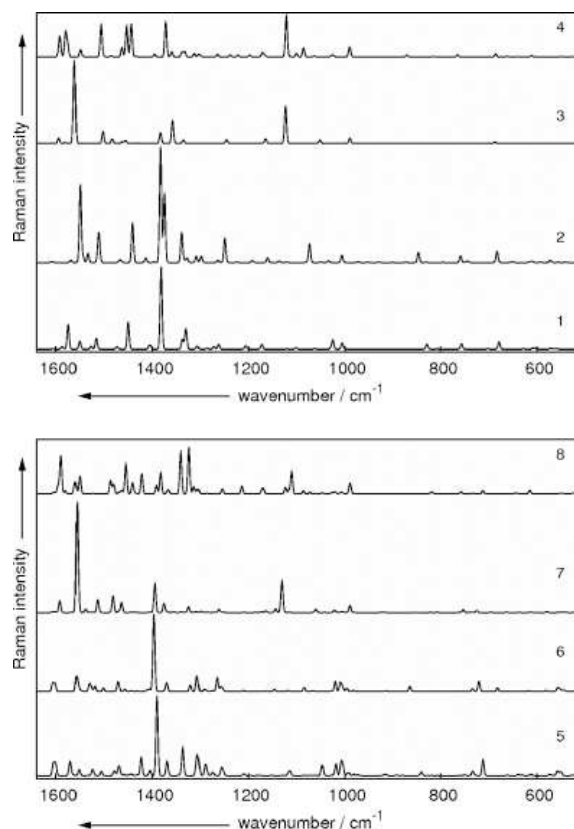


Figure 5. Calculated Raman spectra of ligands **1–4** and the complexes **5–8**.

As found in the experimental Raman spectrum, the number of bands visible in the spectrum decreases if dppz is substituted with phac groups. The reason for this was tentatively discussed in the context of the experiments and can now be corroborated by the calculations. The absolute Raman activity of the band 22 used for normalization increases by a factor of 30 due to the fact that the phac ligand induces a higher polarizability of the phenanthroline part. Considering this fact, it is clear that only a few bands, of which the Raman activity increases by a comparable factor, appear in the spectrum. With the help of the calculated normal modes, these bands are assigned to vibrations of phenanthroline, phac groups or the coupled vibration of both. The bands that are found only in the Raman spectrum of **3**, namely the bands 10, 17, 20, 21 and 47, belong to vibrations where the phac groups contribute only (10, 17 and 20) or dominantly (21 and 47) to the respective vibration. In contrast to this, Raman bands that are assigned to vibrations where phac is not involved show Raman activities comparable to those of ligand **1** or **2**. Due to normalization to the band 22, which shows an increased absolute Raman activity in the presence of the phac groups, these latter ones are not detectable in the spectrum but are included in Table 2.

The calculated Raman spectrum of ligand **4** contains a higher number of bands as compared to the calculated spectrum of **3**. Here the phac groups induce a higher polarizability within the dppz backbone and not only within the phenazine part to which they are connected. Hence, the intensity of Raman bands of both parts of the molecule is increased and more bands become visible

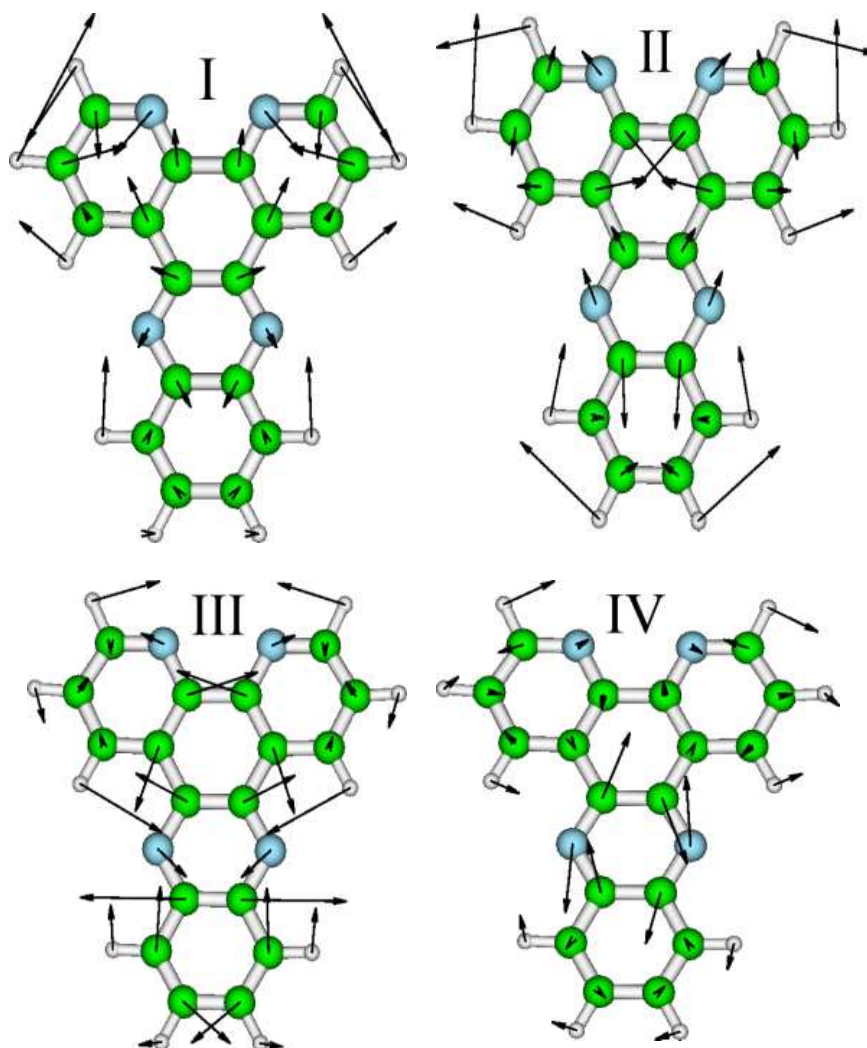


Figure 6. Normal coordinates for the four Raman modes discussed exemplarily No. 16 (I), 30 (II), 40 (III) and 48 (IV) (Table 2). The displacement of the atoms is depicted by arrows. The Roman numbering is used for the discussion of these bands in the text.

in the spectrum. Compared to the other ligands, there are five new bands, namely 24, 36, 41, 42 and 55 (Table 2). These bands belong to modes in which the phenazine couples to the phac groups, so that their Raman activity is increased dramatically.

All experimental Raman bands could be assigned to calculated Raman modes. By this it was possible to explain or corroborate several features that were obtained in the experimental spectra, such as the appearance or disappearance of modes depending on the substitution or shifts of wavenumbers and Raman intensities, with the help of the DFT calculations.

Discussion of individual modes

To obtain a thorough insight into the coupling between the phenanthroline and the phenazine moiety and how this coupling is reflected in the vibrational properties of the molecule, the discussion now focuses on a set of individual characteristic Raman modes. In particular, the substitution dependence of their

atomic displacement and wavenumber shifts is analyzed in detail. The vibrational features of dppz can be discussed exemplarily considering these characteristic bands. The normal modes of the respective vibrations are shown in Fig. 6. Referring to Table 2 these bands are: (I) the ring-breathing mode of the dppz pyridine rings (band No. 16), (II) a CH deformation mode at 1272 cm^{-1} where both parts of dppz are involved (band No. 30), (III) a mode with dominant ring stretching contributions of the two benzene rings in dppz (band No. 40) and (IV) the asymmetric ring stretching mode of the central pyrazine ring in the phenazine moiety (band No. 48).

Vibration (I) is an outstanding example of a mode that involves solely atoms of the phenanthroline part and which is therefore influenced only by structure variations on the phenanthroline moiety (Fig. 6). Other bands with the same characteristics are 5, 22, 32, 35, 51, 53 and 56 (Table 2). For vibration (I) the various substitutions discussed in this work lead to unexpectedly large wavenumber shifts of the associated band. While substitution

with Br causes a shift of nearly 50 cm^{-1} from 1025 cm^{-1} (ligand **1**) to 1073 cm^{-1} (ligand **2**), the phac groups shift this vibration in the opposite direction by 102 cm^{-1} to 923 cm^{-1} (Fig. 4). This behaviour is in contrast to ligand **4** where this band is not shifted, which demonstrates that properties of the phenazine sphere can be varied without effecting the structural properties of the phenanthroline sphere. It should be noted that there are obviously some more bands observable in the experimental Raman spectra of **2** and **3** around 1025 cm^{-1} (Fig. 4). Hence, without a detailed normal mode analysis by DFT calculations these bands would have been assigned to the ring-breathing mode of **2** and **3**. Thus, the enormous shift induced by the substituents – most likely – would not have been recognized and a false Raman band assignment might easily have happened.

Normal mode (III) is a ring stretching mode of the two benzene rings of dppz (Fig. 6). For **1** and **2** it is the most intense mode in both the experimental and calculated Raman spectrum (Figs 4 and 5). Considering the noncoordinated ligands only, this band is an example for a purely phenazine-centered vibration (Fig. 6). Consequently, the wavenumber position of (III) is unaffected by phenanthroline substitution. Only in the Raman spectrum of **4** a shift by 10 cm^{-1} to lower wavenumbers, as compared to **1**, is observed. This hints to the fact that the phenazine sphere can be varied independently of the phenanthroline sphere. However, this changes upon complexation with Ru (see discussion below).

In contrast to (I) and (III), vibration (II) – a CH deformation vibration – is chosen because it is delocalized over the entire dppz structure (Fig. 6). Thus, it constitutes a prominent example for bands whose wavenumber positions are influenced by all substitutions investigated irrespective of the substitution position. An analogous behavior is observed for the bands 9, 25, 34 and 50 (Table 2). Band (II) is shifted either by substitution on the phenanthroline part (23 cm^{-1} to lower wavenumbers by Br and 26 cm^{-1} by phac) and on the phenazine part (7 cm^{-1} by phac). These shifts are both observable in the experimental as well as calculated spectra. The wavenumber shift of mode (I) in the phenazine-substituted species **4** is rather small, but increases upon complexation with the ruthenium center. This finding will be discussed later in more detail in the context of the complex spectra. The presence of (II) and the other vibrations, which are delocalized over the complete dppz structure, indicates that the two parts of dppz may not be treated as two completely separate units even though properties of either moiety can be tuned independently.

Vibration (IV) is the asymmetric ring stretching of the dppz pyrazine ring (Fig. 6). In the calculated spectra, the wavenumber position of IV is affected significantly only by the phac groups on the phenazine sphere. A similar behavior can be found for the modes 3, 8 and 21 (Table 2). As discussed earlier, vibrations of the phenazine sphere are not observable in the Raman spectrum of **3**. Hence, this band is only observable for the ligands **1** and **2** in the experimental Raman spectra (Fig. 4). There, it is only shifted slightly by 4 cm^{-1} due to Br substitution as predicted by the calculation. By substituting the phenazine sphere with phac groups, like in ligand **4**, the absolute Raman activity of this band increases approximately by a factor of 30. Therefore, this band is one of the dominating bands in the Raman spectrum of **4** (Figs 4 and 5). Compared to (I), the wavenumber shift induced by phac substitution (10 cm^{-1}) is quite small. This can be explained by the fact that phac is not bound directly to the vibrating pyrazine

ring and accordingly the induced changes are overall smaller as compared to vibrations of the phenanthroline sphere.

These examples show that the vibrations of dppz can be classified into four species:

1. phenanthroline vibrations, which can be spectrally tuned by substitutions on the phenanthroline part;
2. coupled vibrations that show that the two parts of dppz are not entirely free of interaction;
3. vibrations that depend on changes of the phenanthroline sphere in the ruthenium complexes only, thus revealing complexation-induced changes of the dppz properties;
4. phenazine vibrations that are influenced only by direct structural modifications of the phenazine sphere.

In concluding this section, it should be noted that with the help of DFT calculations and a detailed normal mode analysis deep insight into the molecular properties of dppz can be gained. It is found that the phenanthroline sphere may be varied independently on phenazine and vice versa. However, both parts may not be regarded as single molecular units. Furthermore – from a methodological point of view – the results presented here constitute a nice example of how the use of DFT calculations helps preventing wrong Raman band assignment.

Complexation-induced changes in the vibrational properties

The knowledge gained about the structural properties of dppz and their influence on substitution patterns will now be transferred to a discussion of the respective ruthenium complexes. The calculated Raman spectra of the investigated ruthenium complexes are depicted in Fig. 5. In contrast to the experimental Raman spectra of the complexes **5** and **6** (Fig. 4), the Raman intensity of band 40 within the calculations (Fig. 5) is disproportionately overrated, which makes this band the dominating one in the calculated complex spectra. Hence, the intensity patterns of the calculated complex spectra are more like the experimental ligand spectra rather than those of the other complexes. In contrast to the Raman intensities, the calculations were able to predict the wavenumber shifts that are induced by the introduction of the ruthenium center to the dppz ligands.

The experimental bands of the tbbpy groups, which are introduced upon complexation (Fig. 4), i.e. band no. 15, 18, 19, 26, 29, 37 and 46 (Table 2), are detected clearly in the calculated spectra. Aside from these bands which can be assigned to tbbpy by visual inspection of the experimental Raman spectra, a theoretical analysis of the normal modes reveals the presence of even more vibrations that are assigned to tbbpy, i.e. band no. 12, 13, 14, 27, 49, 58 and 59 (Table 2).

Let us exemplarily consider the changes upon phenazine substitution by phac. Generally, in the Raman spectrum of the complex **8**, identical changes are observed as in the respective one of the noncoordinated ligand **4** (Fig. 5). But in the Raman spectrum of **8**, the largest changes of Raman intensities compared to the spectrum of the unbound ligand occur between 1400 and 1600 cm^{-1} (Fig. 5). Particularly, the bands that are solely observed upon substitution on the phenazine sphere show different intensities and are shifted in their wavenumber position. This finding points towards the fact that Ru coordination has an influence not only on the phenanthroline moiety but also on the phenazine part of dppz.

The most dominant changes induced by complexation become obvious by a closer inspection of the four highlighted vibrations

(Fig. 6). Vibration (I) is shifted by 20 cm^{-1} to higher wavenumbers in the complexes **5**, **6** and **8** as compared to the spectra of the ligands (Table 2). This was somehow expected, since the Ru–N bond withdraws electron density out of the pyridine rings. However, vibration (I) is not shifted for complex **7** compared to ligand **3**. Apparently, the phac groups have the ability to compensate the changes in electron density in the pyridine rings.

Complexation induces a wavenumber shift of vibration (II) (Fig. 6) that is independent on substitution on the phenanthroline sphere and lies in the range of 17 cm^{-1} . Here the phac groups on the phenazine sphere lead to a completely different behavior as compared to the unbound ligands. The phac groups induce a shift of this vibration by 44 cm^{-1} to higher wavenumber, which is different for the noncoordinated ligand, where this shift was only 7 cm^{-1} toward lower wavenumbers. This can be rationalized when considering the fact that the phenazine sphere is influenced by complexation that takes place on the phenanthroline part. This fact is clearly pronounced in vibrations (III) and (IV), too. For complex **5**, the wavenumber position of vibration (III) is shifted by 10 cm^{-1} to higher wavenumbers due to complexation (i.e. **1** vs **5**). For the unbound ligands, substitution on the phenanthroline part does not show any influence on the wavenumber positions of this vibration (III), which is centered on the phenazine part only (Fig. 6). This behavior changes slightly when considering the ruthenium complexes, where a rather small wavenumber shift in the same order of magnitude for substitutions on the phenanthroline and on the phenazine sphere can be found. This finding is confirmed by comparing the calculation results with the experimental spectra. Band III (40, see Table 2) in the experimental Raman spectra of the unbound ligands shifts by 7 cm^{-1} to higher wavenumbers due to Br substitution on the phenanthroline part, while for the corresponding complexes a shift of 15 cm^{-1} to higher wavenumbers is observed in the experimental Raman spectra. This behavior demonstrates that substituents on the phenanthroline sphere influence the phenazine part.

The influence of complexation on vibration (IV) is quite similar to that on vibration (II). The shift of around 10 cm^{-1} due to complexation, i.e. **1** versus **5** to lower wavenumbers, does not depend upon substitution with phac at the phenanthroline part. However, as compared to the noncoordinated ligands, the shift induced by the phac groups at the phenazine sphere is much bigger. Thus, upon complexation the variability of the dppz phenazine sphere is increased.

Conclusion

We have presented an extensive study on the substitution-induced effects of novel dipyrrophenazine derivatives and their Ru complexes. The study was performed using the powerful combination of Raman spectroscopy and high-level DFT calculations. With respect to the ground state properties, the unbound ligand dppz was found to be separable into two different moieties – i.e. a phenanthroline part and a phenazine part. It was shown that the structural properties of the two parts of the unbound ligands can be altered independently by side-specific substitution. Upon complexation of the different ligands with the Ru(tbbpy)₂ moiety, coupling between the phenazine and the phenanthroline moieties is observed – i.e. substitution of the phenanthroline part influences the properties of the phenazine part and vice versa. Hence, a detailed insight into the structural properties and the resultant vibrational structure of novel dipyrrophenazine derivatives and their Ru complexes is obtained. The results exemplarily

highlight the usefulness of a combined Raman–DFT approach in studying molecular structural properties.

Acknowledgements

C. K. gratefully acknowledges funding by a Ph.D. scholarship of the Deutsche Bundesstiftung Umwelt (DBU), while B. D. is grateful for financial support by the Fonds der Chemischen Industrie.

References

- [1] M. Schmitt, J. Popp, *J. Raman Spectrosc.* **2006**, *37*, 20.
- [2] K. Jalkanen, J. Würtz, V. Jürgensen, A. Claussen, A. Rahim, M. Jensen, R. Wade, F. Nardi, C. Jung, I. Degtyarenko, R. Nieminen, F. Herrmann, M. Knapp-Mohammady, T. Niehaus, K. Frimand, S. Suhai, *Int. J. Quantum Chem.* **2006**, *106*, 1160.
- [3] C. Herrmann, M. Reiher, *Top. Curr. Chem.* **2006**, *268*, 85.
- [4] G. Denti, S. Campagna, L. Sabatino, S. Serroni, M. Ciano, V. Balzani, *Proc. Int. Conf.* **1991**, *8*, 27.
- [5] V. Balzani, A. Juris, M. Venturi, S. Campagna, S. Serroni, *Chem. Rev.* **1996**, *96*, 759.
- [6] N. Damrauer, G. Cerullo, A. Yeh, T. Boussie, C. Shank, J. McCusker, *Science* **2007**, *275*, 54.
- [7] V. Balzani, *Electrontransfer in Chemistry*, vol. 5, Wiley-VCH Verlag GmbH Weinheim: Weinheim, Germany, **2001**.
- [8] S. Campagna, F. Puntoriero, F. Nastasi, G. Bergamini, V. Balzani, *Top. Curr. Chem.* **2007**, *280*, 117.
- [9] S. Rau, B. Schäfer, D. Gleich, E. Anders, M. Rudolph, M. Friedrich, M. H. Görls, H. W. Henry, J. Vos, *Angew. Chem.* **2006**, *118*, 6361.
- [10] R. Konduri, H. Ye, F. MacDonell, S. Serroni, S. Campagna, K. Rajeshwar, *Angew. Chem. Int. Ed.* **2002**, *41*, 3185.
- [11] S. Tschierlei, B. Dietzek, M. Karnahl, S. Rau, F. MacDonnell, M. Schmitt, J. Popp, *J. Raman Spectrosc.* **2008**, *39*, 557.
- [12] M. Schwalbe, B. Schäfer, H. Görls, S. Rau, S. Tschierlei, M. Schmitt, J. Popp, G. Vaughan, W. Henry, J. Vos, *Eur. J. Inorg. Chem.* **2008**, *3310*.
- [13] E. Amouyal, A. Homsy, *J. Chem. Soc. Dalton Trans.* **1990**, 1841.
- [14] R. Nair, B. Cullum, J. Murphy, *Inorg. Chem.* **1997**, *36*, 962.
- [15] J. P. Sauvage, J. C. Chambron, *Chem. Phys. Lett.* **1991**, *182*, 603.
- [16] E. Olson, D. Hu, A. Hörmann, A. Jonkmann, M. Arkin, E. Stemp, J. Barton, P. Barbara, *J. Am. Chem. Soc.* **1997**, *119*, 11458.
- [17] C. Coates, P. Callaghan, J. McGarvey, J. Kelly, P. Kruger, M. Higgins, *J. Raman Spectrosc.* **2000**, *31*, 283.
- [18] A. Friedman, J. Chambron, J. Sauvage, N. Turro, J. Barton, *J. Am. Chem. Soc.* **1990**, *112*, 4960.
- [19] Y. Jenkins, A. Friedman, N. Turro, J. Barton, *Biochemistry* **1992**, *31*, 10809.
- [20] R. Hartshorn, J. Barton, *J. Am. Chem. Soc.* **1992**, *114*, 5919.
- [21] J. Fees, W. Kaim, M. Moscherosch, W. Matheis, J. Klima, M. Krejčik, S. Zalis, *Inorg. Chem.* **1993**, *32*, 166.
- [22] B. Schäfer, H. Görls, M. Presselt, M. Schmitt, J. Popp, W. Henry, J. Vos, S. Rau, *Dalton Trans.* **2006**, *18*, 2225.
- [23] C. Coates, J. Olofsson, M. Coletti, J. McGarvey, B. Önfelt, P. Lincoln, B. Norden, E. Tuite, P. Matousek, A. Parker, *J. Phys. Chem. B.* **2001**, *105*, 12654.
- [24] M. Brennaman, J. Alstrum-Acevedo, C. Fleming, P. Jang, T. Meyer, J. Papanikolas, *J. Am. Chem. Soc.* **2002**, *124*, 15094.
- [25] J. Olofsson, L. Wilhelmsson, P. Lincoln, *J. Am. Chem. Soc.* **2004**, *126*, 15458.
- [26] M. Brennaman, T. Meyer, J. Papanikolas, *J. Phys. Chem. A* **2004**, *108*, 9938.
- [27] C. Turro, S. Bossmann, Y. Jenkins, J. Barton, N. Turro, *J. Am. Chem. Soc.* **1995**, *117*, 9026.
- [28] S. Tschierlei, M. Presselt, C. Kuhnt, A. Yartsev, T. Pascher, V. Sundström, M. Karnahl, M. Schwalbe, B. Schäfer, S. Rau, M. Schmitt, B. Dietzek, J. Popp, *Chem. Eur. J.* **2009**, *15*, 7678.
- [29] B. Önfelt, P. Lincoln, B. Norden, J. Spencer Baskin, A. Zewail, *Proc. Natl. Acad. Sci.* **2000**, *97*, 5708.
- [30] B. Dietzek, D. Akimov, W. Kiefer, S. Rau, J. Popp, M. Schmitt, *Laser Phys. Lett.* **2007**, *4*, 121.
- [31] B. Dietzek, W. Kiefer, J. Blumhoff, L. Böttcher, S. Rau, D. Walther, U. Uhleman, M. Schmitt, J. Popp, *Chem. Eur. J.* **2006**, *12*, 5105.

- [32] C. Hermann, J. Neugebauer, M. Presselt, U. Uhlemann, M. Schmitt, S. Rau, J. Popp, M. Reiher, *J. Phys. Chem. B* **2007**, *111*, 6078.
- [33] J. Olofsson, B. Önfelt, P. Lincoln, *J. Phys. Chem. A* **2004**, *108*, 4391.
- [34] R. Ahlrichs, M. Bär, M. Häser, H. Horn, C. Kölmel, *Chem. Phys. Lett.* **1989**, *162*, 165.
- [35] A. Becke, *Phys. Rev. A* **1988**, *38*, 3098.
- [36] J. Perdew, *Phys. Rev. B* **1986**, *33*, 8822.
- [37] B. Dunlap, J. Connolly, J. Sabin, *J. Chem. Phys.* **1979**, *71*, 3396.
- [38] A. Schäfer, C. Huber, R. Ahlrichs, *J. Phys. Chem.* **1994**, *100*, 5829.
- [39] T. Dunning, *J. Chem. Phys.* **1989**, *90*, 1007.
- [40] D. Woon, T. Dunning, *J. Chem. Phys.* **1993**, *98*, 1358.
- [41] D. Woon, T. Dunning, *J. Chem. Phys.* **1994**, *100*, 2975.
- [42] D. Andrae, U. Häußermann, M. Dolg, M. Stoll, H. Preuß, *Theor. Chem. Acta.* **1990**, *77*, 123.
- [43] J. Neugebauer, M. Reiher, C. Kind, A. Hess, *J. Comput. Chem.* **2002**, *23*, 895.
- [44] A. Winter, C. Friebe, M. Chipor, U. Schubert, M. Presselt, B. Dietzek, B. Schmitt, J. Popp, *ChemPhysChem* **2009**, *10*, 787.

[CK2] **Substitution-controlled ultrafast excited-state processes in Ru-dppz-derivatives**

Der Nachdruck der folgenden Publikation erfolgt mit freundlicher Genehmigung der PCCP Owner Societies.

Reproduced with permission from:

C. Kuhnt, M. Karnahl, S. Tschierlei, K. Griebenow, M. Schmitt, B. Schäfer, S. Krieck, H. Görls, S. Rau, B. Dietzek, J. Popp, SUBSTITUTION-CONTROLLED ULTRAFAST EXCITED-STATE PROCESSES IN RU-DPPZ-DERIVATIVES, *Phys. Chem. Chem. Phys.*, **2010**, *12*, 1357-1368.

Copyright 2010 PCCP Owner Societies.

Substitution-controlled ultrafast excited-state processes in Ru–dppz-derivatives†

Christian Kuhnt,^{‡a} Michael Karnahl,^{‡b} Stefanie Tschierlei,^a Kristin Griebenow,^c Michael Schmitt,^a Bernhard Schäfer,^b Sven Krieck,^b Helmar Görls,^b Sven Rau,^{*d} Benjamin Dietzek^{*ac} and Jürgen Popp^{ac}

Received 31st July 2009, Accepted 13th November 2009

First published as an Advance Article on the web 16th December 2009

DOI: 10.1039/b915770k

Ru–dppz (dppz = dipyrido[3,2-*a*:2',3,3'-*c*]phenazine) complexes play an important role as environmentally sensitive luminescence sensors and building blocks for larger supramolecular compounds. Their photophysical properties are known to be highly sensitive to intermolecular solvent–solute interactions and solvent bulk-properties. Here, the synthesis and characterisation of a novel Ru–dppz derivative is reported. The potential of drastically tuning the photophysical properties of such complexes is exemplified, by introducing very simple structural modifications, namely bromine, into the dppz-ligand scaffold. The photophysics *i.e.* nature of excited states and the excited-state relaxation pathway of the various complexes has been investigated by means of electrochemical measurements, steady-state emission experiments and femtosecond time-resolved spectroscopy. It could be shown that the location of bromine substitution influences the relative energy between a luminescent and a non-luminescent metal-to-ligand charge-transfer state and therefore quenches or facilitates transitions between both. Hence it is illustrated that the luminescent properties and the underlying ultrafast excited-state dynamics of the complexes can be controlled by structural variations, *i.e.* by intramolecular interactions as opposed to changes in the intermolecular interactions.

1. Introduction

Ruthenium polypyridine complexes are interesting building blocks for supramolecular architectures because they are chemically very stable, redox active and display a rich photochemistry.^{1–4} This combination of properties has rendered them an intensively investigated model system for artificial photosynthesis,⁵ dyes in dye sensitised solar cells,^{6,7} biomolecular probes⁸ and light driven catalysis.⁹ The sensitivity of their emission properties towards their surroundings can be utilised for the detection of diverse analytes such as metal ions,^{10–13} oxygen¹⁴ and biological macromolecules like DNA.^{15–23} Particularly, ruthenium complexes of dipyrido-[3,2-*a*:2',3,3'-*c*]phenazine, dppz, play an important role for the latter application.

These complexes display an interesting photochemistry: The [(bpy)₂Rudppz]²⁺ complex is non-luminescent in aqueous solution but displays a relatively strong emission upon addition of double stranded DNA. This so-called *light-switch effect*, which refers to an alteration of the luminescent properties by changes in the intermolecular *i.e.* solvent–complex interactions, may be explained by the existence of two states both associated with the dppz framework. The bright state is most often described as a ³MLCT state residing on the phenanthroline part of the dppz whereas the dark state is associated with the phenazine part of dppz.^{20,23–27} The nature of this dark excited state is still subject to debate, descriptions put forward include a ³ILCT (intra-ligand charge transfer) and a ³ππ* state.^{28–33} A wide variety of spectroscopic techniques has been utilised to address the question how these two states interconvert and how to influence the luminescence and excited-state processes as well as the light-switch effect. These techniques include resonance Raman spectroscopy, picosecond time-resolved resonance Raman spectroscopy, femtosecond transient absorption spectroscopy and temperature dependent time-resolved luminescence spectroscopy.^{23,25,28,29,34–36}

Aside from these spectroscopic investigations, considering different chemical substitution patterns of the dppz with identical substituents should open an alternative route towards elucidating the photophysics of these complexes. In this context the structures **I** and **II** (see Scheme 1) of methyl-substituted dppz-complexes are known in the literature. A comparison of the respective luminescence properties shows that the lifetime of the excited state is influenced by the

^a Institute of Physical Chemistry, Friedrich-Schiller-University Jena, Helmholtzweg 4, 07743 Jena, Germany.

E-mail: benjamin.dietzek@uni-jena.de

^b Institute of Inorganic and Analytical Chemistry, Friedrich-Schiller-University Jena, August-Bebel-Straße 2, 07743 Jena, Germany

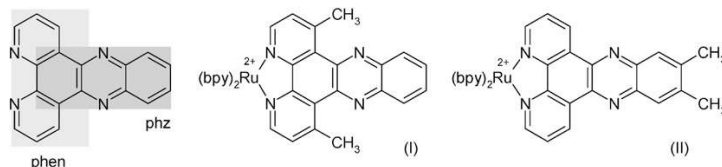
^c Institute of Photonic Technology Jena e.V., Albert-Einstein-Straße 9, 07745 Jena, Germany

^d Department of Chemistry and Pharmacy, Friedrich-Alexander-University Erlangen-Nürnberg, Egerlandstraße 1, 91058 Erlangen, Germany.

E-mail: sven.rau@chemie.uni-erlangen.de

† Electronic supplementary information (ESI) available: NMR spectra. CCDC reference number 617549. For ESI and crystallographic data in CIF or other electronic format see DOI: 10.1039/b915770k

‡ These authors contributed equally to the work.



Scheme 1 Constituent parts of dppz (phen = 1,10-phenanthroline and phz = phenazine) and the structures of **I** and **II**. The two conceptually different compartments phz and phen of the dppz-moiety are highlighted.

position at which the methyl substituent is introduced as **I** displays 820 ns³⁷ and **II** 300 ns.²⁹ Furthermore, the light-switch effect is disabled in compound **I**, which has been explained by a pure steric protection of the phenazine nitrogen atoms.^{29,37} Other possibilities to control the excited-state properties of dppz-complexes with the help of substitutions have been examined by George and coworkers who used rhenium as the metal center. They showed by means of time-resolved infrared spectroscopy that the destination of photoinitiated charge-transfer of $[\text{Re}(\text{Cl})_3(\text{py})(11,12\text{-X}_2\text{dppz})]^+$ -complexes—with $\text{X} = \text{H, F, methyl, CO}_2\text{ethyl}$ —depends on X .^{38–40}

Here, to the best of our knowledge, we present the first detailed ultrafast time-resolved comparative study on the influence of substitution at both dppz compartments on the photophysics and photochemistry of its ruthenium complexes. We chose bromine substitutions which we introduced at the 2,7-position (**L2**) and at the 11,12-position (**L3**) of dppz (see Scheme 2). Since bromine substitution in the 2,7-position has no steric effect on the phenazine nitrogens substitution-induced electronic interactions can be deciphered without contributions from steric interactions. Furthermore, from a previous study on related dibromophenanthroline complexes it is known that bromine affects the photophysics of such systems.^{41,42} The substitution pattern with bromine in the 11,12-position is known from the literature.⁴³ The emission properties of the corresponding ruthenium complex (**Ru3**) *i.e.* $[(\text{tbbpy})_2\text{Ru}(\text{dppz-Br}_2)](\text{PF}_6)_2$ (tbbpy = 4,4'-di-*tert*-butyl-2,2'-bipyridine, dppz-11,12-Br₂ = 11,12-dibromo-dipyrido-[3,2-*a*:2',3'-*c*]phenazine) showed a lack of emission in polar aprotic environment and emission in less polar solvents.⁴³ However, the ultrafast excited-state processes that underlie this behaviour remained to be investigated, which constitutes one focus in the work at hand. For comparative reasons the unsubstituted ruthenium dppz complex (**Ru1**) was included in this study. The photophysical properties of the three complexes **Ru1–Ru3**, *i.e.* $[(\text{tbbpy})_2\text{Ru}(\text{dppzR}_2)](\text{PF}_6)_2$ (dppz = dipyrido-[3,2-*a*:2',3'-*c*]phenazine, with R representing the bromine/hydrogen substituents at different positions), were investigated using an array of techniques including electrochemistry, resonance Raman (rR) spectroscopy, ultrafast transient absorption and time-resolved luminescence spectroscopy. This approach allowed us to characterise the location of the excited state using rR spectroscopy and to unravel the ultrafast dynamics of subsequently formed states.

Experimental

Synthesis

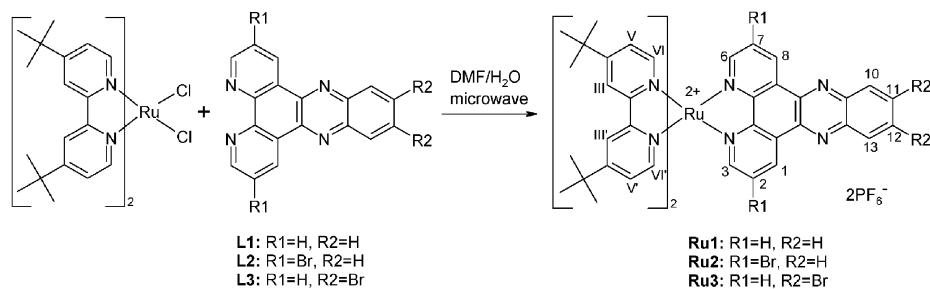
If not stated otherwise all solvents were of HPLC grade and used as purchased. 1,10-Phenanthroline-monohydrate,

o-phenylenediamine, bromine, NH_4PF_6 and all other materials were of commercial grade and used without further purification. $[(\text{tbbpy})_2\text{RuCl}_2]$, 4,4'-di-*tert*-butyl-2,2'-bipyridine (tbbpy), 3,8-dibromo-1,10-phenanthroline (phenBr₂), 1,10-phenanthroline-5,6-dione (phenO₂), dipyridophenazine (dppz), 11,12-dibromodipyridophenazine (dppz-11,12-Br₂) and **Ru3** $[(\text{tbbpy})_2\text{Ru}(\text{dppz-11,12-Br}_2)](\text{PF}_6)_2$ were prepared according to literature methods.^{41,43–49}

All dipyridophenazine type ligands dppzR₂ (**L1–L3**) (with R = H or Br at different positions) were complexed with $[(\text{tbbpy})_2\text{RuCl}_2]$ (where tbbpy = 4,4'-di-*tert*-butyl-2,2'-bipyridine) by application of a microwave-assisted method for preparation of heteroleptic ruthenium complexes (see Scheme 2).⁴⁸ All complexes contain tbbpy to increase the solubility in less polar organic solvents. The respective complexes of the type $[(\text{tbbpy})_2\text{Ru}(\text{dppzR}_2)](\text{PF}_6)_2$ were isolated in good yields between 61 and 84% and in short reaction times of approximately 3 h. All compounds were structurally characterised using two dimensional ¹H- and ¹³C-NMR methods, electrospray ionisation mass spectroscopy (ESI), elemental analyses and IR-spectroscopy.

2,7-Dibromodipyridophenazine (dppz-2,7-Br₂) L2. A mixture of 3,8-dibromo-1,10-phenanthroline-5,6-dione (0.20 g, 0.54 mmol) and *o*-phenylenediamine (98%, 0.06 g, 0.55 mmol) was refluxed in 75 ml dry ethanol for 7 h. After that time the dark yellow suspension was filtered, washed well with water, methanol and diethyl ether. The precipitate was dried *in vacuo*. Yield = 76% (0.18 g); M (C₁₈H₈N₄Br₂) = 440.1 g mol⁻¹; anal. calcd for C₁₈H₈N₄Br₂*1H₂O: C = 47.19, H = 2.20, N = 12.23; found: C = 47.31, H = 1.98, N = 12.08; MS (DEI): *m/z* = 220 (50%, M²⁺/2), 280 (30%, M⁺-2Br), 359 (40%, M⁺-Br), 440 (100% M⁺); ¹H-NMR (400 MHz, CDCl₃/CF₃COOD, 300 K): δ = 10.18 (d, 2H, *J* = 2.0 Hz, 3 + 6), 9.33 (d, 2H, *J* = 2.0 Hz, 1 + 8), 8.53 (dd, 2H, *J* = 6.8 Hz and *J* = 3.6 Hz, 10 + 13), 8.17 (dd, 2H, *J* = 6.8 Hz and *J* = 3.6 Hz, 11 + 12) ppm; ¹³C-NMR (100 MHz, CDCl₃/CF₃COOD, 300 K): δ = 124.54, 130.03, 130.72, 133.79, 137.80, 137.92, 141.74, 143.68, 149.79 ppm.

$[(\text{tbbpy})_2\text{Ru}(\text{dppz})](\text{PF}_6)_2$ Ru1. $[(\text{tbbpy})_2\text{RuCl}_2]$ (0.128 g, 0.18 mmol) and an equimolar amount of dipyridophenazine (0.05 g, 0.18 mmol) were suspended in DMF–H₂O (90 ml/12 ml) and heated at reflux for 3 h using microwave irradiation (150 W). Then the cooled reaction mixture was filtered, followed by evaporation of the solvent on the rotary evaporator. After that the reddish brown complex was dissolved in a mixture of ethanol and water. The addition of an excess of NH_4PF_6 to the red solution leads to a precipitate, which was filtered, washed with water and diethylether and dried *in vacuo*. Further



Scheme 2 Synthesis and labelling of the presented ligand **L1–L3** and their corresponding ruthenium complexes **Ru1–Ru3**.

purification was obtained by recrystallisation from acetone/water. Yield = 83% (0.18 g); M ($C_{54}H_{58}N_8RuP_2F_{12}$) = 1210.08 g mol⁻¹; anal. calcd for $C_{54}H_{58}N_8RuP_2F_{12}$: C = 53.59, H = 4.83, N = 9.26; found: C = 53.69, H = 4.71, N = 9.18; MS (ESI in methanol): m/z = 919 (5%) $[M-2PF_6-H]^+$, 1065 (100%) $[M-PF_6]^+$; ¹H-NMR (400 MHz, CD₃CN, 300 K): δ = 9.65 (dd, 2H, J = 8.0 Hz and J = 1.2 Hz, 3 + 6), 8.52 (d, 2H, J = 2.0 Hz, H III), 8.49 (d, 2H, J = 1.6 Hz, H III'), 8.47 (dd, 2H, J = 6.4 Hz and J = 3.2 Hz, 10 + 13), 8.14 (dd, 2H, 11 + 12), 8.12 (dd, 2H, 1 + 8), 7.91 (dd, 2H, J = 8.4 Hz and J = 5.6 Hz, 2 + 7), 7.69 (d, 2H, J = 6.0 Hz, H VI), 7.60 (d, 2H, J = 6.0 Hz, H VI'), 7.48 (dd, 2H, J = 6.0 Hz and J = 2.0 Hz, H V), 7.24 (dd, 2H, J = 6.0 Hz and J = 2.0 Hz, H V'), 1.45 (s, 18H, *tert*-butyl), 1.35 (s, 18H, *tert*-butyl) ppm; ¹³C-NMR (100 MHz, CD₃CN 300 K): δ = 30.43, 30.52, 36.28, 36.38, 122.51, 122.59, 125.49, 125.66, 128.35, 130.63, 131.79, 133.50, 134.13, 141.03, 143.78, 151.67, 152.06, 152.40, 154.41, 157.81, 158.04, 163.66, 163.77 ppm; IR (KBr, cm⁻¹): ν (C–CH₃) = 2963 cm⁻¹ (s), ν (C=C–) = 1616 cm⁻¹ (s), ν (C=N–) = 1483 cm⁻¹ (s), ν (C=C–) = 1415 cm⁻¹ (s), ν (PF₆⁻) = 840 cm⁻¹ (s). Crystal data of **Ru1**:† [$C_{54}H_{58}N_8Ru$]²⁺ 2[PF₆]⁻ * 1.25 C₂H₅N * 0.25 C₄H₁₀O Mr = 1279.94 g mol⁻¹, red-brown prism, size 0.07 × 0.06 × 0.03 mm³, triclinic, space group P $\bar{1}$, a = 16.6339(2), b = 17.8896(4), c = 23.0113(5) Å, α = 99.969(1), β = 102.875(1), γ = 112.505(1)°, V = 5907.7(2) Å³, T = -90 °C, Z = 4, ρ_c = 1.439 g cm⁻³, μ (Mo-K α) = 4.04 cm⁻¹, $F(000)$ = 2632, 41167 reflections in $h(-19/21)$, $k(-19/23)$, $l(-27/29)$, measured in the range $4.13^\circ \leq \Theta \leq 27.46^\circ$, completeness Θ_{max} = 98.2%, 26567 independent reflections, R_{int} = 0.0549, 16487 reflections with $F_o > 4\sigma(F_o)$, 1455 parameters, 0 restraints, $R1_{obs}$ = 0.0770, $wR2_{obs}$ = 0.1741, $R1_{all}$ = 0.1382, $wR2_{all}$ = 0.2103, GOOF = 1.033, largest difference peak and hole: 1.269/-0.752 e Å⁻³.⁴⁷

[(tbbpy)₂Ru(dppz-2,7-Br₂)](PF₆)₂ **Ru2.** Starting from 2,7-dibromodipyridophenazine (dppz-2,7-Br₂, 0.04 g, 0.09 mmol) and [(tbbpy)₂RuCl₂] the same standard procedure as for the synthesis of [(tbbpy)₂Ru(dppz)](PF₆)₂ (see above) was used. Yield = 78% (0.09 g); M ($C_{54}H_{56}N_8Br_2RuP_2F_{12}$) = 1367.86 g mol⁻¹; anal. calcd for $C_{54}H_{56}N_8Br_2RuP_2F_{12} \cdot 1H_2O$: C = 46.80, H = 4.22, N = 8.09; found: C = 46.69, H = 4.11, N = 7.37; MS (ESI in methanol): m/z = 1078 (10%) $[M-2PF_6]^+$, 1223 (100%) $[M-PF_6]^+$; ¹H-NMR (400 MHz, CD₃CN, 300 K): δ = 9.64 (d, 2H, J = 2.0 Hz, 3 + 6), 8.52 (d, 2H, J = 2.0 Hz, H III), 8.49 (d, 2H, J = 1.6 Hz, H III'),

8.46 (dd, 2H, J = 6.8 Hz and J = 3.6 Hz, 10 + 13), 8.18 (dd, 2H, J = 6.8 Hz and J = 3.6 Hz, 11 + 12), 8.09 (dd, 2H, J = 1.6 Hz, 1 + 8), 7.67 (d, 2H, J = 6.0 Hz, H VI'), 7.64 (d, 2H, J = 6.0 Hz, H VI), 7.48 (dd, 2H, J = 6.0 Hz and J = 2.0 Hz, H V), 7.29 (dd, 2H, J = 6.0 Hz and J = 2.0 Hz, H V'), 1.50 (s, 18H, *tert*-butyl), 1.37 (s, 18H, *tert*-butyl) ppm; ¹³C-NMR (100 MHz, CD₃CN 300 K): δ = 31.07, 31.11, 31.50, 36.95, 37.03, 123.39, 124.86, 126.03, 126.34, 131.32, 132.85, 134.74, 137.03, 140.71, 144.61, 150.54, 152.84, 153.50, 155.84, 158.31, 158.66, 164.67, 164.74 ppm; IR (KBr, cm⁻¹): ν (C–CH₃) = 2959 cm⁻¹ (s), ν (C=C–) = 1615 cm⁻¹ (s), ν (C=N–) = 1482 cm⁻¹ (s), ν (C=C–) = 1414 cm⁻¹ (s), ν (PF₆⁻) = 836 cm⁻¹ (s).

The microwave-assisted reactions were carried out using the Microwave Laboratory Systems MLS EM-2 microwave system. Elemental analyses were performed by the Micro-analytical Laboratory of the Friedrich-Schiller University Jena. ¹H-NMR and ¹³C-NMR spectra were recorded at ambient temperature on a Bruker AC 200 or AC 400 MHz spectrometer (¹H: 400.25 MHz, ¹³C: 100.65 MHz). All spectra were referenced to TMS or deuterated solvent as an internal standard (measured values for δ are given in ppm and for J in Hz). The mass spectra were obtained using a SSQ 710, Finnigan MAT SSQ 710 instrument at the Friedrich Schiller University Jena. Electrospray ionisation-mass spectra (ESI) were recorded on a Finnigan MAT 95 XL. The positive ESI mass spectra were achieved with voltages of 3–4 kV applied to the electrospray needle. Infrared spectra were determined by using a Perkin-Elmer FTIR spectrometer System 2000 and KBr blanks of the corresponding samples.

Crystal structure determination

The crystal-structure analyses† were carried out on a Enraf Nonius Kappa CCD diffractometer, using graphite monochromated Mo-K α radiation. The crystals are mounted in a stream of cold nitrogen, in a distance of 29 mm to the crystal detector. Data were corrected for Lorentz and polarisation effects but not for absorption.^{48,49,51,52} The structures were solved by direct methods (SHELXS⁵³) and refined by full-matrix least squares techniques against F_o^2 (SHELXL-97⁵⁴). The hydrogen atoms were included at calculated positions with fixed thermal parameters during the final stages of the refinement. All nonhydrogen atoms were refined anisotropically.⁵⁴ The molecular illustrations were drawn using the program XP (SIEMENS Analytical X-ray Instruments, Inc.).⁵⁰

Electrochemistry

Electrochemical data were obtained by cyclic voltammetry using a conventional single-compartment three-electrode cell arrangement in combination with a potentiostat "AUTOLAB[®], eco chemie". As working electrode a 0.196 cm² Pt disk, auxiliary electrode was used: glassy carbon and reference electrode Ag/AgCl (3 M KCl). The measurements were carried out in anhydrous and nitrogen purged ACN with 0.1 M tertbutylammonium tetrafluoroborate as supporting electrolyte. All potentials are referenced by the ferrocenium/ferrocene couple ($E(\text{Fc}/\text{Fc}^+) = 0.45 \text{ V}$).

Photophysics

For the photophysical measurements the complexes were dissolved in aerated acetonitrile. Acetonitrile was chosen since a straight forward photophysical behaviour of Ru–dppz-complexes dissolved in this solvent as compared to alcohols or water was shown.^{23,28,55} If not stated otherwise all experiments were performed at room temperature (22 °C in an air-conditioned laboratory). Absorption spectra were taken prior and subsequent to all measurements to ensure photochemical stability of the samples.

The time-resolved transient absorption set-up is described in detail elsewhere.⁵⁶ Briefly, the output of an amplified Ti:Sapphire laser (*Libra*, Coherent Inc.) was split in two beams, one of which was used to pump a non-collinear optical-parametric amplifier (*TOPASwhite*, LightConversion Ltd.). The TOPAS output pulses were spectrally tuned to 510 nm and served as pump-pulses in our pump-probe experiments. A fraction of the Ti:Sapphire output was employed to generate a supercontinuum by focusing the 800 nm fundamental into a Ti-sapphire plate. This supercontinuum served as a broad-band probe in the transient absorption experiments. In these experiments the probe pulses were focused into the sample by means of a 500 mm focal-length spherical mirror, while the reference pulses were biasing the sample and were directed onto the detector. Probe-pulses were spatially and temporally overlapped at the sample position with the pump pulses, which were focused into the sample by means of a 1000 mm focal-length quartz lens. The different focus conditions were chosen to ensure homogeneous excitation of the sample over the entire probe volume. The energy of the pump pulses was chosen to be 0.5 μJ, while typical probe intensities fall into the range of hundreds of nJ. Probe- and reference intensities were detected on a double-stripe diode array and converted into differential absorption (ΔA) signals using a commercially available detection system (Pascher Instruments AB).

For a kinetic analysis the broad-band ΔA signals recorded as function of the delay time (t) and the probe wavelength (λ_{pr}) were chirp corrected and subsequently subjected to a global fit routine as e.g. described in^{57,58} using a sum of exponential functions for fitting:

$$\Delta A(t, \lambda_{\text{pr}}) = \phi(\lambda_{\text{pr}}) + \sum_{i=1}^n A_i(\lambda_{\text{pr}}) \cdot e^{-t/\tau_i};$$

with $\phi(\lambda_{\text{pr}})$ being a constant offset to simulate pump-induced absorption changes on time-scales not captured by the

delay-time range accessible in our experiments (2 ns). The $A_i(\lambda_{\text{pr}})$ represent pre-exponential factors of the kinetic components τ_i . The plot of these pre-exponential factors $A_i(\lambda_{\text{pr}})$ corresponds to the so called decay-associated spectra (DAS) of the kinetic components τ_i . In order to avoid prominent contributions from coherent artefacts to the data analysis^{59,60} the pulse-overlap region was ignored in the data fitting procedure.

Fluorescence lifetimes were obtained by time-correlated single photon counting. As light source a Ti-Sapphire laser (Tsunami, Newport Spectra Physics GmbH) was used whose repetition rate was reduced by a pulse selector (Model 3980, Newport Spectra-Physics GmbH) to 800 kHz. The output was frequency doubled in a second harmonic generator (Newport Spectra-Physics GmbH) to create the 435 nm pump beam. The emission was recorded using a Becker & Hickel PMC-100-4 photon-counting module with 150 ps response-limited time resolution. To control the temperature of the sample an Oxford Instruments ITC 503 intelligent temperature monitor and control unit was used. Steady-state absorption spectra were recorded on a Jasco V-670 spectrophotometer, the fluorescence spectra were measured from dilute solutions using a Jasco FP-6200 spectrofluorimeter. Luminescence quantum yields were measured with diluted solutions (optical density < 0.05) using [Ru(bpy)₃]Cl₂ in non-degassed water ($\Phi = 0.028$) as reference (margin of error = 10%).⁶¹

The resonance Raman spectra were recorded in a conventional 90°-scattering arrangement. Excitation light at 458, 476 and 488 nm was delivered by an argon ion laser (Coherent Innova 300C MotoFreD Ion Laser) and used for resonant excitation in the range of the Ru–MLCT absorption band. A rotating cell was employed to prevent heating of the samples. No changes in the absorption spectra of the samples could be observed after exposure to the laser light. The scattered light was collected with a lens ($f_1 = 35 \text{ mm}$) and subsequently focused ($f_2 = 50 \text{ mm}$) onto the entrance slit of an Acton SpectraPro 2758i spectrometer. The dispersed light was detected using a CCD-camera (Princeton Instruments Spec-10 400B/LN back-illuminated). To obtain the best signal-to-noise ratio the concentration of the sample was optimised in the mM range.

Results and discussion

Synthesis and characterization

The different dppzR₂-ligands were prepared by Schiff-base coupling between an orthophenyldiamine derivative and a potentially substituted 1,10-phenanthroline-5,6-dione in alcoholic solution. Thus, the bromine substituted dppz-2,7-Br₂ ligand for **Ru2** was synthesised *via* a condensation reaction between 3,8-dibromophenanthroline-5,6-dione (phenBr₂O₂) and 1,2-diaminobenzene with a yield of more than 75%. The therefore required 3,8-dibromophenanthroline-5,6-dione was obtained from 3,8-dibromo-1,10-phenanthroline (phenBr₂) which was easily oxidised to the corresponding phenBr₂O₂ in a yield of 67% using literature methods.^{41,44-47,49} The subsequent synthesis of the corresponding ruthenium complexes **Ru1** and **Ru2** was accomplished using microwave heating within 3 h and with good yields of above 80%.⁴⁸

Structural characterisation was accomplished using various NMR techniques, MS and elemental analysis. Based on these investigations a conventional octahedral coordination was suggested. These hypotheses were supported by a solid state X-ray structure for **Ru1** (Fig. 1).

The Ru–N bond lengths and angles of **Ru1** are in the typical range for Ru polypyridine complexes. In the solid state structure of **Ru1** the deviation from planarity within the dppz ligand is with 0.049 Å, similar to the reported value of 0.038 Å for **Ru3** which is negligible.⁴³ All three complexes show a concentration-dependent behaviour in ¹H-NMR experiments. The signals corresponding to the dppz ligands are significantly shifted upon variation of the concentration (data presented in the ESI†). This behaviour is indicative of π – π -interactions in solution involving this ligand as seen by Kol and co-workers for similar ligands.^{62,63} Significant interaction is also found in the solid state structure of **Ru3**.⁴³ Here two complex molecules are facing each other in an angle of nearly 180° allowing an interaction of the dppz ligands. A different arrangement could be observed for **Ru1**. Here dppz–dppz interaction is accomplished with both complexes in a mutually perpendicular orientation. The arrangement of two neighbouring complexes of **Ru1** is different to that of **Ru3**. The distance between both dppz planes for **Ru1** is 3.24 Å, which is even shorter than the

3.54 Å observed for **Ru3** (Fig. 1). Comparing **Ru1** and **Ru3** no significant differences in bond lengths and angles around the ruthenium centre or within the dppz ligand can be observed.

Electrochemistry

Cyclic voltammograms of **Ru1**–**Ru3** are consistent with metal-based reversible oxidation and several ligand-based reduction steps,⁶⁴ which are presented in Table 1. In comparison to the unsubstituted dppz ligand in **Ru1** ($E_{\text{ox}}^{\text{Ru(II)/III}} = 0.85$ V) the oxidation potentials of Ru(II)/III in **Ru2** lead towards more positive values, whereas in **Ru3** the oxidation is not affected by the substitution pattern. The first ligand-based reduction step of the phen moiety of dppz (Fig. 2) of **Ru1** is located at –1.34 V and the influence of the electron-withdrawing ability of the bromo substituents in 2,7-position results in a positive shift of 70 mV in **Ru2**. Fees *et al.* describes a cathodic shift of about 100 mV upon going from the unsubstituted dppz ligand to its dimethyl derivative.²⁰ The second and third reductions at around –1.9 V and –2.1 V, respectively, are ascribed to the stepwise one-electron tbbpy-based reduction reactions occurring at potentials less negative than the second reduction of the dppz ligand. The latter takes place at –2.48 to –2.50 V in **Ru1** to **Ru3** and is obviously not markedly affected either by the introduction of –I-substituents like Br or by the substitution pattern.

Steady-state spectroscopy

Fig. 3 comprises the absorption (A) and emission spectra (B) of **Ru1**–**Ru3**. In accordance with the literature^{24,34} the absorption spectra show two distinct electronic transitions in the spectral range above 330 nm. The shortwave absorption band is attributed to a π – π^* transition located on the dppz-ligand, while the longwave transition in the visible parts of the spectrum is assigned to a metal-to-ligand-charge transfer (MLCT) transition. As it is apparent from the data shown in Fig. 3, introduction of bromine substitution at the 11,12-position of the dppz, *i.e.* at the phenazine moiety (phz) (**Ru3**), does not alter the spectral characteristics of the

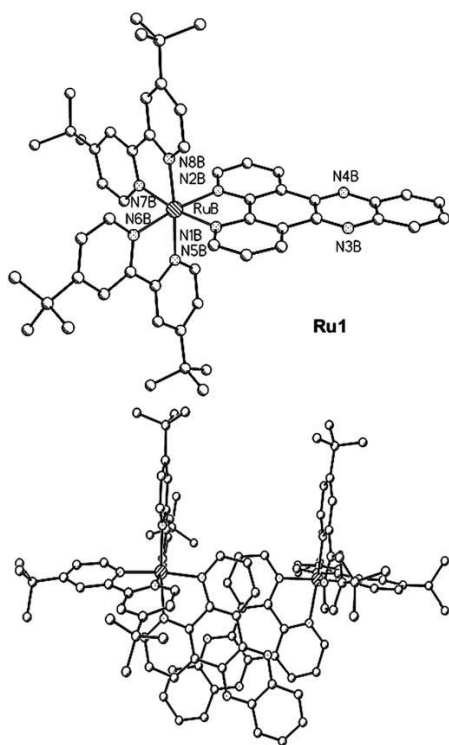


Fig. 1 Top: solid state X-ray structure and numbering scheme of molecule B of **Ru1**, selected bond length and angles of molecule B of **Ru1**: RuB–N1B 2.059(5), RuB–N2B 2.084(4), RuB–N5B 2.070(4), RuB–N6B 2.048(4), RuB–N7B 2.059(4), RuB–N8B 2.053(4); and angles in: N1B–RuB–N2B 79.34 (17), N5B–RuB–N6B 78.11(17), N7B–RuB–N8B 78.64 (17); Bottom: π – π -interaction of **Ru1** in the solid state between the two symmetry independent molecules A and B.

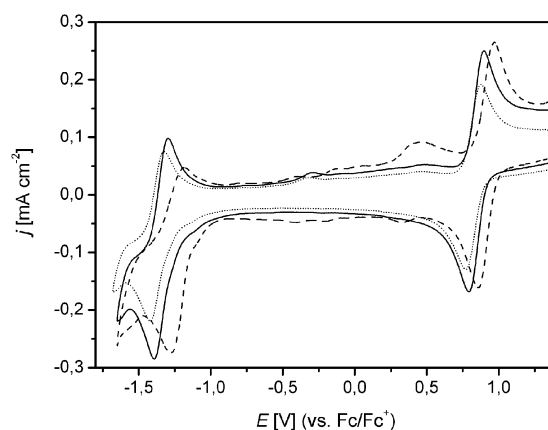


Fig. 2 Cyclic voltammograms of the ruthenium oxidation reaction and the first phenazine based reduction step in comparison to the substitution pattern (scan rate 100 mV s⁻¹). The data for **Ru1**, **Ru2**, **Ru3** is shown as solid line, dashed line and dotted line, respectively.

Table 1 Electrochemical data: Half-wave potentials E [V] (vs. Fc/Fc⁺) in ACN^a

Compound	E_{ox}	$E_{\text{red}}^{\text{I}}$	$E_{\text{red}}^{\text{II}}$	$E_{\text{red}}^{\text{III}}$	$E_{\text{red}}^{\text{IV}}$
Ru1 [Ru(tbbpy) ₂ (dppz)](PF ₆) ₂	0.85	-1.34	-1.86	-2.11	-2.48
Ru2 [Ru(tbbpy) ₂ (dppz-2,7-Br ₂)](PF ₆) ₂	0.90	-1.27	-1.87	-2.11	-2.50
Ru3 [Ru(tbbpy) ₂ (dppz-11,12-Br ₂)](PF ₆) ₂	0.84	-1.36	-1.86	-2.08	-2.47

^a The electrochemical measurements were carried out in anhydrous and nitrogen purged ACN with 0.1 M tetrabutylammonium tetrafluoroborate as supporting electrolyte.

MLCT-band significantly (see inset Fig. 3), which remains very similar to the absorption band of **Ru1**.⁴³ However, the π - π^* transition is shifted to lower energies. Contrary, substitution of Br at the 2,7-position of the dppz ligand and thus at the phenanthroline moiety (phen) of the ligand (**Ru2**) leaves the π - π^* transition unchanged. For **Ru2**, however, a splitting of the MLCT band is observed yielding one transition at roughly 430 nm with a pronounced longwave shoulder at 490 nm (see inset Fig. 3). We verified that all optical spectroscopy experiments were performed in a concentration range, in which the spectroscopic features change linearly with concentration. Therefore, we do not observe any intramolecular effects caused by dimer structures as seen in the NMR experiments, which are generally conducted with complex concentrations in the mM range, which is much higher than the concentration in the 20 μ M used for all optical spectroscopy experiments.

The luminescence quantum yields and lifetimes for **Ru1**–**Ru3** are given in Table 2. In **Ru2** the luminescence quantum yield (2×10^{-2}) is increased by a factor of 2 compared to the unsubstituted complex **Ru1** (1×10^{-2}). An opposite effect is obtained for **Ru3**, where the luminescence quantum yield drops drastically, so that the complex appears non-luminescent.⁴³ Furthermore, the luminescence spectra changes upon introduction of bromine substitution in the 2,7-position: compared to **Ru1** (emission maximum at 650 nm) the emission of **Ru3** appears at 670 nm and hence 460 cm^{-1} red-shifted.

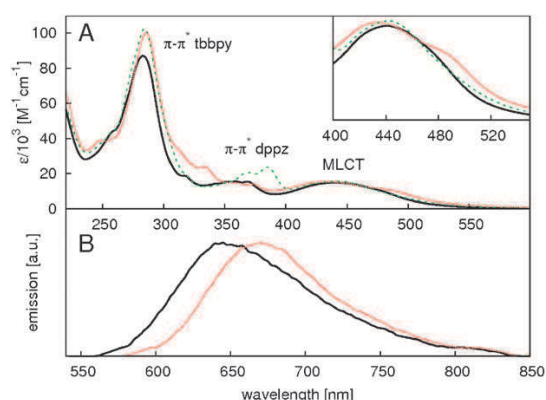


Fig. 3 shows the absorption (A) and emission spectra (B) of **Ru1** (black solid line), **Ru2** (red dotted line) and **Ru3** (green dashed line). The absorption spectra are normalised to the maximum MLCT absorption, the shape of which is highlighted in the inset. The emission spectra of **Ru1** and **Ru2** are normalised to the maximum emission. **Ru3** does not show any emission.

It is known that the luminescence lifetime of **Ru1** is (highly) temperature-dependent (in a range for τ_ϕ between 200 ns to 1300 ns) due to the equilibrium between the dark phz-centered and the bright phen-centered states.²⁸ As shown in Fig. 4 this is not the case for **Ru2** in acetonitrile, where the emission lifetime is almost constant over a broad temperature range. This finding indicates that the bromine substitution on the phen-sphere significantly stabilises the bright state and quenches the charge-transfer to the phz-centered dark state. Otherwise the luminescence lifetime should increase for lower temperatures. This result is kind of surprising in the way that even the well-known deactivation *via* a metal-centered excited state in Ru–polypyridine-complexes can be excluded.^{28–30,65} This also shows that the luminescence lifetime of the bright-state in **Ru2** drastically decreases following the introduction of bromine to dppz's phen-sphere.

The molecular origin of the double-peak MLCT-absorption of **Ru2** can be understood on the basis of the rR data. rR spectroscopy highlights the Franck–Condon active vibrational modes, *i.e.* coupled to the electronic transition.⁶⁶ Hence, it can be utilised to decipher the nature of an electronic transition in multi-chromophore systems and transition metal complexes.^{41,67–69} The rR data obtained in acetonitrile for **Ru1**, **Ru2** and for comparison of [Ru(tbbpy)₃]²⁺ are summarised in Fig. 5 and in Table 3. The rR spectra of **Ru1**, normalised to the solvent band at 920 cm^{-1} , were measured using Raman excitation wavelengths of 458 and 488 nm and thus in resonance with the MLCT-transition. The obtained spectra show enhanced Raman bands which can be assigned to vibrations of both ligands, tbbpy and **L1**.^{25,70,71} However, this situation is changed when considering **Ru2**. As can be seen upon excitation in the maximum of the MLCT transition at 458 nm of **Ru2**, the enhanced modes can be assigned to both ligands, tbbpy and **L2**. For a detailed mode assignment based on the comparison of non-resonant Raman spectra and DFT calculations the reader is referred to.³⁶ However, in comparison to **Ru1** the Raman intensity variation using longer excitation wavelengths is different.

Excitation at long wavelengths result in dominant contributions from the **L2** ligand as can be seen through a comparison of the Raman bands located at 1558 (**L2**) with

Table 2 Summary of emission lifetimes τ_ϕ and quantum yields ϕ as inferred from time-dependent luminescence measurements

	Ru1	Ru2	Ru3
τ_ϕ/ns	100	190	— ^a
ϕ	1×10^{-2}	2×10^{-2}	— ^a

^a The complex appears non-luminescent.

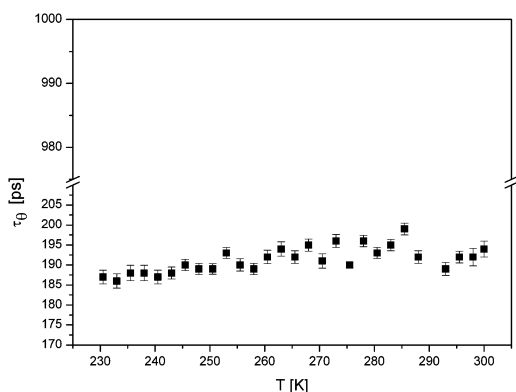


Fig. 4 Temperature dependence of the emission lifetime τ_0 of **Ru2** in acetonitrile. The y-axis is scaled to the normal window of temperature-dependent shifts of luminescence lifetimes of Ru-polypyridine complexes to indicate the specific behaviour of **Ru2**.²⁸

1541/1538 (tbbpy) and 1483/1484 (tbbpy) with 1470/1471 cm^{-1} (**L2**). Thus, we conclude that introduction of Br in the 2,7-positions of the dppz lowers the transition energy of the Ru \rightarrow dppz-MLCT transition, while leaving the Ru \rightarrow tbbpy-MLCT transition unaffected. This effect also explains the appearance of the double-peak structure in the absorption spectrum of **Ru2**. Contrary, no changes in the MLCT-band of **Ru3** are observed as compared to **Ru1**. Schäfer *et al.* could show by means of rR spectroscopy that excitation of **Ru3** in

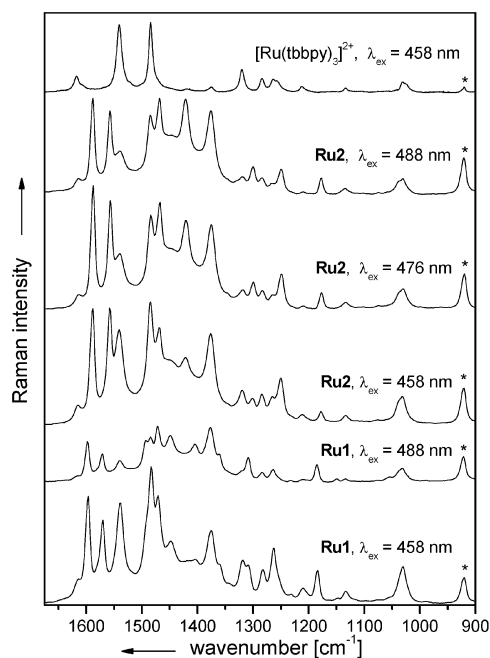


Fig. 5 Resonance Raman spectra of **Ru1**, **Ru2** and for comparison of $[\text{Ru}(\text{tbbpy})_3]^{2+}$ dissolved in ACN (solvent bands are marked with *). The complexes were excited at different wavelengths lying within the first absorption band (Fig. 3). The spectra of **Ru2** are normalised to the solvent band at 920 cm^{-1} .

Table 3 Summary of the resonance Raman bands of **Ru1**, **Ru2** and for comparison of $[\text{Ru}(\text{tbbpy})_3]^{2+}$. The solvent bands are marked with *. Mode positions are given in cm^{-1}

$[\text{Ru}(\text{tbbpy})_3]^{2+}$	Ru1	Ru2
920*	920*	920*
1031	1030	1033
1134	1134	1133
	1184	1179
1212	1211	1211
1265	1264	1250
1284	1282	1284
		1301
1320	1318	1319
1375*	1376*	1376*
	1405	1421
	1448	
	1471	1470
1484	1483	1484
1541	1538	1541
	1570	1558
	1596	1588
1617	1616	1615

the red edge of the MLCT transition results in a predominant MLCT excitation of the substituted dppz ligand.⁴³ This excitation-wavelength dependent absorption behaviour of **Ru3** is quite similar to **Ru1** and not as pronounced as for **Ru2**.

Already the considerations about the absorption spectra, as discussed above, indicate that bromine substitution at the 2,7-positions of dppz (**Ru2**) selectively influences the electronic structure of the phen part of the Ru-dppz complexes. Substitution at the 11,12-position (**Ru3**) and hence at the phz moiety on the other hand leaves the electronic structure of the phen unaffected, while it at the same time selectively influences the dppz π - π^* -transition. This observation illustrates that the latter transition dominantly concerns π -electrons from the phz part of the ligand architecture.

Further evidence of this phen-phz-separation, which has been discussed in the context of electrochemistry experiments²⁰ and is indicated by the steady-state absorption spectra shown above, is obtained from the luminescence data presented here. Luminescence of Ru-dppz complexes originates from the dppz-ligands by the formally spin-forbidden $^3\text{MLCT} \rightarrow \text{S}_0$ -transition, while population of a phz-centered dark state provides an efficient mechanism for fluorescence quenching.^{23,28,30,72} In this context it is notable that the luminescence quantum yield of **Ru2** is enhanced compared to **Ru1**, while luminescence is not observed for **Ru3**. Furthermore, substitution of bromine in the 2,7-position results in a prolonged luminescence lifetime of **Ru2**. While **Ru1** shows a luminescence lifetime of 180 ns (100 ns) in deaerated (aerated) acetonitrile at room temperature, **Ru2** shows a lifetime of 460 ns (180 ns). Similar results have been obtained with related phenanthroline-based complexes.⁴¹ Here bromine substitution in the 3,8-position (equivalent to 2,7 in dppz) resulted in prolongation of lifetime and increased location of the $^1\text{MLCT}$ at long wavelength excitation.

This data reveals the drastic influence of the molecular structure on the luminescence quantum yield. The luminescence of Ru-dppz complexes can be tuned by altering the intermolecular interactions as compared to the

environmentally induced tuning of the luminescence characteristics of dppz-complexes.^{18,23,73} Thus, the results presented here exemplify the possibility to alter the luminescence properties by tailoring (non-sterical) intramolecular interactions. This finding indicates a stabilisation (destabilisation) of the phen-centered MLCT compared to the phz-centered dark state upon introduction of bromine in the 2,7-position, *i.e.* at the phen moiety, (11,12-position, *i.e.* substitution at the phz moiety). This finding has potential implications for the explanation of the nature of the excited state, which are discussed in the following.

Nature of the excited-states. The substitution dependent emission properties of the complexes allow us to shed some new light on the nature of the states involved in the excited-state deactivation of the complexes at hand. In particular the nature of the phz-centered dark state has been disputed in literature. Some authors refer to the dark state as MLCT and the solvent-dependent properties of this state, as well as its temperature dependent population in respect to the phen-centered MLCT state, have been discussed extensively.^{23,27,28,74} However, others refer to the state as a π - π^* state.^{28–33,72} The results discussed here reveal that bromine substitution at the phen moiety increases the emission quantum yield. This shows that despite the introduction of a heavy atom into the molecular architecture, the Br-substituent does not affect the phen-centered MLCT by introducing a higher triplet–singlet interconversion rate due to an increased spin–orbit coupling. The latter is expected to result in a significantly faster excited-state decay and hence in a decreased emission quantum yield. In contrary, bromine substitution at the 2,7-positions increases the luminescence quantum yield compared to **Ru1**, therefore, we conclude that the effect of bromine substitution does not affect the deactivation of excited states with charge-transfer character.

In contrast to 2,7-substitution, bromine substitution at the 11,12 position of the phz moiety significantly reduces the luminescence quantum yield, which can be assigned to an increased triplet–singlet interconversion rate of a phz-centered state. As it was just argued for **Ru2**, the effect of bromine substitution on states with charge-transfer character is completely opposite, *i.e.* increasing lifetime and quantum yield of emission. Therefore the observed loss of emission in **Ru3** might indicate a $\pi\pi^*$ character of the dark state. Such a $\pi\pi^*$ state could be prone to heavy-atom induced singlet–triplet interconversion and hence would allow us to rationalise the experimental results. However, the observed absence of luminescence in **Ru3** might also be accounted for by a MLCT state, in which the electron lies on the phenazine moiety of dppz, *i.e.* some sort of charge-separated state. Such a state might non-radiatively decay with a reduced rate as compared to the phen-centered MLCT. Although we added additional data to the debate, our experimental results are not capable of resolving this long-standing question.

In the remainder of the paper, we will focus on ultrafast time-resolved spectroscopy in order to unravel the details of the photoinduced excited-state relaxation. Thereby, the structure–dynamics relationship underlying these substitution-dependent luminescence properties are revealed.

Ultrafast time-resolved spectroscopy. The photophysics of the complexes was triggered by absorption of a pump pulse at 510 nm, *i.e.* by excitation of the complexes in the MLCT transition. Subsequent ultrafast processes are interrogated by means of transient absorption spectroscopy as described above.

Fig. 6 comprises the global differential absorption changes of **Ru1–Ru3**. At first glance all complexes show comparable excited-state relaxation behaviours. Upon light absorption a positive differential absorption band rises, while in the spectral region probed in this study, *i.e.* 520 nm to 685 nm, no ground-state bleach or stimulated-emission bands are observable. The maximum of the excited-state absorption (ESA) band is located at 590 nm for **Ru1** and **Ru3** and at 600 nm for **Ru2**. The shape of the ΔA spectra is generally in good agreement with spectra recorded for related complexes. In particular, the spectra are in correspondence to long-lived ESA obtained for other dppz-based Ru complexes.^{55,69} When comparing the long-lived ΔA spectra of **Ru1** and **Ru2** with the spectrum of **Ru3**, it becomes apparent that the decrease of the ΔA band towards long probe wavelengths becomes more pronounced for **Ru3**. This results in an almost symmetric ΔA band shape for **Ru3**, while significant contributions to the ΔA signal of **Ru1** and **Ru2** can be seen even at the red edge of our probing window (roughly 30% of the maximum signal). Furthermore, the overall intensity of the ΔA band of **Ru3** is approximately four times higher compared to the bands of **Ru1** and **Ru2**.⁷⁵ This finding resembles recent results on the structurally related complexes $[\text{Ru}(\text{tbbpy})_2\text{tpphz}]^{2+}$ and $[\text{Ru}(\text{tbbpy})_2\text{tpphzPdCl}_2]^{2+}$. For these systems it was shown that the excited-state absorption cross-section increases approximately twofold upon coordination of $[\text{Ru}(\text{tbbpy})_2\text{tpphz}]^{2+}$ with the PdCl_2 -moiety.⁶⁹

Aside from these spectral changes, for the complexes **Ru1** and **Ru3** the dynamics are complete after a few hundred ps, while the excited-state dynamics of **Ru2** comes to a halt in only a few ps. **Ru3** on the other hand reveals a biphasic rise on a time-scale comparable to **Ru1**, which however is followed by a decay of the band.

To further analyse the two-dimensional $\Delta A(\tau_{\text{pr}}, t)$ data more quantitatively a global fitting routine was applied as described above. The result of this approach is summarised in Fig. 8 and Table 4. The prominent substitution-induced effect on the excited-state relaxation kinetics highlighted in Fig. 8 is mirrored in the different abundances of kinetic components for either of the complexes: All three complexes show a fast ps-component (τ_1), which is followed by a second rise-component in the range of 100–200 ps (τ_2) only for **Ru1** and **Ru3**. The slowest kinetic component (τ_3) is visible in the ΔA data of **Ru3** only, where it appears as a decay of the signal.

For more detailed considerations we turn to Fig. 7, which depicts the DAS of compounds **Ru1–Ru3**. The DAS corresponding to the constant in the multiexponential fit function reveals a long-lived excited-state absorption in **Ru1–Ru3**, which resembles the prominent spectral features discussed already. The build-up of the excited-state absorption band is reflected in negative amplitudes of the DAS corresponding to τ_1 and τ_2 for all complexes. For **Ru1** and **Ru3** the $\text{DAS}(\tau_1, \tau_2)$ generally follow the inverted shape of the long-lived excited-state absorption spectrum, while for **Ru2** only negligible

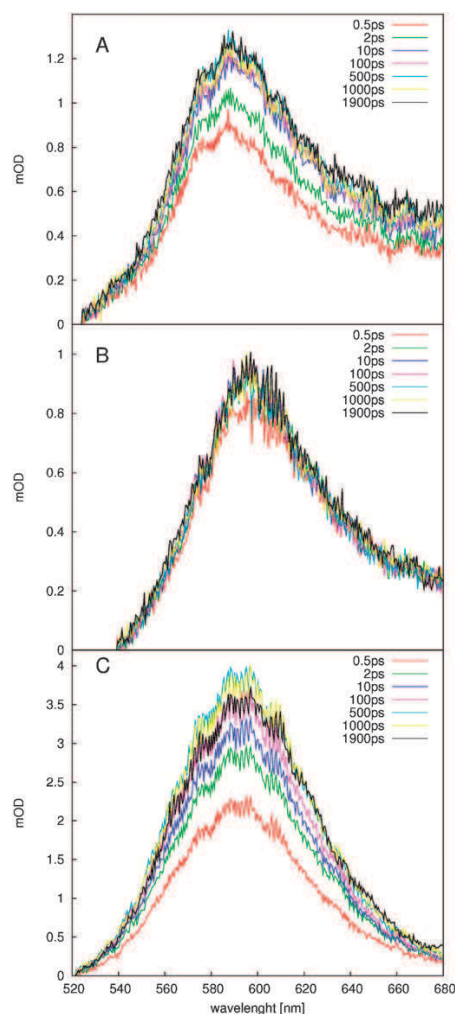


Fig. 6 Different absorption spectra of **Ru1** (A), **Ru2** (B) and **Ru3** (C) recorded at different delay times, which are given in the inset.

Table 4 summarises the characteristic decay times τ_i obtained from a global fit of the ΔA data. τ_3 denotes a decay time, while $\tau_{1,2}$ refer to a build-up of the ΔA band for all complexes. It has to be noted, that the actual value of τ_3 represents an estimate only due to the limited range of delay times accessible in our experimental setup. However, the actual value of τ_3 is of minor importance for the following argumentation

	Ru1	Ru2	Ru3
τ_1/ps	2.4	1.3	1.0
τ_2/ps	150	—	200
τ_3/ns	—	—	10^a

^a This component appears as a signal decay.

differential absorption changes on a time-scale corresponding to τ_1 are observed for probe-wavelengths longer than 630 nm.

Generally, the photophysics of Ru–polypyridine complexes involve ultrafast (sub-200 fs) inter-system crossing (ISC) from the initially photoexcited $^1\text{MLCT}$ to the $^3\text{MLCT}$ ⁷⁶—a process

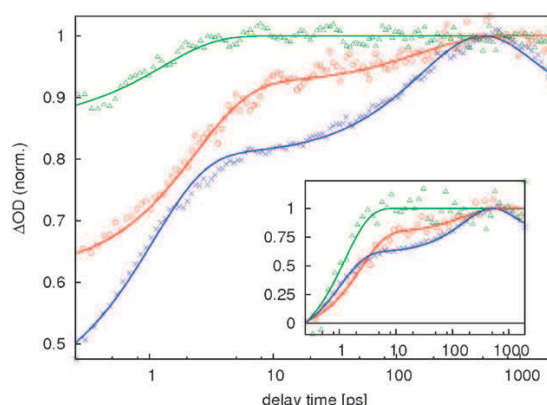


Fig. 7 Normalised differential absorption kinetics reflecting the temporal behaviour of the broad visible DA of **Ru1** (circles), **Ru2** (triangles) and **Ru3** (crosses) band are shown. The two-dimensional experimental data was integrated over the probe wavelengths to obtain kinetics, which were subsequently normalised to the maximum signal. Symbols refer to experimental data, while solid lines indicate the results of the global fitting approach as discussed in the text. The inset shows the data in a min–max-normalisation representation.

which escapes detection in these experiments due to strong contributions from coherent artefacts, which hamper the data analysis in roughly the first 200 fs after photoexcitation.^{59,68,77} The fastest process apparent in our experiments occurs on a ps time-scale. We assign this process to thermal equilibration of the rapidly formed dppz- $^3\text{MLCT}$ state as previously observed for related complexes.^{66,78–80}

Subsequent to the formation of the equilibrated $^3\text{MLCT}$ state, the system relaxes to the phz-centered state, which in the nomenclature of Barbara and coworkers is referred to as MLCT.^{2,23} This relaxation takes place on a 100-ps timescale, which is in agreement with reports on related complexes in acetonitrile.⁵⁵ It is interesting to note that such a relaxation step is absent in the case of **Ru2**. Furthermore, for **Ru3** a yet slower kinetic component is observed, the characteristic time of which is roughly estimated to be 10 ns. The latter τ_3 -component is spectrally characterised by the decay of the broad excited-state absorption band and assigned to the overall non-radiative decay of the excited-state population.

Substitution-controlled excited-state dynamics. In the remainder of the paper we shall discuss the influence of the specific bromine substitution pattern on the excited-state dynamics in **Ru2** and **Ru3** compared to **Ru1**: In all three complexes the formation of the equilibrated $^3\text{MLCT}$ state is kinetically viable. From the rR data (monitoring the Franck–Condon point) and experiments on related complexes (monitoring the ps-relaxation dynamics upon photoexcitation)^{25,70,71} it is apparent that this process characterised by τ_1 leads to the population of a dppz-centered MLCT state localised on the phen part of the ligand, which is energetically lowered compared to the tbbpy-centered MLCT states. While **Ru1** and **Ru3** show further ps and ns decay components, the ultrafast excited-state dynamics in **Ru2** are arrested after a few ps. To understand this result the effect of

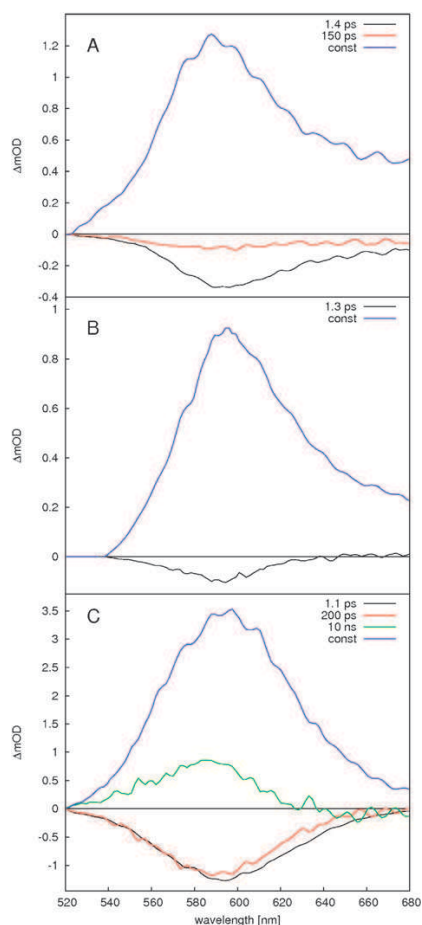


Fig. 8 Decay-associated spectra (DAS) reflecting the photoinduced processes in **Ru1** (A), **Ru2** (B) and **Ru3** (C).

the bromine substitution in the 2,7-position must be also considered to tentatively rationalise the changes within the luminescence quantum yields. The Br-substitution at the phen stabilises the bright MLCT (phen centered) state with respect to the dark phz-centered $^3\pi\pi^*$ state to an extent that inhibits further relaxation *via* the phz-channel (Scheme 3). The latter channel is open for **Ru1** and **Ru3** as indicated by the presence of the respective kinetic component (τ_2). Bromine substitution at the 11,12-position of phz on the other hand stabilises the phz-centered state with respect to the MLCT and hence reduces the luminescence quantum yield. Furthermore, it increases the non-radiative decay rate of the phz-centered $^3\pi\pi^*$ state to an extent, that the decay of the excited-state absorption becomes already visible within the range of delay times accessible in our experiments.

This kinetic viewpoint is corroborated by the differences in the long-lived differential absorption spectra as discussed above. The decrease in ΔA -signal towards longer probe-wavelengths in **Ru3** can be attributed to the absence of a $^3\text{MLCT} \rightarrow S_n$ excited-state absorption, which is expected to be observed at the red edge of our probe window.⁵⁵ Coates *et al.*⁵⁵ observed a similar effect for the ESA of $\text{Ru}(\text{phen})_2\text{dppz}^{2+}$

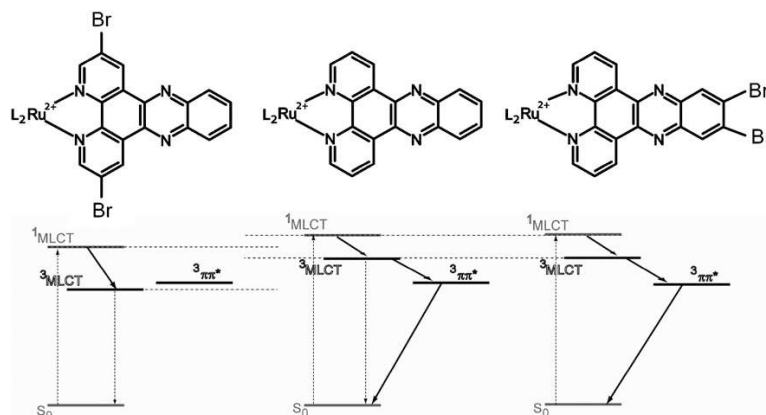
when dissolved in solvents of different proticity: while in ACN a red-component is visible in the ΔA -spectra on a 100-ps time scale, it is absent when dissolving the complex in either water containing buffer or methanol. While Coates *et al.* discuss the photophysics of $\text{Ru}(\text{phen})_2\text{dppz}^{2+}$ in the context of a solvent-induced light-switch effects, similar analogous effects can be introduced by various substitution pattern of the dppz structure.

Thus, the experiments presented here constitute an example for a clear structure–dynamics correlation, where the luminescent properties and the underlying ultrafast excited-state dynamics are controlled by locally dependent substitution of bromine—and not by variations of the environment of the complexes as in conventional light-switch experiments. The time-resolved experiments show that such effect is achieved by not only modifying decay characteristics but actually blocking certain decay channels, indicating that strong intramolecular electron transfer gradients can be achieved by the here-discussed substitution pattern. This finding opens the doorway of combining intra- and intermolecular effects to mutually enhance (or suppress, respectively) the driving force for intramolecular electron transfer across the dipyrrophenazine unit. This might be of particular interest as Ru–Pd tetrapyrrophenazine complexes, containing dppz as building blocks, have been shown to be suitable supra-molecular catalysts for the visible light-driven production of hydrogen.

Conclusions

Synthesis and structural characterisation of a novel dppz-derivative, 2,7-dibromodipyrrophenazine, in concert with its Ru-complex, *i.e.* $[(\text{tbbpy})_2\text{Ru}(\text{dppz-2,7-Br}_2)](\text{PF}_6)_2$, are presented and the photophysical properties of this complex are compared to the light-induced processes in structurally related Ru–dppz complexes. The substitution patterns discussed here do not only shift the excited-state spectra of the corresponding Ru-complexes or accelerate/decelerate particular relaxation steps but block entire relaxation pathways. Therefore, the results presented here allow for a direct correlation of structural modifications with distinct kinetic components in the excited-state dynamics of the complexes. We rationalise this drastic effect of the different substitution patterns by a substitution-dependent energy difference between the bright phen-centered state and the dark phz-centered state. Introduction of bromine at the 2,7-position, *i.e.* at the phen moiety, stabilises the bright state of the dppz ligand to the extent that no further relaxation to the dark phz state is possible. Hence, the luminescence quantum yield is increased and the ultrafast excited-state relaxation is arrested after formation of the relaxed $^3\text{MLCT}$ state. On the contrary, substituting bromine at the 11,12-position of phz stabilises the dark state (relative to the bright state), reduces the luminescence quantum yield and accelerates the non-radiative decay of excited molecules back to the ground-state (Scheme 3).

Thus, the results presented show the drastic influence of minimal alterations of the molecular structure on the ultrafast excited-state dynamics and the subsequent



Scheme 3 A schematic presentation of the molecular origin for the substitution-dependent excited-state processes in **Ru1–Ru3** (left: **Ru2**, center: **Ru1**, right: **Ru3**). Horizontal lines represent electronic state involved in the photophysics of the complexes, while dashed (solid) arrows refer to radiative (non-radiative) transitions. L refers to a tbppy-ligand.

ns-radiative properties. It could be shown, that introduction of bromine into the ligand structure induces position-dependent effects, which can be understood based on the well known $-I$ and $+M$ -effect of bromine.⁸¹ The results presented in this study detail a route for the design of ligand system and their respective Ru-complexes with optimised electron-transfer properties, *i.e.* tpphz-based systems for tuning the catalytic activity in Ru/Pd-heterodinuclear complexes. Additionally, our results on the side-specific electronic effects of substitution indicate an important starting point for the introduction of organic substituents to extend the molecular architecture and control the electronic properties of the dppz ligand. Finally, the prolongation of the excited-state lifetime of the more reactive phen-centered excited charge-transfer state upon introduction of bromine in the 2,7-positions opens a doorway for the optimisation of, for instance, photocatalytic processes. Therefore, the herein presented results are expected to have a broad impact for the design of novel ligand architectures and tuning of the photophysical and photochemical properties of Rudppz complexes.

Acknowledgements

We are grateful for Denis Akimov's help with the experimental setup. S. R. and M. K. gratefully acknowledge financial support by the DFG and the SFB 583. S. K. is very grateful to the Verband der Chemischen Industrie (VCI/FCI) for a PhD grant. B. D. and J. P. acknowledge financial support by the Fonds der Chemischen Industrie, while C. K. thanks the Deutsche Bundesstiftung Umwelt for a PhD fellowship.

References

- J. Lehn, in *Supramolecular Chemistry: Concepts and Perspectives*, Wiley-VCH, Weinheim, 1995, pp. 1–262.
- V. Balzani, A. Juris, M. Venturi, S. Campagna and S. Serroni, *Chem. Rev.*, 1996, **96**, 759–833.
- F. Scandola, C. Chiorboli, M. T. Indelli and M. A. Rampi, in *Electron Transfer in Chemistry*, ed. V. Balzani, Wiley-VCH, Weinheim, 2001, vol. 3, p. 337.
- S. Campagna, F. Puntoriero, F. Nastasi, G. Bergamini and V. Balzani, *Top. Curr. Chem.*, 2007, **280**, 117–214.
- A. J. Esswein and D. G. Nocera, *Chem. Rev.*, 2007, **107**, 4022–4047.
- M. Grätzel, *Nature*, 2001, **414**, 338–344.
- M. Grätzel, *Inorg. Chem.*, 2005, **44**, 6841–6851.
- H. B. Gray and J. R. Winkler, *Proc. Natl. Acad. Sci. U. S. A.*, 2005, **102**, 3534–3539.
- S. Rau, D. Walther and J. G. Vos, *Dalton Trans.*, 2007, 915–919.
- J. B. Cooper, M. G. B. Drew and P. D. Beer, *J. Chem. Soc., Dalton Trans.*, 2001, 392–401.
- P. D. Beer and E. J. Hayes, *Coord. Chem. Rev.*, 2003, **240**, 167–189.
- P. D. Beer, F. Szemes, P. Passaniti and M. Maestri, *Inorg. Chem.*, 2004, **43**, 3965–3975.
- S. Rau, T. Büttner, C. Temme, M. Ruben, H. Gørls, D. Walther, M. Duati, S. Fanni and J. G. Vos, *Inorg. Chem.*, 2000, **39**, 1621–1624.
- B. D. MacCraith, C. M. McDonagh, G. O'Keefe, E. T. Keyes, J. G. Vos, B. O'Kelly and J. F. McGilp, *Analyst*, 1993, **118**, 385–388.
- J.-C. Chambron, J.-P. Sauvage, E. Amouyal and P. Koffi, *New J. Chem.*, 1985, **9**, 527–529.
- A. E. Friedman, J.-C. Chambron, J.-P. Sauvage, N. J. Turro and J. K. Barton, *J. Am. Chem. Soc.*, 1990, **112**, 4960–4962.
- J.-P. Sauvage and J.-C. Chambron, *Chem. Phys. Lett.*, 1991, **182**, 603–607.
- Y. Jenkins, E. A. Friedman, J. N. Turro and K. J. Barton, *Biochemistry*, 1992, **31**, 10809–10816.
- R. M. Hartshorn and J. K. Barton, *J. Am. Chem. Soc.*, 1992, **114**, 5919–5925.
- J. Fees, W. Kaim, M. Moscherosch, W. Matheis, J. Klíma, M. Krejčík and S. Zláliš, *Inorg. Chem.*, 1993, **32**, 166–174.
- C. Turro, S. H. Bossmann, Y. Jenkins, J. K. Barton and N. J. Turro, *J. Am. Chem. Soc.*, 1995, **117**, 9026–9032.
- I. Haq, P. Lincoln, D. Suh, B. Norden, B. Z. Chowdhry and J. B. Chaires, *J. Am. Chem. Soc.*, 1995, **117**, 4788–4796.
- E. J. C. Olson, D. Hu, A. Hörmann, A. M. Jonkman, M. R. Arkin, E. D. A. Stemp, J. K. Barton and P. F. Barbara, *J. Am. Chem. Soc.*, 1997, **119**, 11458–11467.
- E. Amouyal, A. Homsí, J.-C. Chambron and J.-P. Sauvage, *J. Chem. Soc., Dalton Trans.*, 1990, 1841–1845.
- J. R. Schoonover, W. D. Bates and T. J. Meyer, *Inorg. Chem.*, 1995, **34**, 6421–6422.
- G. Pourtois, D. Beljonne, C. Moucheron, S. Schumm, A. Kirsch-De Mesmaeker, R. Lazzaroni and J. Bredas, *J. Am. Chem. Soc.*, 2004, **126**, 683–692.
- Y. Sun, D. A. Lutterman and C. Turro, *Inorg. Chem.*, 2008, **47**, 6427–6434.
- M. K. Brennaman, J. H. Alstrum-Acevedo, C. N. Fleming, P. Jang, T. J. Meyer and J. M. Papanikolas, *J. Am. Chem. Soc.*, 2002, **124**, 15094–15098.

- 29 M. K. Brennaman, T. J. Meyer and J. M. Papanikolas, *J. Phys. Chem. A*, 2004, **108**, 9938–9944.
- 30 J. Olofsson, B. Onfelt and P. Lincoln, *J. Phys. Chem. A*, 2004, **108**, 4391–4398.
- 31 S. Fantacci, F. De Angelis, A. Sgamellotti and N. Re, *Chem. Phys. Lett.*, 2004, **396**, 43–48.
- 32 E. R. Batista and R. L. Martin, *J. Phys. Chem. A*, 2005, **109**, 3128–3133.
- 33 M. Atsumi, L. González and C. Daniel, *J. Photochem. Photobiol., A*, 2007, **190**, 310–320.
- 34 W. Chen, C. Turro, L. Friedman, J. Barton and N. Turro, *J. Phys. Chem. B*, 1997, **101**, 6995–7000.
- 35 C. G. Coates, J. Olofsson, M. Coletti, J. J. McGarvey, B. Onfelt, P. Lincoln, B. Norden, E. Tuite, P. Matousek and A. W. Parker, *J. Phys. Chem. B*, 2001, **105**, 12653–12664.
- 36 C. Kuhnt, S. Tschierlei, M. Karnahl, S. Rau, B. Dietzek, M. Schmitt and J. Popp, *J. Raman Spectrosc.*, 2009, DOI: 10.1002/jrs.2534.
- 37 N. Komatsuzaki, R. Katoh, Y. Himeda, H. Sugihara, H. Arakawa and K. Kasuga, *J. Chem. Soc., Dalton Trans.*, 2000, 3053–3054.
- 38 M. K. Kuimova, D. C. Grills, P. Matousek, A. W. Parker, X.-Z. Sun, M. Towrie and M. W. George, *Vib. Spectrosc.*, 2004, **35**, 219–223.
- 39 J. Dyer, C. M. Creely, J. C. Penedo, D. C. Grills, S. Hudson, P. Matousek, A. W. Parker, M. Towrie, J. M. Kelly and M. W. George, *Photochem. Photobiol. Sci.*, 2007, **6**, 741–748.
- 40 M. K. Kuimova, X.-Z. Sun, P. Matousek, D. C. Grills, A. W. Parker, M. Towrie and M. W. George, *Photochem. Photobiol. Sci.*, 2007, **6**, 1158–1163.
- 41 M. Karnahl, S. Kriek, H. Görls, S. Tschierlei, M. Schmitt, J. Popp, D. Chartrand, G. S. Hanan, R. Groarke, J. G. Vos and S. Rau, *Eur. J. Inorg. Chem.*, 2009, 4962–4971.
- 42 M. Karnahl, S. Tschierlei, C. Kuhnt, B. Dietzek, M. Schmitt, J. Popp, M. Schwalbe, S. Kriek, H. Görls, F. W. Heinemann and S. Rau, *Dalton Trans.*, 2010, **39**, DOI: 10.1039/b917484b.
- 43 B. Schäfer, H. Görls, M. Presselt, M. Schmitt, J. Popp, W. Henry, J. G. Vos and S. Rau, *Dalton Trans.*, 2006, 2225–2231.
- 44 M. Yamada, Y. Tanaka, Y. Yoshimoto, S. Kuroda and I. Shimao, *Bull. Chem. Soc. Jpn.*, 1992, **65**, 1006–1011.
- 45 D. Tzalis, Y. Tor, S. Failla and J. S. Siegel, *Tetrahedron Lett.*, 1995, **36**, 3489–3490.
- 46 R. Eisenberg and W. Paw, *Inorg. Chem.*, 1997, **36**, 2287–2293.
- 47 C. Dietrich-Buchecker, M. C. Jiménez and J.-P. Sauvage, *Tetrahedron Lett.*, 1999, **40**, 3395–3396.
- 48 S. Rau, B. Schäfer, A. Grüßing, S. Schebesta, K. Lamm, J. Vieth, H. Görls, D. Walther, M. Rudolph, U. W. Grummt and E. Birkner, *Inorg. Chim. Acta*, 2004, **357**, 4496–4503.
- 49 S. Ott and R. Faust, *Synthesis*, 2005, 3135–3139.
- 50 The data deposited at the Cambridge Crystallographic Data Centre under CCDC-617549 contain the supplementary crystallographic data for **Ru1** excluding structure factors.
- 51 *COLLECT Data Collection Software*, B. V. Nonius, Netherlands, 1998.
- 52 Z. Otwinowski and W. Minor, *Methods Enzymol.*, 1997, **276**, 307–326.
- 53 G. M. Sheldrick, *Acta Crystallogr., Sect. A: Found. Crystallogr.*, 1990, **46**, 467–473.
- 54 G. M. Sheldrick, *SHELXL-97*, University of Göttingen, Germany, 1997.
- 55 C. G. Coates, P. Callaghan, J. J. McGarvey, J. M. Kelly, L. Jacquet and A. Kirsch-De Mesmaeker, *J. Mol. Struct.*, 2001, **598**, 15–25.
- 56 R. Siebert, D. Akimov, M. Schmitt, A. Winter, U. S. Schubert, B. Dietzek and J. Popp, *ChemPhysChem*, 2009, **10**, 910–919.
- 57 A. R. Holzwarth, *Adv. Photosynth.*, 1996, **3**, 75–92.
- 58 B. Dietzek, S. Tschierlei, G. Hermann, A. Yartsev, T. Pascher, V. Sundström, M. Schmitt and J. Popp, *ChemPhysChem*, 2009, **10**, 144–150.
- 59 A. L. Dobryakov, J. Ruthmann and N. P. Ernsting, *Phys. Rev. A: At., Mol., Opt. Phys.*, 1999, **59**, 2369–2384.
- 60 B. Dietzek, T. Pascher, V. Sundström and A. Yartsev, *Laser Phys. Lett.*, 2007, **4**, 38–43.
- 61 K. Nakamura, *Bull. Chem. Soc. Jpn.*, 1982, **55**, 2697–2705.
- 62 S. D. Bergman, I. Goldberg, A. Barbieri and M. Kol, *Inorg. Chem.*, 2005, **44**, 2513–2523.
- 63 D. Gut, I. Goldberg and M. Kol, *Inorg. Chem.*, 2003, **42**, 3483–3491.
- 64 A. Juris, V. Balzani, F. Barigelletti, S. Campagna, P. Belser and A. V. Zelevsky, *Coord. Chem. Rev.*, 1988, **84**, 85–277.
- 65 F. Barigelletti, L. De Cola, V. Balzani, P. Belser, A. v. Zelevski, F. Vögtle, F. Ebmeyer and S. Grammenudi, *J. Am. Chem. Soc.*, 1989, **111**, 4662–4668.
- 66 A. B. Myers, *Chem. Rev.*, 1996, **96**, 911–926.
- 67 S. Tschierlei, B. Dietzek, M. Karnahl, S. Rau, F. M. MacDonnell, M. Schmitt and J. Popp, *J. Raman Spectrosc.*, 2008, **39**, 557–559.
- 68 B. Dietzek, W. Kiefer, J. Blumhoff, L. Böttcher, S. Rau, D. Walther, U. Uhlemann, M. Schmitt and J. Popp, *Chem.–Eur. J.*, 2006, **12**, 5105–5115.
- 69 S. Tschierlei, M. Presselt, C. Kuhnt, A. Yartsev, T. Pascher, V. Sundström, M. Karnahl, M. Schwalbe, B. Schäfer, S. Rau, M. Schmitt, B. Dietzek and J. Popp, *Chem.–Eur. J.*, 2009, **15**, 7678–7688.
- 70 W. R. Browne and J. McGarvey, *Coord. Chem. Rev.*, 2006, **250**, 1696–1709.
- 71 C. G. Coates, P. L. Callaghan, J. J. McGarvey, J. M. Kelly, P. E. Kruger and M. E. Higgins, *J. Raman Spectrosc.*, 2000, **31**, 283–288.
- 72 J. Olofsson, L. M. Wilhelmsson and P. Lincoln, *J. Am. Chem. Soc.*, 2004, **126**, 15458–15465.
- 73 N. Armaroli, L. D. Cola, V. Balzani, J.-P. Sauvage, C. O. Dietrich-Buchecker and J. M. Kern, *J. Chem. Soc., Faraday Trans.*, 1992, **88**, 553–6.
- 74 A. C. Benniston, P. Matousek and A. W. Parker, *J. Raman Spectrosc.*, 2000, **31**, 503–507.
- 75 Care was taken to ensure that for all experiments samples with identical optical densities, *i.e.* OD = 0.5 at the excitation wavelength, and identical pump-pulse intensities, *i.e.* 500 nJ per pulse, were used.
- 76 N. H. Damrauer, G. Cerullo, A. Yeh, T. R. Bousie, C. V. Shank and J. K. McCusker, *Science*, 1997, **275**, 54–57.
- 77 S. Wallin, J. Davidsson, J. Modin and L. Hammarström, *J. Phys. Chem. A*, 2005, **109**, 4697–4704.
- 78 A. C. Bhasikuttan, M. Suzuki, S. Nakashima and T. Okada, *J. Am. Chem. Soc.*, 2002, **124**, 8398–8405.
- 79 B. Dietzek, D. Akimov, W. Kiefer, S. Rau, J. Popp and M. Schmitt, *Laser Phys. Lett.*, 2007, **4**, 121–125.
- 80 It should be noted that Coates *et al.* discussed a state with a ps lifetime, which proceeds the formation of the dppz-MLCT state. This precursor-state was observed in [Ru(phen)₂dppz]²⁺ and according to Coates *et al.* should not be spectroscopically visible in our probe-range (ref. 35). However, as different molecular species are considered here, we cannot definitely rule out contributions from an analogous “precursor”-state to the ps-component observed here.
- 81 F. A. Carey and R. J. Sundberg, in *Organische Chemie–Ein Weiterführendes Lehrbuch*, ed. H. J. Schäfer, D. Hoppe, G. Erker, Wiley VCH, Weinheim, 1st edn, 1995, p. 201.

[CK3] Tuning of Photocatalytic Hydrogen Production and Photoinduced Intramolecular Electron Transfer Rates by Regioselective Bridging Ligand Substitution

Der Nachdruck der folgenden Publikation erfolgt mit freundlicher Genehmigung von Wiley-VCH Verlag GmbH & Co. KGaA.

Reproduced with permission from:

M. Karnahl, C. Kuhnt, F. Ma, A. Yartsev, M. Schmitt, B. Dietzek, S. Rau, J. Popp, TUNING OF PHOTOCATALYTIC HYDROGEN PRODUCTION AND PHOTOINDUCED INTRAMOLECULAR ELECTRON TRANSFER RATES BY REGIOSELECTIVE BRIDGING LIGAND SUBSTITUTION, *Chem. Phys. Chem.*, **2011**, *12*, 2101-2109

Copyright 2011 Wiley-VCH Verlag GmbH & Co. KG KGaA., Weinheim

DOI: 10.1002/cphc.201100245

Tuning of Photocatalytic Hydrogen Production and Photoinduced Intramolecular Electron Transfer Rates by Regioselective Bridging Ligand Substitution

Michael Karnahl,^[e] Christian Kuhnt,^[b] Fei Ma,^[c] Arkady Yartsev,^[c] Michael Schmitt,^[b] Benjamin Dietzek,^{*,[b, d]} Sven Rau,^{*,[a]} and Jürgen Popp^[b, d]

Artificial photosynthesis based on supramolecular photocatalysts offers the unique possibility to study the molecular processes underlying catalytic conversion of photons into chemical fuels in great detail and to tune the properties of the photocatalyst by alterations of the molecular framework. Herein we focus on both possibilities in studying the photocatalytic reduction of protons by derivatives of the well-known photocatalyst [(tbbpy)₂Ru(tpphz)PdCl₂](PF₆)₂ [4,4'-di-*tert*-butyl-2,2'-bipyridine (tbbpy), tetrapyrido[3,2-*a*:2',3'-*c*:3'',2''-*h*:2''',3'''-*j*]phenazine (tpphz)]. We report on a modified photocatalyst where the crucial bridging ligand tpphz is substituted by bromine and investigate the effect of the structural variation on the catalytic properties of the complex and its ultrafast intramolecular

charge transfer behavior. It is found that structural modification stabilizes the phenanthroline-centered metal-to-ligand charge-transfer state on the tpphz moiety, thereby reducing the electron transfer gradient across the entire electron-relaying bridging ligand and at the same time accelerating nano-second ground-state recovery. The same structural modifications cause an overall reduction of the catalytic activity of the complex. Thus, the results highlight the potential of small structural variations in the molecular framework of supramolecular catalysts in understanding the photoinduced charge-transfer processes and optimizing their catalytic performance.

1. Introduction

An ever-increasing demand for energy combined with depleting stocks of fossil fuels makes the use of solar energy very interesting.^[1–5] The conversion of solar energy into electricity using solar cells is already technologically developed. In this regard, photochemical molecular devices on the basis of dye molecules attached to semiconducting electrode surfaces opened an interesting alternative to conventional silicon solar cells.^[2,6,7] An alternative concept is light-driven catalysis, where solar energy is used to drive chemical reactions, which store the energy of the light in chemical bonds. These energy-rich molecules can be efficiently stored, transported and used as fuels. Heterogeneous photocatalysts that are capable of splitting water into hydrogen and oxygen have been developed and current developments suggest that a more detailed understanding of the nature of the catalytically active surface-bound species is evolving.^[8,9] Inspired by the delicate architecture of biological photosynthesis, supramolecular photocatalysts that are capable of using visible light to reduce protons to molecular hydrogen in the presence of a reducing agent have been developed.^[10–12]

These novel photocatalysts are composed of at least three essential building blocks:^[10–14] they consist of a photocenter (photosensitizer), a molecular bridge and a catalytic center. This modular construction concept might open a route towards tunable catalytic systems. Recently, several of these intramolecular catalysts have been realized by combining a ruthenium chromophore and a reaction center such as platinum, palladium, rhodium or cobalt bridged by an appropriate

ligand.^[15–18] The prominent role of the bridging ligand is not only the combination of the two metal centers. Rather it should allow a directed photoinduced electron transfer, serve

[a] Prof. Dr. S. Rau⁺⁺⁺

*Institute of Inorganic Chemistry
University Ulm
Albert-Einstein-Allee 11, 89081 Ulm (Germany)
Fax: (+49) 731-5023039
E-mail: sven.rau@uni-ulm.de*

[b] C. Kuhnt,^{*} Prof. Dr. M. Schmitt, Dr. B. Dietzek,⁺⁺ Prof. Dr. J. Popp

*Institute of Physical Chemistry and Abbe Center of Photonics
Friedrich-Schiller-University Jena
Helmholtzweg 4, 07743 Jena (Germany)
Fax: (+49) 3641-948309
E-mail: benjamin.dietzek@uni-jena.de*

[c] Dr. F. Ma, Prof. Dr. A. Yartsev

*Department of Chemical Physics
Lund University
Getingevägen 60, S-22241 Lund (Sweden)*

[d] Dr. B. Dietzek,⁺⁺ Prof. Dr. J. Popp

*Institute of Photonic Technology (IPHT) Jena e.V.
Albert-Einstein-Straße 9, 07745 Jena (Germany)*


[e] Dr. M. Karnahl^{*}

*Department of Photochemistry and Molecular Science
Uppsala University
Lägerhydds väg 1, 75237 Uppsala (Sweden)*

[*] These authors contributed equally to the work.

[++] Correspondence regarding ultrafast spectroscopy

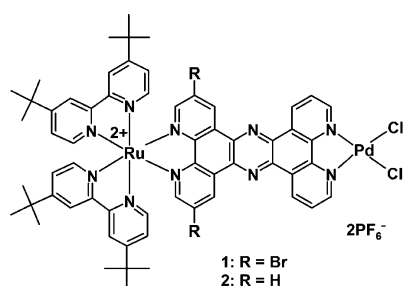
[+++] Correspondence regarding synthesis and catalysis

 Supporting information for this article is available on the WWW under <http://dx.doi.org/10.1002/cphc.201100245>.

as an electron reservoir and tune the interaction between both metal centers, that is, limiting detrimental back electron transfer.

Recently it has been shown that the location of the first excited state, ¹MLCT, in the known photocatalyst [(tbbpy)₂Ru(tpphz)PdCl₂](PF₆)₂ [4,4'-di-*tert*-butyl-2,2'-bipyridine (tbbpy), tetrapyrido[3,2-*a*:2',3'-*c*:3'',2''-*h*:2''',3''''-*j*]phenazine (tpphz)] is of fundamental importance for the catalytic activity of this complex.^[19] If the excited state is localized on the peripheral bipyridine ligands, a significantly lower catalytic efficiency is observed as compared to the localization of the excited state on the bridging ligand. These results lead to a new design concept for photocatalysts termed Frank–Condon point (FCP) design.^[19] One direct consequence of this concept is the development of bridging ligands that are substituted in such a way that an increased likelihood of location of the ¹MLCT on the bridging ligand state can be expected.

Based on what is known regarding the influence of bridging ligands on the photochemistry of multinuclear metal complexes, several additional factors have to be taken into account.^[20] It has to be considered that other properties of the bridging ligand such as electron storage and stabilization of the reaction-center components are also crucial for the overall catalytic activity in addition to effects deduced from the FCP-design concept.^[21–23] For these reasons we chose to investigate a regioselective substituted tpphz bridging ligand in a ruthenium–palladium complex, which is able to evolve hydrogen (Scheme 1). By comparison with the well-known corresponding unsubstituted ruthenium complex [(tbbpy)₂Ru(tpphz)PdCl₂](PF₆)₂,^[24] conclusions about the resulting structure–property relationships could potentially be deduced. In addition to the



Scheme 1. Chemical structure of the different tpphz-based heterodinuclear ruthenium complexes [(tbbpy)₂Ru(Br₂tpphz)PdCl₂](PF₆)₂ **1** and [(tbbpy)₂Ru(tpphz)PdCl₂](PF₆)₂ **2** investigated herein.

light-driven supramolecular photocatalysis, the underlying electron transfer processes were investigated in detail by time-resolved transient absorption experiments in the femtosecond-to-nanosecond regime.

2. Results and Discussion

2.1. Photospectroscopy

To study the photophysical properties and the photoinduced electron transfer in **1** (Scheme 1), steady-state absorption and emission spectroscopy was applied in concert with time-resolved differential absorption spectroscopy. The data obtained hereby were considered in comparison to the unsubstituted and previously studied complex **2** (Scheme 1).^[24]

Steady-State Spectroscopy

The absorption spectra of **1** reveal four maxima between 250 and 600 nm (Figure 1). The first one, at 286 nm is assigned to ligand-centered π – π^* transitions of the tbbpy ligand. The maxima at 361 and 381 nm belong to π – π^* transitions located on the tpphz ligand. It is apparent that these absorption features are rather unaffected by the introduction of bromine to the molecular frame in the 3,16-position. In contrast, the metal-to-ligand charge-transfer (MLCT) transition, which is assigned to the absorption band in the visible part of the spectrum, is significantly affected by substitution with bromine. For **1** the maximum of the transition is shifted to shorter wavelengths as compared to **2**. Furthermore, a shoulder becomes visible at longer wavelengths, that is, at approximately 484 nm. The appearance of this shoulder is in agreement with studies on the related [(tbbpy)₂Ru(dppz-2,7-Br₂)]²⁺-complex (dppz = dipyrido[3,2-*a*:2',3'-*c*]phenazine)^[25] and reveals the presence of two distinct MLCT states which are populated upon photoexcitation of **1**. These states are associated with the two different ligands tbbpy and tpphz.^[24] While in **2** the tbbpy- and tpphz-associated MLCT states are close to degenerate, that is, a single broad MLCT band is observed, the introduction of bromine in the 3,16-positions stabilizes the tpphz-associated MLCT, leading to the appearance of the aforementioned shoulder. The observed absorption characteristics are generally in agreement with similar observations for this class of Ru–polypyridine complexes.^[11,23,24,26–29]

In addition to the absorption spectra, Figure 1 and Table 1 summarize the steady-state emission characteristics of **1**. For recording the emission spectra, excitation was performed at 435 nm. In contrast to **2**, where the emission is below the sensitivity of the instrument,^[11] **1** exhibits detectable solvent-polarity-dependent luminescence. By increasing the solvent polarity, the quantum yield (life time) decreases from 2.4×10^{-2} (198 ns) in dichloromethane (DCM), to 0.3×10^{-2} (84 ns) in acetonitrile (ACN), respectively.

Table 1. Emission quantum yields (Φ) and lifetimes (τ) of **1** in various solvents (and their solvent polarity parameter ϵ).

Solvent	ϵ ^[39]	$\Phi \times 10^{-2}$	τ [ns]
ACN (CH ₃ CN)	37.5	0.3	84
Ethanol (C ₂ H ₅ OH)	24.3	0.7	128
DCM (CH ₂ Cl ₂)	8.9	2.4	198

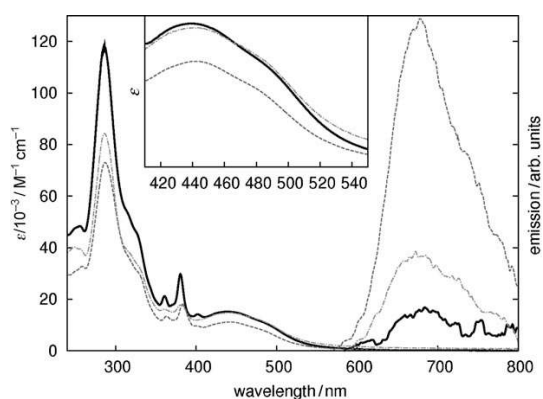


Figure 1. Absorption and emission spectra (> 600 nm) of **1** in ACN (—), ethanol (---) and DCM (----). The inset highlights the spectral shape of the MLCT band.

The origin for these solvent-dependent luminescence characteristics is found in the nature of the excited states involved in the excited-state relaxation. Generally in Ru–polypyridine complexes, photoexcitation into the ¹MLCT state is followed by intersystem crossing into a ³MLCT state, which is promoted by the presence of the heavy central ion.^[30–33] The lowest lying ³MLCT state in **1** and **2** is located on the phenanthroline part of tpphz. From there two distinct relaxation pathways are possible: First, intraligand charge transfer yielding a phenazine-centered excited state, which is followed by a fast radiationless deactivation to the ground state or further charge transfer to the Pd center coordinated to the tpphz ligand. Second, radiative decay of the phenanthroline-centered MLCT state is possible.^[27,34–38] The weight of each relaxation channel depends on the solvent, as the phenazine-centered dark state is stabilized in more polar solvents due to its increased molecular dipole moment. Consequently, the excited-state equilibrium is shifted towards the phenanthroline-centered state when the polarity of the solvent is decreased, that is, electron transfer to the Pd center is partially inhibited and luminescence increases. The bromine substitution has the same effect. Considering the luminescence properties of **1** indicates that the luminescent (phenanthroline-centered) MLCT state is stabilized by the electron-withdrawing effect of bromine. This finding is in line with literature reports on the luminescence properties of related Ru^{II}-polypyridine complexes.^[25]

Ultrafast Experiments

Overall Photophysics of **1** in a Polar Water-Free Solvent

Ultrafast transient absorption experiments were performed to obtain direct insight into the photoinduced charge-transfer processes in **1**. Excited-state dynamics were initiated by absorption of a pump pulse at 510 nm, that is, by photoexcitation of the MLCT transition (Figure 2). We first discuss the pump–probe data obtained in ACN in some detail before comparing them to the data collected in different solvent environments.

The time-dependent differential-absorption spectra (see Figure 2) of **1** in ACN show a broad structureless excited-state absorption (ESA) band extending between 540 and 700 nm with its maximum at around 590 nm. Following photoexcitation, the signal rises during the first few hundreds of picoseconds. This signal build-up is followed by a small decrease in

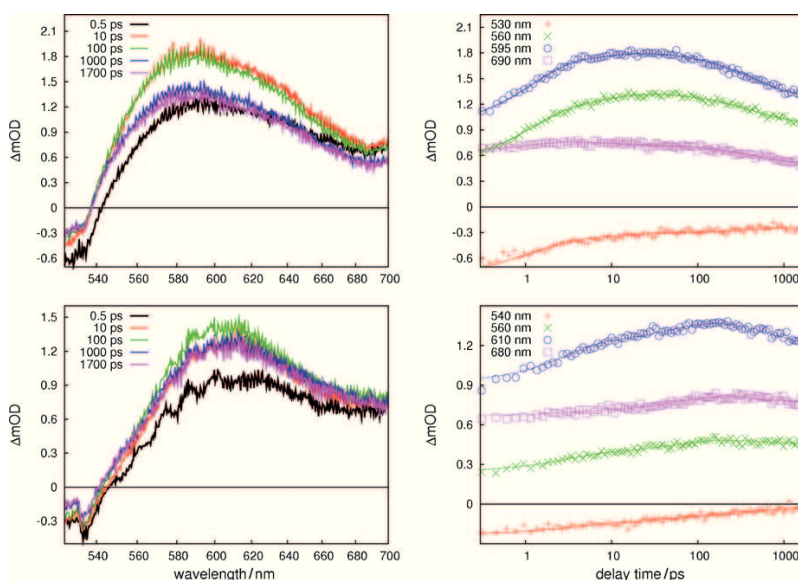


Figure 2. Results of transient absorption measurements of **1** are depicted for ACN solutions (top) and DCM solutions (bottom). The left panel gives the transient spectra at representative delay-times between pump and probe. The kinetics for selected wavelengths are depicted in the right panel.

the ESA band for longer delay times extending towards the longest experimentally available delay time which is 1.8 ns in this particular experimental geometry. Within the experimentally accessible time window, only slight spectral shifts of the ESA band are observed upon visual inspection of the data. For quantitative analysis a global fitting routine is applied [see Eq. (1) in the Experimental Section], revealing that three kinetic components (τ_i) are sufficient to fit a kinetic model to the data. The spectral signatures of the individual kinetic processes are depicted by the corresponding decay-associated spectra (DAS, Figure 3).

Thus the discussion of the experimental results obtained for **1** in ACN starts from the characteristic decay times τ_i and the DAS (Figure 3). The fastest process ($\tau_1 = 1.1$ ps) builds up the

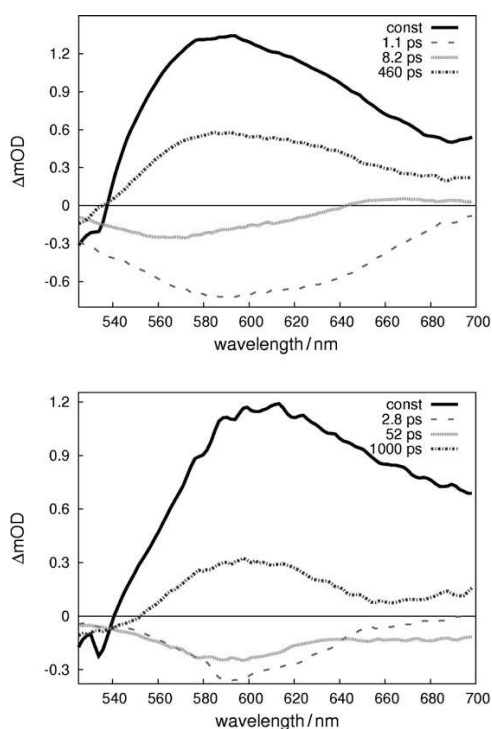


Figure 3. DAS of **1** in ACN (top) and DCM (bottom), which reflect the relaxation dynamics.

ESA band as reflected by the negative amplitudes of the DAS. Subsequently, the ESA increases slightly in the blue part of the spectrum ($\lambda_{pr} < 640$ nm), while a decrease of the band is observed in the red part ($\tau_2 = 8.2$ ps). The third process ($\tau_3 = 460$ ps) reflects a decrease of the ESA over the entire spectral range.

In order to discuss the molecular nature of these ultrafast processes, we turn to the photophysics of **2** that has been reported previously.^[24] Here, an initial ps process ($\tau_1 = 1.1$ ps) is assigned to equilibration of the ³MLCT state on the tpphz ligand. This kinetic process most likely contains contributions from interligand hopping processes, vibrational cooling and intramolecular vibrational energy redistribution.^[40–44] The actual ¹MLCT → ³MLCT intersystem crossing cannot be observed due to the insufficient temporal resolution in our experiments. The DAS of the 8.2 ps component in **1** resembles the spectral features of the 5 ps component in **2**, which is due to intraligand charge transfer (ILCT), yielding the excited state which is localized at the phenazine sphere of tpphz.^[27,38] The spectral characteristics of the third, that is, the 460 ps process lead to the assignment of this kinetic component to a ligand-to-metal charge transfer (LMCT) from tpphz to the PdCl₂ center. This assignment stems from spectral and kinetic analogies of the photophysics of **1** and **2** as well as that of [(bpy)₂Ru^{II}tpphzOs^{III}-(bpy)]₂⁴⁺.^[24,27,38]

Despite the spectroscopic similarities between **1** and **2**, the photophysics of **1** reveal two remarkable differences in the ultrafast data as compared to **2**. First, the DAS (τ_2), that is, forma-

tion of the ILCT, shows a red-shift of 30 nm. As the spectral information of a DAS depicts relative energies between the two states involved, the red-shift indicates that the phenanthroline-centered state is stabilized by the introduction of the bromine substituents. Consequently, the electron-transfer process to the phenazine-centered state becomes less favored and the transition is decelerated from 5 to 8 ps. The same effect is obtained for the LMCT to the palladium(II) centre, which compared to **2**, is slower and accompanied by a red-shifted DAS (see also Table 2). These findings indicate that the introduction of bro-

Table 2. Comparison of the picosecond kinetic components of [(tbbpy)₂Ru(Br₂tpphz)PdCl₂] **1** and [(tbbpy)₂Ru(tpphz)PdCl₂] **2** in dependence of the solvent.

	[(tbbpy) ₂ Ru(tpphz)PdCl ₂] 2		[(tbbpy) ₂ Ru(Br ₂ tpphz)PdCl ₂] 1	
	ACN	DCM	ACN	DCM
τ_1 [ps]	0.8	1.0	1.1	2.8
τ_2 [ps]	5	19	8.2	52
τ_3 [ps]	310	740	460	1000

[a] Previously published data,^[24] which is summarized here for the sake of clarity.

mine flattens the electron-transfer gradient in general, leading to a deceleration of the subsequent electron-transfer steps. This is, to the best of our knowledge, the first example for this class of Ru-complexes, for which a chemical variation of one part of the molecule influences the electron transfer gradient across an entire supramolecular framework. This opposes the general aspect of locally varying excited-state dynamics in the vicinity of substituents. It also provides a new viewpoint on existing electrochemical studies where the influence of substituents are locally restricted only to small moieties of the entire complex.^[25,45–47]

In order to reveal any ns processes in the excited-state relaxation of **1** and **2**, transient-absorption experiments were performed using a setup with an accessible temporal window of 15 ns. Here, we focused on the dynamics of the ground-state bleach (GSB) in the spectral region between 490 and 520 nm for either of the complexes **1** and **2**. As shown in Figure 4 (for

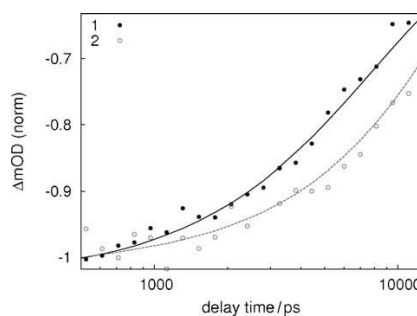


Figure 4. Nanosecond ground-state recovery kinetics of **1** (solid symbols) and **2** (open symbols) in ACN integrated over the spectral region of GSB. The recovery of ground-state bleach occurs faster for **1** (7.2 ns) than for **2** (≥ 30 ns).

spectral information see Figure S5 of the Supporting Information), these experiments identified a ns component, which is characterized by a characteristic time of $\tau_4 = 7.2$ ($\tau_4 \geq 30$) ns for **1** (**2**). It should be pointed out that due to the limited temporal window accessible in this experiment the value of 30 ns as obtained from the fit presents a lower-boundary estimate for the actual characteristic time. For both complexes it is found that the respective ns component causes significant ground-state recovery. Hence, this deactivation process is directly competing with catalysis for which the charge centered on the Pd centre is crucial.

Solvent Effects on the Ultrafast Dynamics: Impact of Solvent Polarity

In order to yield information about the solvent dependence of the electron-transfer processes, the ultrafast measurements were also performed in the less polar (compared to ACN) solvent DCM.^[39] In this solvent, the stabilization of charge-transfer states is supposed to be reduced and hence the driving force for intramolecular electron transfer is lowered. This solvent-induced impact on the driving force of electron transfer is detailed in this section.

The ESA spectra of **1** in DCM are generally red-shifted by 20–30 nm compared to the spectra obtained for ACN and additionally the band shape appears modified. A shoulder in the red part of the spectrum, observed in ACN, is now absent. In solutions of **1** in DCM the processes described above for ACN as solvent are retained, as indicated by the same spectral features of the DAS. However, generally the kinetic processes appear decelerated in DCM (right panel in Figure 2 and Table 2). Within the first 2.8 ps charge separation, interligand hopping and vibrational cooling take place, leading to a phenanthroline-centered ³MLCT state. This process is followed by an ILCT to the phenazine sphere of the bridging ligand ($\tau_2 = 52$ ps). The third step is, as for ACN, assigned to a charge transfer to the Pd center. Notably, the DAS of all kinetic components except for the fast 2.8 ps process reveal a red-shift as compared to the situation of **1** in ACN. The DAS corresponding to τ_1 and τ_3 reveal bands that are spectrally narrowed compared to those obtained in ACN. Similarly, the 20–30 nm red-shift of the DAS associated with the ILCT (τ_2) as compared to that in ACN indicates a solvent-induced decrease in the energy gap between the two phenanthroline- and phenazine-located states involved. The energetic difference is lowered in DCM and as a result the driving force for the charge transfer between both states is reduced and the excited-state charge transfer processes are slowed down in the less polar environment.

Solvent Effects on the Ultrafast Dynamics: Impact of the Addition of Water

Up to now the photoinduced charge-transfer dynamics was discussed as they occur in neat solvents. However, complex **1** becomes photocatalytically active only in complex water-containing solvent mixtures. In order to approach the investigation

of the photoinduced dynamics in such complex solvent mixtures, transient absorption spectroscopy experiments of both **1** and **2** were performed in a mixture of 90% ACN and 10% H₂O (Figures 5 and 6 and Figure S4 in the Supporting Information). In general, it is found that the influence of water on the quali-

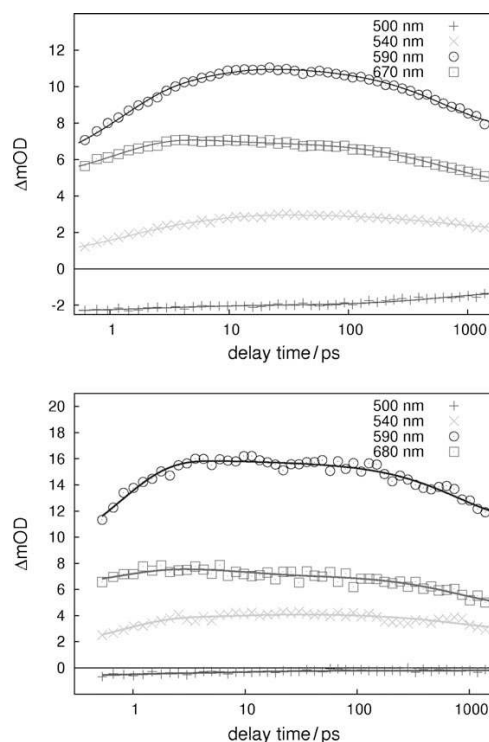


Figure 5. Transient kinetics of **1** (top) and **2** (bottom) in the ACN/H₂O solvent mixture at chosen probe wavelength after excitation with light at 480 nm.

tative features of the electron migration processes is minor. Compared to the situation in pure ACN, no spectral changes are observed. Hence, the photophysics of **1** and **2** as detailed above for pure ACN can be translated to the ACN/H₂O solvent mixture. However, adding water affects the rate of the individual charge transfer steps as documented in Figure 6. While for **1** the fastest process, charge localization on the tpphz-centered MLCT, occurs in roughly 1 ps as in pure ACN, the subsequent ILCT is decelerated to a characteristic time constant of 10.5 ps upon adding H₂O. While this change is minor, a more significant deceleration is observed for the LMCT, which needs approximately 800 ps in ACN/H₂O, a time which is nearly double that in pure ACN. The DAS (Figure 6), however, reveal that these electron migrations are accompanied by, at most, minor spectral changes when comparing both solvents.

An analogous argumentation can be followed describing the photophysics of **2** in the solvent mixture. The rates of the initial two processes are not affected and only slightly decelerated compared to ACN as solvent, yielding time constants of 1.2 and 6.1 ps, respectively. Analogous to **1**, the LMCT is slowed down to a characteristic time of 850 ps upon adding

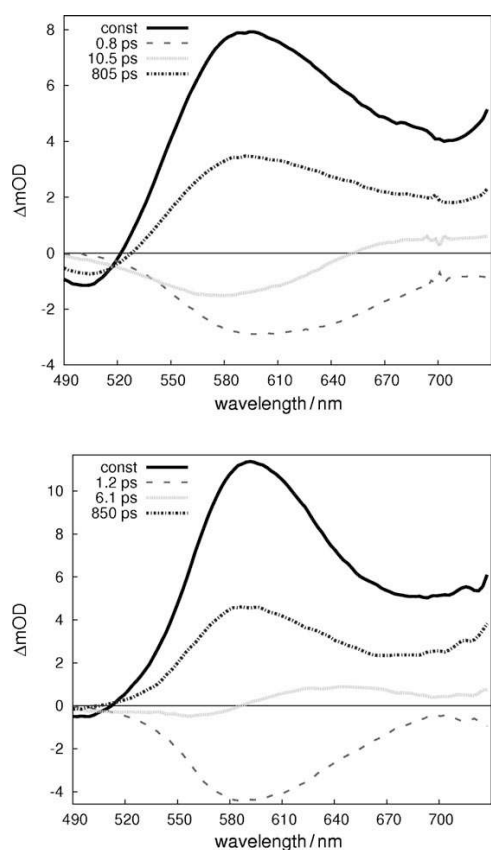


Figure 6. DAS of **1** (top) and **2** (bottom) in the ACN/H₂O mixture.

H₂O. As found for complex **1**, for **2** the transient spectra as well as the DAS reveal no differences for ACN/H₂O compared to pure ACN. In conclusion, it can be stated that the addition of water to an ACN solution exerts the same effect on the excited-state dynamics for both **1** and **2**. Nevertheless, the data show that in the ACN/H₂O solvent mixtures the time constants characterizing the LMCT are practically equal for both complexes. This points to the fact that the alterations of the electron transfer gradient caused by the substitution of bromine are significantly compensated by intermolecular, that is, solvent-induced effects. However, such reduced electron transfer rates are also observed when **1** and **2** are dissolved in the less polar solvent DCM. But, despite the situation in DCM, the addition of water to ACN has only a minor effect on the rate of both initial processes of charge separation. Thus, it is concluded that the mere polarity effects of the solvent mixture of ACN/H₂O cannot account for the change in electron-transfer rates. Other effects such as specific interactions between water molecules

and the complexes must be taken into consideration for explanation.

Photocatalysis and Hydrogen Production

The new heterodinuclear ruthenium complex [(tbbpy)₂Ru(Br₂tpphz)PdCl₂](PF₆)₂ **1** was tested towards its catalytic activity in the field of light-driven hydrogen production and compared to [(tbbpy)₂Ru(tpphz)PdCl₂](PF₆)₂ **2** as explained in refs. [11, 19].

The photocatalytic activity was determined by a commercially available LED array ($\lambda = 470 \pm 10$ nm, $P = 10$ mW cm⁻²) in combination with a specialized air-cooled photomicroreactor. Irradiation times of 18 h were found to be most effective for maximum hydrogen production^[48] in the presence of triethylamine (TEA) acting as a sacrificial electron donor.

Table 3 and Figure 7 display the influence of the bromine substituents and the water addition onto the photocatalytic activity of **1** and **2** in ACN in the presence of 2 M TEA for different water concentrations. To ensure comparability apart from the water concentration, all other reaction conditions such as catalyst concentration ($c = 0.07$ mM) and radiation time ($t = 18$ h) were kept constant. As can be seen, **2** displays a generally higher turnover number (TON) than **1** (Table 3 and Figure 7). One possible reason for the inferior catalytic activity of **1** could be due to the electron-withdrawing bromine substituents (–I effect), slowing the photoelectron transfer from the ruthenium unit over the bridging ligand to the palladium center (when comparing the photophysics of **1** and **2** in neat solvents). However, this tentative explanation contradicts the results of the ultrafast electron transfer investigations in the ACN/H₂O mixtures. Thus, it is concluded that the increased catalytic activity

Table 3. Examination of the photocatalytic activity of **1** and **2** in terms of TON for two different amounts of water content. In order to compare the catalytic results with the photophysics the different electron transfer times for the LMCT (ligand-to-metal-charge transfer) and GSR (ground-state recovery) are shown in dependency to the substitution.

	TON		τ_3 (LMCT)		τ_4 (GSR)
H ₂ O content	2 vol%	10 vol%	0 vol%	10 vol%	0 vol%
[(tbbpy) ₂ Ru(Br ₂ tpphz)PdCl ₂] 1	68.5	67.3	460 ps	850 ps	7.2 ns
[(tbbpy) ₂ Ru(tpphz)PdCl ₂] 2	153.2	209.8	310 ps	805 ps	≥ 30 ns

of **2** is not related to alterations in the sub-ns dynamics upon bromine substitution. Nonetheless, the long-time-scale differential absorption data indicate that a some-nanosecond deactivation channel is favored in **1** as compared to **2**, which might be due to the influence of the heavy atom on electronic states of the tpphz moiety itself and which might contribute to the inferior catalytic turnover of **1**. Alternatively, one might postulate that slower processes, for example, associated with the second electron transfer, are influenced by bromine substitution and affect the catalytic activity.

For both complexes, the catalytic activity is higher in the presence of water. The TON of complex **2** increases largely upon the addition of water and reached a maximum of (238.3 ± 11.4) for a water concentration of about 15 vol% (see

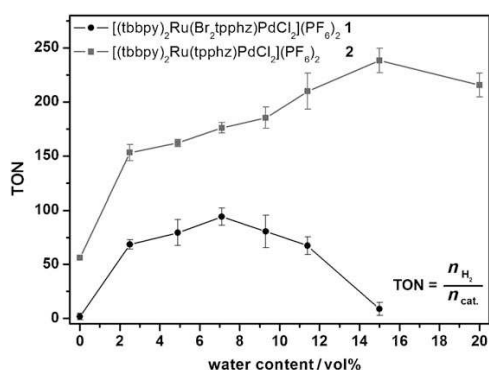


Figure 7. Examination of the photocatalytic activity of **1** and **2** in terms of TON (turnover number = number of H₂ molecules evolved per each catalyst molecule under continuous 470 ± 10 nm, $P = 10 \text{ mW cm}^{-2}$ LED irradiation for 18 h) versus the water content (vol%). All samples contained 0.07 mM of the photocatalyst and 2 M TEA (final concentrations) in an acetonitrile–water mixed solution. All reactions were carried out at a constant temperature of 21 °C. The error bars are calculated by multiplying the student's distribution (95%) with the standard deviation of the arithmetic mean.

Figure 7). This enhanced turnover number is significant higher than the recently published TON of 146.2 for complex **2**, which was obtained under different conditions at a water content of 10 vol% after laser irradiation of 10 h at 476 nm.^[19] A further raise of the water content above 15 vol%, however, reduces the TON. Another important fact is that the introduction of the bromine into the tpphz frame in the 3,16-position leads to a clear decrease in the turnover number and a reduced tolerance of water. For instance, the catalytic activity of complex **1**, expressed as TON, reaches only 45% if compared with **2** for a water content of 2.5 vol% [TON = 68.5 (**1**) instead of 153.2 (**2**)]. Moreover, the maximum TON of 94.2 ± 8.0 for **1** is reached much earlier at a water content of only 7.1 vol% (Figure 7).

Based only on this catalytic data, the activating effect of water is difficult to evaluate. It might for instance be the result of the altered solvent polarity, increased proton mobility, or the propensity of water molecules to act as ligands at the Pd center. Taking the results of the ultrafast experiments into account, a more detailed analysis of the water effect is possible. As described above, it was found that the presence of water does not change this ultrafast electron migration qualitatively and only slows the LMCT, that is, independent of the addition of water, identical light-induced processes are observed with only minor variations in the reaction rates. Considering this, we can exclude that the altered polarity of the water-containing mixture influences the first charge separation process. This shows that the effect of water on the catalytic activity of the tpphz complexes discussed here cannot be assigned to a mere polarity effect on the electron transfer, which would influence the charge transfer characteristics of the first charge-transfer step in a very similar manner as changing the solvent from DCM to ACN. As the LMCT process to the palladium centre is believed to be associated with the dissociation of the chloride ligand,^[11] a positive effect of the increased polarity on this highly polar process can be excluded as well. Another interest-

ing feature observed for both complexes is the maximum TON reached as a function of water addition. This shows that the addition of water has (at least) two competing effects on the catalytic reaction and the balance between both effects apparently depends on the substitution pattern of the complex. These considerations lead to the conclusion that water influences the catalytic activity by acting further downstream of the reaction cascade, that is, that it influences the stability of the charge-separated states, the efficiency of the second charge transfer process or the re-reduction of the photo-oxidized Ru^{III} center. Further mechanistic studies will focus on elucidating the effect of water on the catalytic efficiency in more detail. Hence, prospective investigations will focus on the electrochemistry, reaction kinetics and the photophysics of either complex as a function of water addition.

3. Conclusions

In conclusion, we discussed in detail the photophysical and catalytic properties of a new regioselective substituted tpphz-based photocatalyst. The introduced bromine substituents in $[(\text{tbbpy})_2\text{Ru}(\text{Br}_2\text{tpphz})\text{PdCl}_2](\text{PF}_6)_2$ lead to a deceleration of the electron-transfer rates and is associated with a decrease in the catalytic activity. It could be shown that slight variations, such as the introduction of bromine, of the bridging ligand have a profound impact on the catalytic performance of these compounds. Hence, careful optimization of the bridging ligands provides great opportunities and challenges. Therefore, exact design of the bridging ligands may be crucial for the goal to increase the activity of supramolecular photocatalysts. The quite significant impact of minor changes on tetrapyridophenazine-based complexes in supramolecular devices on the intramolecular electron transfer rates and catalytic turnover suggests the great potential of such supramolecular photocatalysts with tunable photophysical and photochemical properties. The detailed investigation of the effect of added water on the ultrafast electron transfer events and the catalytic activity of **1** and **2** has led to the following conclusions: The increased polarity of the water-containing mixture does not positively influence the photochemistry of the first photoinduced electron transfer reaction. The terminal LMCT from the bridging ligand to the palladium centre is even significantly slowed down in the presence of 10% water. This process leaves the palladium centre in its reduced form, for which water might not be a suitable ligand. Furthermore, water exerts a second effect, namely to decrease the catalytic activities, promoted by the introduction of bromine, at higher concentrations. These observations suggest that the reason for the observed positive effect of water on the catalytic activity is most likely correlated with processes occurring at a later stage during the catalytic reaction.

Experimental Section

Materials and Methods: The synthesis and the subsequent steps to ensure purity of both complexes **1** and **2** is described in the electronic supporting information (ESI).

Photocatalysis: Photocatalytic hydrogen production experiments were carried out in gas chromatography (GC) vials placed in a self-made and air-cooled photomicroreactor for maintaining room temperature (21 °C) under continuous LED ($\lambda = 470 \pm 10$ nm) irradiation. The LED sticks used for these experiments were manufactured by Innotas Elektronik GmbH (Germany) and provide a power of approximately 10 mW cm^{-2} (at 12 V). Full specifications and representative pictures regarding the technical equipment for hydrogen production and the determination via GC were published recently.^[19]

Each sample was prepared in a separate and commercially available GC vial (diameter = 13 mm, VWR) with a known headspace of 3 mL and a given ratio from headspace to solution of 3 mL/2 mL. Furthermore, the GC vials were loaded in the dark and under argon flow. The gas phase above the solution was probed by inserting a gas-tight GC syringe through a septum and analyzing the amount of hydrogen in the gas phase using GC.

Hydrogen was measured by headspace GC on a Varian CP3800 chromatograph equipped with a thermal conductivity detector and a CP7536 Plot Fused Silica 25 MX 0.32 MMID column (length = 25 m, layer thickness = 30 μm) with nitrogen as carrier gas (99.999% purity), which was calibrated with pure hydrogen earlier.

Photophysics: For the photophysical measurements both complexes **1** and **2** were dissolved in ACN and DCM and ethanol. All solvents were of spectroscopic grade (purity higher than 99.9%) and used without further purification. All experiments were performed at constant room temperature (22 °C) and under aerated conditions. Absorption spectra were recorded prior and subsequent to all measurements to ensure photochemical stability of the samples.

For the time-resolved transient absorption experiments with the time range of 1.8 ps two setups were used. One setup is described in detail by Siebert et al.^[49] and was used to employ a pump beam with a wavelength of 510 nm. The second setup used to record the solvent-dependent pump-probe data was built up as follows: One part (about 1 W) of the 800 nm output of an amplified Ti:Sapphire laser (Legend, Coherent Inc.) was split into two beams, one of which was used to pump an optical-parametric amplifier (TOPAS-C). The TOPAS output pulses were spectrally tuned to 480 nm and served as pump pulses in our pump-probe experiments. This beam was sent over a 600 mm delay line in order to realize the temporal delay between the pump and the probe pulses. The residual fraction of the fundamental was employed for supercontinuum generation in a sapphire plate used as a broadband probe in the transient absorption experiments. The probe light was then split into two beams, one of which was focused into the sample by means of a 500 mm focal length spherical mirror, while the second beam was used as reference. To ensure homogeneous excitation of the probe spot, the pump beam was only weakly focused by a 1000 mm focal length lens into the sample and spatially overlapped with the probe beam. The energy of the pump pulses was chosen to be 0.5 μJ and the mutual polarization between pump and probe pulses was set to the magic angle. Probe and reference intensities were detected on a double-stripe diode array and converted into differential absorption (ΔA) signals using a commercially available detection system (Pascher Instruments AB, Sweden).

For data evaluation, the two-dimensional differential-absorption (ΔA) data set, which is recorded as a function of the delay time (t) and the probe wavelength (λ_{pr}), was chirp corrected numerically and treated with a global fitting procedure using a sum of exponential functions [Eq. (1)]^[50]

$$\Delta A(t, \lambda_{\text{pr}}) = \phi(\lambda_{\text{pr}}) + \sum_{i=1}^n A_i(\lambda_{\text{pr}}) e^{-t/\tau_i} \quad (1)$$

The constant offset ϕ simulates long-lived pump-induced absorption changes in the sample, which decay on a time-scale much longer than the range covered in our experiments, that is, ~ 2 ns. The wavelength-dependent pre-exponential factors $A_i(\lambda_{\text{pr}})$ yield the decay-associated spectra (DAS), which contain the spectral characteristics of each individual kinetic component associated with τ_i . The pulse-overlap region was ignored during the fitting process to make sure that no contributions from coherent artefacts affect the data analysis.^[42, 51]

The setup used to record the long-time window differential absorption data is described in detail by De et al.^[52]

Steady-state experiments were performed in solutions with aerated acetonitrile at room temperature (22 °C). The steady-state absorption spectra were recorded with a Jasco V-670 spectrophotometer. For emission spectra the solutions were diluted (optical density < 0.05) and a Jasco FP-6200 spectrofluorimeter was used. To detect the absolute emission quantum yields a solution of $[\text{Ru}(\text{bpy})_3]\text{Cl}_2$ in non-degassed water ($\Phi = 0.028$) was used as reference.^[53] Time-correlated single-photon counting was employed to obtain fluorescence lifetimes, where a Ti-sapphire laser (Tsunami, Newport Spectra-Physics GmbH) reduced in its repetition rate by a pulse selector (Model 3980, Newport Spectra-Physics GmbH) to 800 kHz was employed as light source. The laser output was frequency doubled in a second harmonic generator (Newport Spectra-Physics GmbH) to create a pump-beam at 435 nm. For detection of emission photons a Becker & Hickel PMC-100-4 photon counting module with 150 ps response limited time resolution was employed.

Acknowledgements

This work was financially supported by the Deutsche Forschungsgemeinschaft (DFG). S. R. gratefully acknowledges support from the Collaborative Research Centre 583. C. K. thanks the Deutsche Bundesstiftung Umwelt (DBU) for a Ph.D. fellowship and DYNA for a traveling grant. B.D. acknowledges financial support by the Fonds der Chemischen Industrie.

Keywords: hydrogen · photocatalysis · photochemistry · supramolecular chemistry · time-resolved spectroscopy

- [1] N. S. Lewis, D. G. Nocera, *Proc. Natl. Acad. Sci. USA* **2006**, *103*, 15729–15735.
- [2] N. Armaroli, V. Balzani, *Angew. Chem.* **2007**, *119*, 52–67; *Angew. Chem. Int. Ed.* **2007**, *46*, 52–66.
- [3] J. Balzani, A. Credo, M. Venturi, *ChemSusChem* **2008**, *1*, 26–58.
- [4] A. Magnuson, M. Anderlund, O. Johansson, P. Lindblad, R. Lomoth, T. Polivka, S. Ott, K. Stensjö, S. Styring, V. Sundström, L. Hammarström, *Acc. Chem. Res.* **2009**, *42*, 1899–1909.
- [5] D. G. Nocera, *Chem. Soc. Rev.* **2009**, *38*, 13–15.
- [6] M. Grätzel, *Nature* **2001**, *414*, 338–344.
- [7] M. Grätzel, *Inorg. Chem.* **2005**, *44*, 6841–6851.
- [8] K. Maeda, N. Sakamoto, T. Ikeda, H. Ohtsuka, A. Xiong, D. Lu, M. Kanehara, T. Teranishi, K. Domen, *Chem. Eur. J.* **2010**, *16*, 7750–7759.
- [9] X. Chen, J. Zhang, X. Fu, M. Antonietti, X. Wang, *J. Am. Chem. Soc.* **2009**, *131*, 11658–11659.
- [10] S. Rau, D. Walther, J. G. Vos, *Dalton Trans.* **2007**, 915–919.
- [11] S. Rau, B. Schäfer, D. Gleich, E. Anders, M. Rudolph, M. Friedrich, H. Görls, W. Henry, J. G. Vos, *Angew. Chem.* **2006**, *118*, 6361–6364; *Angew. Chem. Int. Ed.* **2006**, *45*, 6215–6218.
- [12] A. J. Esswein, D. G. Nocera, *Chem. Rev.* **2007**, *107*, 4022–4047.

- [13] K. Rangan, S. M. Arachchige, J. R. Brown, K. J. Brewer, *Energy Environ. Sci.* **2009**, *2*, 410–419.
- [14] A. Inagaki, M. Akita, *Coord. Chem. Rev.* **2010**, *254*, 1220–1239.
- [15] H. Ozawa, M. Haga, K. Sakai, *J. Am. Chem. Soc.* **2006**, *128*, 4926–4927.
- [16] M. Elvington, J. Brown, S. M. Arachchige, K. J. Brewer, *J. Am. Chem. Soc.* **2007**, *129*, 10644–10645.
- [17] P. Lei, L. Hammarström, M. Hedlund, R. Lomoth, H. Rensmo, O. Johansson, *J. Am. Chem. Soc.* **2008**, *130*, 26–27.
- [18] A. Fihri, V. Artero, M. Razavet, C. Baffert, W. Leibl, M. Fontecave, *Angew. Chem.* **2008**, *120*, 574–577; *Angew. Chem. Int. Ed.* **2008**, *47*, 564–567.
- [19] S. Tschierlei, M. Karnahl, M. Presselt, B. Dietzek, J. Guthmuller, L. González, M. Schmitt, S. Rau, J. Popp, *Angew. Chem.* **2010**, *122*, 4073–4076; *Angew. Chem. Int. Ed.* **2010**, *49*, 3981–3984.
- [20] V. Balzani, S. Campagna, G. Denti, A. Juris, S. Serroni, M. Venturi, *Coord. Chem. Rev.* **1994**, *132*, 1–13.
- [21] H. Ozawa, Y. Yokoyama, M. Hagab, K. Sakai, *Dalton Trans.* **2007**, 1197–1206.
- [22] M. Schwalbe, M. Karnahl, H. Görls, D. Chartrand, F. Laverdiere, G. S. Hanan, S. Tschierlei, B. Dietzek, M. Schmitt, J. Popp, J. G. Vos, S. Rau, *Dalton Trans.* **2009**, 4012–4022.
- [23] M. Karnahl, S. Tschierlei, C. Kuhnt, B. Dietzek, M. Schmitt, J. Popp, M. Schwalbe, S. Kriek, H. Görls, F. W. Heinemann, S. Rau, *Dalton Trans.* **2010**, *39*, 2359–2370.
- [24] S. Tschierlei, M. Presselt, C. Kuhnt, A. Yartsev, T. Pascher, V. Sundström, M. Karnahl, M. Schwalbe, B. Schäfer, S. Rau, M. Schmitt, B. Dietzek, J. Popp, *Chem. Eur. J.* **2009**, *15*, 7678–7688.
- [25] C. Kuhnt, M. Karnahl, S. Tschierlei, K. Griebenow, M. Schmitt, B. Schäfer, S. Kriek, H. Görls, S. Rau, B. Dietzek, J. Popp, *Phys. Chem. Chem. Phys.* **2010**, *12*, 1357–1368.
- [26] J. Bolger, A. Gourdon, E. Ishow, J. Launay, *Inorg. Chem.* **1996**, *35*, 2937–2944.
- [27] C. Chiorboli, C. A. Bignozzi, F. Scandola, E. Ishow, A. Gourdon, J. P. Launay, *J. Inorg. Chem.* **1999**, *38*, 2402–2410.
- [28] N. Komatsuzaki, R. Katoh, Y. Himeda, H. Sugihara, H. Arakawa, K. Kasuga, *J. Chem. Soc. Dalton Trans.* **2000**, 3053–3054.
- [29] S. Tschierlei, B. Dietzek, M. Karnahl, S. Rau, F. M. MacDonnell, M. Schmitt, J. Popp, *J. Raman Spectrosc.* **2008**, *39*, 557–559.
- [30] A. Juris, V. Balzani, F. Barigelletti, S. Campagna, P. Belser, A. von Zelewski, *Coord. Chem. Rev.* **1988**, *84*, 85–277.
- [31] V. Balzani, A. Juris, M. Venturi, S. Campagna, S. Serroni, *Chem. Rev.* **1996**, *96*, 759–834.
- [32] M. H. Damrauer, G. Cerullo, A. Yeh, T. R. Bousie, C. V. Shank, J. K. McCusker, *Science* **1997**, *275*, 54–57.
- [33] A. Cannizzo, F. van Mourik, W. Gawelda, G. Zgrablic, C. Bressler, M. Chergui, *Angew. Chem.* **2006**, *118*, 3246–3248; *Angew. Chem. Int. Ed.* **2006**, *45*, 3174–3176.
- [34] M. K. Brennamann, J. H. Alstrum-Acevedo, C. N. Fleming, P. Jang, T. J. Meyer, J. M. Papanikolas, *J. Am. Chem. Soc.* **2002**, *124*, 15094–15098.
- [35] J. Olofsson, B. Önfelt, P. Lincoln, *J. Phys. Chem. A* **2004**, *108*, 4391–4398.
- [36] C. G. Coates, J. Olofsson, M. Coletti, J. J. McGarvey, B. Önfelt, P. Lincoln, B. Norden, E. Tuite, P. Matousek, A. W. Parker, *J. Phys. Chem. B* **2001**, *105*, 12653–12664.
- [37] J. Olofsson, L. M. Wilhelmsson, P. Lincoln, *J. Am. Chem. Soc.* **2004**, *126*, 15458–15465.
- [38] C. Chiorboli, M. A. J. Rodgers, F. Scandola, *J. Am. Chem. Soc.* **2003**, *125*, 483–491.
- [39] C. Reichardt, *Angew. Chem.* **1965**, *77*, 30–40.
- [40] A. C. Bhasikuttan, M. Suzuki, S. Nakashima, T. Okada, *J. Am. Chem. Soc.* **2002**, *124*, 8398–8405.
- [41] B. Dietzek, W. Kiefer, J. Blumhoff, L. Böttcher, S. Rau, D. Walther, U. Uhlemann, M. Schmitt, J. Popp, *Chem. Eur. J.* **2006**, *12*, 5105–5115.
- [42] B. Dietzek, T. Pascher, V. Sundström, A. Yartsev, *Laser Phys. Lett.* **2007**, *4*, 38–43.
- [43] G. Benkö, J. Kallioinen, J. E. I. Korppi-Tommola, A. Yartsev, V. Sundström, *J. Am. Chem. Soc.* **2002**, *124*, 489–493.
- [44] S. Wallin, J. Davidsson, J. Modin, L. Hammarström, *J. Phys. Chem. A* **2005**, *109*, 4697–4704.
- [45] R. H. Hartshorn, J. K. Barton, *J. Am. Chem. Soc.* **1992**, *114*, 5919–5925.
- [46] B. Schäfer, H. Görls, M. Presselt, M. Schmitt, J. Popp, W. Henry, J. G. Vos, S. Rau, *Dalton Trans.* **2006**, 2225–2231.
- [47] M. Karnahl, H. Görls, S. Tschierlei, M. Schmitt, J. Popp, D. Chartrand, G. S. Hanan, R. Groarke, J. G. Vos, S. Rau, *Eur. J. Inorg. Chem.* **2009**, 4962–4971.
- [48] M. Karnahl, S. Rau, J. G. Vos, S. Tschierlei, M. Schmitt, B. Dietzek, S. Styring, P. Huang, **2011**, submitted.
- [49] R. Siebert, D. Akimov, M. Schmitt, A. Winter, U. S. Schubert, B. Dietzek, J. Popp, *ChemPhysChem* **2009**, *10*, 910–919.
- [50] B. Dietzek, S. Tschierlei, G. Hermann, A. Yartsev, T. Pascher, V. Sundström, M. Schmitt, J. Popp, *ChemPhysChem* **2009**, *10*, 144–150.
- [51] S. A. Kovalenko, A. L. Dobryakov, J. Ruthman, N. P. Ernstring, *Phys. Rev. A* **1999**, *59*, 2369–2384.
- [52] S. De, T. Pascher, M. Maiti, K. G. Jespersen, T. Kesti, F. Zhang, O. Inganas, A. Yartsev, V. Sundström, *J. Am. Chem. Soc.* **2007**, *129*, 8466–8472.
- [53] K. Nakamura, *Bull. Chem. Soc. Jpn.* **1982**, *55*, 2697–2705.

Received: March 29, 2011
Published online on June 16, 2011

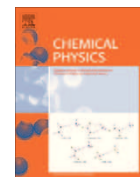
[CK4] Synthesis and photophysics of a novel photocatalyst for hydrogen production based on a tetrapyridoacridine bridging ligand

Der Nachdruck der folgenden Publikation erfolgt mit freundlicher Genehmigung von Elsevier B.V..

Reproduced with permission from:

M. Karnahl, C. Kuhnt, F. W. Heinemann, M. Schmitt, S. Rau, J. Popp, B. Dietzek, SYNTHESIS AND PHOTOPHYSICS OF A NOVEL PHOTOCATALYST FOR HYDROGEN PRODUCTION BASED ON A TETRAPYRIDOACRIDINE BRIDGING LIGAND, *Chem. Phys.*, **2012**, 393, 65-73

Copyright 2011 Elsevier B.V.



Synthesis and photophysics of a novel photocatalyst for hydrogen production based on a tetrapyridoacridine bridging ligand

Michael Karnahl^{a,1}, Christian Kuhn^{b,1}, Frank W. Heinemann^c, Michael Schmitt^b, Sven Rau^{d,*}, Jürgen Popp^{b,e}, Benjamin Dietzek^{b,e,*}

^a Department of Photochemistry and Molecular Science, The Ångström Laboratory, Uppsala University, Box 523, 75120 Uppsala, Sweden

^b Institute of Physical Chemistry and Abbe Center of Photonics, Friedrich-Schiller-University Jena, Helmholtzweg 4, 07743 Jena, Germany

^c Department of Chemistry and Pharmacy, Friedrich-Alexander-University Erlangen-Nürnberg, Egerlandstraße 1, 91058 Erlangen, Germany

^d Institute of Inorganic Chemistry I, University Ulm, Albert-Einstein-Allee 11, 89091 Ulm, Germany

^e Institute of Photonic Technology (IPHT) Jena e.V., Albert-Einstein-Straße 9, 07745 Jena, Germany

ARTICLE INFO

Article history:

Received 20 October 2011

In final form 18 November 2011

Available online 8 December 2011

Keywords:

Photocatalysis

Ultrafast dynamics

Molecular photocatalyst

Impact of water on the catalytic properties

Hydrogen

ABSTRACT

Molecular photocatalysts allow for selectively tuning their function on a molecular level based on an in-depth understanding of their chemical and photophysical properties. This contribution reports the synthesis and photophysical characterization of the novel molecular photocatalyst [(tbbpy)₂Ru(tpac)PdCl₂]²⁺ **RutpacPd** (with tpac = tetrapyrido[3,2-a:2',3'-c:3'',2''-h:2''',3'''-j]acridine) and its mononuclear building block. Furthermore, detailed photocatalytic activity measurements of **RutpacPd** are presented. The introduction of the tpac-ligand into the molecular framework offers a potential route to reduce the impact of water as compared to the well-studied class of **RutpphzPd** (with tpphz = tetrapyrido[3,2-a:2',3'-c:3'',2''-h:2''',3'''-j]phenazine) complexes. The distinct impact of water on the electron-transfer processes in tpphz-ligands stems from the possibility of water to form hydrogen bonds to the phenazine nitrogen atoms and will potentially be reduced when replacing the phenazine by the acridine unit. The effect of this structural variation on the catalytic properties and the underlying ultrafast intramolecular charge transfer behavior will be discussed in detail.

© 2011 Elsevier B.V. All rights reserved.

1. Introduction

The development of proton reduction catalysts for hydrogen fuel generation is at the heart of a future “Hydrogen Economy” [1–5]. Therefore, photocatalytic water splitting with molecular devices is a rapidly developing area of catalysis as it may present a potential solution towards the increasing energy demand and limited resources of fossil fuels [1,2,6–10]. In general, several distinct processes have to occur within the molecules in order to allow catalysis to take place. Light absorption has to be coupled to an electron transfer process which ultimately must lead to the reduction at a catalytic center [8,10–15]. A detailed mechanistic understanding for this interplay has recently been developed for the heterodinuclear complex [(tbbpy)₂Ru(tpphz)Pd(Cl)₂]²⁺ (tbbpy = 4,4'-di-*tert*-butyl-2,2'-bipyridin, tpphz = tetrapyrido[3,2-a:2'3'-c:3'',2''-h:2''',3'''-j]phenazine) **RutpphzPd** (see Fig. 1) [14,16,17]. This catalyst produces up to 238 mol of H₂ per mol of catalyst under irradiation with visible

light in the presence of a sacrificial electron donor (triethylamine TEA) and water (15 vol.%). In this case the water serves as an additional proton source and influences the solvent polarity, the proton mobility and also the first photoinduced electron transfer reaction [17]. Based on electrochemical and EPR spectroscopic investigations the tpphz bridging ligand serves as an electron storage side which is charged under light illumination [18]. However, overall the bridging ligand plays an even more dominant role for the catalytic activity. The combination of ultrafast spectroscopy and excitation wavelength dependent resonance Raman spectroscopy revealed that efficient catalysis only takes place when the first excited ¹MLCT state is localized on the tpphz bridging ligand [14] and that ultrafast charge separation processes within the ligand scaffold are part of the catalytic mechanism [16].

Due to this dominant role of the bridging ligand several different tetrapyridophenazine based bridging ligands tpphzR_n (n = 2 or 4) with different kinds and number of substituents were developed [19]. Subsequently, a correlation between the well-defined place of the bromine substitution and the resulting photophysical properties of the corresponding ruthenium complexes could be established [17,19]. In addition, the effect of this structural variation on the catalytic activity and its underlying ultrafast intramolecular charge transfer behavior were recently studied on **RuBr₂tpphzPd**,

* Corresponding authors. Address: Institute of Photonic Technology (IPHT) Jena e.V., Albert-Einstein-Straße 9, 07745 Jena, Germany (B. Dietzek).

E-mail addresses: sven.rau@uni-ulm.de (S. Rau), benjamin.dietzek@ipht-jena.de (B. Dietzek).

¹ These authors contributed equally to this work.

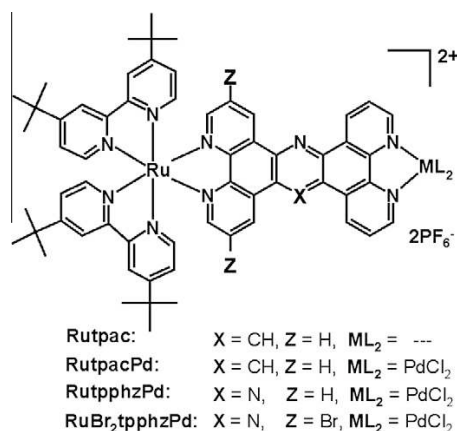


Fig. 1. Generalized chemical structure of the mono- and heterodinuclear ruthenium complexes with their different bridging ligands investigated in this study.

containing two bromine substituents at the tpphz bridge (Fig. 1). The introduction of these electron-withdrawing bromines into the tpphz frame had a broad influence and lead to a reduction of the electron-transfer rates in association with a decreased catalytic activity [17]. This lower catalytic activity of **RuBr₂tpphzPd** compared to **RutpphzPd** could potentially correlate with the results from ultrafast spectroscopical measurements, which illustrate that different excited-state decay pathways are competing with the charge transfer to the catalytic center. This fact becomes even more substantial upon introduction of heavy halogen atoms into the bridging ligand structure [17]. Furthermore, it has been shown that considering different loss mechanisms (like triplet–triplet annihilation) is important for the design of improved molecular artificial photosynthetic devices [20,21].

A further aspect of mono- and dinuclear ruthenium complexes with phenazine-based tpphz bridging ligands is their interaction with water in the excited state, i.e., the nitrogens of the phenazine moiety are prone to form hydrogen bonds with the solvent [22–24]. In particular, studies on Ru-dppz model systems (dppz = dipyrido[3,2-a:2',3'-c]phenazine) revealed that the luminescent MLCT-state is quenched upon increasing water concentrations [25–27]. However, by detailed investigations on the catalytic activity of **RutpphzPd** it was observed that water, which might serve as substrate for the catalytic hydrogen production, has an optimal concentration range in between 10 and 15 vol.% and that already minor amounts of water strongly increase the catalytic activity [14,17]. Nonetheless, apparently an opposing effect comes into action at higher water concentrations, limiting the catalytic turnover. This might be in connection with the disadvantageous effect of water on the long-lived excited state in ruthenium complexes bearing a phenazine moiety, where the stability is perhaps negatively influenced by water.

Based on this line of arguments it is quite clear that novel bridging ligands with a decreased water sensitivity of the excited state and altered electron storage capacities of the central sphere would yield valuable insights into the properties determining catalytic activity. Tetrapyridoacridine (tetrapyrido[3,2-a:2',3'-c:3'',2''-h:2''',3''-j]acridine, tpac, Fig. 1) possesses similar coordination spheres compared to the tpphz ligand and a central acridine moiety in contrast to the phenazine moiety in tpphz. Previous photophysical investigations of [(phen)₂Ru(tpac)]²⁺ and [(phen)₂Ru(tpac)Ru(phen)₂]⁴⁺ showed that the excited states are less sensitive towards water, that the two metal centers exhibit no electrochemical communication and that the excited state is mainly localized on the tpac ligand [28–30]. Thus, tpac presents an interesting bridging ligand for

the generation of intramolecular photocatalysts, which potentially yields important insights into the construction requirements for the development of related systems.

Here, we present the synthesis and structural characterization of two novel complexes [(tbbpy)₂Ru(tpac)]²⁺ **Rutpac** and [(tbbpy)₂Ru(tpac)PdCl₂]²⁺ **RutpacPd** (see Fig. 1). In addition, UV–vis, steady-state emission and time-resolved transient-absorption spectroscopy in dependence on the solvent environment are shown. By combination of these different spectroscopic techniques together with the characterization of the catalytic potential of **RutpacPd**, this study will help to present the versatility of tpac based heterodinuclear photocatalysts for photo hydrogen production.

2. Experimental section

2.1. Materials and methods

The synthetic procedures are based on standard literature methods [17–19,31], which were partially modified in this work. The exact experimental conditions for the preparation of **Rutpac** and **RutpacPd** are given in the synthesis section below. Subsequently the resulting products were analyzed by means of elemental analysis, mass spectrometry (ESI-MS), NMR spectroscopy (¹H NMR and H,H-COSY) and in case of **Rutpac** by single crystal X-ray analysis.

Furthermore, the precursors 4,4'-di-tert-butyl-2,2'-bipyridine (tbbpy), tetrapyrido[3,2-a:2',3'-c:3'',2''-h:2''',3''-j]acridine and the Pd(CH₃CN)₂Cl₂-adduct were synthesized as described previously [17,28,32]. If not stated otherwise all required materials (e.g. 2,2'-bipyridine, 5-amino-1,10-phenanthroline, RuCl₃·xH₂O or NH₄PF₆) were of commercial grade (solvents of HPLC grade) and used without further purification. Acetonitrile (ACN) used for photoinduced catalytic hydrogen production experiments was dried over calcium hydride and triethylamine (TEA) was dried over sodium before being freshly distilled under argon.

Nuclear Magnetic Resonance (NMR) spectra were recorded at ambient temperature on a Bruker AC 400 MHz spectrometer (¹H: 400.25 MHz). The proton assignment was done with the help of 2D-experiments. All spectra were referenced to TMS (tetramethylsilane) or to residual proton-solvent references (¹H: CDCl₃: 7.26 ppm, CD₃CN: 1.94 ppm) as an internal standard. In the assignments, the chemical shift (in ppm) is given first, followed by the multiplicity of the signal in brackets (s: singlet, d: doublet, dd: double doublet, m: multiplet), the number of protons and finally the value of the coupling constants in Hertz if applicable. Electrospray ionisation-Mass spectra were obtained on a Finnigan MAT 95 XL instrument at the Friedrich-Schiller University, Jena. The positive ESI-MS spectra were achieved with voltages of 3–4 kV applied to the electrospray nozzle. Elemental analysis was performed by the Microanalytical Laboratory of the University Jena.

2.2. Preparation of [(tbbpy)₂Ru(tpac)](PF₆)₂ (**Rutpac**)

In order to obtain the mononuclear ruthenium complex a purple solution of the (tbbpy)₂RuCl₂-precursor (0.11 g, 0.15 mmol) in ethanol/water (120 ml/40 ml) was slowly added dropwise to a boiling ethanol solution of a 1.5-equivalent-excess of tetrapyridoacridine (tpac, 0.89 mg, 0.23 mmol). During this reaction time the mixture was continuously heated to reflux and the orange suspension turned to a red solution. After 4 h the major solvent part was distilled off and then the remaining tpac-ligand was filtered off from the cooled solution and washed with a small portion of ethanol. After removal of most of the ethanol from the clear filtrate using the rotary evaporator an excess of NH₄PF₆ was added to

the complex solution. The yielded red precipitate was filtered, washed well with water, a little bit of ethanol and diethyl ether. Finally, the complex was purified by recrystallization and dried in vacuo. Despite the fact, that the heteroaromatic tpac-ligand contains two similar coordination spheres for binding the ruthenium precursor only the mononuclear compound **Rutpac** was isolated with a yield of 72% (0.14 g).

M ($C_{61}H_{61}N_9RuP_2F_{12}$) = 1311.2 g mol⁻¹; Anal. calcd. for $C_{61}H_{61}N_9RuP_2F_{12} \cdot 1H_2O$: C = 55.12, H = 4.78, N = 9.48; found: C = 54.75, H = 5.16, N = 9.20; MS (ESI in acetonitrile): m/z = 511 (20%) [(M-2PF₆)/2]²⁺, 1166 (100%) [M-PF₆]⁺ with matching isotopic pattern; ¹H NMR (400 MHz, CD₃CN, 300 K, c = 5.6 mmol l⁻¹): 9.95 (s, 1H), 9.73 (dd, 1H, J = 7.6 and 0.4 Hz), 9.56 (dd, 1H, J = 8.0 and 0.4 Hz), 9.37 (dd, 1H, J = 8.0 and 0.4 Hz), 9.27 (dd, 1H, J = 8.0 and 0.4 Hz), 8.66 (m, 2H), 8.56 (d, 2H, *bpy*), 8.51 (d, 2H, *bpy*), 8.16 (m, 2H), 7.88 (m, 4H), 7.82 (d, 2H, J = 5.6 Hz, *bpy*), 7.74 (dd, 2H, *bpy*), 7.50 (d, 2H, *bpy*), 7.31 (dd, 2H, *bpy*), 1.47 (s, 18H, *tert.butyl*), 1.33 (s, 18H, *tert.butyl*) ppm; UV-vis (acetonitrile): λ_{max} = 460 nm.

2.3. Preparation of [(*tbbpy*)₂Ru(tpac)PdCl₂](PF₆)₂ (**RutpacPd**)

This heterodinuclear complex was synthesized by the reaction of [(*tbbpy*)₂Ru(tpac)](PF₆)₂ with the Pd(CH₃CN)₂Cl₂-adduct in DCM under inert conditions [17]. Hence, a light red solution of [(*tbbpy*)₂Ru(tpac)](PF₆)₂ (40 mg, 0.03 mmol) and a slight excess of Pd(CH₃CN)₂Cl₂ (10 mg, 0.04 mmol) was refluxed in 40 ml freshly distilled dichloromethane (DCM) for 18 h under argon atmosphere. During this time the color changed to dark red. Thereafter the solution was filtered clear and the solvent was completely removed under reduced pressure. Finally, the reaction product was taken up again in a small amount of ethanol and then precipitated with an excess of an aqueous NH₄PF₆ solution. The resulting solid was isolated by filtration, washed well with water, a small portion of ethanol and diethyl ether. Subsequent drying in vacuo resulted in a dark red solid. Yield: 38 mg (84%).

M ($C_{61}H_{61}N_9RuPdCl_2P_2F_{12}$) = 1488.5 g mol⁻¹; MS (ESI in acetonitrile and methanol): m/z = 599 (20%) [(M-2PF₆)/2]²⁺, 1166 (40%) [M-PdCl₂-PF₆]⁺, 1376 (30%) [M-PF₆+MeOH]⁺ with matching isotopic pattern; ¹H NMR (400 MHz, CD₃CN, 300 K, c = 5.6 mmol l⁻¹): 10.07 (s, 1H), 9.92 (dd, 1H, J = 8.0 and 0.4 Hz), 9.64 (dd, 1H, J = 8.0 and 0.4 Hz), 9.49 (dd, 1H, J = 8.4 and 0.4 Hz), 9.31 (dd, 1H, J = 8.0 and 0.4 Hz), 9.07 (dd, 1H, J = 4.8 and 0.8 Hz), 8.96 (dd, 1H, J = 4.8 and 0.8 Hz), 8.55 (d, 2H, *bpy*), 8.50 (d, 2H, *bpy*), 8.27 (m, 2H), 8.09 (m, 4H), 7.83 (d, 2H, *bpy*), 7.73 (dd, 2H, *bpy*), 7.50 (d, 2H, *bpy*), 7.28 (dd, 2H, *bpy*), 1.47 (s, 18H, *tert.butyl*), 1.35 (s, 18H, *tert.butyl*) ppm; UV-vis (acetonitrile): λ_{max} = 462 nm.

2.4. Crystallography

A suitable single crystal of **Rutpac** was selected, embedded in protective perfluoropolyalkyether oil and transferred into the cold nitrogen gas stream of the diffractometer. Intensity data were collected at 150 K on a Bruker Kappa APEX II IμS Duo diffractometer using MoK_α radiation (λ = 0.71073 Å, QUAZAR focusing Montel optics). Data were corrected for Lorentz and polarization effects, semi-empirical absorption corrections were performed on the basis of multiple scans using SADABS [33]. The structure was solved by direct methods and refined by full-matrix least-squares procedures on F² using SHELXTL NT 6.12 [34]. All non-hydrogen atoms were refined with anisotropic displacement parameters. All hydrogen atoms were placed in positions of optimized geometry, their isotropic displacement parameters were tied to those of their corresponding carrier atoms by a factor of 1.2 or 1.5. The tpac ligand is disordered in a way that the atoms N2 and C25 change their positions. The refinement of the disorder resulted in site occupancies of 67(5)% for N2 and C25 and 33(5)% for N2A and C25A. One of the PF₆⁻ anions is dis-

ordered, two alternative orientations were refined resulting in site occupancies of 61.9(6)% for P2 – F25 and 38.1(6)% for P2A – F25A, respectively. SAME, ISOR, and SIMU restraints were applied in the refinement of the disordered structure parts.

The compound crystallizes with a total number of 2.5 water molecules that are disordered over five different sites. No hydrogen atoms were included for these disordered solvent molecules. Complete data for the X-ray crystal structure determination of **Rutpac** were deposited (CCDC-848418). These data can be obtained free of charge from the Cambridge Crystallographic Data Center via www.ccdc.cam.ac.uk/data_request/cif (or from Cambridge Crystallographic Data Center, 12 Union Road, Cambridge, CB2 1EZ, UK; fax: +44-1223-336-033; e-mail: deposit@ccdc.cam.ac.uk).

2.5. Crystal Data of *Rutpac*

[$C_{61}H_{61}N_9Ru$]²⁺2[PF₆]⁻2.5[H₂O] ($C_{61}H_{66}F_{12}N_9O_{2.5}P_2Ru$), Mr = 1356.24 g mol⁻¹, red crystals, crystal size 0.15 × 0.03 × 0.02 mm, triclinic, space group *P*-1, *a* = 11.532(1), *b* = 12.888(2), *c* = 22.282(2) Å, α = 93.846(2), β = 92.302(2), γ = 94.369(2)°, *V* = 3291.1(5) Å³, *T* = 150(2) K, *Z* = 2, ρ_{calcd.} = 1.369 g cm⁻³, absorption coefficient = 0.369 mm⁻¹, *F*(000) = 1394, 31,546 reflections in *h*(-14/14), *k*(-15/15), *l*(-27/27), measured in the range 3.08° ≤ θ ≤ 25.68°, completeness θ_{max} = 98.1%, 12,253 independent reflections, *R*_{int} = 0.0417, 9400 observed reflections [*I* > 2σ(*I*)], 883 parameters, 352 restraints, *R*_{1obs} = 0.0659, *wR*_{2obs} = 0.1600, *R*_{1all} = 0.0901, *wR*_{2all} = 0.1731, *Goof* on *F*² = 1.118, largest difference peak and hole: 1.318/–1.091 e Å⁻³.

2.6. Photocatalysis

Photocatalytic hydrogen production experiments were accomplished by using appropriate gas chromatography (GC) vials (5 ml) placed in a self-made and air-cooled photomicroreactor for maintaining room temperature (21 °C) under continuous LED (λ = 470 ± 10 nm) irradiation. The commercially available LED sticks applied for these experiments were manufactured by Innatas Elektronik GmbH (Germany) and provide an intensity of approximately 10 mW cm⁻² (at 12 V). Full specifications and representative pictures regarding the technical equipment for hydrogen production and the determination via GC were presented before [14,17].

2.7. Photophysics

If not stated otherwise the solvents acetonitrile (ACN) and dichloromethane (DCM) were used as purchased (spectroscopic grade, purity > 99.9%) and all measurements were performed with aerated solvents at room temperature (22 °C). To guarantee the photophysical stability of the samples UV-vis spectra were taken prior and subsequent to all experiments.

Steady-state UV-vis absorption spectra were recorded with a JASCO V-670 photospectrometer. The solutions were diluted (OD < 0.05 at 445 nm) to record steady-state emission spectra using a Jasco FP-6200 spectrofluorimeter. Quantum yield measurements were performed in reference to solutions of [Ru(*bpy*)₃]Cl₂ in non-degassed water (φ = 0.028) [35]. Time-correlated single-photon counting determined the luminescence lifetimes: The output of a Ti-Sapphire laser (Tsunami, Newport Spectra-Physics GmbH) was frequency-doubled and used as pump beam at 435 nm. To detect the luminescence a Becker & Hickel PMC-100-4 photon counting module with 150-ps response time and a pulse-to-pulse repetition rate of 800 kHz was used.

The setup used for pump-probe spectroscopy was published earlier [17]. Briefly, a pump pulse at 480 nm, with an average energy of 0.5 μJ per pulse was spatially and temporally overlapped in the sample volume with a supercontinuum white-light probe. To

avoid polarization effects, the mutual polarization between pump and probe pulses was set to magic angle.

The entire differential absorption (ΔA) data set, recorded as a function of the delay time Δt between pump pulse and probe continuum and the probe-wavelength λ_{pr} , is treated by a global fit routine for data analysis. The fit routine uses a sum of exponentials as fit function:

$$\Delta A(t, \lambda_{pr}) = \Phi(\lambda_{pr}) + \sum_{i=1}^n A_i(\lambda_{pr}) \cdot e^{-\Delta t/\tau_i}$$

The constant offset $\Phi(\lambda_{pr})$ accounts for long-lived pump-induced absorption changes, which decay on a larger time-scale than the experimental accessible time window of 1.6 ns. The wavelength-dependent pre-exponential factors $A_i(\lambda_{pr})$ contain the spectral characteristics of each individual kinetic component associated with τ_i and represent the so called *decay-associated spectra* (DAS). Each data set was numerically chirp corrected before fitting. The pulse-overlap region was ignored during the fitting process to avoid contributions from coherent artifacts [36,37]. As a consequence of the data handling, processes occurring faster than in about 500 fs are not resolved.

3. Results and discussion

3.1. Synthesis and structural characterization

The synthesis of the heterodinuclear complex [(tbbpy)₂Ru(tpac)PdCl₂](PF₆)₂ **RutpacPd** (see Fig. 1) was carried out according to standard methods by the reaction of [(tbbpy)₂Ru(tpac)](PF₆)₂ **Rutpac** with Pd(ACN)₂Cl₂ in DCM under inert conditions [17,18]. By doing so **RutpacPd** was obtained in high yield (84%), which is in very good agreement to the yields obtained for the analogous compounds **RutpphzPd** (88%) and **RuBr₂tpphzPd** (84%).

The subsequent structural characterization was performed by means of multidimensional NMR methods (H,H-COSY), MS (ESI) and also by single crystal X-ray analysis for **Rutpac**. ESI mass spectroscopy with matching isotopic pattern confirmed the composition of both ruthenium complexes. While for **Rutpac** the [M–1PF₆]⁺ peak was found as the most intense peak, in case of **RutpacPd** the [M–1PF₆+MeOH]⁺ and the [(M–2PF₆)/2]²⁺ peak could be assigned to the corresponding fragments.

Based on the results of the ¹H- and the H,H-COSY spectra two bipyridine signal sets and 13 proton signals related to the tpac-ligand could be determined. The occurrence of only one heterocyclic N-atom in the acridine moiety leads to an asymmetry of the tpac ligand as compared to the tpphz ligand. Hence, the tpac-ligand gives rise to 13 different ¹H NMR signals in both complexes (**Rutpac** and **RutpacPd**), which are partially overlapping in the aromatic region [28]. Nevertheless, a very striking singlet proton signal can be assigned to the isolated CH group of the acridine moiety with a chemical shift of 9.95 ppm for **Rutpac** and 10.07 ppm (in CD₃CN) for **RutpacPd**. Furthermore, these proton NMR signals of the bridging ligand are typically very sensitive towards the coordination of a second metal center [17,18,29,41]. For instance, the low field signal at 9.73 ppm, which belongs to the free phenanthroline side of **Rutpac**, undergoes a downfield shift of about 0.19 ppm towards 9.92 ppm after introduction of the PdCl₂ unit. These observations are in good agreement with some analogous mono- and dinuclear tpac/tpphz compounds [17,29,38].

Orange-red single crystals of **Rutpac** suitable for X-ray characterization were obtained from an acetone/water solution. The result of the X-ray crystallographic analysis is shown in Fig. 2 and confirms the proposed conventional structure for this kind of ruthenium polypyridine complexes [18,19,39]. The central ruthenium ion is coordinated by six nitrogen donor atoms of the polypyridine

chelate ligands in an approximated octahedral fashion. The tpac ligand appears to be largely planar and π - π interactions between two neighboring tpac ligands lead to the formation of stacked dimers in the solid state (see Fig. 2), which is in accordance with related Ru-complexes [19,27,40]. This finding might also explain the observed concentration-dependent proton-NMR signals in some of these compounds [19,41,42], which was also reported for **Rutpac** [29,38] (Table 1).

3.2. Catalytic activity

The newly developed heterodinuclear ruthenium complex **RutpacPd** was tested towards its photocatalytic activity for light-driven hydrogen production (see Fig. 3). By using the same conditions and experimental setup its catalytic activity, expressed as turnover number (TON), could be compared to those of [(tbbpy)₂Ru(tpphz)PdCl₂](PF₆)₂ **RutpphzPd** and [(tbbpy)₂Ru(3,16-Br₂tpphz)PdCl₂](PF₆)₂ **RuBr₂tpphzPd** [14,17]. The presence of 2 M triethylamine (TEA), acting as a sacrificial electron donor, and irradiation times of 18 h were found to be most effective for a maximum hydrogen production.

As expected, for all these complexes the catalytic activity is higher in the presence of water and is already largely increased by the addition of small amounts of water (in the range between 2 and 10 vol.%, see Fig. 3). However, **RutpacPd** (as does **RuBr₂tpphzPd**) shows reduced turnover numbers as compared to **RutpphzPd** (see Table 3). **RutpacPd**, **RuBr₂tpphzPd** and **RutpphzPd** possess different maximal TONs of 139, 94 and 238, respectively, measured after 18 h of irradiation. This means that rather small structural modifications, for instance replacing the phenazine by an acridine unit, induce a reduction of the catalytic activity. The impact of this structural modification on the spectroscopic properties and photo-induced dynamics with respect to the catalytic capability will be discussed in the following section.

3.3. Photophysics

The photophysical properties of **Rutpac** and **RutpacPd** were studied by means of UV-vis absorption and emission spectroscopy in concert with ultrafast transient absorption spectroscopy. Furthermore, the impact of the solvents on the photophysical properties is investigated as the charge-transfer reactions in Ru-polypyridine complexes generally depend on the solvent polarity [17,43–45]. Following, the observation of water-content dependent catalytic turnover, comparative photophysical measurements of **Rutpac** and **RutpacPd** were carried out in acetonitrile (ACN), dichloromethane (DCM) and a mixture of ACN with 10 vol.% H₂O.

3.4. Steady-state spectroscopy

The UV-vis absorption spectra of **Rutpac** and **RutpacPd** in ACN and DCM (see Fig. 4 and Table 2) show features typical for Ru-polypyridine complexes [31,46–48]. Both compounds reveal four absorption maxima: The band at 280 nm belongs to π - π^* transitions of the terminal tbbpy ligands, while the two maxima at 350 and 370 nm can be assigned to π - π^* transitions of the tpac ligand. The broad band in the visible range, i.e. between 400 and 500 nm, belongs to the metal-to-ligand charge transfer (MLCT) from the central Ru-ion to the coordinating ligands. Furthermore, a solvent-independent shoulder is apparent at 475 nm. In summary, the UV-vis absorption spectrum of **RutpacPd** is similar to the spectra of **RutpphzPd** and **RuBr₂tpphzPd** with somewhat different MLCT maxima (see Table 2) [17,18].

Both complexes **Rutpac** and **RutpacPd** show a clear emission after MLCT excitation (see Fig. 4). The emission maximum of **Rutpac** is located at 612 nm in ACN, with an emission quantum yield

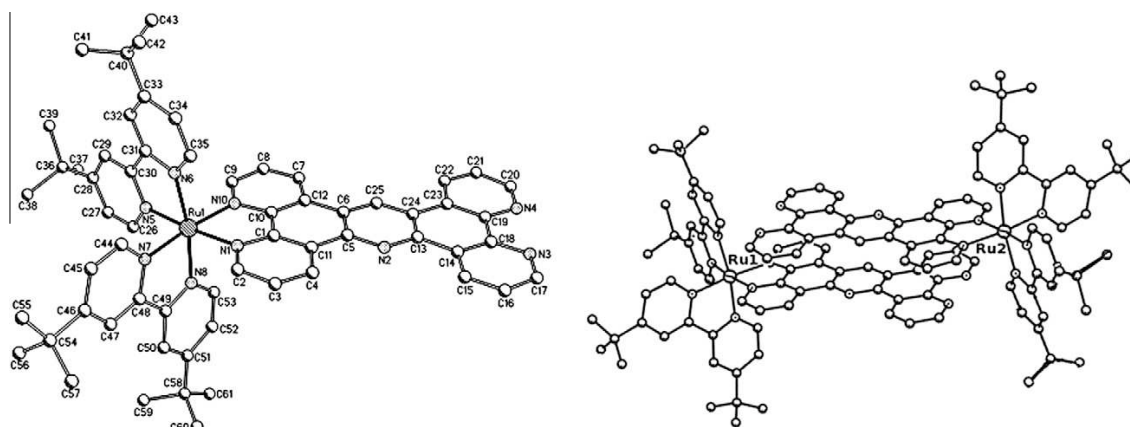


Fig. 2. Molecular structure (left: numbering scheme, right: its dimeric arrangement) of **Rutpac** (H-atoms and PF_6^- -anions are omitted for clarity). Relevant bond distances (in Å) and bond angles (in $^\circ$) are listed in Table 1.

Table 1
Selected bond lengths (Å) and angles ($^\circ$) of **Rutpac**.

Rutpac	Bond lengths (in Å)	Rutpac	Angles (in $^\circ$)
Ru(1)–N(1)	2.068(5)	N(10)–Ru(1)–N(1)	79.46(18)
Ru(1)–N(5)	2.049(5)	N(6)–Ru(1)–N(5)	77.94(19)
Ru(1)–N(6)	2.047(5)	N(6)–Ru(1)–N(7)	94.07(18)
Ru(1)–N(7)	2.053(5)	N(5)–Ru(1)–N(7)	90.29(18)
Ru(1)–N(8)	2.059(5)		
Ru(1)–N(10)	2.064(4)	C(2)–N(1)–C(1)	117.5(5)
C(1)–C(10)	1.442(8)	C(9)–N(10)–C(10)	118.0(5)
C(5)–C(6)	1.414(9)		
N(1)–C(1)	1.366(7)	C(5)–N(2)–C(13)	121.1(6)
N(2)–C(5)	1.340(8)	C(24)–C(25)–C(6)	122.2(6)

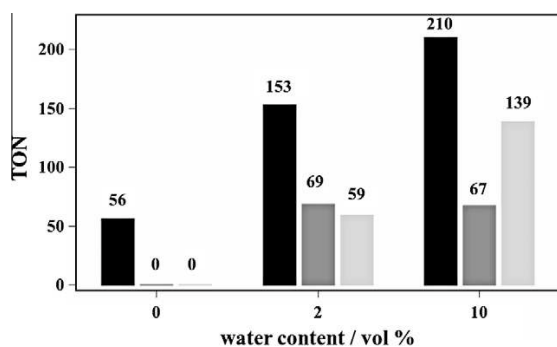


Fig. 3. Illustration of the photocatalytic activity of **RutpphzPd** (black), **RuBr₂tpphzPd** (dark gray) and **RutpacPd** (light gray) for three different amounts of water content, keeping all other reaction conditions constant (18 h irradiation time, $\lambda = 470 \pm 10$ nm, $P = 10$ mW cm⁻²). In addition, all samples contained 2 M TEA in an acetonitrile–water mixed solution under argon atmosphere.

Table 2
Summary of the photophysical and catalytic data of **RutpphzPd**, **RuBr₂tpphzPd** and **RutpacPd** presented in this paper. The Δ values (in parentheses) refer to the difference between the respective values of the heterodinuclear complex minus the mononuclear precursor.

Complex	λ_{abs} [nm] ($\Delta\lambda_{\text{abs}}$)	λ_{em} [nm] ($\Delta\lambda_{\text{em}}$)	Φ	τ [ns] ($\Delta\tau$)	Solvent (catalysis)	Donor (catalysis)	TON (time [h])	Ref.
RutpacPd	475(0)	617 (+5)	0.008	180(+27)	ACN + 10%	TEA	138.7 (18)	This study
	ACN	ACN	ACN	ACN (aer.)	H ₂ O			
RutpphzPd [†]	445(0)	650 (+12)	–	27(–127)	ACN + 15%	TEA	238.3 (18)	[17,18]
	ACN	ACN	ACN	ACN (aer.)	H ₂ O			
RuBr ₂ tpphzPd [†]	484(+6)	675 (+14)	0.003	84(–134)	ACN + 7.1%	TEA	94.2 (18)	[17,19]
	ACN	ACN	ACN	ACN (aer.)	H ₂ O			

[†] The data of **RutpphzPd** and **RuBr₂tpphzPd** are used for comparison and taken from Rau et al. [18] and Karnahl et al. [17,19] (aer. = aerated/oxygen containing solvent).

of 1.6×10^{-2} and an emission lifetime of 153 ns (Table 3). The changes of the luminescence properties of **Rutpac** induced by adding 10 vol.% water to the ACN solution are rather small, resulting in a quantum yield of 1.8×10^{-2} and an emission lifetime of 162 ns. In DCM the quantum yield of the **Rutpac** emission rises to 5.5×10^{-2} and the emission lifetime becomes 900 ns as the luminescence undergoes a hypsochrome shift of 9 nm (244 cm⁻¹) to 603 nm. The rise of the emission lifetime and quantum yield in DCM originates from the decreased solvent polarity, which favors the population of the emissive phenanthroline-centered charge-transfer state (³MLCT-phen) [21,29]. In contrast, a second charge-transfer state exists, which – in analogy to dppz (dppz = dipyrdo[3,2-a:2',3'-c]phenazine) and tpphz complexes – is assumed to be located on the acridine moiety of tpac (³MLCT-ac). Population of this state will increase the dipole moment of the complex contrary to a population of the ³MLCT-phen state. Hence, the population of the ³MLCT-ac state is significantly reduced (enhanced) in the unpolar (polar) solvent DCM (ACN) [29,44,47,49,50]. As the ³MLCT-ac state is prone to non-radiative decay **Rutpac** emission is increased in the unpolar solvent DCM.

Introduction of the Pd-ion induces a small redshift of the emission by 5 nm (130 cm⁻¹) and a drop of the luminescence quantum yield, which is independent of the solvent (see Tables 2 and 3). As summarized in Table 2, this redshifted emission upon PdCl₂-coordination is typical for this series of complexes. Especially the significant drop of the quantum yield reveals the presence of a more efficient non-radiative deactivation channel in **RutpacPd**. This decay channel is attributed to electron transfer to the Pd-core (see below for a discussion of the ps time-resolved spectroscopic data). Furthermore, in pure ACN the luminescence lifetime of **RutpacPd** (180 ns) is slightly longer than the lifetime of the precursor **Rutpac** (153 ns), which could possibly add to the lower

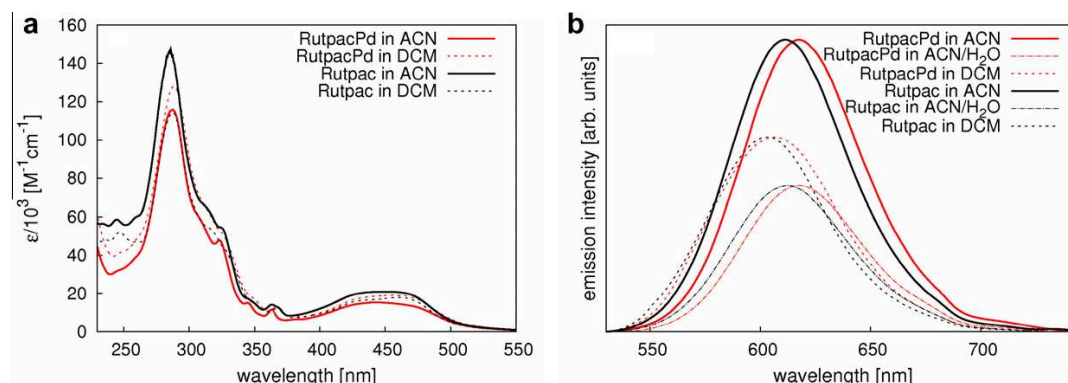


Fig. 4. UV-vis absorption (a) and emission (b) spectra of Rutpac and **RutpacPd**. For better comparability the intensities of the normalized emission spectra are scaled.

Table 3

Emission data (emission maxima λ_{em}) of **Rutpac** and **RutpacPd** in dependence of the solvent environment (the ACN/H₂O mixture contains 10 vol.% H₂O). Typical errors in determining the quantum yields Φ are in the order of 20%, while the luminescence lifetimes τ are measured with a relative error of 1%.

Complex	λ_{em} [nm]			$\Phi \times 10^{-2}$			τ [ns]		
	ACN	DCM	ACN/H ₂ O	ACN	DCM	ACN/H ₂ O	ACN	DCM	ACN/H ₂ O
Rutpac	612	603	612	1.6	4.6	1.8	153	900	162
RutpacPd	617	607	617	0.8	0.8	0.6	180	170	90

catalytic activity of **RutpacPd** in comparison to **RutpphzPd**. However, upon addition of 10 vol.% H₂O to the ACN solution, the emission lifetime of **RutpacPd** drops significantly to 90 ns. This value is then in the same order of magnitude as the lifetimes of **RutpphzPd** and **RuBr₂tpphzPd** (see Table 3).

This behavior of **RutpacPd** after water addition differs from the results obtained for **Rutpac**. On the other hand a comparison of the **RutpacPd** luminescence lifetimes in ACN and DCM indicates that the altered solvent polarity cannot account for this observation. However, this finding might indicate that water (within the investigated concentration range) dominantly interacts with the Pd-ion, e.g. by exchange of a Cl⁻ anion with a water molecule as suggested for **RutpphzPd** before [16].

Overall, the steady-state spectroscopic results of **RutpacPd** (see Table 2) exhibit similar features like those of **RutpphzPd** and the exchange of one single N-atom in the phenazine unit against a CH-group results in comparable UV-vis, emission and catalytic

properties. Anyway, the photoinduced dynamics, which are discussed in the following section, reveal notable effects of the acridine moiety which might have an influence on the catalytic reactions.

3.5. Ultrafast transient absorption spectroscopy

Transient absorption data of **Rutpac** and **RutpacPd** were also recorded in ACN, ACN/H₂O and DCM, after MLCT excitation at 480 nm. The spectral window accessed by the probe-light was between 490 and 720 nm, covering a broad visible excited-state absorption (ESA) band. The transient spectra of both species (see Figs. 5 and 6) show similar spectral features for all three solvents: a ground-state bleach below 520 nm is accompanied by ESA bands with solvent-specific maxima.

Fig. 5 depicts typical transient absorption spectra (a) and photoinduced kinetics (b) of **Rutpac** in different solvents. The maximum

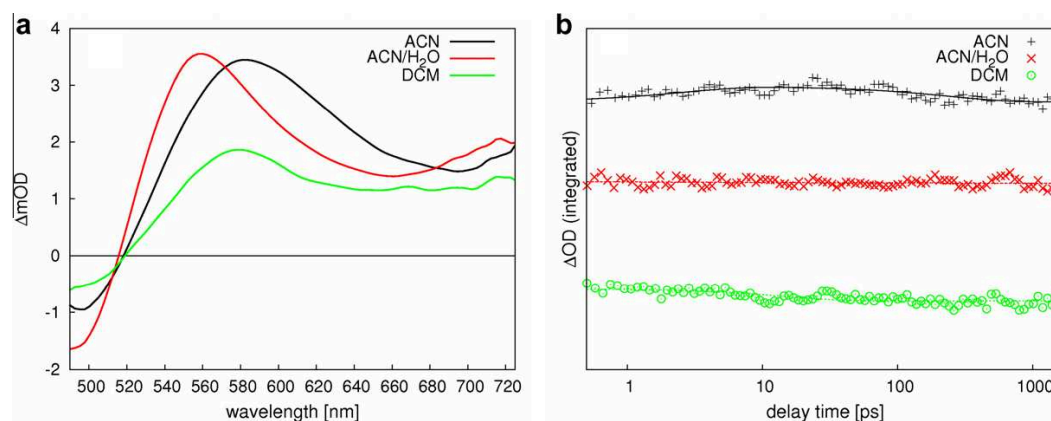


Fig. 5. Transient absorption spectra (a) of **Rutpac** recorded 10 ps after excitation at 480 nm and the integrated transient kinetics (b) in different solvents.

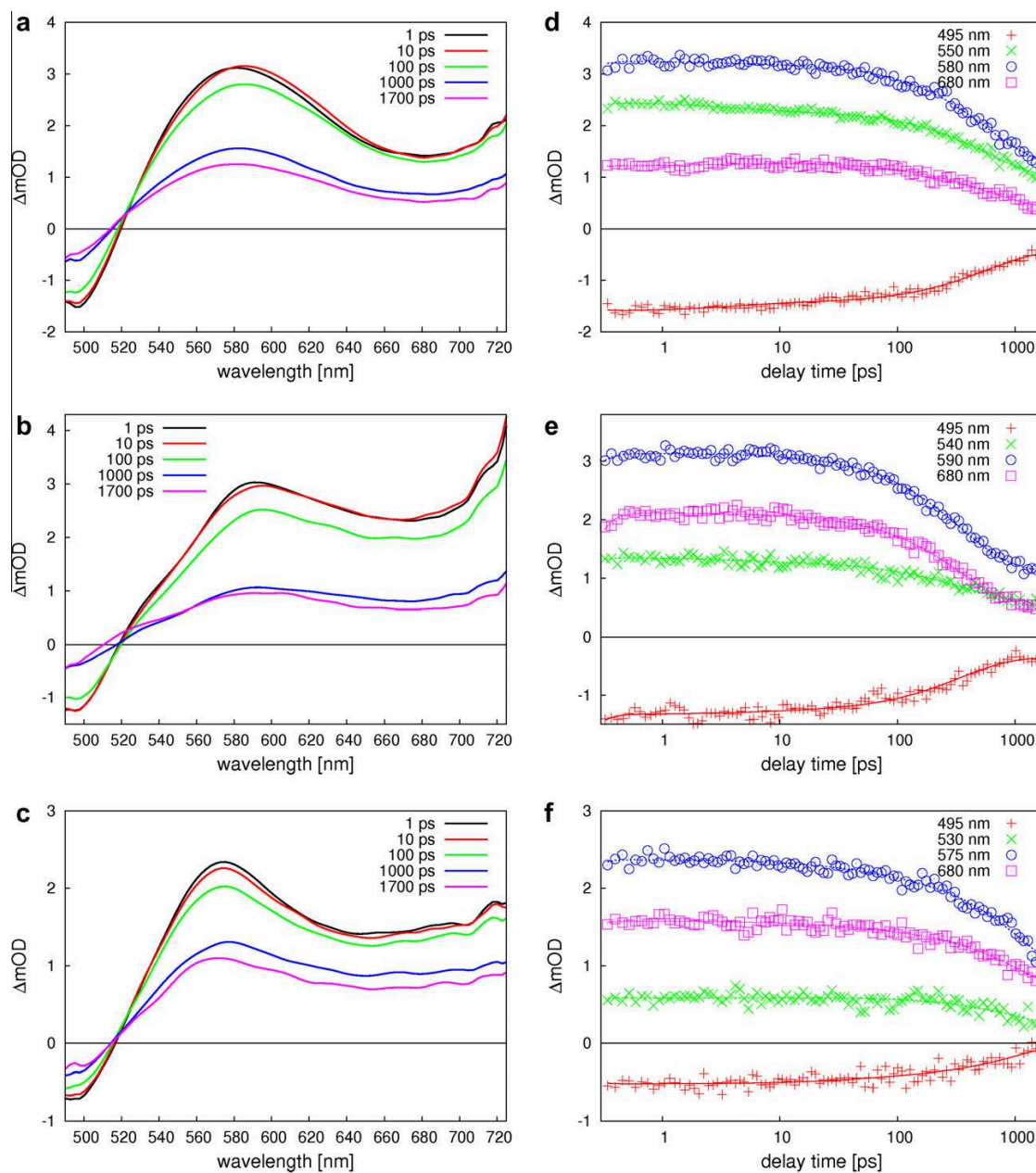


Fig. 6. Transient spectra (left) and kinetics (right) of **RutpacPd** in three different solvent environments (ACN, top; ACN/H₂O, middle; DCM, bottom) after excitation at 480 nm.

of the transient absorption appears at 585 nm in ACN and is slightly blue shifted to 580 nm in DCM and to 560 nm upon addition of water to ACN. Irrespective of the solvent the transient absorption spectra show barely any temporal evolution within the experimental accessible time window of 1.6 ns. This is reflected in the transient kinetics (Fig. 5b), which resemble the dynamics of the ESA band by plotting the ΔOD signal spectrally integrated over the ESA band as a function of delay time. This representation fails to account for potentially subtle spectral band shifts, but it highlights the existing kinetic behavior, which might arise for several reasons: On the one hand, the excited states dynamics might be faster than the temporal resolution of our experiment, i.e. occurring within the

first 500 fs and can therefore not be resolved with our time-resolved spectrometer. On the other hand, the photoinduced processes might be too slow to cause significant ΔOD changes within the experimentally accessible time window of 1.6 ns. Finally, the photoinduced charge-transfer processes might be associated with very small spectral changes, so that these are not visible inside the experimentally achievable signal-to-noise ratio. This explanation however would be in contrast to the ultrafast transient absorption results of the related Ru-dppz and Ru-tpphz complexes [16,17,51].

The transient absorption spectra of **RutpacPd** in ACN and DCM resemble central features of the spectra of **Rutpac** and only small

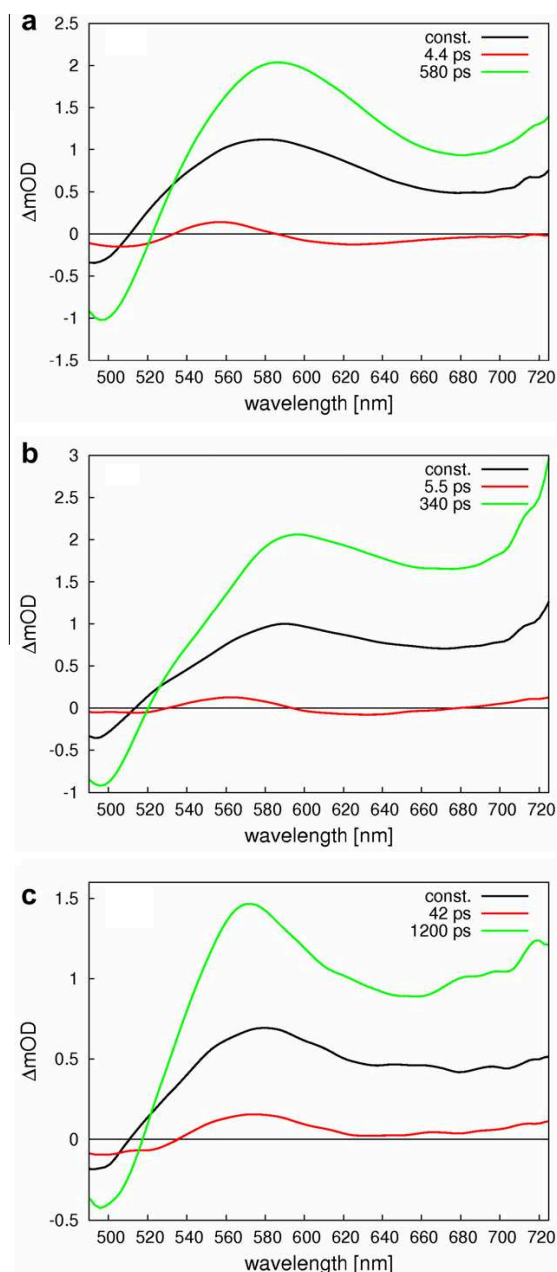


Fig. 7. Decay-associated spectra of **RutpacPd** in the different solvent environments: pure ACN (a), mixture of ACN and 10 vol.% H₂O (b) and DCM (c).

spectral shifts were found when comparing the ESA shapes of the mononuclear complex with those of the dinuclear species in both solvents (see Figs. 5 and 6). This situation is significantly different for the ACN/H₂O mixture. Here, the introduction of a Pd-center induces a shift of the ESA from 550 to 590 nm (see Figs. 5 and 6). The excited-state dynamics of **RutpacPd** reveal two features irrespective of the solvent: on a short time-scale a blue shift of the ESA band appears and a global decay of the differential absorption signal is observed for long timescales. The characteristic time constants describing the photoinduced dynamics of **RutpacPd** can be best fitted to $\tau_1 = 4.4$ and $\tau_2 = 580$ ps in ACN. The assignment of these

time-constants to the underlying charge-transfer dynamics is done in comparison to the related **Rutpphz**-complexes [16,44]. Based on this comparison the τ_2 -component is assigned to a ligand-to-metal charge transfer (LMCT) from the ac-unit to the Pd-center. As the LMCT originates from the ³MLCT-ac state, it is expected that ISC (¹MLCT-phen → ³MLCT-phen) and ILCT (³MLCT-phen → ³MLCT-ac) have taken place prior, i.e. on a timescale much faster than $\tau_1 = 4.4$ ps.

Coming back to the discussion on the relatively uniform transient kinetics observed for **Rutpac**, this finding argues for the fact that also in the mononuclear complex the photoinduced processes take place rather rapidly and are associated with very little spectral changes. Therefore, we can conclude that the previously raised option that the photoinduced processes in **Rutpac** being very slow, is likely not to hold true.

In different solvent environments the same kinetic components of **RutpacPd** are observed, however, with altered characteristic time-constants (see Fig. 7). In DCM the kinetics are decelerated to $\tau_1 = 42$ and $\tau_2 = 1200$ ps, a solvent-dependent behavior also known for related tpphz- and dppz-complexes [16,17,51]. This is due to the fact that the charge-transfer states are destabilized in the unpolar solvent DCM as compared to ACN [16,17,51]. The addition of 10 vol.% water to ACN has only a minor impact on the polarity and accordingly only minor alterations of the photoinduced dynamics are observed. Figs. 6 and 7 show, that the addition of water has mainly a quantitative impact, i.e. two kinetic components with similar spectral characteristics are observed. The first one ($\tau_1 = 5.5$ ps) reflects charge-localization on the tpac ligand, while cooling and ILCT are nearly unaffected by the presence of water. In contrast, the second time-constant, $\tau_2 = 340$ ps, is smaller in the ACN/H₂O solvent mixture compared to pure ACN. The sole acceleration of the LMCT after addition of water supports the conclusion already drawn from the steady-state luminescence experiments, that the H₂O molecules directly interact with the Pd-center and not with the tpac bridging ligand [16]. Therefore, the impact of water is not significantly reduced by the replacement of the phenazine against the acridine unit. In other words, the effect of substituting one N-atom in the bridging ligand versus a CH-group is rather small, compared to the strong influence of the catalytic PdCl₂-center, which was identical in all three investigated complexes.

4. Summary and conclusion

Two novel Ru-polypyridine complexes, [(tbbpy)₂Ru(tpac)PdCl₂]²⁺ **RutpacPd** (with tpac = tetrapyrido[3,2-a:2',3'-c:3'',2''-h:2''',3'''-j]acridine) and [(tbbpy)₂Ru(tpac)]²⁺ **Rutpac**, have been synthesized, characterized and investigated with respect to their spectroscopic and photocatalytic properties for the light-driven generation of molecular hydrogen. In particular, the photophysical and photochemical studies aimed at detailing the effect of the bridging tpac ligand on the photocatalytic behavior and the light-induced dynamics of the complexes in comparison to well established systems bearing a tetrapyridophenazine (tpphz) ligand [14,16,17,20,29]. It was shown that **RutpacPd** is less catalytically active compared to the tpphz-containing counterpart. Furthermore, comparing the luminescence results of the mononuclear and the dinuclear species, i.e. **Rutpac** and **RutpacPd**, it becomes apparent that the acridine moiety is less prone to interact with the solvent water by forming hydrogen bonds than the phenazine unit in tpphz. Instead, the impact of water on the luminescence properties of the **RutpacPd** photocatalyst is attributed to direct interactions of water molecules with the coordinated Pd-ion by, e.g., replacing a chloro ligand by a water molecule. This possible replacement of a chloro ligand by a water molecule is also observed in similar Ru-complexes and therefore underlines a more general feature of photocatalysts including a catalytic PdCl₂ center [16,18]. Furthermore, the ultrafast

photoinduced dynamics show barely any dynamic changes of the differential absorption spectra on a ps-timescale, indicating that the photoinduced intraligand charge-transfer dynamics takes place on a rapid sub-ps timescale and is associated with only minor spectral changes. In contrast to the mononuclear building block **Rutpac**, the photoinduced dynamics in the dinuclear complex **RutpacPd** reveal photoinduced charge-transfer from the photoactive Ru-unit to the catalytically active Pd-center on a sub-ns timescale. These results are consistent with reports on related compounds [16,44,52]. In conclusion, the work presented here constitutes an important stepping stone investigating of the modular design approach to molecular photocatalysts building on the successfully established catalysts of the **RutpphPd** family [12,14,18], thereby, potentially paving the way to an improved design of photocatalysts for the production of molecular hydrogen.

Acknowledgements

M.K. likes to thank the Wenner-Gren Foundation for a PostDoc fellowship. C.K. is grateful to the Deutsche Bundesstiftung Umwelt (DBU) for a PhD fellowship and B.D. and J.P. for financial support by the Fonds der Chemischen Industrie (FCI). This research was supported financially by the Thüringer Ministerium für Bildung, Wissenschaft und Kultur (PhotoMIC, Grant No. B 514-09049).

References

- [1] N.S. Lewis, D.G. Nocera, Proc. Natl. Acad. Sci. USA 103 (2006) 15729.
- [2] N. Armbaroli, V. Balzani, Angew. Chem. Int. Ed. 46 (2007) 52.
- [3] J. Balzani, A. Credo, M. Venturi, ChemSusChem 1 (2008) 26.
- [4] A. Zuttel, A. Borgschulte, L. Schlapbach (Eds.), Hydrogen as a Future Energy Carrier, Wiley-VCH, Weinheim, 2008.
- [5] A. Boddien, D. Mellmann, F. Gärtner, R. Jackstell, H. Junge, P.J. Dyson, G. Laurency, R. Ludwig, M. Beller, Science 333 (2011) 733.
- [6] A. Magnuson, M. Anderlund, O. Johansson, P. Lindblad, R. Lomoth, T. Polivka, S. Ott, K. Stensjö, S. Styring, V. Sundström, L. Hammarström, Acc. Chem. Res. 42 (2009) 1899.
- [7] T.R. Cook, D.K. Dogutan, S.Y. Reece, Y. Surendranath, T.S. Teets, D.G. Nocera, Chem. Rev. 110 (2010) 6474.
- [8] H. Ozawaa, K. Sakai, Chem. Commun. 47 (2011) 2227.
- [10] V. Artero, M. Chavarot-Kerlidou, M. Fontecave, Angew. Chem. Int. Ed. 50 (2011) 7238.
- [11] A.J. Esswein, D.G. Nocera, Chem. Rev. 107 (2007) 4022.
- [12] S. Rau, D. Walthner, J.G. Vos, Dalton Trans. (2007) 915.
- [13] M. Wang, Y. Na, M. Gorlov, L. Sun, Dalton Trans. (2009) 6458.
- [14] A. Inagaki, M. Akita, Coord. Chem. Rev. 254 (2010) 1220.
- [15] S. Tschierlei, M. Karnahl, M. Presselt, B. Dietzek, J. Guthmüller, L. Gonzales, M. Schmitt, S. Rau, J. Popp, Angew. Chem. 122 (2010) 4073; Angew. Chem. Int. Ed. 49 (2010) 3981.
- [16] S. Tschierlei, M. Presselt, C. Kuhnt, A. Yartsev, T. Pascher, V. Sundström, M. Karnahl, M. Schwalbe, B. Schäfer, S. Rau, M. Schmitt, B. Dietzek, J. Popp, Chem. Eur. J. 15 (2009) 7678.
- [17] M. Karnahl, C. Kuhnt, F. Ma, A. Yartsev, M. Schmitt, B. Dietzek, S. Rau, J. Popp, Chem. Phys. Chem. 12 (2011) 2101.
- [18] S. Rau, B. Schäfer, D. Gleich, E. Anders, M. Rudolph, M. Friedrich, H. Görls, W. Henry, J. G. Vos, Angew. Chem. 118 (2006) 6361; Angew. Chem. Int. Ed. 45 (2006) 6215.
- [19] M. Karnahl, S. Tschierlei, C. Kuhnt, B. Dietzek, M. Schmitt, J. Popp, M. Schwalbe, S. Kriech, H. Görls, F.W. Heinemann, S. Rau, Dalton Trans. 39 (2010) 2359.
- [20] C. Kuhnt, M. Karnahl, M. Schmitt, S. Rau, B. Dietzek, J. Popp, Chem. Commun. 47 (2011) 3820.
- [21] C. Kuhnt, M. Karnahl, S. Rau, M. Schmitt, B. Dietzek, J. Popp, Chem. Phys. Lett. 516 (2011) 45.
- [22] J. Preuß, A. Gieren, W. Hoppe, V. Zunker, Liebigs Ann. Chem. (1973) 221.
- [23] J. Olofsson, B. Onfelt, P. Lincoln, J. Phys. Chem. A 108 (2004) 4391.
- [24] D.A. McGovern, A. Selmi, J.E. O'Brien, J.M. Kelly, C. Long, Chem. Commun. (2005) 1402.
- [25] R.M. Hartshorn, J.K. Barton, J. Am. Chem. Soc. 114 (1992) 5919.
- [26] E.J.C. Olson, D. Hu, A. Hormann, A.M. Jonkman, M.R. Arkin, E.D.A. Stemp, J.K. Barton, P.F. Barbara, J. Am. Chem. Soc. 119 (1997) 11458.
- [27] M. Schwalbe, M. Karnahl, S. Tschierlei, U. Uhlemann, M. Schmitt, B. Dietzek, J. Popp, R. Groake, J.G. Vos, S. Rau, Dalton Trans. 39 (2010) 2768.
- [28] M. Demeunynck, C. Moucheron, A. Kirsch-De Mesmaeker, Tetrahedron Lett. 43 (2002) 261.
- [29] B. Elias, L. Herman, C. Moucheron, A. Kirsch-De Mesmaeker, Inorg. Chem. 46 (2005) 4979.
- [30] L. Herman, B. Elias, F. Pierard, C. Moucheron, A. Kirsch-De Mesmaeker, J. Phys. Chem. A 111 (2007) 9756.
- [31] J. Bolger, A. Gourdon, E. Ishow, J. Launay, Inorg. Chem. 35 (1996) 2937.
- [32] S. Rau, B. Schäfer, A. Grüßing, S. Schebesta, K. Lamm, J. Vieth, H. Görls, D. Walthner, M. Rudolph, U.W. Grummt, E. Birkner, Inorg. Chim. Acta 357 (2004) 4496.
- [33] SADABS 2.06, Bruker AXS, Inc., Madison, WI, USA, 2002.
- [34] SHELXTL NT 6.12, Bruker AXS, Inc., Madison, WI, USA, 2002.
- [35] K. Nakamura, Bull. Chem. Soc. Jpn. 55 (1982) 2697.
- [36] A.L. Dobryakov, J. Ruthman, N.P. Ernsting, Phys. Rev. A 59 (1999) 2369.
- [37] B. Dietzek, T. Pascher, V. Sundström, A. Yartsev, Laser Phys. Lett. 4 (2007) 38.
- [38] A. Boisdenghien, C. Moucheron, A. Kirsch-De Mesmaeker, Inorg. Chem. 44 (2005) 7678.
- [39] M. Karnahl, S. Kriech, H. Görls, S. Tschierlei, M. Schmitt, J. Popp, D. Chartrand, G.S. Hanan, R. Groarke, J.G. Vos, S. Rau, Eur. J. Inorg. Chem. (2009) 4962.
- [40] B. Schäfer, H. Görls, M. Presselt, M. Schmitt, J. Popp, W. Henry, J.G. Vos, S. Rau, Dalton Trans. (2006) 2225.
- [41] D. Gut, I. Goldberg, M. Kol, Inorg. Chem. 42 (2003) 3483.
- [42] S.D. Bergman, M. Kol, Inorg. Chem. 44 (2005) 1647.
- [43] A.C. Bhasikuttan, M. Suzuki, S. Nakashima, T. Okada, J. Am. Chem. Soc. 124 (2002) 8398.
- [44] C. Chiorboli, M. Roger, F. Scandola, J. Am. Chem. Soc. 125 (2003) 483.
- [45] Y. Sun, C. Torro, Inorg. Chem. 49 (2010) 5025.
- [46] C. Chiorboli, C.A. Bignozzi, F. Scandola, E. Ishow, A. Gourdon, J.P. Launay, J. Inorg. Chem. 38 (1999) 2402.
- [47] N. Komatsuzaki, R. Katoh, Y. Himeda, H. Sugihara, H. Arakawa, K. Kasuga, Dalton Trans (2000) 3053.
- [48] S. Tschierlei, B. Dietzek, M. Karnahl, S. Rau, F.M. MacDonnell, M. Schmitt, J. Popp, J. Raman Spectrosc. 39 (2008) 557.
- [49] M. Brennamann, J. Alstrum-Acevedo, C. Fleming, P. Jang, T. Meyer, J. Papanikolas, J. Am. Chem. Soc. 124 (2002) 15094.
- [50] J. Olofsson, L. Wilhelmsson, P. Lincoln, J. Am. Chem. Soc. 126 (2004) 15458.
- [51] C. Kuhnt, M. Karnahl, S. Tschierlei, K. Griebenow, M. Schmitt, B. Schäfer, S. Kriech, H. Görls, S. Rau, B. Dietzek, J. Popp, Phys. Chem. Chem. Phys. 12 (2010) 1357.
- [52] C. Chiorboli, S. Fracasso, F. Scandola, S. Campagna, S. Serroni, R. Konduri, F.M. MacDonnell, Chem. Commun. (2003) 1658.

[CK5] Excited-state annihilation in a homodinuclear ruthenium complex

Der Nachdruck der folgenden Publikation erfolgt mit freundlicher Genehmigung der Royal Society of Chemistry.

Reproduced with permission from:

C. Kuhnt, M. Karnahl, M. Schmitt, S. Rau, B. Dietzek, J. Popp, EXCITED-STATE ANNIHILATION IN A HOMODINUCLEAR RUTHENIUM COMPLEX, *Chem. Comm.*, **2011**, 47, 3820-3821

Copyright 2011 The Royal Society of Chemistry

Cite this: *Chem. Commun.*, 2011, **47**, 3820–3821

www.rsc.org/chemcomm

COMMUNICATION

Excited-state annihilation in a homodinuclear ruthenium complex†

Christian Kuhnt,^a Michael Karnahl,^b Michael Schmitt,^a Sven Rau,^c Benjamin Dietzek^{*ad} and Jürgen Popp^{ad}

Received 22nd October 2010, Accepted 28th January 2011

DOI: 10.1039/c0cc04555a

Ultrafast excited-state annihilation in a homodinuclear ruthenium complex is observed. This coordination compound constitutes a model system for approaches towards artificial photosynthetic systems. The observation of pump-intensity dependent triplet–triplet annihilation highlights the importance of considering various loss mechanisms in the design of artificial photosynthetic assemblies.

Ru–polypyridine complexes are promising building blocks for artificial photosystems, *i.e.* to convert solar energy into chemical energy, as their photophysical and photochemical properties are easily tunable by structural modifications.^{1–4} To increase the light harvesting efficiency of supramolecular photocatalysts, attempts have been made to connect more than one photoactive metal center (*i.e.* most conventionally a Ru^{II} center) to a catalytically active metal center *via* a bridging ligand with multiple coordination spheres.^{5,6} In general, such architecture poses the challenge not only to design the interaction of the photoactive with the catalytically active metal center but also to tailor the interactions between the individual photoactive metal centers. In order to shed light on the latter we investigate the excitation light intensity dependence of the photophysics of the homodinuclear Ru-complex [(tbbpy)₂Ru(tpphz)Ru(tbbpy)₂]⁴⁺ (tbbpy = 4,4'-di-*tert*-butyl-2,2'-bipyridin, tpphz = tetrapyrido[3,2-a:2'3'-c:3''-2''-h:2'''-3''']phenazine) (**Ru**) (see Fig. 1). The photophysics of the closely related system [(bpy)₂Ru(tpphz)Ru(bpy)₂]⁴⁺ have been interrogated in the low-excitation intensity regime.⁷ Both complexes are related to the heterodinuclear complex [(tbbpy)₂Ru(tpphz)PdCl₂]²⁺, which presents a supramolecular photocatalyst following the up to date implemented concept of connecting a single photoactive unit with one catalytically active center.^{8,9}

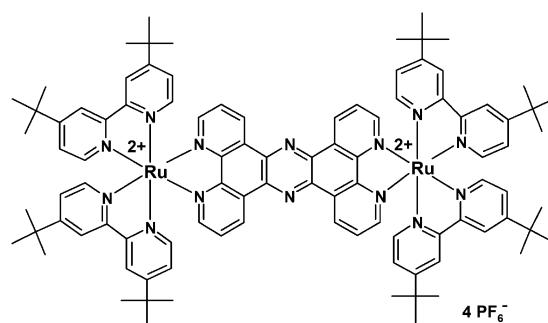


Fig. 1 Chemical structure of the investigated dinuclear complex **Ru**.

Such pump-intensity dependent processes, which are at the core of this investigation, are typically known for conducting polymers.^{10,11} In these systems pump-intensity dependent kinetics are generally assigned to the simultaneous excitation of two excitons in close proximity, *i.e.* a distance shorter than the product of exciton diffusion speed and observation time, and resultant exciton–exciton annihilation, which constitute an additional decay channel for photoexcited chromophores. The data presented here show to the best of our knowledge for the first time triplet–triplet annihilation in a homodinuclear transition metal complex. Therefore, the benchmark results discussed in the following present an important constraint that needs to be taken into account when designing artificial photosynthetic systems.

The absorption spectrum of **Ru** shows four main bands in the UV/Vis region, *i.e.* π - π^* -transitions of the tbbpy- and tpphz ligands at 290 and 370 nm, respectively, the d-d-transition of the Ru^{II} ion as shoulder at 320 nm and finally the broad and structureless MLCT band centered at 445 nm. In the transient absorption experiments the MLCT band is excited in its red flank at 510 nm, while the photoinduced dynamics are recorded using a supercontinuum white-light probe pulse covering the spectral range from 520 to 750 nm. The absorption cross section for **Ru** is $3.8 \times 10^{-17} \text{ cm}^2$ at the pump wavelength.

The differential absorption (ΔOD) data of **Ru** are characterized by contributions of ground-state bleach (GSB) below 530 and the excited-state absorption (ESA) above 530 nm with a maximum at 560 nm. Within the experimental accessible time delay of 1.8 ns no significant ESA band shifts are observed. While in the low-pump-intensity regime, *i.e.* $9.3 \times 10^{15} \text{ photons cm}^{-2}$ per excitation pulse, a build-up of the ESA is observed over the entire range of delay times accessible.

^a Institute for Physical Chemistry, Friedrich-Schiller-University Jena, Jena Center of Soft Matter and Abbe Center of Photonics, Helmhotzweg 4, 07743 Jena, Germany

^b Institute for Inorganic and Analytical Chemistry, Friedrich-Schiller-University Jena, August-Bebel-Straße 2, 07743 Jena, Germany

^c Department of Chemistry and Pharmacy, Friedrich-Alexander-University Erlangen-Nürnberg, Egerlandstraße 1, 91058 Erlangen, Germany

^d Institute of Photonic Technology Jena e.V., Albert-Einstein-Straße 9, 07745 Jena, Germany. E-mail: benjamin.dietzek@uni-jena.de

† Electronic supplementary information (ESI) available: Complete ΔOD data for both low and high-concentration limit, details on the fitting procedure, schematic presentation of states involved in the photophysics. See DOI: 10.1039/c0cc04555a

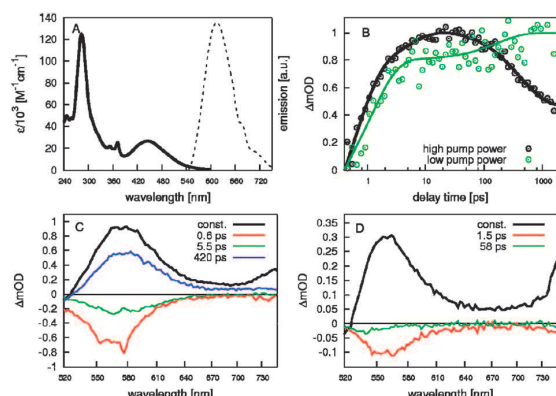


Fig. 2 Absorption and emission spectra of **Ru** (A) and transient kinetics recorded in the maximum of the ESA band (B); for comparison the data were normalized to the maximum amplitude. Decay-associated spectra for high (C) and low (D) excitation intensities.

This changes when the pump intensity is increased to 4.6×10^{16} photons cm^{-2} per excitation pulse: In this situation the ESA signal increases over the first roughly 30 ps and subsequently decreases to about half of the maximal signal within the time range accessible. For quantitative analysis the data were fitted globally using three or four kinetic components associated with characteristic decay times τ_i . Fig. 2 summarizes the data and the result of the global-fit data analysis.[†]

As indicated above and illustrated in Fig. 2 an increase in pump intensity qualitatively alters the excited state dynamics as reflected in the temporal dependence of the ESA band. Irrespective of the pump intensity a ~ 1 ps component is observed, which corresponds to the formation of the tpphz-centered ³MLCT state following excitation of the ¹MLCT.^{7,8} In the low-intensity regime this is followed by the population of the phenazine-centered state with a time-constant of 58 ps in **Ru**. Subsequently no further changes are observed in the experimentally accessible time window. This situation is qualitatively altered in the high-intensity regime. Here **Ru** shows different photophysics after the formation of the tpphz-centered ³MLCT, which is followed by two kinetic components. These components are characterized by time constants of 5.5 and 420 ps. The first one is assigned to an intra-ligand charge-transfer (ILCT) transferring the charge from a phenanthroline-centered to a phenazine-centered excited state.⁸ The ILCT appears accelerated upon increase of the pump intensity and – at the same time – a third component ($\tau_3 = 420$ ps) becomes apparent as a decay of the ESA signal.

This pump-intensity dependent turnover between two qualitatively different photophysical situations, *i.e.* an exclusive ESA increase at low pump intensities and an ESA decay on a 100 ps timescale at high pump intensities, points to an excitation-intensity dependent deactivation mechanism of excited states. At high pump intensities both photoactive centers of the same dinuclear complex might be excited, which gives rise to intramolecular interactions between excited states centered on either of the Ru^{II} units. To exclude intermolecular interactions between triplet states localized in different complexes, which might form dimers at high concentrations, dilution measurements were also performed. In contrast to the

apparent dependence of the photoinduced dynamics on the pump intensity, a variation of the solute concentration by an order of magnitude did not influence the dynamics observed.[†]

The electrochemistry of **Ru** indicates that the phenazine part of the bridging ligand is only capable of being singly reduced. However, simultaneous photoexcitation of the phenanthroline-centered MLCT states (yielding two ³MLCT(phen) states after inter system crossing) of the individual ruthenium centers in **Ru** is possible. This is followed by ILCT from one of the Ru(1)–³MLCT(phen) and a Ru(2)–³MLCT(phz) states, the latter referring to a state centered on the phenazine part of the tpphz ligand. The interaction of these two ³MLCT states will lead to the deactivation of one of the states and simultaneous formation of a singly excited unit on a time scale of 420 ps. This phenomenon is known from the photophysics of conducting polymers and generally referred to as exciton–exciton-annihilation.^{10,11} Furthermore, such process has been observed in assemblies of chromophores in polymeric units and in dendrimers of chromophores, where it is termed triplet–triplet or singlet–singlet annihilation respectively.^{12,13} Upon excited-state annihilation the system is most likely left in a ³MLCT(phz) state while the overall number of excited states is reduced. Hence, the excited-state absorption is reduced.

The results presented show for the first time the presence of pump-intensity dependent excited-state relaxation process in a homodinuclear complex, in which two photoactive transition metal centers are bridged by an electron relaying ligand. Combining various photoactive centers with a catalytically active center is one promising approach in designing molecular artificial photosynthetic devices – a situation in which the interaction of different photoactive centers needs to be taken into account. Therefore, the results presented here constitute an important benchmark in describing a potentially devastating deactivation channel for excited states in multi-chromophoric artificial photosynthetic systems.

Notes and references

- C. Chiorboli, S. Fracasso, M. Ravaglia, F. Scandola, S. Campagna, K. L. Wouters, R. Konduri and F. M. MacDonnell, *Inorg. Chem.*, 2005, **44**, 8368.
- A. Inagaki and M. Akita, *Coord. Chem. Rev.*, 2010, **254**, 1220.
- S. Rau, D. Walther and J. G. Vos, *Dalton Trans.*, 2007, 915.
- C. Kuhnt, M. Karnahl, S. Tschierlei, K. Griebenow, M. Schmitt, B. Schäfer, S. Kriek, H. Görls, S. Rau, B. Dietzek and J. Popp, *Phys. Chem. Chem. Phys.*, 2010, **12**, 1357.
- M. Elvington, J. Brown, S. M. Arachchige and K. J. Brewer, *J. Am. Chem. Soc.*, 2007, **129**, 10644.
- T. D. Pilz, N. Rockstroh and S. Rau, *J. Coord. Chem.*, 2010, **63**, 2727.
- C. Chiorboli, M. A. J. Rodgers and F. Scandola, *J. Am. Chem. Soc.*, 2003, **125**, 483.
- S. Tschierlei, M. Presselt, C. Kuhnt, A. Yartsev, T. Pascher, V. Sundström, M. Karnahl, M. Schwalbe, B. Schäfer, S. Rau, M. Schmitt, B. Dietzek and J. Popp, *Chem.–Eur. J.*, 2009, **15**, 7678.
- S. Tschierlei, M. Karnahl, M. Presselt, B. Dietzek, J. Guthmüller, L. Gonzalez, M. Schmitt, S. Rau and J. Popp, *Angew. Chem., Int. Ed.*, 2010, **49**, 3981.
- J. M. Hodgkiss, A. R. Campbell, R. A. Marsh, A. Rao, S. Albert-Seifried and R. H. Friend, *Phys. Rev. Lett.*, 2010, **104**, 177701.
- J. G. Scheblykin, A. Yartsev, T. Pullerits, V. Gulbinas and V. Sundström, *J. Phys. Chem. B*, 2007, **111**, 6303.
- G. B. Shaw and J. M. Papanikolas, *J. Phys. Chem. B*, 2002, **106**, 6156.
- J. Larsen, B. Bruggemann, T. Polivka, V. Sundström, E. Akesson, J. Sly and M. J. Crossley, *J. Phys. Chem. A*, 2005, **109**, 10654.

[CK6] The impact of bromine substitution on the photophysical properties of a homodinuclear Ru–tpphz–Ru complex

Der Nachdruck der folgenden Publikation erfolgt mit freundlicher Genehmigung von Elsevier B.V..

Reproduced with permission from:

C. Kuhnt, M. Karnahl, S. Rau, M. Schmitt, B. Dietzek, J. Popp, THE IMPACT OF BROMINE SUBSTITUTION ON THE PHOTOPHYSICAL PROPERTIES OF A HOMODINUCLEAR RU–TPPHZ–RU COMPLEX, *Chem. Phys. Lett.* **2011**, *516*, 45-50

Copyright 2011 Elsevier B.V.



Contents lists available at SciVerse ScienceDirect

Chemical Physics Letters

journal homepage: www.elsevier.com/locate/cplett

The impact of bromine substitution on the photophysical properties of a homodinuclear Ru–tpphz–Ru complex

Christian Kuhnt^a, Michael Karnahl^b, Sven Rau^c, Michael Schmitt^a, Benjamin Dietzek^{a,d,*}, Jürgen Popp^{a,d}

^aInstitute of Physical Chemistry and Abbe Center of Photonics, Friedrich-Schiller-University Jena, Helmholtzweg 4, 07743 Jena, Germany

^bDepartment of Photochemistry and Molecular Science, The Ångström Laboratory, Uppsala University, Box 523, 75120 Uppsala, Sweden

^cInstitute of Inorganic Chemistry I, University Ulm, Albert-Einstein-Allee 11, 89091 Ulm, Germany

^dInstitute of Photonic Technology (IPHT) Jena e.V., Albert-Einstein-Straße 9, 07745 Jena, Germany

ARTICLE INFO

Article history:

Received 23 June 2011

In final form 22 September 2011

Available online 29 September 2011

ABSTRACT

Ruthenium–polypyridine complexes play an important role as photosensitizers in supramolecular photocatalysis. Using multiple Ru-centers within a single supramolecular catalyst might be a promising path for improving its efficiency. The connection of several chromophores may, however, lead to direct interaction amongst individual photoactive centers, which is at the core of the work at hand. The work focuses on the photophysics of [(tbbpy)₂Ru(3,16-Br₂-tpphz)Ru(tbbpy)₂](PF₆)₄ (**1**, tpphz = tetrapyrrodo[3,2-a:2',3'-c:3'',2''-h:2''',3'''-j]phenazine, tbbpy = 4,4'-di-*tert*-butyl-2,2'-bipyridine) and aims at detailing the impact of the bromine substituents on bridging ligand photoinduced intramolecular charge-transfer dynamics. It is shown that the introduction of the bromine reduces the driving force for intra-ligand charge-transfer steps and impacts exciton–exciton annihilation at high pump intensities.

© 2011 Elsevier B.V. All rights reserved.

1. Introduction

Ruthenium–polypyridine complexes possess versatile photophysical properties for which they play an important role for the development of new photosensitizers and molecular sensors [1,2]. These complexes find application as optical sensors, e.g. for DNA sensing or cell imaging [3–5], as dyes in dye-sensitized solar cells [6,7] and as light-harvesting units in supramolecular photocatalysts [8–10]. A central advantage of such systems is the tunability of their photophysical properties either by variation of environmental parameters, such as solvent, temperature and pH [11,12] or by alterations of their chemical structure, e.g. by introducing substituents [13–15].

The latter strategy, i.e. the alteration of photophysical properties by structural modifications, is a common approach in designing supramolecular photocatalysts. Such devices consist of essentially three functional and structural units, which are (i) a photoactive center, e.g. a Ru–polypyridine center, (ii) a catalytically active center, e.g. a coordinated metal ion such as Pd, Pt or Rh and (iii) a molecular bridge that connects both centers and enables intermolecular electron transfer [16,17]. Following the design strategies of natural photosynthetic systems one effort is to combine multiple chromophores with the photocatalytically active

unit [18–20]. This strategy increases the number of harvested photons because the absorption-cross-section of the catalyst rises nearly linearly with the number of Ru-centers [21,22]. Various ligand structures have been exploited to connect multiple Ru-units, to build for instance dendrimeric structures. Among these structures the tpphz-bridging ligand (tpphz = tetrapyrrodo[3,2-a:2',3'-c:3'',2''-h:2''',3'''-j]phenazine) has proven to be well suited [21,23]. Aside from increasing the absorption cross-section of the catalysts another advantage of introducing multiple chromophoric units is the tunability of the absorption spectrum of the catalyst. By altering the chemical properties of the individual chromophores, for instance by introduction of substituents, the energetic positions of the metal-to-ligand charge transfer (MLCT) states involved in visible light absorption of Ru-units are shifted individually and hence the absorption spectrum of the photocatalyst can be broadened to cover a larger part of the solar spectrum.

However, introducing multiple chromophoric units to a photocatalyst may also lead to unwanted interactions among the individual photoactive centers, i.e. annihilation of excited states. Such processes are well known for systems with high numbers of chromophoric units like conjugated polymers and dendrimers where they play an important role for the performance of the supramolecular systems [24,25]. Building on previous studies on the excited-state annihilation processes in [(tbbpy)₂Ru(tpphz)-Ru(tbbpy)₂](PF₆)₄ (**2**) [26], this study focuses on the substitution effect by introducing bromine to the tpphz bridging ligand, e.g. the effect of non-degenerate excited-states for the excited-state annihilation process in similar model compounds. To this end the

* Corresponding author at: Institute of Physical Chemistry and Abbe Center of Photonics, Friedrich-Schiller-University Jena, Helmholtzweg 4, 07743 Jena, Germany. Fax: +49 3641206399.

E-mail address: benjamin.dietzek@uni-jena.de (B. Dietzek).

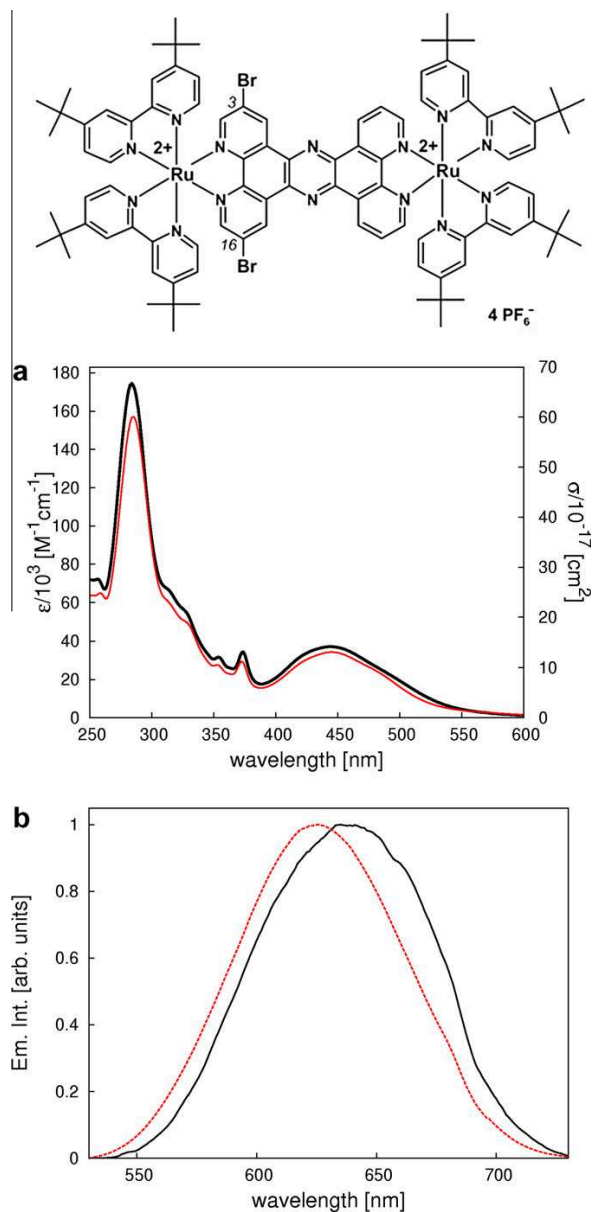


Figure 1. The molecular structure of **1**; (a) the absorption spectra in ACN (black) and DCM (red) and (b) the emission spectra of **1** in ACN (black) and DCM (red) are depicted. The excitation wavelength for the transient absorption measurements was $\lambda = 505$ nm. (For interpretation of the references in color in this figure legend, the reader is referred to the web version of this article.)

complex [(tbbpy)₂Ru(3,16-Br₂-tpphz)Ru(tbbpy)₂](PF₆)₄ (**1**, tbbpy = 4,4'-di-*tert*-butyl-2,2'-bipyridine; see Figure 1a) is investigated. The substitution of the tpphz bridging ligand influences the photophysical properties of the chromophoric unit as known from mononuclear Ru(dppz)-(dppz = dipyrido[3,2-a:2',3'-c]phenazine) and Ru(tpphz)-complexes [13,27–29]. The electron-withdrawing effect of the bromine-substituents leads to a stabilization of the MLCT states which are located on the brominated part of the bridging ligand while leaving the overall geometry of the complexes unchanged [14,30].

This contribution is organized as follows: After some experimental remarks, the first part presents the spectroscopic characterization of [(tbbpy)₂Ru(3,16-Br₂-tpphz)Ru(tbbpy)₂](PF₆)₄ (**1**) by steady-state absorption and emission spectroscopy. This is followed by ultrafast transient-absorption spectroscopic investigations of the charge-transfer kinetics in dependence on the excitation power. Finally, a summarizing discussion concludes.

2. Experimental

2.1. Synthesis

The preparation and structural characterization of complex **1** is presented in the ESI. The synthesis procedure was performed according to literature methods and the resulting product was analyzed by means of elemental analysis, mass spectrometry (ESI-MS), NMR spectroscopy (¹H-NMR, ¹³C-NMR and H,H-COSY) and IR spectroscopy (Figures S1 and S2) [14,26,29].

2.2. Photophysics

For the photophysical measurements **1** was dissolved in aerated acetonitrile (ACN) or aerated dichloromethane (DCM). Both solvents were of spectroscopic grade (purity >99.99%) and used without further purification. If not stated otherwise, the experiments were performed at room-temperature (stabilized by air-conditioning to 22 °C). Prior and subsequent to all experiments UV/Vis absorption spectra were taken to ensure photophysical stability of the Ru-complexes.

Steady-state UV/Vis absorption spectra were recorded with a JASCO V-670 photospectrometer. The steady-state emission spectra were recorded with a JASCO FP-6200 spectrofluorimeter using diluted solutions (optical density <0.05). Absolute quantum yield measurements were performed in reference to solutions of [Ru(bpy)₃]Cl₂ in non-degassed water ($\Phi = 0.028$) [31].

The setup for the time-resolved transient absorption experiments has been described previously [32]. Briefly, fs pulses at 505 nm were used to excite the sample and the subsequent photo-initiated processes were recorded by transient absorption using a white-light supercontinuum as probe. The mutual polarization between pump and probe was set to magic angle. Adjusting the pump energy was realized with a Berek compensator in concert with a linear polarizer.

The entire differential absorption (ΔA) data set, recorded as a function of the delay time t and the probe-wavelength λ_{pr} , is treated by a global fit routine for data analysis [33]. The fit routine uses a sum of exponentials as fit function:

$$\Delta(t, \lambda_{pr}) = \Phi(\lambda_{pr}) + \sum_{i=1}^n A_i(\lambda_{pr})e^{-t/\tau_i}$$

The constant offset $\Phi(\lambda_{pr})$ accounts for long-lived pump-induced absorption changes, which decay on a time-scale longer than the experimental accessible time window of 1.7 ns. The wavelength-dependent pre-exponential factors $A_i(\lambda_{pr})$ contain spectral characteristics for each individual kinetic component associated to τ_i and correspond to the so called *decay-associated spectra* (DAS). Each data set was numerically chirp corrected before fitting. The pulse-overlap region was ignored during the fitting process to avoid contributions from coherent artefacts [34,35]. Thus, processes occurring in a window of up to approximately 500 fs are not resolved.

3. Results and discussion

The spectroscopic properties of **1** were obtained with steady-state UV/Vis absorption and emission spectroscopy as well as

ultrafast transient absorption spectroscopy. The analysis of the data is carried out and discussed in comparison to the unsubstituted complex **2** [26].

3.1. Steady-state spectroscopy

The absorption spectra of **1** in ACN and DCM (see Figure 1a) exhibit the common features for Ru–tpphz complexes [21–23]. Four absorption bands are identified in either solvent. The three UV-absorption bands at 284 in ACN (284 in DCM), 354 (352) and 374 (372) nm are accompanied by a broad structureless band in the visible region centered at 444 (444) nm. The absorption band at 284 nm is assigned to a $\pi\pi^*$ -transition of the terminal tbbpy-ligands while the $\pi\pi^*$ -transitions of the 3,16-Br₂tpphz bridge cause the two absorption bands at 354 and 374 nm. Finally, the band with a maximum at 444 nm belongs to mixed MLCT transitions from the Ru-ions to both the tbbpy-ligands and the 3,16-Br₂tpphz ligand [28,36]. In comparison to the unbrominated analogon **2** a red-shift of both tpphz-associated $\pi\pi^*$ -transitions is apparent. These spectral shifts – from 351 to 354 nm and 371 to 374 nm in ACN – are caused by the bromine substituents leading to a decrease in energy of the respective π^* -orbitals.

3.1.1. Effect of solvent polarity

Upon excitation at 445 nm **1** shows emission both in ACN and DCM (Figure 1b). The maximum of the emission in ACN (637 nm) is shifted by 276 cm⁻¹ as compared to DCM (626 nm). Furthermore, the emission quantum yield increases from 0.76×10^{-3} (ACN) to 7.3×10^{-3} (DCM) (see Table 1). The reason for these solvent induced shifts lies in the nature of the excited states, which are involved in the charge-migration process after the excitation of Ru–polypyridine complexes. This will be discussed in the following: Excitation of the ¹MLCT is followed by rapid intersystem crossing to a ³MLCT-state.[37–39] Initially the ³MLCT-state is supposed to be delocalized, i.e. the excess charge density is spread over all ligands.[13,40] Subsequently the delocalized ³MLCT relaxes into a ³MLCT–tpphz–phen state, i.e. the excess electron density is dominantly localized on the phenanthroline moiety of the tpphz ligand. From there a non-radiative transition to an excited state located on the phenazine moiety of the tpphz ligand (³MLCT–tpphz–phz) takes place. These two tpphz centered states differ in their luminescence properties: while the ³MLCT–tpphz–phen shows luminescence, the ³MLCT–tpphz–phz is dark. Hence, the emission properties of the complex are determined by the interplay between the ³MLCT–tpphz–phz and ³MLCT–tpphz–phen states. In **1** these may be localized either on the bromine-substituted or the unsubstituted phenanthroline part of the tpphz unit. Generally, the interplay between these two states can be tuned by bulk properties of the solvent, like polarity or viscosity, the temperature or specific interactions with the chemical environment.[12,13,15,41] The ³MLCT–tpphz–phz is stabilized in polar solvents because of its larger dipole moment as compared to ³MLCT–tpphz–phen. Consequently the luminescence quantum yield of **1** is higher in DCM than in ACN.

3.1.2. Effect of bromine substitution

The introduction of bromine substituents stabilizes the ³MLCT–tpphz–phen state via its withdrawing inductive (–I) effect. This

leads to a red-shift of the emission of **1** as compared to the reference complex **2**. In ACN the emission maximum is shifted from 616 (**2**) to 637 nm (**1**) ($\Delta E = 535 \text{ cm}^{-1}$, emission quantum yield of both **1** and **2** << 1%) and in DCM from 609 (**2**) to 626 nm (**1**) ($\Delta E = 446 \text{ cm}^{-1}$, emission quantum yield of both **1** and **2** $\approx 1\%$). This finding is in accordance with studies on the related systems Ru-(3,16-Br₂tpphz)-Pd and Ru-(2,7-Br₂dppz) for which it was additionally shown that dissolution in less polar solvents increases the emission quantum yield [13,29]. For **1**, however, this behavior is not observed. Instead, the emission quantum yield of **1** is slightly lower than that of **2** (see Table 1). This finding is attributed to the asymmetric substitution pattern in **1**, which causes the presence of two distinct ³MLCT–tpphz–phen states, which are denoted ³MLCT–tpphz–phen_H for the unsubstituted moiety and ³MLCT–tpphz–phen_{Br} for the substituted part (see also Scheme 1). ³MLCT–tpphz–phen_{Br} is solely responsible for the emission of **1**, explaining the red-shift of the emission and the absence of a secondary emission shoulder spectrally similar to the emission of **2**: It is known from Ru-(3,16-Br₂tpphz)-Pd that the bromine substituents influence excited states in their vicinity [29]. As it is depicted in Scheme 1 the ³MLCT–tpphz–phen_{Br} and ³MLCT–tpphz–phz states are both stabilized by the bromine substituents. Hence, after excitation of the ³MLCT–tpphz–phen_H in **1**, charge transfer to the ³MLCT–tpphz–phz state quenches luminescence of the tpphz–phen_H centered charge-transfer state. On the other hand, bromine substitution causes a reduced ³MLCT–tpphz–phen_{Br}–³MLCT–tpphz–phz energy difference due to the stabilization of the ³MLCT–tpphz–phen_{Br} state. Consequently, a thermal equilibrium between the ³MLCT–tpphz–phz and the ³MLCT–tpphz–phen_{Br} state can be established along the lines described by Brennamann et al. [12]. Hence, irrespective of exciting one particular of the two Ru-centers in **2** only ³MLCT–tpphz–phen_{Br}-emission is observed.

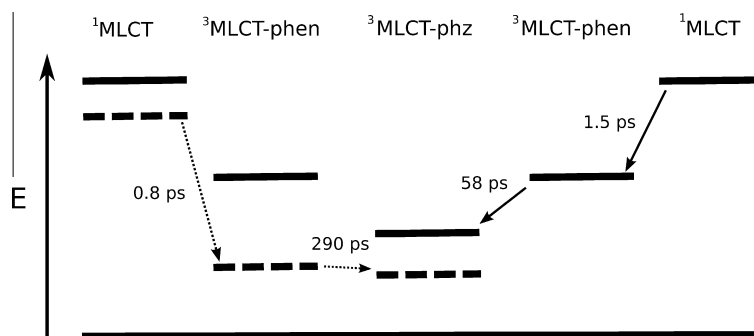
3.2. Transient absorption spectroscopy

Transient absorption spectra of **1** were taken in the temporal window from 500 fs to 1.7 ns after excitation. Excitation pulses were centered at 505 nm, i.e. in resonance with the red flank of the ¹MLCT absorption band (Figure 1). The spectral window of the probe light was chosen between 525 and 750 nm. In this spectral region two distinct transient absorption bands are visible (see Figure 2). The two excited-state absorption (ESA) bands at 590 and 730 nm are accompanied by the onset of ground-state-bleach (below 540 nm) for the entire range of delay times experimentally accessible. However, no significant spectral shifts are apparent. Therefore, the temporal evolution of the signal can be visualized by spectrally integrating the $\Delta A(t, \lambda_{pr})$ data in the range between 580 and 600 nm. The resultant normalized kinetics is depicted in Figure 3. Upon excitation with 100 nJ/pulse a bimodal increase of the ESA signal is observed (green curve, Figure 3) characteristic for this type of Ru complexes [13,29,40,41]. The corresponding characteristic time constants can be fitted to $\tau_1 = 0.8 \text{ ps}$ and $\tau_2 = 290 \text{ ps}$. The spectral characteristics, i.e. the decay-associated spectra (DAS), associated with τ_1 and τ_2 are displayed in Figure 4a.

The first component τ_1 is assigned to inter-system crossing, charge localization on the tpphz-ligand and vibrational cooling within the ³MLCT–tpphz–phen state.[18,42–44] Thus within the

Table 1
Emission quantum-yields ($\times 10^{-3}$) of **1** and **2** in acetonitrile (ACN) and dichloromethane (DCM) solution under aerated conditions after excitation of the MLCT band at 445 nm.

Solvent	λ_{max} (UV/vis absorption) [nm]		λ_{max} (emission) [nm]		Φ ($\times 10^{-3}$)	
	1	2	1	2	1	2
ACN	284; 354; 374; 444	283; 351; 371; 445	637	616	0.76	1.62
DCM	284; 352; 372; 444	285; 352; 371; 449	626	605	7.26	8.08



Scheme 1. Energy diagram of the excited states involved in the charge-transfer processes. The excited states of the symmetrical complex **2** (unsymmetrical complex **1**) are shown as solid (dashed) lines. The influence of the bromine substituents, i.e. stabilizing one of the $^3\text{MLCT-tpphz-phenphen}_{\text{Br}}$ and the $^3\text{MLCT-tpphz-phz}$ states, are illustrated (phen = phenanthroline moiety, phz = phenazine moiety). Notably, the effect of bromine substitution impacts only one of the two Ru-polypyridine centers in the complex (here shown in the left of the diagram) while leaving the energetic of the MLCT-states of the unsubstituted center unaltered. The characteristic time constants describe the intramolecular charge transfer processes at low pump intensities.

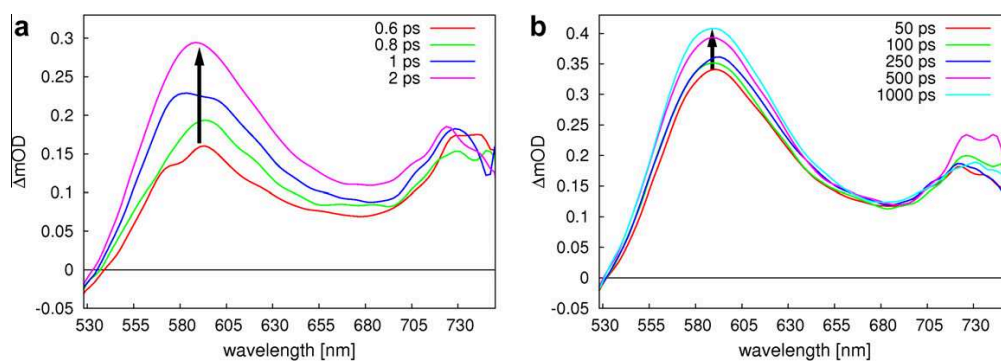


Figure 2. Transient absorption spectra of **1**, for short (a) and long delay-times (b).

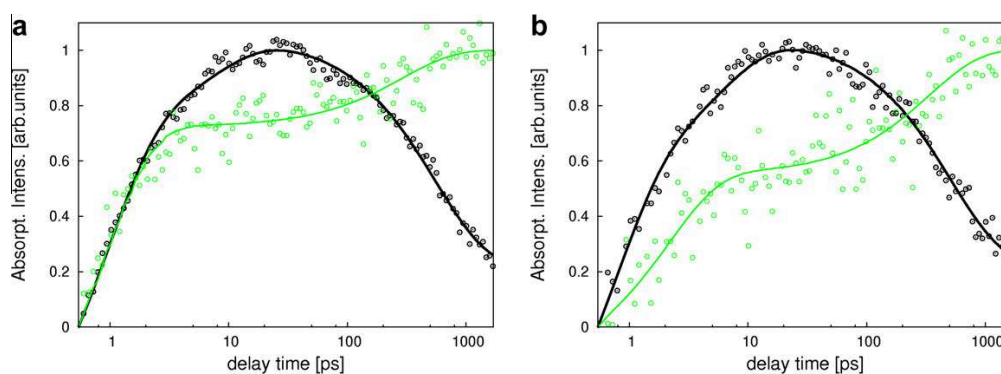


Figure 3. Transient kinetics of the maximum in the transient absorption bands of **1** for low (green) and high (black) pump-intensity and for a high (a) and low (b) concentration.

first picoseconds after excitation of the $^1\text{MLCT}$ the system relaxes to a thermalized $^3\text{MLCT-tpphz-phen}$ state followed by intra-ligand charge-transfer to the $^3\text{MLCT-tpphz-phz}$ state characterized by τ_2 . The assignment of the τ_2 -process is based on the DAS of related Ru-tpphz complexes and the absorption spectrum of the reduced phenazine moiety [29,40,41,45].

3.2.1. Effect of pump-intensity

Figure 3a includes a second transient kinetic (black curve) reflecting the photoinduced dynamics in **1** for different excitation

conditions with otherwise unchanged parameters. The pump-photon flux was increased from 9.3×10^{15} photons cm^{-2} per excitation pulse (low pump intensity) to 4.6×10^{16} photons cm^{-2} per excitation pulse (high pump intensity). The spectral changes induced by the increased pump-intensity are minor and summarized in the ESI. Like for the low pump intensity two ESA bands, centered at 595 and 735 nm, as well as the onset of the ground-state bleach below 535 nm are present. However, significant impact of the pump intensity on the transient kinetics is observed (see Figure 3). For increased pump intensity two rise components ($\tau_1 = 0.9$ ps and

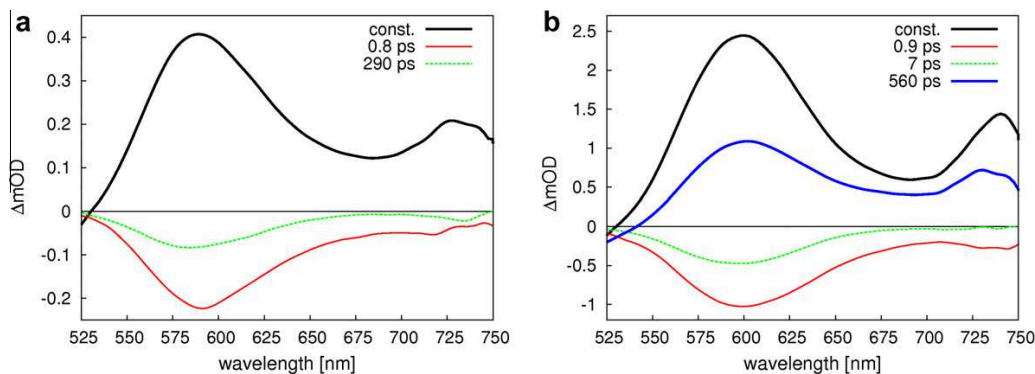


Figure 4. Decay-associated spectra (DAS) of **1** for low (a) and high (b) pump intensity.

$\tau_2 = 7$ ps) contribute to the signal. The bimodal signal rise is followed by an ESA decay. The processes associated with τ_1 are assigned to inter-system crossing, charge localization on the tpphz-ligand and vibrational cooling within the $^3\text{MLCT-tpphz-phen}$ state,[18,42–44] while τ_2 corresponds to the intra-ligand charge transfer populating the $^3\text{MLCT-tpphz-phz}$ state. This assignment of τ_2 to an ILCT, which is significantly accelerated upon increasing the pump intensity, is based on the spectral shape of the respective DAS in comparison to studies on related complexes.[13,29,30,40] The acceleration of the ILCT upon increased pump intensity has been previously observed for complex **2** but its underlying molecular mechanism remains unclear at the moment. The ILCT is followed by an ESA decay with $\tau_3 = 590$ ps.

The dynamic process associated with τ_3 in the high pump-intensity regime reduces the number of excited states and hence indicates a deactivation mechanism induced by the interaction of excited states. These excited state interactions can be either intra- or intermolecular in nature. For several related Ru–polypyridines it is known that π -stacking dimers are formed at high concentrations [13,14,46,47]. Therefore, the dependence of the decay at high pump intensities on the complex concentration was studied. To do so the solutions were diluted up to one order of magnitude. The results (see Figure 3b) for the kinetics and ESI for the transient spectra) show that the decay of the ESA does not depend on the complex concentration within the concentration range probed. Hence, the deactivation mechanism responsible for the characteristic high pump-intensity features is supposed to be intramolecular in nature, i.e. it is observed when the probability to excite both photoactive centers in a single complex **1** is significant. Thus, it is assumed that the interaction of the $^3\text{MLCT-tpphz-phz}$ state with one of the $^3\text{MLCT-tpphz-phen}$ states is the deactivation mechanism manifested in the data. As a result of this interaction, one excited state is deactivated and finally the $^3\text{MLCT-tpphz-phz}$ state is formed.

3.2.2. Effect of bromine substitution

An analogous pump-intensity dependence was found for the unsubstituted complex **2**. [26] However, the introduction of bromine substituents induces changes in the excited-state properties, which shall be discussed in the following. Aside from the slower excited-state annihilation upon introduction of bromine substituents ($\tau_3 = 420$ ps in **2** and $\tau_3 = 590$ ps in **1**) the most notable difference in the transient spectra is the appearance of the ESA band centered at 730 nm. Due to the temporal dependence of the signal in this spectral region, i.e. it is generally following the temporal evolution of the ESA in the shorter-wavelength region, the origin of this band remains unclear, but most likely it indicates the pres-

ence of discrete triplet states lying energetically above the $^3\text{MLCT-tpphz-phen}$ and $^3\text{MLCT-tpphz-phz}$ states [32]. Furthermore, the aforementioned energetic stabilization of the $^3\text{MLCT-tpphz-phen}_{\text{Br}}$ state as compared to the $^3\text{MLCT-tpphz-phen}_{\text{H}}$ state can also be observed in the transient spectra. After excitation with low pump intensity the ESA band of **1** is broadened, compared to **2**, indicating a mixed excitation of $^3\text{MLCT-tpphz-phen}_{\text{Br}}$ and $^3\text{MLCT-tpphz-phen}_{\text{H}}$. Furthermore the maximum of the ESA of **1** is bathochromatically shifted compared to **2** from 560 to 585 nm ($\Delta E = 908 \text{ cm}^{-1}$) which means, that the energy of the $^3\text{MLCT-tpphz-phen}_{\text{Br}}$ state is decreased as compared to the energy of the $^3\text{MLCT-tpphz-phen}_{\text{H}}$ state. Hence, the driving force for the transition, i.e. localization of the $^3\text{MLCT}$ on the tpphz-phen_{Br} moiety, is increased and the first transition step is slightly accelerated in the brominated complex from 1.5 for **2** to 0.8 ps for **1**. This time constant now represents a mixture of processes namely the localization of excitation on either of the non-symmetrical Ru-centers. As the energy between the $^3\text{MLCT-tpphz-phen}_{\text{Br}}$ and $^3\text{MLCT-tpphz-phz}$ state is reduced, the driving force of the transition between these two states decreases resulting in a slower ILCT (58 ps for **2** and 290 ps for **1**). The deceleration of the ILCT can be even seen after excitation with high pump intensity, a situation in which ILCT for **2** occurs with a time constant of 5.5 ps as compared to 7 ps for **1** [26]. The deceleration of the annihilation process in the brominated complex fits quite well with the finding that bromine substituents generally slow down charge-transfer processes in related Ru–polypyridine complexes.[13,29] This general effect of bromine substituents at the phenanthroline moiety of Ru–polypyridines can be also observed for the annihilation.

The transient absorption experiments on **1** revealed charge-transfer dynamics upon excitation with low pump energy, while at high pump energies excited-state annihilation is observed. The introduction of bromine to the phenanthroline moiety of the tpphz bridging ligand lowers the energy of the associated charge-transfer-state ($^3\text{MLCT-tpphz-phen}$), leading to acceleration of the initial charge-localization and a deceleration of the following charge transfer steps.

4. Conclusion

The photophysics of the new homodinuclear complex $[(\text{tbbpy})_2\text{Ru}(3,16\text{-Br}_2\text{-tpphz})\text{Ru}(\text{tbbpy})_2](\text{PF}_6)_4$ (**1**) were discussed in detail and compared to those of $[(\text{tbbpy})_2\text{Ru}(\text{tpphz})\text{Ru}(\text{tbbpy})_2](\text{PF}_6)_4$ (**2**). This system is especially interesting as it combines two non-degenerate photoactive Ru-centers. The bromine substituents selectively introduced to one of the photoactive centers lead to a bathochromatic shift of the emission and to a reduced

emission quantum yield. These results indicate that after excitation of the $^3\text{MLCT-tpphz-phen}$ in **1** $^3\text{MLCT-tpphz-phen}_\text{H} \rightarrow \text{MLCT-tpphz-phz}$ charge transfer takes place irreversibly depopulating the electronic state associated with the chromophoric unit and, hence, quenching $^3\text{MLCT-tpphz-phen}_\text{H}$ -associated emission. This situation is different when the $^3\text{MLCT-tpphz-phen}_\text{Br}$ state is directly excited. This state is closer in energy to the $^3\text{MLCT-tpphz-phz}$ state and consequently an excited-state equilibrium between the $^3\text{MLCT-tpphz-phen}_\text{Br}$ and the $^3\text{MLCT-tpphz-phz}$ states is formed, which serves as a reservoir for excited-states that can decay radiatively back to the ground state. Furthermore, it was shown that the ultrafast charge-transfer kinetics in **1** are decelerated as compared to the complex $[(\text{tbbpy})_2\text{Ru}(\text{tpphz})\text{Ru}(\text{tbbpy})_2](\text{PF}_6)_4$ (**2**) upon specific introduction of the bromine substituents. The latter results highlight the fact that the bromine substituents do not only affect the energetics of the charge-transfer state localized on the phenanthroline but also on the adjacent phenazine moiety. An increase of the pump-intensity leads to a fundamental change in the photoinduced kinetics of **1**. This suggests an intramolecular excited-state annihilation mechanism upon excitation of the MLCT states centered on both Ru-chromophores. Such excited-state annihilation is well known in dendrimers or conjugated polymers and inhere it is reported – to the best of our knowledge for the first – in a dinuclear transition metal complex with two non-identical chromophoric units. A comparison of the annihilation processes in **1** and **2** shows that the bromine substituents, which lifts the degeneracy of the MLCT excited states, only affect the rate but not the nature of the process itself. This finding points to the importance of considering interactions among multiple chemical distinct chromophoric units when designing future supramolecular photocatalytic device applications.

Acknowledgements

C.K. thanks the Deutsche Bundesstiftung Umwelt for a PhD fellowship, M.K. thanks The Wenner-Gren Foundation and B.D. and J.P. acknowledge financial support by the Fonds der Chemischen Industrie. S.R. acknowledges financial support by the DFG, the SFB 583 and the GRK 1626. Furthermore, financial support by the Thüringer Ministerium für Bildung, Wissenschaft und Kultur (Grant No. B 514-09 049, PhotoMIC) is highly acknowledged.

Appendix A. Supplementary data

Supplementary data associated with this article can be found, in the online version, at doi:10.1016/j.cplett.2011.09.056.

References

- [1] S. Campagna, F. Puntoriero, F. Nastasi, G. Bergamini, V. Balzani, *Top. Curr. Chem.* 280 (2007) 117.
- [2] L. Hammarström, O. Johansson, *Coord. Chem. Rev.* 254 (2010) 2546.
- [3] Y. Jenkins, E.A. Friedmann, J.N. Turro, K.J. Barton, *Biochemistry* 31 (1992) 10809.
- [4] U. Neugebauer, Y. Pellegrin, M. Devocelle, R.J. Forster, W. Signac, N. Moran, T.E. Keyes, *Chem. Commun.* 44 (2008) 5307.
- [5] V. Fernandez-Moreira, F.L. Thorp-Greenwood, M.P. Coogan, *Chem. Commun.* 46 (2010) 186.
- [6] M. Grätzel, *Nature* 414 (2001) 338.
- [7] H.B. Gray, *Proc. Natl. Acad. Sci. USA* 102 (2005) 3534.
- [8] S. Rau et al., *Angew. Chem.* 118 (2006) 6361.
- [9] P.D. Beer, E.J. Hayes, *Coord. Chem. Rev.* 240 (2003) 167.
- [10] H. Ozawa, K. Sakai, *Chem. Comm.* 47 (2011) 2227.
- [11] C. Turro, S. Bossmann, Y. Jenkins, J. Barton, N. Turro, *J. Am. Chem. Soc.* 117 (1995) 9026.
- [12] M. Brennamann, J. Alstrum-Acevedo, C. Fleming, P. Jang, T. Meyer, J. Papanikolas, *J. Am. Chem. Soc.* 124 (2002) 15094.
- [13] C. Kuhnt et al., *Phys. Chem. Chem. Phys.* 12 (2010) 1357.
- [14] M. Karnahl et al., *Dalton Trans.* 39 (2010) 2359.
- [15] J. Olofsson, L.M. Wilhelmsson, P. Lincoln, *J. Am. Chem. Soc.* 126 (2004) 14458.
- [16] J.-M. Lehn, J.-P. Sauvage, *Nouv. J. Chim.* 1 (1977) 449.
- [17] A.J. Esswein, D.G. Nocera, *Chem. Rev.* 107 (2007) 4022.
- [18] B. Dietzek et al., *Chem. Eur. J.* 12 (2006) 5105.
- [19] M. Elvington, J. Brown, S.M. Arachchige, K.J. Brewer, *J. Am. Chem. Soc.* 129 (2007) 10644.
- [20] T.D. Pilz, N. Rockstroh, S. Rau, *J. Coord. Chem.* 63 (2010) 2727.
- [21] S. Campagna, S. Serroni, S. Bodige, F.M. MacDonnell, *Inorg. Chem.* 38 (1999) 692.
- [22] S. Bodige, A.S. Torres, D.J. Maloney, D. Tate, G.R. Kinzel, A.K. Walker, F.M. MacDonnell, *J. Am. Chem. Soc.* 119 (1997) 10364.
- [23] E. Ishow et al., *Inorg. Chem.* 37 (1998) 3603.
- [24] I.G. Scheblykin, A. Yartsev, T. Pullerits, V. Gulbinas, V. Sundström, *J. Phys. Chem. B* 111 (2007) 6303.
- [25] F. Laquai, Y.-S. Park, J.-J. Kim, T. Basché, *Macromol. Rapid Commun.* 30 (2009) 1203.
- [26] C. Kuhnt, M. Karnahl, M. Schmitt, S. Rau, B. Dietzek, J. Popp, *Chem. Comm.* 47 (2011) 3820.
- [27] M.K. Brennamann, T.J. Meyer, J.M. Papanikolas, *J. Phys. Chem. A* 108 (2004) 9938.
- [28] N. Komatsuzaki, R. Katoh, Y. Himeda, H. Sugihara, H. Arakawa, K. Kasuga, *Dalton Trans.* (2000) 3053.
- [29] M. Karnahl et al., *Chem. Phys. Chem.* 12 (2011) 2101.
- [30] C. Kuhnt et al., *J. Raman Spectrosc.* 41 (2010) 922.
- [31] K. Nakamura, *Bull. Chem. Soc. Jpn.* 55 (1982) 2697.
- [32] R. Siebert, D. Akimov, M. Schmitt, A. Winter, U.S. Schubert, B. Dietzek, J. Popp, *Chem. Phys. Chem.* 10 (2009) 910.
- [33] B. Dietzek, S. Tschierlei, G. Hermann, A. Yartsev, T. Pascher, V. Sundström, M. Schmitt, J. Popp, *Chem. Phys. Chem.* 10 (2009) 144.
- [34] A.L. Dobryakov, J. Ruthmann, N.P. Ernstring, *Phys. Rev. A* 59 (1999) 2369.
- [35] B. Dietzek, T. Pascher, V. Sudström, A. Yartsev, *Laser Phys. Lett.* 4 (2007) 38.
- [36] J. Bolger, A. Gourdon, E. Ishow, J. Launay, *Inorg. Chem.* 35 (1996) 2937.
- [37] A. Juris, V. Balzani, F. Barigelletti, S. Campagna, P. Belser, A. von Zelewski, *Coord. Chem. Rev.* 84 (1988) 85.
- [38] V. Balzani, A. Juris, M. Venturi, S. Campagna, S. Serroni, *Chem. Rev.* 96 (1996) 759.
- [39] M.H. Damrauer, G. Cerullo, A. Yeh, T.R. Bousie, C.V. Shank, J.K. McCusker, *Science* 275 (1997) 54.
- [40] S. Tschierlei et al., *Chem. Eur. J.* 15 (2009) 7678.
- [41] C. Chiorboli, M. Roger, F. Scandola, *J. Am. Chem. Soc.* 125 (2003) 483.
- [42] A.C. Bhasikuttan, M. Suzuki, S. Nakashima, T. Okada, *J. Am. Chem. Soc.* 124 (2002) 8398.
- [43] S. Wallin, J. Davidson, J. Modin, L. Hammarström, *J. Phys. Chem. A* 109 (2005) 4697.
- [44] G. Benkö, J. Kalliainen, J.E.I. Korppi-Tommola, A.P. Yartsev, V. Sundström, *J. Am. Chem. Soc.* 124 (2002) 489.
- [45] M. Fujita, A. Ishida, T. Majima, S. Takamuku, *J. Phys. Chem.* 100 (1996) 5382.
- [46] D. Gut, I. Goldberg, M. Kol, *Inorg. Chem.* 42 (2003) 3483.
- [47] S.D. Bergman, I. Goldberg, A. Barbieri, M. Kol, *Inorg. Chem.* 44 (2005) 2513.

B. Autorenschaft der Publikationen

[CK1] **Investigation of substitution effects on novel Ru–dppz complexes by Raman spectroscopy in combination with DFT methods**

Christian Kuhnt	quantenchemische Rechnungen, Auswertung und Diskussion der Daten, Erstellung des Manuskriptes
Stefanie Tschierlei	Ramanspektroskopie, Auswertung und Diskussion der Daten, Erstellung des Manuskriptes
Michael Karnahl	Synthese und Charakterisierung der untersuchten Substanzen, Diskussion und Korrektur des Manuskriptes
Sven Rau	Konzept- und Ergebnisdiskussion, Diskussion und Korrektur des Manuskriptes
Benjamin Dietzek	Konzept- und Ergebnisdiskussion, Diskussion und Korrektur des Manuskriptes
Michael Schmitt	Projektleitung, Konzept- und Ergebnisdiskussion, Diskussion und Korrektur des Manuskriptes
Jürgen Popp	Konzept- und Ergebnisdiskussion, Diskussion und Korrektur des Manuskriptes

[CK2] **Substitution-controlled ultrafast excited-state processes in Ru-dppz-derivatives**

Christian Kuhnt	Absorptions- und Emissionsspektroskopie, zeitaufgelöste transiente Absorptionsspektroskopie, Auswertung und Diskussion der Daten, Erstellung des Manuskriptes
Michael Karnahl	Synthese und Charakterisierung der untersuchten Substanzen, Erstellung des Manuskriptes
Stefanie Tschierlei	Resonanz-Raman-Spektroskopie, Auswertung und Diskussion der Daten, Erstellung des Manuskriptes
Kristin Griebenow	Absorptions- und Emissionsspektroskopie, zeitaufgelöste transiente Absorptionsspektroskopie
Michael Schmitt	Konzept- und Ergebnisdiskussion, Diskussion und Korrektur des Manuskriptes
Bernhard Schäfer	Charakterisierung der untersuchten Substanzen
Sven Kriek	elektrochemische Messungen, Auswertung und Diskussion der Daten
Helmar Görls	Röntgenstrukturanalyse
Sven Rau	Projektleitung Synthese, Konzept- und Ergebnisdiskussion, Diskussion und Korrektur des Manuskriptes
Benjamin Dietzek	Projektleitung Spektroskopie, Konzept- und Ergebnisdiskussion, Diskussion und Korrektur des Manuskriptes
Jürgen Popp	Konzept- und Ergebnisdiskussion, Diskussion und Korrektur des Manuskriptes

[CK3] Tuning of Photocatalytic Hydrogen Production and Photoinduced Intramolecular Electron Transfer Rates by Regioselective Bridging Ligand Substitution

Michael Karnahl	Synthese und Charakterisierung der untersuchten Substanzen, Messungen der katalytischen Eigenschaften, Auswertung und Diskussion der Daten, Erstellung des Manuskriptes
Christian Kuhnt	Absorptions- und Emissionsspektroskopie, zeitaufgelöste transiente Absorptionsspektroskopie, Auswertung und Diskussion der Daten, Erstellung des Manuskriptes
Fei Ma	zeitaufgelöste transiente Absorptionsspektroskopie
Arkady Yartsev	Konzept- und Ergebnisdiskussion, Diskussion und Korrektur des Manuskriptes
Michael Schmitt	Konzept- und Ergebnisdiskussion, Diskussion und Korrektur des Manuskriptes
Benjamin Dietzek	Projektleitung Spektroskopie, Konzept- und Ergebnisdiskussion, Diskussion und Korrektur des Manuskriptes
Sven Rau	Projektleitung Synthese und Katalyse, Konzept- und Ergebnisdiskussion, Diskussion und Korrektur des Manuskriptes
Jürgen Popp	Konzept- und Ergebnisdiskussion, Diskussion und Korrektur des Manuskriptes

[CK4] Synthesis and photophysics of a novel photocatalyst for hydrogen production based on a tetrapyridoacridine bridging ligand

Michael Karnahl	Synthese und Charakterisierung der untersuchten Substanzen, Messungen der katalytischen Eigenschaften, Auswertung und Diskussion der Daten, Erstellung des Manuskriptes
Christian Kuhnt	Absorptions- und Emissionsspektroskopie, zeitaufgelöste transiente Absorptionsspektroskopie, Auswertung und Diskussion der Daten, Erstellung des Manuskriptes
Frank. W. Heinemann	Röntgenstrukturanalyse
Michael Schmitt	Konzept- und Ergebnisdiskussion, Diskussion und Korrektur des Manuskriptes
Sven Rau	Projektleitung Synthese und Katalyse, Konzept- und Ergebnisdiskussion, Diskussion und Korrektur des Manuskriptes
Jürgen Popp	Konzept- und Ergebnisdiskussion, Diskussion und Korrektur des Manuskriptes
Benjamin Dietzek	Projektleitung Spektroskopie, Konzept- und Ergebnisdiskussion, Diskussion und Korrektur des Manuskriptes

[CK5] Excited-state annihilation in a homodinuclear ruthenium complex

Christian Kuhnt	Absorptions- und Emissionsspektroskopie, zeitaufgelöste transiente Absorptionsspektroskopie, Auswertung und Diskussion der Daten, Erstellung des Manuskriptes
Michael Karnahl	Synthese und Charakterisierung der untersuchten Substanz, Diskussion und Korrektur des Manuskriptes
Michael Schmitt	Konzept- und Ergebnisdiskussion, Diskussion und Korrektur des Manuskriptes
Sven Rau	Projektleitung Synthese und Katalyse, Konzept- und Ergebnisdiskussion, Diskussion und Korrektur des Manuskriptes
Benjamin Dietzek	Projektleitung Spektroskopie, Konzept- und Ergebnisdiskussion, Diskussion und Korrektur des Manuskriptes
Jürgen Popp	Konzept- und Ergebnisdiskussion, Diskussion und Korrektur des Manuskriptes

[CK6] The impact of bromine substitution on the photophysical properties of a homodinuclear Ru–tpphz–Ru complex

Christian Kuhnt	Absorptions- und Emissionsspektroskopie, zeitaufgelöste transiente Absorptionsspektroskopie, Auswertung und Diskussion der Daten, Erstellung des Manuskriptes
Michael Karnahl	Synthese und Charakterisierung der untersuchten Substanz, Erstellung des Manuskriptes
Michael Schmitt	Konzept- und Ergebnisdiskussion, Diskussion und Korrektur des Manuskriptes
Sven Rau	Projektleitung Synthese und Katalyse, Konzept- und Ergebnisdiskussion, Diskussion und Korrektur des Manuskriptes
Benjamin Dietzek	Projektleitung Spektroskopie, Konzept- und Ergebnisdiskussion, Diskussion und Korrektur des Manuskriptes
Jürgen Popp	Konzept- und Ergebnisdiskussion, Diskussion und Korrektur des Manuskriptes

C. Liste der im Rahmen der Arbeit erzielten Veröffentlichungen

Veröffentlichungen in referierten Zeitschriften, die in diese Arbeit eingehen

1. M. Karnahl, C. Kuhnt, F. W. Heinemann, M. Schmitt, S. Rau, J. Popp, B. Dietzek, SYNTHESIS AND PHOTOPHYSICS OF A NOVEL PHOTOCATALYST FOR HYDROGEN PRODUCTION BASED ON A TETRAPYRIDOACRIDINE BRIDGING LIGAND, *Chem. Phys.*, **2012**, *393*, 65-73
2. C. Kuhnt, M. Karnahl, S. Rau, M. Schmitt, B. Dietzek, J. Popp, THE IMPACT OF BROMINE SUBSTITUTION ON THE PHOTOPHYSICAL PROPERTIES OF A HOMODINUCLEAR RU–TPPHZ–RU COMPLEX, *Chem. Phys. Lett.* **2011**, *516*, 45-50
3. M. Karnahl, C. Kuhnt, F. Ma, A. Yartsev, M. Schmitt, B. Dietzek, S. Rau, J. Popp, TUNING OF PHOTOCATALYTIC HYDROGEN PRODUCTION AND PHOTOINDUCED INTRAMOLECULAR ELECTRON TRANSFER RATES BY REGIOSELECTIVE BRIDGING LIGAND SUBSTITUTION, *Chem. Phys. Chem.*, **2011**, *12*, 2101-2109
4. C. Kuhnt, M. Karnahl, M. Schmitt, S. Rau, B. Dietzek, J. Popp, EXCITED-STATE ANNIHILATION IN A HOMODINUCLEAR RUTHENIUM COMPLEX, *Chem. Comm.*, **2011**, *47*, 3820-3821
5. C. Kuhnt, M. Karnahl, S. Tschierlei, K. Griebenow, M. Schmitt, B. Schäfer, S. Kriek, H. Görls, S. Rau, B. Dietzek, J. Popp, SUBSTITUTION-CONTROLLED ULTRAFAST EXCITED-STATE PROCESSES IN RU–DPPZ-DERIVATIVES, *Phys. Chem. Chem. Phys.*, **2010**, *12*, 1357-1368
6. C. Kuhnt, S. Tschierlei, M. Karnahl, S. Rau, B. Dietzek, M. Schmitt., J. Popp; INVESTIGATION OF SUBSTITUTION EFFECTS ON NOVEL RU–DPPZ COMPLEXES BY RAMAN SPECTROSCOPY IN COMBINATION WITH DFT METHODS, *J. Raman Spectrosc.*, **2010**,

41, 922-932

Öffentliche Vorträge

1. TIME- AND FREQUENCY-RESOLVED CHARACTERIZATION OF SUBSTITUTION EFFECTS ON DNA-INTERCALATORS

Frühjahrssymposium des JungChemikerForums der GDCh, 2009, Essen

Posterpräsentationen

1. ANNIHILATION OF EXCITED STATES IN HOMODINUCLEAR RUTHENIUM COMPLEXES

110. Hauptversammlung der Deutschen Bunsen-Gesellschaft für Physikalische Chemie (Bunsentagung), 2011, Berlin

C. Kuhnt, M. Karnahl, S. Rau, M. Schmitt, B. Dietzek, J. Popp

2. FREQUENZ- UND ZEITAUFGELÖSTE CHARAKTERISIERUNG VON SUBSTITUTIONSEFFEKTEN AN DNA-INTERKALATOREN

108. Hauptversammlung der Deutschen Bunsen-Gesellschaft für Physikalische Chemie (Bunsentagung), 2009, Köln

C. Kuhnt, S. Tschierlei, K. Griebenow, R. Schmeissner, M., S. Rau, B. Dietzek, M. Schmitt, J. Popp

D. Danksagung

Ich möchte diese Gelegenheit nutzen, allen zu danken, die zum Gelingen dieser Arbeit beigetragen haben. An erster Stelle steht dabei Professor Dr. Jürgen Popp, der mir die Möglichkeit gab, die Dissertation innerhalb seiner Arbeitsgruppe anzufertigen und die vorhandenen Arbeitsräume, Laboratorien und Geräte sowohl an der Universität Jena als auch am IPHT zu nutzen.

Für seine unmittelbare wissenschaftliche Betreuung, zahlreiche Diskussionen, seine zielführende Hartnäckigkeit und die wertvolle Unterstützung bei der Erstellung von Manuskripten und Vorträgen danke ich Professor Dr. Benjamin Dietzek.

Prof. Dr. Sven Rau und Dr. Michael Karnahl gebühren aufrichtiger Dank als zuverlässige Kooperationspartner ohne deren Leistungen in der Synthese der untersuchten Substanzen meine Arbeit nicht möglich gewesen wäre. Diese fruchtbare Kooperation wird auch durch die gemeinsamen Publikationen dokumentiert, welche dank der sorgfältig ausgearbeiteten Beschreibungen der Synthese an Qualität und Relevanz gewonnen haben.

Ich bedanke mich bei Professor Arkady Yartsev für die Möglichkeit, die Laboratorien der Universität Lund zu nutzen sowie Grigory Smolentsev und Fei Ma für die Unterstützungen bei den Messungen und der Auswertung und Diskussion der Ergebnisse.

Weiterhin möchte ich mich bei Dr. Stefanie Tschierlei bedanken, welche mir nach Betreuung der Diplomarbeit zu Beginn meiner Promotion den Umstieg von der Theoretischen Chemie zur Spektroskopie erleichterte und mit der ich oft und gerne hilfreiche, wissenschaftliche Diskussionen führen konnte.

Zum erfolgreichen Gelingen meiner Arbeit haben auch Kristin Griebenow und Roman Schmeissner beigetragen. Beide lieferten als Diplomanden einen wissenschaftlichen Beitrag. Desweiteren konnte ich dank ihnen wertvolle Erfahrungen bei der Betreuung ihrer Arbeiten sammeln.

Den Mitgliedern der Nachwuchsarbeitsgruppe "Ultrakurzzeitspektroskopie" danke ich für die stets kollegiale Unterstützung während der gemeinsamen Zeit in Büro und Labor. Vor allem den Kollegen, mit denen ich mir die Büros teilte, möchte ich an dieser Stelle gesondert danken für ihr offenes Ohr bei kleineren und größeren Problemen, welche

D. Danksagung

sowohl die Arbeit als auch der Alltag mit sich brachten.

Ich bedanke mich bei der Deutschen Bundesstiftung Umwelt für die Aufnahme in das Promotionsstipendienprogramm und der damit zusammenhängenden finanziellen Unterstützung. Besonders erwähnenswert sind die durchgeführten Stipendiatenseminare, welche aufgrund der großartigen Teilnehmer Herausforderung und Vergnügen zugleich darstellten.

Für den nötigen Rückhalt im Privatleben sorgte mein wunderbarer Freundeskreis, wofür ich mich hiermit herzlichst bedanke. Ich danke vor allem Susi für die Hilfe zu allen möglichen Gelegenheiten und dafür, immer die richtigen Fragen gestellt zu haben, die zum Weiterdenken zwangen.

Meinen Eltern danke ich für die Unterstützung sowie die Geduld, die sie hatten und immer noch mit mir haben. Mein größter Dank für Alles gilt Christin für das Vertrauen, den Rückhalt und die Unterstützung.

E. Lebenslauf

Persönliche Daten

Name	Christian Kuhnt
Geburtstag	12.05.1983
Geburtsort	Weißenfels

Schulbildung

1989-1993	Grundschule Erfurt
1993-2001	Heinrich-Mann-Gymnasium Erfurt

Zivildienst

08/2001 - 07/2002	Christliches Jugenddorfwerk Deutschland
-------------------	---

Hochschulausbildung

10/2002 - 09/2007	Studium der Chemie (Diplom) an der Friedrich-Schiller-Universität Jena
11/2007 - 05/2013	Dissertation am Institut für physikalische Chemie der Friedrich-Schiller-Universität Jena

Jena, den:

F. Selbständigkeitserklärung

Ich erkläre, dass ich die vorliegende Arbeit selbständig angefertigt und keine anderen als die angegebenen Hilfsmittel und Quellen verwendet habe.

Jena, den

Christian Kuhnt